Spring 2018

Torsional behavior of RC beams strengthened with PBO-FRCM composite

Meyyada Y. Alabdulhady

TORSIONAL BEHAVIOR OF RC BEAMS STRENGTHENED WITH PBO-FRCM COMPOSITE

by

MEYYADA YAHYA MOHAMMED ALABDULHADY

A DISSERTATION

Presented to the Faculty of the Graduate School of the

MISSOURI UNIVERSITY OF SCIENCE AND TECHNOLOGY

In Partial Fulfillment of the Requirements for the Degree

DOCTOR OF PHILOSOPHY

in

CIVIL ENGINEERING

2018

Approved by

Dr. Lesley H. Sneed, Advisor

Dr. John J. Myers

Dr. Mohamed A. ElGawady

Dr. K. Chandrashekhara

Dr. Victor Birman

PUBLICATION DISSERTATION OPTION

This dissertation has been prepared in the style of publications in professional journals.

Paper I (7-42) is a manuscript entitled “Torsional Strengthening of Reinforced Concrete Beams with Externally Bonded Composites: A State of the Art Review” is intended for submission to the Journal of Construction and Building Materials (ELSEVIER).

Paper II (43-80) is a manuscript entitled “Torsional Behavior of RC Beams Strengthened with PBO-FRCM Composite – An Experimental Study” has been published in the Journal of Engineering Structures (ELSEVIER), Volume 139, pp. 393-405.

Paper III (81-123) is a manuscript entitled “A Study of the Effect of Fiber Orientation on the Torsional Behavior of RC Beams Strengthened with PBO-FRCM Composite” has been published in the Journal of Construction and Building Materials (ELSEVIER), Volume 166, pp. 839-854.

Paper IV (124-161) is a manuscript entitled “Finite Element Study on the Behavior of RC Beams Strengthened with PBO-FRCM Composite under Torsion” has been published in the Journal of Composite Structures (ELSEVIER), Volume 179, pp. 326-339.

Paper V (162-198) is a manuscript entitled “Analytical Study on the Torsional Behavior of Reinforced Concrete Beams Strengthened with FRCM Composite” has been submitted to the Journal of Composites for Construction (American Society of Civil Engineers (ASCE)).

ABSTRACT

Externally bonded fiber reinforced cementitious matrix (FRCM) composites have been investigated recently as an alternative to fiber reinforced polymer (FRP) composites to overcome certain shortcomings such as the inability to install on wet surfaces or in low temperatures, low fire resistance, low glass transition temperature, low reversibility, and lack of vapor permeability. This study includes an inclusive investigation of the torsional behavior of RC beams strengthened with externally bonded polyparaphenylene benzo-bisoxazole (PBO)-FRCM composite material. A comprehensive review and discussion of the previous experimental, analytical, and numerically-simulated torsional behavior of RC beams strengthened with FRP composite was introduced to gain a better understanding of their behavior. Then, an experimental campaign was conducted that included 11 solid rectangular RC beams, one without strengthening and 10 that were externally strengthened with PBO-FRCM composite. The effect of different parameters such as number of wrapped sides, the continuity of composite layer, number of composite layers, and fiber orientation on the torsional behavior in terms of strength, rotational ductility, and failure mode was investigated. Finite element and analytical models of the PBO-FRCM-strengthened beams were developed and verified with the experimental results. The contribution of the composite to the torsional strength was estimated based on the measured strain using design provisions for FRP-strengthened beams to examine the applicability of these provisions to the FRCM composite system. Furthermore, a comparison with other composite systems was conducted to compare the efficiency of the PBO-FRCM composite system on increasing the torsional strength of RC beams.

ACKNOWLEDGMENTS

My first thanks and appreciations are for my advisor Dr. Lesly Sneed. She was surrounding me with her help and guidance all the time. All her advice and recommendations helped to improve the overall quality of my work. I ask GOD to bless and keep her safe for her family, friends, and students.

I would also like to thank all my committee members, Drs. John Myers, Mohamed A. ElGawady, K. Chandrashekhara and Victor Birman for their valuable suggestions and guidance. I really appreciate that they have devoted their valuable time to help improve this work.

Many thanks and appreciations are also goes to the staff in the Structure High Bay Lab at Missouri S&T, John Bullock, Brian Swift, Gary Abbott, Greg Leckrone, Jason Cox, and Mike Lusher. My colleagues Ahmed Gheni, Zuhair Aljaberi, Zena Aljazaeri, Samantha Wermager, Kristian Krc, and Nikkolas Edgmond also helped me a lot throughout my experimental work.

I am extremely grateful to my parents and brothers for their spiritual support. My special thanks to my loving husband, Khalid Al-jabery, my little angels, and my mother-in-law for their help and support during my Ph.D. program.

This project was funded by the Higher Committee for Education Development in Iraq (HCED), and the composite material was donated by Ruredil S.p.A. of San Donato Milanese, Italy. This financial and donation support is highly appreciated.

TABLE OF CONTENTS

Page

LIST OF ILLUSTRATIONS

PAPER III

PAPER V

LIST OF TABLES

PAPER IV

PAPER V

1. INTRODUCTION

1.1 BACKGROUND

Damage and/or deterioration of reinforced concrete (RC) structures during their service life can be repaired by adding extra reinforcement, which can be achieved by externally bonded composite material. Externally bonded composite is also applicable for strengthening existing structural members to increase the load carrying or ductility capacity for which they were designed. This increase may be required due to changes in use of the structure or to errors in design or construction.

The use of fiber reinforced polymer (FRP) composite has been widely investigated over last several decades as a strengthening technique. The effectiveness of this composite material in infrastructure applications is due to high strength and stiffness, light weight, resistance to corrosion, low thermal conductivity, and flexibility of use. The FRP composite system contains continuous fibers (e.g., carbon or glass) and liquid polymer matrix (e.g., epoxy resin). This system has been used successfully for strengthening of RC beams subjected to flexural, shear, axial, and torsional loading. In spite of the capabilities of this system, FRP composites have several disadvantages including difficulty to install onto wet surfaces or in low temperatures, low fire resistance, low glass transition temperature, and lack of vapor permeability, which are associated with the use of organic matrix.

In last two decades, a new type of composite material called fiber reinforced cementitious matrix (FRCM) composite has been developed to overcome or reduce some of the shortcomings associated with FRP composites. In this system, different types of

fabric meshes are used such as polyparaphenylene benzobisoxazole (PBO), carbon, glass, aramid, basalt, and steel, which are embedded in an inorganic matrix. The use of inorganic matrix results in better compatibility with concrete and masonry substrates as compared with organic material (epoxy resin). The inorganic matrix can also be applied in low temperatures and onto wet surfaces, allows vapor permeability, has better heat resistance and lower cost than the epoxy resin. Alternative names of this system are Textile Reinforced Mortar (TRM), Fiber Reinforced Concrete (FRC), Mineral Based Composites (MBC), Steel Reinforced Grout (SRG), and Textile Reinforced Concrete (TRC).

PBO-FRCM composite has been investigated for strengthening of RC beams subjected to flexural, shear, and axial loading. However, there are no studies in the technical literature on the use of the PBO-FRCM composite for torsional strengthening. Torsion occurs in many structures, such as in the main girders of bridges, which are twisted by transverse beams or slabs. Torsion also occurs in buildings where the edge of a floor slab and its beams are supported by a spandrel beam spanning between the exterior columns. Furthermore, earthquakes can cause torsional forces in buildings. Other cases where torsion may be significant are in curved bridge girders, spiral stairways, and balcony girders. In order to effectively utilize PBO-FRCM composite as a torsional strengthening system for RC beams, the behavior of the strengthened beams must be understood. Therefore, a comprehensive investigation on the torsional behavior of RC beams strengthened with PBO-FRCM composite material is needed.

1.2 OBJECTIVE AND SCOPE OF WORK

The objective of this study was to explore the torsional behavior of RC beams strengthened with externally bonded PBO-FRCM composite material. In order to evaluate the effectiveness of the composite system, experimental, numerical, and analytical studies were conducted in this research. To achieve the objective of this study, the scope of work included the following:

- A comprehensive review of the literature on the fundamental behavior of RC beams strengthened with FRP composites under torsional loading was conducted. Research on FRP-composite strengthened beams was investigated since no such studies have been reported on the torsional strengthening of RC beams using FRCM composites;
- A series of PBO-FRCM-strengthened RC beams was designed, constructed, and tested under torsional loading. Different parameters were investigated including number of wrapped sides, the continuity of composite layer (along the beam length), number of composite layers, and fiber orientation;
- The torsional behavior of the experimentally tested PBO-FRCM-strengthened RC beams was explored in terms of strength, rotational ductility, and failure mode;
- Strains measured in the internal and external reinforcement were analyzed to evaluate the contribution of each component to the torsional strength;

- Design provisions used to estimate the torsional strength of RC beams with fully-wrapped, externally-bonded FRP composites were examined to determine the applicability to beams strengthened with PBO-FRCM composite;
- The efficiency of the PBO-FRCM composite system was compared with that of CFRP and GFRP composites;
- A nonlinear finite element analysis was developed to analyze the experimentally tested beams in order to study more thoroughly the torsional behavior of RC beams strengthened with PBO-FRCM composite material;
- A parametric study was conducted with the verified finite element model to examine the influence of different parameters on the torsional behavior and capacity of RC beams strengthened with PBO-FRCM composite. This study was important to archive more data and provide researchers more information about the most effective parameters that should be considered in design of the PBO-FRCM composite strengthening system.
- An analytical model that was originally developed for FRP-strengthened RC beams was adapted to predict the full torsional response of RC beams strengthened with PBO-FRCM composite.

1.3 RESEARCH SIGNIFICANCE

The importance of the presented work in this dissertation is to understand the fundamental torsional behavior of RC members externally strengthened with PBO-FRCM composite material and the parameters that potentially influence their performance.

1.4 DISSERTATION ORGANIZATION

This dissertation includes three sections. Section 1 gives a brief introduction to the subject area and explains the need for the current research study. The first section also presents the overarching objective and scope of work of the investigation.

Section 2 presents the results of this study in the form of five manuscripts: two published journal papers, one journal paper in press, one journal paper in review, and one that will be submitted for review. The first paper is a detailed literature review to establish the state-of-the-art on the studied topic. The first paper presents a comprehensive summary and review of torsional strengthening of RC beams with FRP composite material, and it includes findings from experimental studies as well as analytical and numerical studies. The second and third papers present the experimental study on torsional strengthening of 11 RC beams, one without strengthening as a control beam and 10 strengthened with PBO-FRCM composite material in different wrapping configurations. The fourth paper presents a numerical study on the behavior of PBO-FRCM-strengthened RC beams and includes a comparison the experimental results. Finally, the fifth paper presents an analytical study in which the full torsional response of

PBO-FRCM-strengthened RC beams is predicted, and results are compared with the experimental results.

Section 3 summarizes the findings and conclusions of this study and proposes future research.

PAPER

I. TORSIONAL STRENGTHENING OF REINFORCED CONCRETE BEAMS WITH EXTERNALLY BONDED COMPOSITES: A STATE OF THE ART REVIEW

Meyyada Y. Alabdulhady, and Lesley H. Sneed

ABSTRACT

The use of externally bonded fiber reinforced composites to strengthen reinforced concrete (RC) structures has been explored extensively in recent decades. While many studies have been conducted on the flexural, shear, and axial strengthening of RC members, far fewer studies have been conducted on torsional strengthening. Thus, the knowledge on the behavior of RC beams strengthened in torsion with externally bonded composites is rather limited. The aim of this paper was to present a comprehensive review and evaluation for torsional strengthening of RC beams using externally bonded composites. A detailed survey of the literature was conducted, and a database of experimental tests was developed and presented. The effectiveness of the strengthening system was examined in terms of geometrical and mechanical characteristics of the RC beam, and composite type and wrapping configuration. Different modes of failure of the strengthened beams were also discussed. Additionally, numerical and analytical methods developed to predict the torsional response of RC beams strengthened with externally bonded composites were summarized and discussed. Finally, recommendations based on the knowledge gained from this study were introduced.

1. INTRODUCTION

Reinforced concrete (RC) members in buildings, bridges, and other structures can be subjected to significant torsional moment, which could lead to failure. The number of studies on the torsional behavior of RC structural members is quite limited due to the fact that torsion is considered a secondary effect compared with flexural and shears behaviors. However, torsional effects can be significant for certain cases such as for spandrel and curved beams in buildings and curved girders in bridges. Furthermore, earthquakes can cause severe torsional damage in structures [1].

Different techniques have been explored for strengthening of RC beams subjected to torsional moment. One technique includes the addition of external reinforcement to the member. The use of fiber reinforced polymer (FRP) composites as an external reinforcement for repairing and strengthening of RC structures has proven to be an effective and efficient technique compared to traditional solutions (e.g., steel jackets [2]). FRP composites are comprised of continuous fibers that are embedded in a polymeric matrix that is used to bind the fibers to the substrate and to transfer stresses between the substrate and fibers. Positive attributes of this material include its high strength-to-weight ratio, resistance to corrosion, low thermal conductivity, and flexibility of use. Experiments have demonstrated that externally bonded FRP composites can be used effectively to strengthen RC beams in torsion [3-14].

Recently, a new type of composite called fiber reinforced cementitious matrix (FRCM) composite has been developed and considered as an alternative to FRP composites. FRCM composites are comprised of continuous fibers embedded in an inorganic (e.g., cementitious) matrix, which affords better compatibility with the concrete

substrate when compared with the organic matrix (epoxy resin) used in FRP composites. FRCM composites can also be applied in low temperatures and on wet surfaces, allow vapor permeability, and have better heat resistance compared to FRP composites. Fibers in FRCM composites are typically bundled to provide better bond between the fibers and matrix. Alternative names of this system are Textile Reinforced Mortar (TRM), Fiber Reinforced Concrete (FRC), Mineral Based Composites (MBC), Steel Reinforced Grout (SRG), and Textile Reinforced Concrete (TRC). Research on the use of FRCM composites in structural strengthening applications is in its infancy, and currently, there are few studies in the technical literature on its use for torsional strengthening of RC members [15] [16].

In this paper, the state of research on torsional strengthening of RC beams with externally bonded fiber reinforced composites is presented. From a detailed survey of the literature, a database of experimental tests is developed and discussed. The effectiveness of the strengthening system is examined in terms of geometrical and mechanical characteristics of the RC beam, composite type, and composite wrapping configuration. Different modes of failure of the strengthened beams are also discussed. Then, numerical and analytical methods developed to predict the torsional response of RC beams strengthened with externally bonded composites are summarized and discussed. Finally, recommendations based on the knowledge gained from this study were introduced. It should be noted that this study is focused on composites bonded to the surface of the member; studies on near surface mounted (NSM) composites [e.g., 17-19] are not included in this survey.

2. EXPERIMENTAL DATABASE

The use of externally bonded composites to strengthen RC beams in torsion has been investigated experimentally since the early 2000s. Fourteen studies on the torsional strengthening of RC beams with externally bonded composites were found in the technical literature. A database that includes the characteristics of the RC beams, the composite strengthening systems, and experimental results was developed and is summarized in Table 1. Eighty beams with different cross-sections, composite types, and wrapping configurations, tested under static loading [3-5, 7-16] or cyclic loading [6] are included in the database. Figure 1 illustrates the different cross-sections and wrapping configurations reported.

In the evaluation of the collected data, the data were subdivided based on the mode of failure. Three main types of failure modes were reported: concrete damage, debonding of the composite from the composite substrate, and fiber rupture. Additional discussion on failure mode is presented in Section 4.

3. EVALUATION OF THE DATABASE AND DISTRIBUTION OF DATA

3.1 GEOMETRY AND MECHANICAL PROPERTIES OF THE STRENGTHENED BEAMS

Figure 2 shows in the increase in torsional strength T_u, relative to the corresponding unstrengthened (control) beam, as a function of the geometrical and mechanical properties of the RC beam. Figure 2 plots the percent increase in T_u as a function of the concrete compressive strength f'_c, volumetric ratio of the internal longitudinal reinforcement $\rho_{sl} = A_{sl}/A_c$, and internal transverse volumetric ratio

$\rho_{st} = \frac{A_{st}}{A_c}\frac{p_t}{s}$, where A_{sl} is the total area of longitudinal bars, A_c is the gross concrete area (A_c=bh), A_{st} is the area of one leg of a stirrup, p_t is the perimeter of a stirrup, and s is the center-to-center spacing of stirrups.

The results in Figure 2 show that the increase in T_u achieved by the external strengthening varies from 0% to 178% with an average of 51%. 75% of the tests were performed on beams with f'_c ranging from 20-40 MPa (Figure 2a). These values of concrete compressive strength are relatively low for new structures but can be considered suitable to represent the compressive strength of existing structures. All beams that exhibited a concrete damage failure mode had concrete compressive strengths in this range. It should be noted that beams with higher concrete compressive strengths, i.e., from 40-80 MPa, did not achieve a higher torsional strengths. This can be explained by the change in failure mode from concrete damage to composite debonding or rupture.

Figure 2b shows that 97% of the tests were performed on beams with ρ_{sl} between 0.5% and 2% (Figure 2b). Furthermore, 95% of the tests were performed on beams with ρ_{st} less than 1.5% (Figure 2c). These ranges are recommended by ACI 445.1R [20] for the internal reinforcement to be under-reinforced in order to avoid a brittle failure by concrete crushing. Under-reinforced beams are capable of continued twist as the reinforcement yields, producing a ductile failure. Figure 2c also shows that the increase in ρ_{st} may reduce the effectiveness of the strengthening system. This phenomenon is due to the RC beams potentially becoming over-reinforced, leading to a brittle failure. Another possible explanation for this trend is the interaction between the internal transverse steel reinforcement and the external strengthening reinforcement, which has been reported for RC beams strengthened in shear with externally bonded composites

[21-24]. It is noted that only one (i.e., [11]) test was conducted with beams without internal transverse reinforcement (i.e., ρ_{st} = 0%), however, the largest increase in torsional strength was achieved by a beam without stirrups.

3.2 COMPOSITE TYPES

As discussed in Section 1, two different types of externally bonded composites have been studied for torsional strengthening of RC beams: FRP composites, in which the fiber is bonded to the concrete substrate by an epoxy resin, and FRCM composites, in which the bonding agent between the fibers and the concrete substrate is an inorganic material. Figure 3 shows the distribution of data in terms of composite type. The majority of the available data (88%) is with FRP composites, while only 12% of the available data is with FRCM composites. For the case of FRP composites, the use of carbon and glass fibers has been studied (70% and 18% of all tests, respectively), whereas PBO fiber is the only fiber type studied for the case of FRCM composites. Figure 3 shows that the largest increases in torsional strength were achieved with CFRP composites, however significantly more tests have been conducted with CFRP composite than other types.

3.2.1 Wrapping Configuration. Torsion moment in unstrengthened RC beams is resisted by closed-loop stirrups due to the circulatory shear flow stresses that are induced by torsion. When a composite strengthening system is applied to the external surface of the beam, the composite fibers should form a closed-loop (4-sided wrapping) around the cross-section. In practice, however, a 4-sided wrapping configuration may not be possible to install if the complete perimeter of the beam is not accessible, such as in the case of a spandrel beam in monolithic construction. Therefore, the use of U-jackets (3-sided

wrapping) has been explored. In the case of U-jackets, the shear flow is not in the form of a closed-loop, and thus efficiency in improving the torsional strength compared to systems with closed-loop reinforcement is expected to be lower. Figure 4 shows that fully wrapped (4-sided) configurations were the most investigated (68%) and produced the largest increases in torsional strength.

Continuity of the composite along the length of the RC beam has also been explored. Results in Figure 4 show that beams with continuous (along the beam length) strengthening configurations achieved larger increases T_u compared to discontinuous strips for both 4-sided and 3-sided wrapping configurations. Certainly continuous configurations have larger reinforcement ratios those discontinuous strips. However, continuity of fibers along the length of the beam also serves to arrest the concrete cracks and preventing them from widening. Furthermore, composite strip width and spacing influences the confinement provided to the concrete, which affects the post-cracking behavior [5].

3.2.2 Fiber Orientation. Several studies have investigated the effect of composite fiber orientation on the effectiveness of fiber reinforced composite strengthening systems. For the case of FRP composites, different authors [3-6,13] have investigated fibers oriented at 0°, 45°, and 90° with respect to the longitudinal axis of the beam. Only one study [16] has investigated different fiber orientations (namely 0°, 45°, and 90°) for FRCM composites. These studies demonstrated that fiber direction has a significant influence on the torsional strength and rotational capacity of a strengthened RC beam.

Regarding distribution of data, Figure 5 shows most beams included in the database were wrapped with 90° fiber orientation (87%). Eight percent of beams were wrapped with 45° fiber orientation, while only 5% were wrapped with 0° fiber orientation. Although the results in Figure 5 show that the maximum increase in torsional strength was achieved by beams with 90° orientated fibers, the 45° fiber orientation is generally considered to be the most effective on increasing the torsional strength since the inclined fibers are oriented perpendicular to the concrete diagonal cracks. In fact, results of FRP-strengthened RC beams showed this to be the case [4-6]. However, no difference in rotational capacity between the 45° and 90° orientations was observed. For the case of FRCM composites, on the other hand, the 90° fiber orientation was found to be more effective in increasing the torsional strength than the 45° fiber orientation since premature debonding of the fibers occurred at the ends of the 45° strips, which contrasted the potential benefits from optimizing the fiber orientation and led to the underutilization of the composite [16]. Additional discussion on failure modes is presented in Section 4. Figure 5 shows that the 0° fiber orientation was not very effective for increasing the torsional strength of FRP- or FRCM-strengthened beams, however, is has been shown to be effective on increasing the cracking torque and post cracking twist by providing higher stiffness while keeping the width of the concrete cracks small [5]. Similarly, the study by He et al. [25] on FRP-strengthened RC columns determined that fibers oriented at 0° provided a minor contribute to the torsional strength of FRP-strengthened RC columns based on strain measurements in the longitudinal fibers.

3.2.3 Composite Fiber Volumetric Ratio, Number of Layers, and Fiber Strain. Figure 6 shows the increase in torsional strength T_u as a function of the

volumetric ratio of the composite fiber reinforcement $\rho_f = \frac{n.t_f.p_f}{A_c}\frac{w_f}{s_f}$, the ultimate strain in the fiber ε_{fu}, and number of composite layers *n*, where t_f is the thickness of the composite, w_f is the width of the composite sheets, and s_f is the center-to-center spacing of the applied composite sheets. Most (86%) of the tests were conducted with ρ_f between 0% and 0.5% (Figure 6a). The maximum increase in torsional strength was achieved for beams with ρ_f between 0.5% and 1%, which had 2 layers of composite as shown in Figure 6b. The majority of tests were conducted on beams with one layer of composite (75%), 20% with two layers, and 5% of the tests with three layers. Although some higher increases in torsional strength occurred by increasing the number of layers from one to two, the effectiveness of the strengthening system appears to be reduced when a larger number of layers are provided. In other words, the increase in torsional strength may not be proportional to the number of composites layers. 83% of the tests investigated had fiber strain between 1% and 2% (Figure 6c), which was corresponds to values for carbon and PBO fibers.

4. MODE OF FAILURE

Failure of unstrengthened RC beams subjected to pure torsion is governed by concrete damage, which can be described as crushing of concrete struts and/or cover spalling. The same type of failure has been reported on the unstrengthened side of FRP-strengthened beams with a U-jacketing configuration. However, the failure of beams with U-jackets was initiated by debonding or delamination of the composite strip at the most stressed region of the concrete-composite adhesive interface. In some cases, peeling of

the FRP strips (intermediate composite debonding, along the crack direction and at the crack location [113]) occurred before crushing of concrete struts, while slippage of the fiber in the cementitious matrix in the FRCM system occurred before failure [15] [16].

Failure of beams with fully wrapped strips was governed by either crushing of concrete struts between the strips or fiber rupture. Rupture of the fiber occurred in fully wrapped beams when the fibers reached their tensile strength before crushing of concrete struts due to compression forces or excessive diagonal cracking associated with diagonal tension forces. In spite of two different strengthening systems using externally bonded composite sheets (FRP and FRCM), the mode of failure for each mentioned condition was the same in both systems.

5. ANCHORAGE SYSTEM

The failure mode associated with premature debonding or delamination of the composite from the substrate is an undesirable failure. This type of failure is often the result of an incomplete loop of the force transferring mechanism provided by the composite. In order to improve the composite fiber efficiency and the performance of the 3-sided wrapped beams, anchorage systems were investigated in various forms, introduced by different researchers [6-7, 13-14]. For the case of FRP-strengthened beams, four types of anchorage systems have been used in an attempt to mitigate debonding of the composite from the concrete substrate: through rods, fasteners, steel angles with fasteners, and extended U-jackets for T-sections as shown in Figure 7. The results revealed that each technique is workable and effective for increasing the torsional strength and rotational capacity of FRP-strengthened beams. This improvement was due

to the shear flow in the anchors, which also delayed composite delamination [6]. This can be seen clearly in Figure 4, where the lower bound value in increasing the torsional strength of 3-sided strips with anchors is higher than the upper bound value of 3-sided strips without anchors. The same observation can be seen for 3-sided continuous with and without anchors.

6. ANALYTICAL MODELS

The torsional behavior of RC beams strengthened with external reinforcement is complex and not well understood. Furthermore, as discussed in Section 2, experimentally tested beams are limited, and additional investigations are needed to understand the complex behavior and to illustrate the contribution of different components (i.e. concrete, internal reinforcement, and external reinforcement) in terms of torsional strength and behavior.

Different approaches have been used to analytically model the behavior of RC beams strengthened in torsion with externally bonded composites. In each approach, the same assumptions were adopted: torsion after cracking is resisted by truss action of compressive stresses in diagonal concrete struts and tensile stresses in the internal (longitudinal and transverse) and external reinforcement. Equilibrium and compatibility equations were implemented with the constitutive laws of an element taken from a member subjected to pure torsion, as shown in Figure 8, to obtain the torsional response.

One of the first analytical models developed to evaluate the torsional capacity of FRP strengthened RC beams was introduced by Ameli and Ronagh [26]. The interaction of different components was considered by implementing the equilibrium and

compatibility equations throughout the loading regime, whereas the ultimate torque of the beam was calculated using the compression field theory (CFT). Reasonably accurate results were obtained from the analytical model. Deifalla and Ghobarah [27] developed an analytical model to predict the full torsional behavior of RC beams strengthened with FRP composite material based on the modified compression field theory (MCFT), the hollow tube analogy, and the compatibility at the corner of the cross section. This model took into account the composite wrapping scheme, even for the case where the FRP is not bonded to all beam faces, FRP contribution, and mode of failure. The analytical model results showed good agreement with the experimental results.

Chalioris [28] introduced an analytical method to predict the full torsional behavior of RC beams strengthened with FRP composite material by employing two different theoretical models: a smeared crack model for plain concrete in torsion and a modified softened truss model which takes into account the contribution of the FRP composite. The proposed model was capable of describing the full torsional response with satisfactory accuracy and the cracking torque and torsional strength. Zojaji and Kabir [29] and Ganganagoudar et al. [30] introduced a modified softened membrane model (SMMT) for torsion with taking into account the influence of externally bonded FRP on the compressive behavior of cracked concrete. The model by Ganganagoudar et al. [30] considered the composite fiber rupture failure mode, while the model by Zojaji and Kabir [29] also included the composite debonding failure mode. Reasonably good agreement was achieved with the tested data.

Chai et al. [31] proposed an analytical method to predict the torsional capacity and behavior of RC multi-cell box girders strengthened with CFRP sheets based on the

extension and modification of the space truss model for torsion (STMT) algorithm. Good agreement between the proposed method and the experimental results was achieved. Shen et al. [32] proposed an analytical model based on the modification of the classical rotating angle softened truss model (RA-STM) for torsion to predict the full torsional behavior of RC beams externally wrapped with FRP composite material with considering the influence of the tensile stress in concrete and the effect of FRP confinement on torsional behavior. Good agreement between the analytical and experimental results indicated the applicability of the analytical model for predicting the torsional behavior of RC beams strengthened with FRP materials both at the pre-cracking and post-cracking stages.

The authors of the analytical studies described above tested the validity of their model by comparing the analytical results with experimental results from other studies. Table 2 summarizes the experimental tests used in the comparison (rows in the table) for each analytical study (columns in the table). Results were compared in terms of cracking torsional moment T_{cr} and/or torsional strength T_u. The comparison of analytical and experimental results is listed in Table 2.

7. NUMERICAL STUDIES

The torsional response of externally bonded fiber reinforced composite strengthened RC beams has been investigated using numerical simulation. Hii and Al-Mahaidi [8] implemented the nonlinear finite element program DIANA [33] to model CFRP-strengthened RC beams with solid and box sections under torsional loading. Good agreement in terms of torque–twist behavior, steel and CFRP reinforcement responses,

crack patterns, and mode of failure was achieved. Ameli et al. [9] modeled CFRP or GFRP-strengthened RC beams with a rectangular cross-section with the nonlinear finite element program ANSYS [34]. The results from modeled beams were in a reasonable agreement with the experimental data. Ganganagoudar et al. [30] used a nonlinear finite element program ABAQUS [35] to model full scale, RC beams strengthened with FRP composite material. A reasonably good agreement was achieved between the predicted and the experimental results. Elwan [36] use the nonlinear finite element program ANSYS [34] to conduct a parametric study on the effect of volumetric ratio of composite, number of composite layers, composite strength, and U-jacket configuration on the torsional behavior of FRP-strengthened rectangular and T-shaped RC beams. Alabdulhady et al. [37] modeled PBO-FRCM-strengthened RC beams with a rectangular cross-section by using a nonlinear finite element program LS-DYNA [38]. Good agreement was achieved between the experimental and the predicted results of the model for the full torsional response. Furthermore, a parametric study was conducted on the effect of concrete compressive strength, FRCM composite strip width, and strip spacing on the torsional behavior and strength. Table 3 summarizes a comparison of FE and corresponding experimental results of these studies in terms of cracking torsional moment T_{cr} and torsional strength T_u.

8. MODELS FOR COMPUTING THE CONTRIBUTION OF THE COMPOSITE TO THE TORSIONAL STRENGTH

Fib [39] and NCHRP Report 655 [40] are currently the only guides applicable to the design of FRP composites for torsional strengthening, whereas no provisions exist for

the design of FRCM composites for torsional strengthening. In the Fib and NCHRP guides, the contribution of the externally bonded composite system T_f is considered additive to the torsional strength of the unstrengthened RC beam T_{RC} as indicated in Equation 1. In this section, this approach is examined using the experimental data from the database in Table 1 in an attempt to evaluate the effective strain in the composite corresponding to the torsional strength of the member.

$$T_f = T_u - T_{RC} \tag{1}$$

Salom et al. [6] and Hii and Al-Mahaidi [10] assumed that the composite around the perimeter of the beam behaves similarly to closed stirrups. Therefore, the torsional contribution from the composite can be calculated from Equation 2, which is similar to the equation for computing the torsional capacity of unstrengthened beams by the ACI code [41].

$$T_f = \frac{2A_0 A_f f_{fe}}{s_f}(cos\,\theta + sin\,\theta) \tag{2}$$

where: A_0 is gross area enclosed by the shear flow path within the composite, $A_f = nw_f t_f$ is the area of the composite, $f_{fe} = \varepsilon_{fe} E_f$ is the effective stress in the composite, ε_{fe} is the effective strain in the composite, E_f is the modulus of elasticity of the composite fibers, θ is the angle between the fiber orientation and the longitudinal axis of the beam, and s_f is the center-to-center spacing of the composite strip along the longitudinal axis.

By substitution of terms, Equation 2 can be rewritten as:

$$T_f = 2.\varepsilon_{fe}.E_f.b.h.\frac{t_f.w_f}{s_f}cot(\theta) \tag{3}$$

For beams strengthened with U-jacket configurations with anchors, Panchacharam and Belarbi [5], recommended that a reduced value of T_f be considered in accordance with Equation 4:

$$T_f = \varepsilon_{fe}.E_f.b.h.\frac{t_f.w_f}{s_f}cot(\theta) \quad (4)$$

According to Equations 3 and 4, provisions for torsional strengthening RC beams with externally bonded fiber reinforced composites require an estimation of the effective strain in the composite fibers ε_{fe} to design the strengthening system. For the case of FRP composites, this value is recommended as ε_{fe} =0.004 [40]. On the other hand, if the contribution of the composite to the torsional strength is known from Equation 1, the effective strain in the fiber can be calculated from Equation 3.

To examine the validity of the aforementioned approach, the contribution of the composite to the torsional strength of the beams in Table 1 was estimated from Equation 1 ($T_{f,test}$) and then compared with the value computed from strains measured in the composite fibers at the ultimate strength of the beam ($T_{f,pred}$). This approach was also used by Alabdulhady et al. [15] to estimate the contribution of the FRCM composite for beams with a 4-sided wrapping configuration by considering the maximum measured strain in the fibers corresponding to the torsional strength. The predicted $T_{f,pred.}$ versus the experimental T_f (Equation 1) are shown in Figure 9.

It should be noted that not all tests in Table 1 are included in Figure 9. Only 50% of the studies reported values of fiber strains (i.e. [4, 6-8, 10-12, 15-16]), and therefore, only tests from these studies are shown in the figure. Figure 9 shows that the majority of the data have higher predicted strengths, which means that this approach overestimates

the contribution of the composite to the torsional strength. This supports the need for a maximum value of the effective strain used in design, which is currently taken at 0.004 for FRP composites. More work is needed to determine a suitable limit for the effective strain for the case of FRCM composites.

9. CONCLUSIONS

This paper provided a comprehensive review of the existing studies on torsional strengthening of RC beams with externally bonded composites. Evaluation of the experimental database, methods of strengthening, mode of failure, anchorage system, the accuracy of existing analytical and FE models, and code provisions were discussed in this paper. The important conclusions from this study are listed below:

1. The experimental evidence showed that externally bonded composite materials can be used to increase the torsional strength of RC beams. For the beams included in the database, the increase in torsional strength varied from 0% to 178% with an average of 51%.
2. U-jacketing (3-sided) and fully wrapped (4-sided) strengthening configurations were the most heavily investigated configurations.
3. Fibers with 0°, 45°, and 90° directions have been investigated. Beams wrapped with 45° fiber orientation was the most effective on increasing the torsional strength, while fibers with 0° had the least contribution to the torsional strength. However, fibers with 0° orientations increased the cracking torsional moment.

4. Continuity of the composite along the beam proved to be more effective than discrete strips due to the effect of fiber continuity on arresting the cracks and preventing them from widening.
5. Failure of beams strengthened with U-jacketing configurations was governed by concrete damage. Failure of beams with fully wrapped strips was dominated by either crushing of concrete struts between the strips or composite fiber rupture. Rupture of the fiber governed the failure of beams with fully wrapped, continuous composite.
6. Different forms of anchorage systems have been investigated such as anchor bars, composite fastened to the top of the beam for rectangular sections, steel angles, and extended U-jacket for T-sections, to overcome debonding of the composite from the concrete substrate. These techniques have proven to be effective for increasing the torsional strength and rotational capacity of FRP-strengthened beams. Additional work is needed to study anchorage of FRCM-strengthened beams.
7. Analytical studies have been conducted to predict the full torsional response of RC beams strengthened with FRP composite material by implementing different approaches including the compression field theory (CFT), softened membrane model for torsion (SMMT), and space truss model for torsion (STMT).
8. Nonlinear finite element programs such as DIANA, ANSYS, ABAQUS, and LS-DYNA have been used to numerically model the response of RC beams strengthened with externally bonded FRP and FRCM composites subjected to torsion.

9. Provisions used to estimate the torsional strength of RC beams with externally bonded composite sheets are applicable for designing or analyzing such beams, with acceptable tolerance.

10. RECOMMENDATIONS

To better understand the torsional behavior of RC beams with externally bonded composites, additional work is needed in the following areas:

1. Very few studies have investigated the behavior of RC beams strengthened with fibers orientated at angles other than 90°. Additional studies are needed to examine the effect of fiber orientation on the torsional response of strengthened beams.
2. Experimental studies on large- or full-scale RC beams are extremely limited. Additional investigation is needed to examine potential size effects.
3. Very few studies exist on torsional strengthening with FRCM composite. Additional work is needed to explore the response of FRCM-strengthened beams with different fiber types.
4. Additional investigation is needed to develop suitable anchorage systems that could improve the torsional capacity of FRCM-strengthened beams with 3-sided wrapping configurations.
5. Analytical models on the full torsional response of FRCM-strengthened beams are in need of development.

6. Although design provisions exist for designing externally bonded FRP strengthening systems, provisions are needed for other composite types including FRCM composites.
7. More investigations are needed for RC beams strengthened with new composite systems such as steel reinforced polymer (SRP) and steel reinforced grout (SRG).

Table 1. Experimental database.

			Cross-section		Concrete	Internal reinf.		Composite										Results	
Ref.	Beam name	Shape	b (mm)	h (mm)	f'_c (MPa)	ρ_{sl} (%)	ρ_{st} (%)	Composite type	Layout	n	w_f (mm)	s_f (mm)	E_f (GPa)	f_f (MPa)	ρ_f (%)	Anchors	% Increase in T_u	Failure mode
[3]	L2	R/s	150	250	21.2	0.837	0.462	CFRP	4-sided 90°S	1	60	120	287	3269	0.118	No	41.0	R
	L3	R/s	150	250	21.2	0.837	0.462	CFRP	4-sided 90°S	3	60	120	287	3269	0.355	No	75.0	CC
	L4	R/s	150	250	23.7	0.837	0.462	CFRP	4-sided 90°S	1	60	120	287	3269	0.118	No	88.0	R
	L5	R/s	150	250	23.7	0.837	0.462	CFRP	4-sided 90°S	3	60	120	287	3269	0.355	No	80.0	CC
	L6	R/s	150	250	23.7	0.837	0.462	CFRP	4-sided 90°S	1	60	150	287	3269	0.095	No	56.0	R
	L7	R/s	150	250	23.7	0.837	0.462	CFRP	4-sided 90°S	3	60	150	287	3269	0.284	No	64.0	CC
	L8	R/s	150	250	23.7	0.837	0.462	CFRP	2-sided 0°S	1	60	70	287	3269	0.076	Yes	12.0	CC
	L9	R/s	150	250	23.7	0.837	0.462	CFRP	2-sided 0°S	1	60	170	287	3269	0.052	Yes	16.0	CC
	L10	R/s	150	250	21.2	0.837	0.46	CFRP	2-sided 0°S/4-sided 90°S	3	60	120	287	3269	0.222	Yes	80.0	R
[4]	C1	R/s	150	350	37	1.148	0.644	CFRP	4-sided 90°C	1	1	1	252	4300	0.314	No	63.2	D
	C2	R/s	150	350	37	1.148	0.644	CFRP	4-sided 90°S	1	100	200	252	4300	0.157	No	26.7	CC
	C3	R/s	150	350	37	1.148	0.644	CFRP	1-side 45°S	1	100	170	252	4300	0.065	No	11.6	CC
	C4	R/s	150	350	37	1.148	0.644	CFRP	4-sided 90°S	1	200	300	252	4300	0.210	No	43.7	CC
	C5	R/s	150	350	37	1.148	0.644	CFRP	4-sided 90°S	1	100	250	252	4300	0.126	No	21.8	CC
	C6	R/s	150	350	37	1.148	0.376	CFRP	4-sided 45°S	1	100	230	252	4300	0.137	No	54.5	R
	G1	R/s	150	350	37	1.148	0.644	GFRP	4-sided 90°C	1	1	1	87	1317	0.672	No	71.9	D
	G2	R/s	150	350	37	1.148	0.644	GFRP	4-sided 90°S	1	100	200	87	1317	0.336	No	19.4	CC
[5]	A90W4	S/s	279.4	279.4	34	1.025	0.537	GFRP	4-sided 90°C	1	1	1	72	1520	0.220	No	149.0	R
	A90S4	S/s	279.4	279.4	34	1.025	0.537	GFRP	4-sided 90°S	1	114.3	228.6	72	1520	0.110	No	90.0	CC
	A0L4	S/s	279.4	279.4	34	1.025	0.537	GFRP	4-sided 0°C	1	1	1	72	1520	0.220	No	62.0	P
	A0L3	S/s	279.4	279.4	34	1.025	0.537	GFRP	3-sided 0°C	1	1	1	72	1520	0.165	No	43.0	P
	B0L4/90S4	S/s	279.4	279.4	26	1.025	0.537	GFRP	4-sided 0°C/90°S	2	114.3	228.6	72	1520	0.220	No	96.0	P
	B90U3-Anch	S/s	279.4	279.4	26	1.025	0.537	GFRP	3-sided 90°S	1	1	1	72	1520	0.165	Yes	39.0	CC
	C90U3	S/s	279.4	279.4	31	1.025	0.537	GFRP	3-sided 90°C	1	1	1	72	1520	0.165	No	35.0	CS
[6]	TB2	L/s	203	305	55	1.781	1.615	CFRP	3-sided 0°/90°C	2	1	1	104	NR	2.846	No	35.2	d
	TB3	L/s	203	305	55	1.781	1.615	CFRP	3-sided +45°/-45°C	2	1	1	104	NR	2.846	Yes	77.9	d
	TB4	L/s	203	305	55	1.781	1.615	CFRP	3-sided 0°/90°C	2	1	1	104	NR	2.846	Yes	52.9	CC
	TB5	L/s	203	305	55	1.781	1.615	CFRP	3-sided 90°C	1	1	1	104	NR	1.423	Yes	46.3	d
[7] [8] [10]	FS050D2	R/s	350	500	56.4	0.628	0.203	CFRP	4-sided 90°S	2	50	300	240	3800	0.057	No	49.2	R
	FH075D1	R/h	350	500	48.9	2.749	0.203	CFRP	4-sided 90°S	1	50	425	240	3800	0.020	No	36.7	R
	FH050D1	R/h	350	500	56.4	2.749	0.203	CFRP	4-sided 90°S	1	50	300	240	3800	0.028	No	51.5	R
	FH050D2	R/h	350	500	52.8	2.749	0.203	CFRP	4-sided 90°S	2	50	300	240	3800	0.057	No	77.6	R
[9]	CFE	R/s	150	350	39	1.532	0.530	CFRP	4-sided 90°C	1	1	1	244	3943	0.314	No	87.0	R
	CFE2	R/s	150	350	39	1.532	0.530	CFRP	4-sided 90°C	2	1	1	244	3943	0.629	No	143.0	R
	CJE	R/s	150	350	39	1.532	0.530	CFRP	3-sided 90°C	1	1	1	244	3943	0.267	No	33.0	D
	CFS	R/s	150	350	39	1.532	0.530	CFRP	4-sided 90°S	1	100	200	244	3943	0.157	No	45.0	R
	CJS	R/s	150	350	39	1.532	0.530	CFRP	3-sided 90°S	1	100	200	244	3943	0.134	No	16.0	D
	GFE	R/s	150	350	36	1.532	0.530	GFRP	4-sided 90°C	1	1	1	73	3373	0.293	No	78.0	R
	GFE2	R/s	150	350	36	1.532	0.530	GFRP	4-sided 90°C	2	1	1	73	3373	0.587	No	110.0	R
	GJE	R/s	150	350	36	1.532	0.530	GFRP	3-sided 90°C	1	1	1	73	3373	0.249	No	32.0	D
	GFS	R/s	150	350	36	1.532	0.530	GFRP	4-sided 90°S	1	100	200	73	3373	0.147	No	34.0	R
	GJS	R/s	150	350	36	1.532	0.530	GFRP	3-sided 90°S	1	100	200	73	3373	0.125	No	14.0	D
[11]	Ra-F(1)	R/s	100	200	27.5	1.005	0	CFRP	4-sided 90°C	1	1	1	230	3900	0.330	No	103.8	R
	Ra-F(2)	R/s	100	200	27.5	1.005	0	CFRP	4-sided 90°C	2	1	1	230	3900	0.660	No	178.4	R
	Ra-Fs150(2)	R/s	100	200	27.5	1.005	0	CFRP	4-sided 90°S	2	150	300	230	3900	0.330	No	26.3	CC
	Rb-F(1)	R/s	150	300	28.8	0.447	0	CFRP	4-sided 90°C	1	1	1	230	3900	0.220	No	44.6	R

Table 1. Experimental database (continued).

	Rb-Fs200(1)	R/s	150	300	28.8	0.447	0	CFRP	4-sided 90°S	1	200	400	230	3900	0.110	No	34.0	CC
	Rb-Fs300(1)	R/s	150	300	28.8	0.447	0	CFRP	4-sided 90°S	1	300	600	230	3900	0.110	No	8.2	CC
	T-FU(1)	T/s	150	300	26.5	0.670	0	CFRP	3-sided 90°C	1	1	1	230	3900	0.136	No	6.0	D
	T-FU(2)	T/s	150	300	26.5	0.670	0	CFRP	3-sided 90°C	2	1	1	230	3900	0.272	No	11.4	D
[12]	ACS1	R/s	150	350	74.39	0.598	0.938	CFRP	4-sided 90°S	1	100	200	240	3800	0.168	No	9.9	D
	ACUJ-anc.	R/s	150	350	72.67	0.598	0.938	CFRP	3-sided 90°C	1	1	1	240	3800	0.285	Yes	52.7	R
	ACW1	R/s	150	350	73.18	0.598	0.938	CFRP	4-sided 90°C	1	1	1	240	3800	0.335	No	48.5	R
	ACW2	R/s	150	350	73.24	0.598	0.938	CFRP	4-sided 90°C	2	1	1	240	3800	0.670	No	75.3	R
	BCS1	R/s	150	350	78.52	1.173	0.938	CFRP	4-sided 90°S	1	100	200	240	3800	0.168	No	9.6	R
	BCUJ-anc.	R/s	150	350	80.56	1.173	0.938	CFRP	3-sided 90°C	1	1	1	240	3800	0.285	Yes	59.5	R
	BCW1	R/s	150	350	78.12	1.173	0.938	CFRP	4-sided 90°C	1	1	1	240	3800	0.335	No	57.6	R
	BCW2	R/s	150	350	74.95	1.173	0.938	CFRP	4-sided 90°C	2	1	1	240	3800	0.670	No	92.6	R
	CCW1	R/s	150	350	73.33	1.532	1.459	CFRP	4-sided 90°C	1	1	1	240	3800	0.335	No	65.1	R
	CCW2	R/s	150	350	74.43	1.532	1.459	CFRP	4-sided 90°C	2	1	1	240	3800	0.670	No	111.8	R
[13]	RB1ER6-50	R/s	150	350	25	1.005	0.545	CFRP	4-sided 90°S	1	50	200	NR	700	0.070	No	17.0	P
	RB1ER6-100	R/s	150	350	25	1.005	0.545	CFRP	4-sided 90°S	1	100	200	NR	700	0.130	No	34.0	P
	LB1ER2	L/s	150	350	25	1.056	0.348	CFRP	3-sided 90°S	1	100	200	NR	700	0.100	Yes	41.7	CC
	LB1ER3	L/s	150	350	25	1.056	0.348	CFRP	3-sided 45°S	1	100	200	NR	700	0.100	No	25.0	D
	LB1ER4	L/s	150	350	25	1.056	0.348	CFRP	3-sided 90°S	1	100	200	NR	700	0.100	Yes	58.3	CC
	LB1ER7	L/s	150	350	25	1.056	0.348	CFRP	4-sided 90°S	1	100	200	NR	700	0.100	No	83.3	CC
	TB1ER1	T/s	120	400	25	1.446	0.571	CFRP	3-sided 90°S	1	100	200	NR	700	0.140	No	30.2	D
	TB1ER5	T/s	120	400	25	1.446	0.571	CFRP	3-sided 90°S	1	100	200	NR	700	0.140	Yes	64.1	D
[14]	ST-S	R/h	250	350	45	1.645	0.332	CFRP	4-sided 90°S	1	100	200	230	4900	0.097	No	22.9	R
	ST-T	R/h	750	350	43	1.645	0.214	CFRP	4-sided 90°S	1	100	200	230	4900	0.060	No	21.7	R
[15] [16]	N-P-3-S-1	R/s	203.2	304.8	39.3	1.290	0.92	PBO-FRCM	3-sided 90°S	1	101.6	203.2	206	3015	0.030	No	7.8	CC
	N-P-3-45S-1	R/s	203.2	304.8	34.5	1.290	0.92	PBO-FRCM	3-sided 45°S	1	101.6	203.2	206	3015	0.030	No	0.0	CC
	N-P-3-C-1	R/s	203.2	304.8	34.5	1.290	0.92	PBO-FRCM	3-sided 90°C	1	1	1	206	3015	0.060	No	0.8	CC
	N-P-4-S-1	R/s	203.2	304.8	39.3	1.290	0.92	PBO-FRCM	4-sided 90°S	1	101.6	203.2	206	3015	0.038	No	29.9	R
	N-P-4-45S-1	R/s	203.2	304.8	34.5	1.290	0.92	PBO-FRCM	4-sided 45°S	1	101.6	203.2	206	3015	0.038	No	17.6	D
	N-P-4-8S-1	R/s	203.2	304.8	34.5	1.290	0.92	PBO-FRCM	4-sided 90°S	1	203.2	304.8	206	3015	0.038	No	28.6	R
	N-P-4-0C-1	R/s	203.2	304.8	34.5	1.290	0.92	PBO-FRCM	4-sided 0°C	1	1	1	206	3015	0.075	No	7.7	D
	N-P-4-C-1	R/s	203.2	304.8	39.3	1.290	0.92	PBO-FRCM	4-sided 90°C	1	1	1	206	3015	0.075	No	61.7	R
	N-P-4-(0/90)C-2	R/s	203.2	304.8	34.5	1.290	0.92	PBO-FRCM	4-sided 90°C	2	1	1	206	3015	0.151	No	79.1	D
	N-P-4-C-2	R/s	203.2	304.8	39.3	1.290	0.92	PBO-FRCM	4-sided 90°C	2	1	1	206	3015	0.151	No	108.9	R

Beam shape: R/s=rectangular/solid, S/s=square/solid, L/s=L-shaped/solid, R/h= rectangular/hollow, T/s= T-shaped/solid.
Composite fiber type: C=carbon, G=glass
Layout: Angle reported is relative to the beam longitudinal axis. C=continuous, S=strip.
Failure mode: D=composite debonding, CC=concrete crushing, R=composite fiber rupture, P=composite peeling, CS=concrete cover spalling, d=composite delamination.
NR=not reported.
% increase in T_u is relative to the corresponding unstrengthened (control) beam.

Table 2. Comparison of analytical and experimental results.

Ref.	Beam name	Ameli and Ronagh [26]		Deifalla and Ghobarah [27]		Chalioris [28]		Zojaji and Kabir [29]		Ganganagoudar et al. [30]		Chai et al. [31]		Shen et al. [32]	
		$T_{cr,ANA.}/T_{cr,exp.}$	$T_{u,ANA.}/T_{u,exp.}$	$T_{cr,ANA.}/T_{cr,exp.}$	$T_{u,ANA.}/T_{u,exp.}$	$T_{cr,ANA.}/T_{cr,exp.}$	$T_{u,ANA.}/T_{u,exp.}$	$T_{cr,ANA.}/T_{cr,exp.}$	$T_{u,ANA.}/T_{u,exp.}$	$T_{cr,ANA.}/T_{cr,exp.}$	$T_{u,ANA.}/T_{u,exp.}$	$T_{cr,ANA.}/T_{cr,exp.}$	$T_{u,ANA.}/T_{u,exp.}$	$T_{cr,ANA.}/T_{cr,exp.}$	$T_{u,ANA.}/T_{u,exp.}$
[11]	Ra-FC(1)	--	--	--	--	0.83*	0.93*	--	--	--	--	--	--	--	--
	Ra-FC(2)	--	--	--	--	0.82*	0.83*	--	--	--	--	--	--	--	--
	Ra-FS150(2)	--	--	--	--	1.04*	1.06*	--	--	--	--	--	--	--	--
	RaS-FS150(2)	--	--	--	--	0.99*	1.02*	0.93	1.01	--	--	--	--	0.78	0.91
	Rb-FC(1)	--	--	--	--	0.82*	1.04*	--	--	--	--	--	--	--	--
	Rb-FS200(1)	--	--	--	--	1.06*	0.95*	--	--	--	--	--	--	--	--
	Rb-FS300(1)	--	--	--	--	1.03*	1.18*	--	--	--	--	--	--	--	--
	RbS-FS200(1)	--	--	--	--	1.04*	0.99*	1.03	1.3	--	--	--	--	--	--
[9]	CFE	--	0.83	--	--	0.99*	0.90*	1.09	0.85	1.00	0.84*	--	--	--	--
	CFE2	--	0.72	--	--	0.96*	0.83*	1.01	0.77	--	--	--	--	--	--
	CJE	--	--	--	--	0.97*	0.94*	--	--	--	--	--	--	--	--
	CFS	--	1.00	--	--	1.00*	1.02*	1.03	0.92	0.89	0.91	--	--	0.88	1.02
	CJS	--	--	--	--	1.01*	0.93*	--	--	--	--	--	--	--	--
	GFE	--	0.75	--	--	0.98*	0.93*	1.08	0.92	--	--	--	--	0.86	0.81
	GFE2	--	0.68	--	--	0.91*	0.95*	--	--	--	--	--	--	--	--
	GJE	--	--	--	--	0.93*	0.96*	--	--	--	--	--	--	--	--
	GFS	--	0.97	--	--	0.91*	1.01*	1.01	1.01	--	--	--	--	1.01	1.05
	GJS	--	--	--	--	0.96*	0.94*	--	--	--	--	--	--	--	--
[5]	A90W4	--	--	--	0.74	1.18*	0.99*	1.11	0.94	1.00	0.93*	--	--	--	--
	A90S4	--	--	--	1.13	1.23*	1.03*	1.05	1.01	0.95	0.96*	--	--	0.90	1.12
	C90U3	--	--	--	1.38	1.22*	1.18*	0.91	1.10	--	--	--	--	--	--
	B90U3-Anch	--	--	--	1.14	1.03*	1.16*	--	--	--	--	--	--	--	--
	A0L4	--	--	--	--	1.00*	1.01*	0.95	1.13	--	--	--	--	--	--
	A0L3	--	--	--	--	1.04*	1.04*	1.28	1.11	--	--	--	--	--	--
	B0L4/90S4	--	--	--	1.07	0.99*	1.04*	--	--	--	--	--	--	0.77	0.96
[4]	C1	--	0.92	--	1.11	0.92*	1.09*	1.26	1.05	--	--	--	--	1.41	1.20
	C2	--	1.13	--	1.41	1.12*	1.19*	1.37	1.14	--	--	--	--	--	--
	C4	--	--	--	1.03	0.94*	1.10*	1.16	1.00	--	--	--	--	--	--
	C5	--	--	--	1.48	1.05*	1.19*	1.29	1.17	--	--	--	--	--	--
	C6	--	--	--	1.15	--	--	--	--	--	--	--	--	--	--
	G1	--	0.81	--	1.22	0.86*	0.97*	1.03	1.06	--	--	--	--	--	--
	G2	--	1.12	--	1.56	0.98*	1.25*	1.21	1.21	--	--	--	--	--	--
[7] [8] [10]	FS050D2	--	--	--	--	1.04*	0.99*	0.91	0.94	--	--	--	--	0.99	1.03
	FH050D2	--	--	--	--	--	--	1.31	0.91	--	--	--	--	--	--

Table 2. Comparison of analytical and experimental results (continued).

[3]	L2	--	--	--	1.45	--	--	--	--	--	--	--	--	--	--
	L3	--	--	--	0.89	--	--	--	--	--	--	--	--	--	--
	L4	--	--	--	0.67	--	--	--	--	--	--	--	--	--	--
	L5	--	1.16	--	0.86	--	--	--	--	--	--	--	--	--	--
	L6	--	1.16	--	1.03	--	--	--	--	--	--	--	--	--	--
	L7	--	--	--	0.93	--	--	--	--	--	--	--	--	--	--
	L10	--	--	--	1.02	--	--	--	--	--	--	--	--	--	--
[31]	ST-S	--	--	--	--	--	--	--	--	--	--	--	0.95	--	--
	ST-T	--	--	--	--	--	--	--	--	--	--	--	0.99	--	--

* represents [1/ ($T_{exp.}$ /$T_{ANA.}$)] from the original reference.

Table 3. Comparison of FE and experimental results.

Ref.	Beam name	$T_{cr,FE.}/T_{cr,exp.}$	$T_{u,FE.}/T_{u,exp.}$
[8]	CS1	0.73	--
	CH1	1.31	--
	FH050D2	--	0.77
[9]	RC	--	0.98
	CFE	--	0.92
	CFE2	--	0.89
	CJE	--	0.99
	CFS	--	1.00
	CJS	--	1.04
	RG	--	0.96
	GFE	--	0.90
	GFE2	--	0.85
	GJE	--	0.98
	GFS	--	1.05
	GJS	--	1.05
[30]	A90W4	0.93*	0.83*
	A90S4	0.70*	0.62*
	CFE	1.00*	1.09*
	CFS	1.03*	0.88*
[36]	CR	--	0.93*
	WR1	--	0.82*
	WR2	--	0.90*
	CT	--	1.18*
	WT1(U-jacket)	--	0.91*
	WT2(Ex. U-jacket)	--	0.82*
[37]	Control	--	1.02
	N-P-4-S-1	--	1.11
	N-P-4-8S-1	--	1.18
	N-P-4-C-1	--	0.99
	N-P-4-(0/90)C-2	--	1.05
	N-P-4-C-2	--	0.94

* Value reported is [1/ ($T_{exp,}$ /T_{FE})] from the original reference.

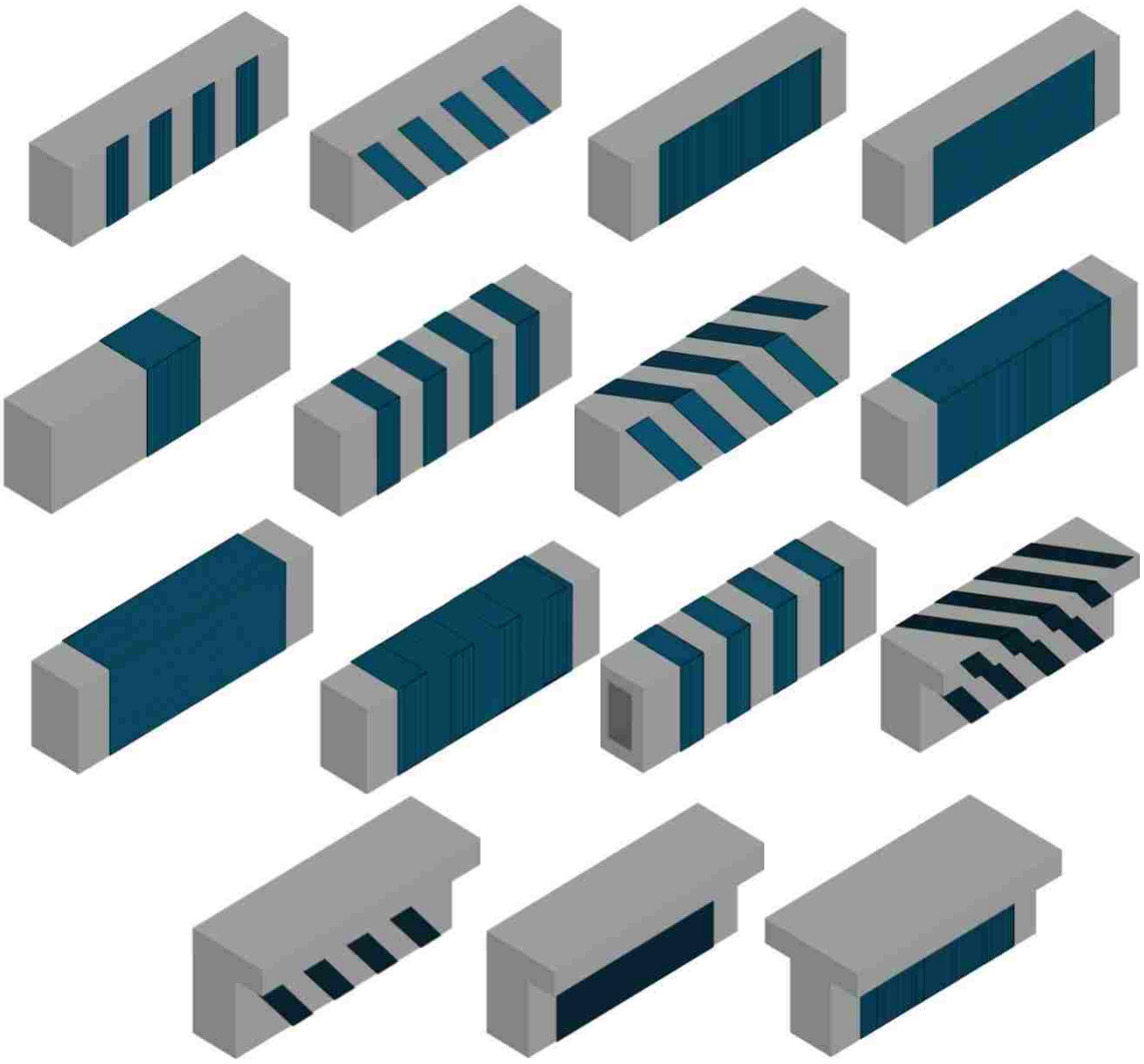

Figure 1. Wrapping configuration of strengthened beams.

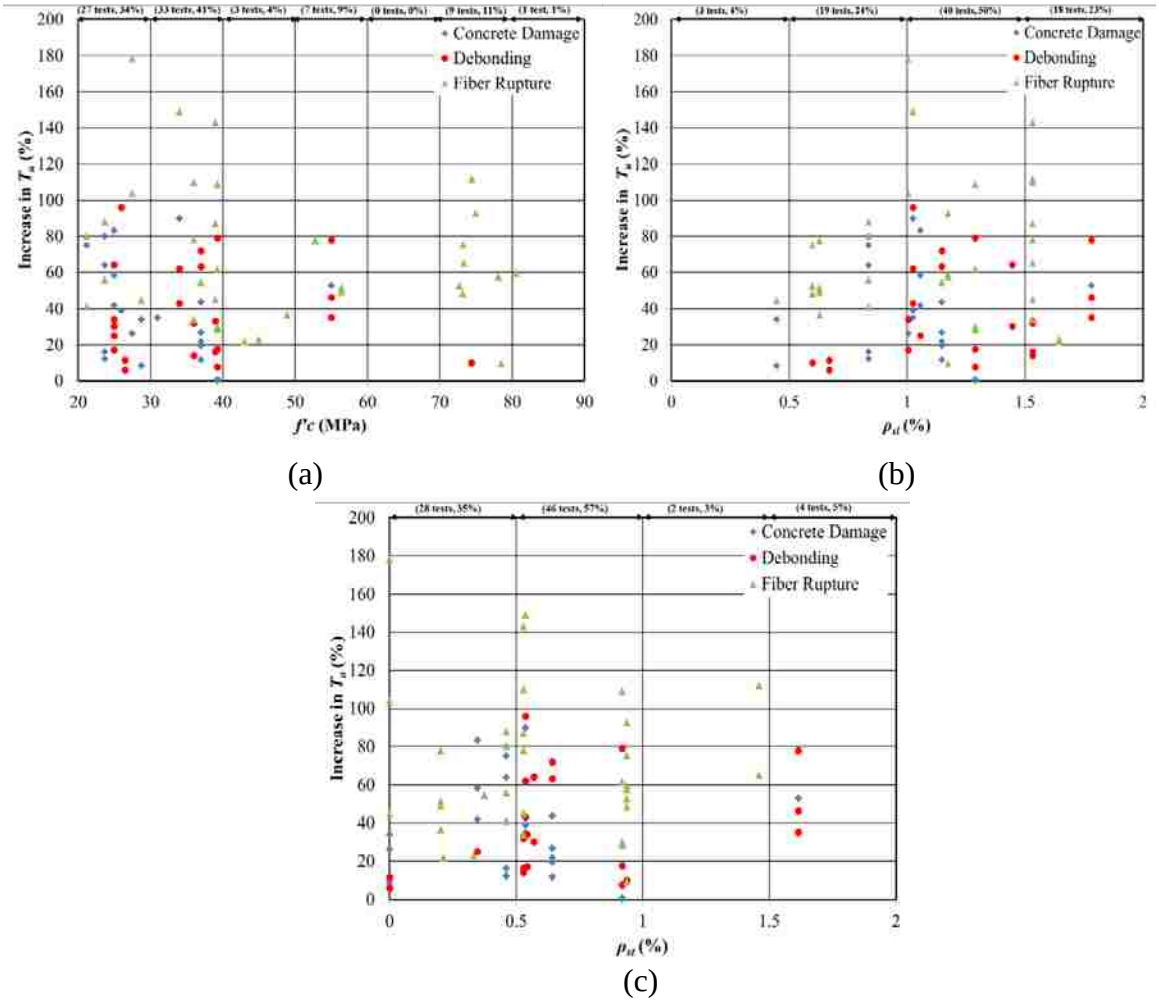

Figure 2. Increase in torsional strength T_u versus (a) f'_c, (b) ρ_{sl}, and (c) ρ_{st}.

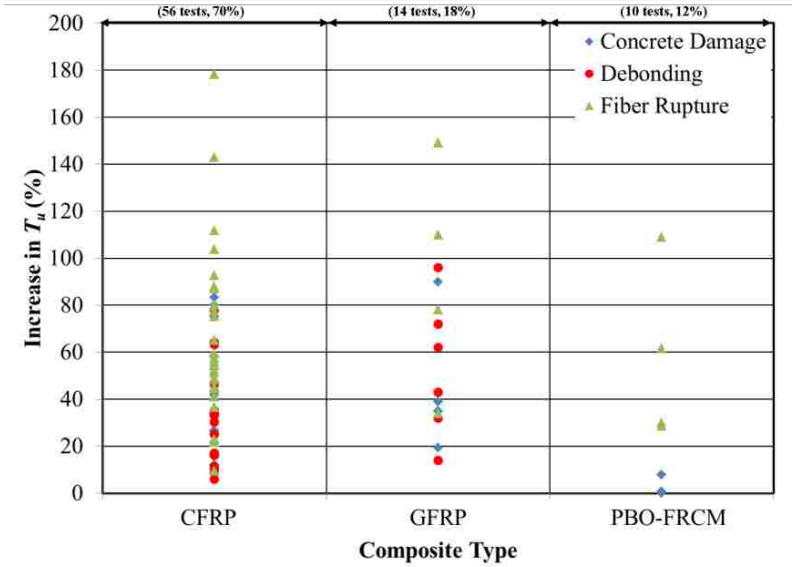

Figure 3. Increase in torsional strength T_u versus composite type.

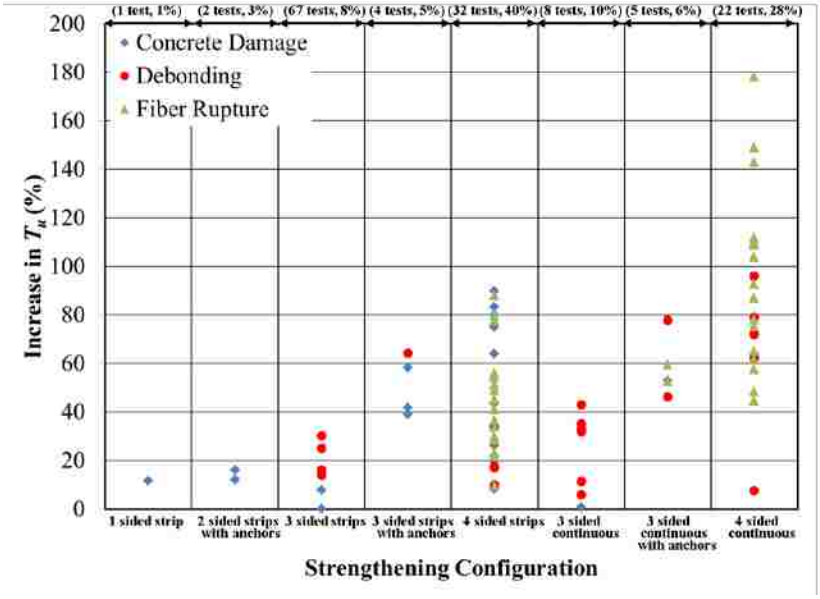

Figure 4. Increase in torsional strength T_u for different strengthening configurations.

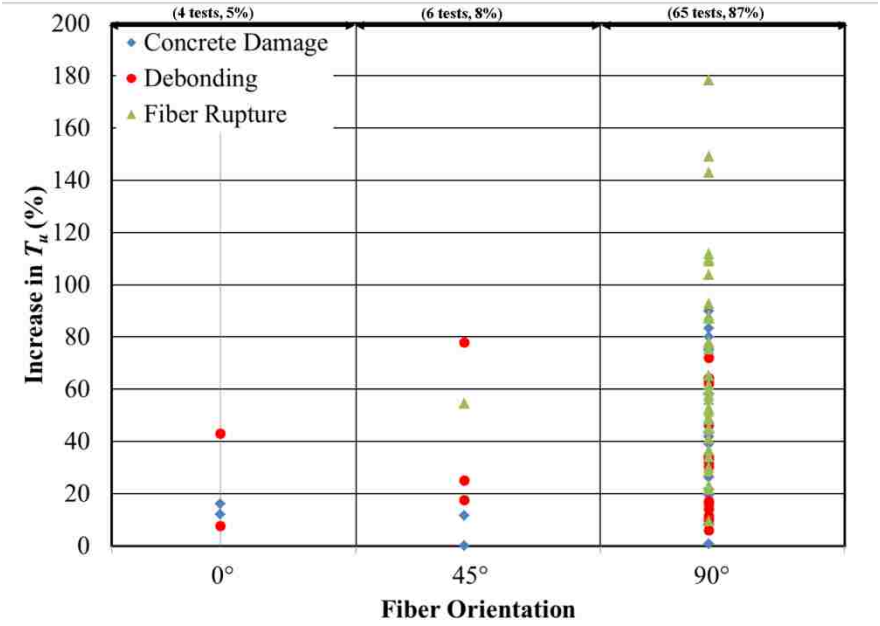

Figure 5. Increase in torsional strength T_u versus fiber orientation.

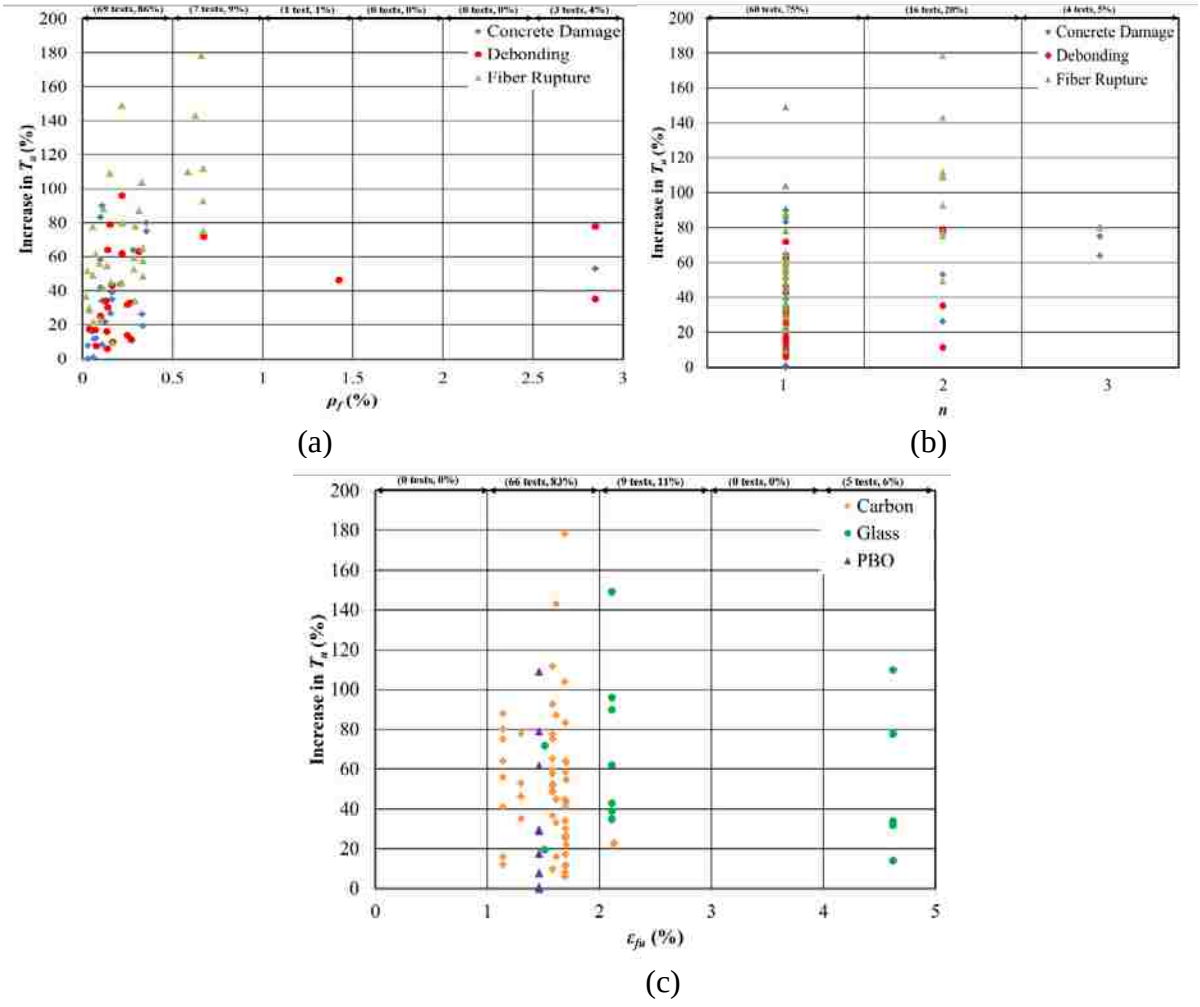

Figure 6. Increase in torsional strength T_u versus (a) ρ_f, (b) ε_{fu}, and (c) n.

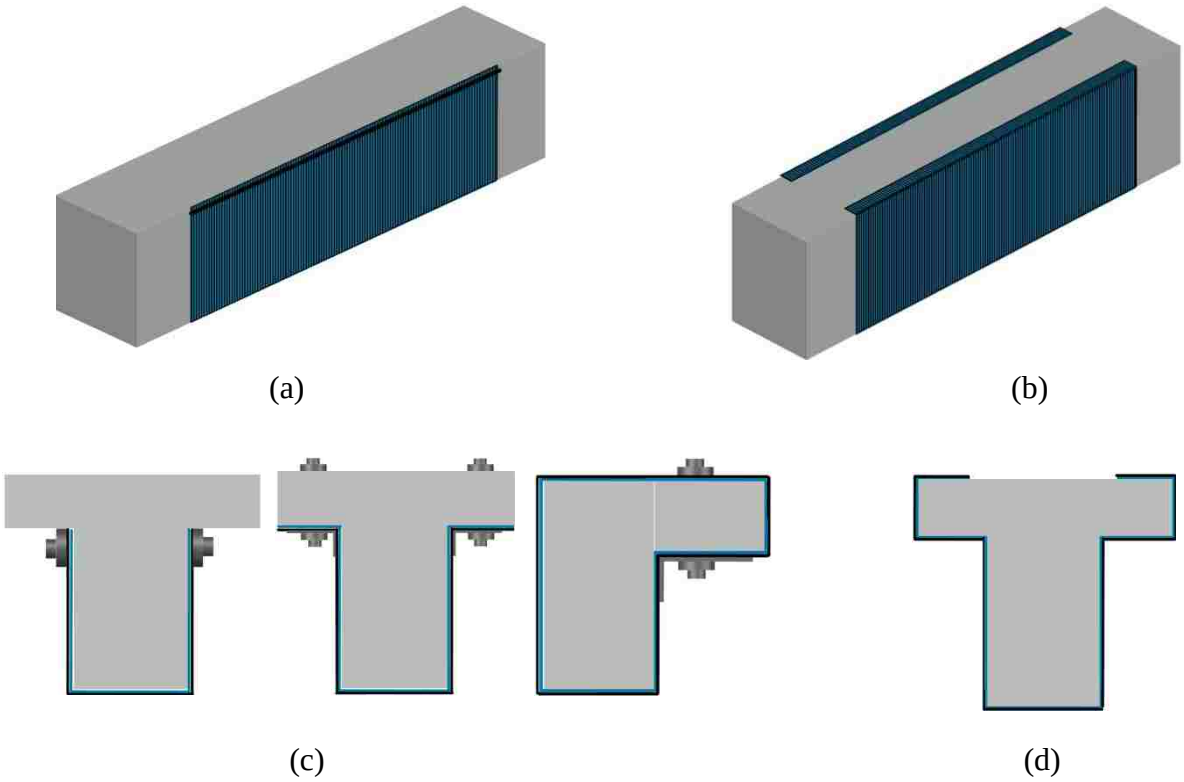

Figure 7. Anchorage system types (a) anchor bar, (b) composite fastened to the top of the beam for rectangular section, (c) steel angle, (d) extended u-jacket for T-section.

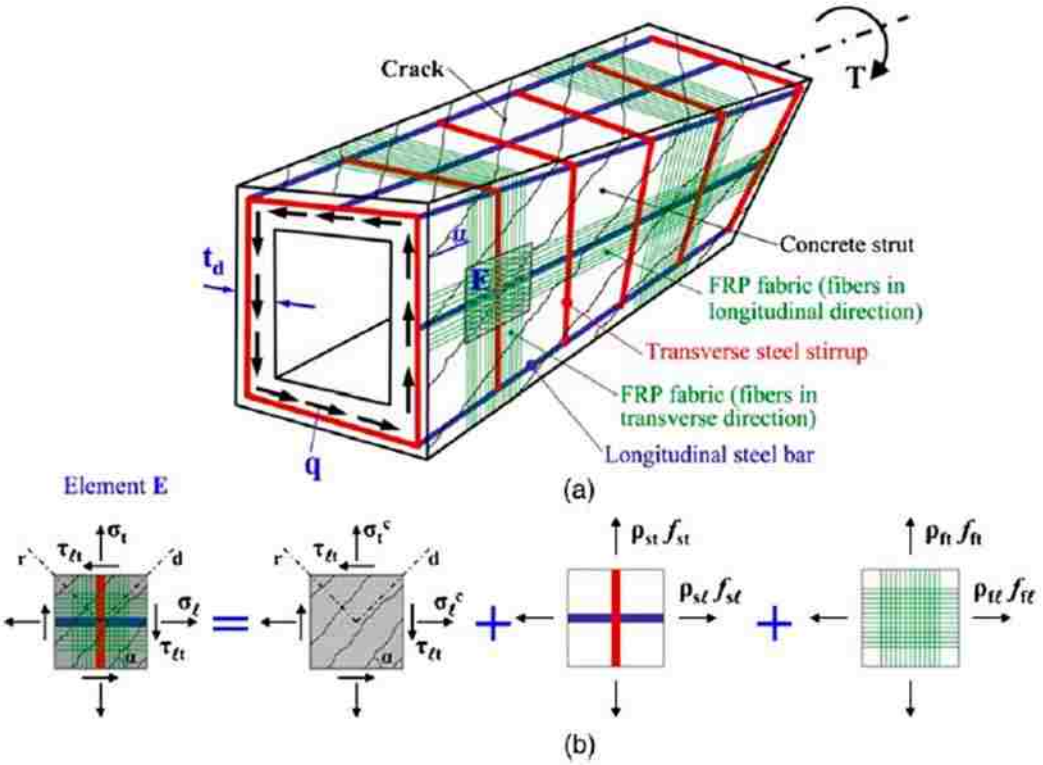

Figure 8. (a) Torsional deformation of a FRP strengthened RC beam, (b) in-plane stresses of an element taken from shear flow zone (adapted from [29]).

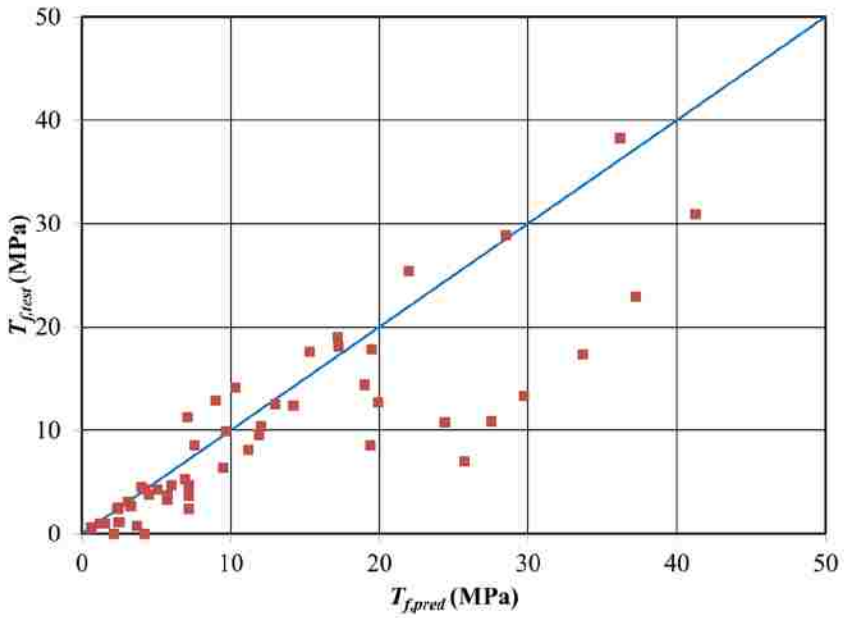

Figure 9. $T_{f,test}$ versus $T_{f,pred.}$

REFERENCES

[1] McCormac, J. C., & Brown, R. H. (2015). *Design of reinforced concrete*. John Wiley & Sons.

[2] Holman, J. W., & Cook, J. P. (1984). Steel plates for torsion repair of concrete beams. *Journal of Structural Engineering*, *110*(1), 10-18.

[3] Zhang, J. W., Lu, Z. T., & Zhu, H. (2001). Experimental study on the behaviour of RC torsional members externally bonded with CFRP. In *FRP Composites in Civil Engineering. Proceedings of the International Conference on FRP composites in Civil Engineering* (No. Volume 1).

[4] Ghobarah, A., Ghorbel, M. N., & Chidiac, S. E. (2002). Upgrading torsional resistance of reinforced concrete beams using fiber-reinforced polymer. *Journal of Composites for Construction*, *6*(4), 257-263.

[5] Panchacharam, S., & Belarbi, A. (2002). Torsional behavior of reinforced concrete beams strengthened with FRP composites. In *First FIB Congress, Osaka, Japan* (Vol. 1, pp. 01-110).

[6] Salom, P. R., Gergely, J., & Young, D. T. (2004). Torsional strengthening of spandrel beams with fiber-reinforced polymer laminates. *Journal of Composites for Construction*, *8*(2), 157-162.

[7] Hii, A. K., & Al-Mahaidi, R. (2006). Experimental investigation on torsional behavior of solid and box-section RC beams strengthened with CFRP using photogrammetry. *Journal of Composites for Construction*, *10*(4), 321-329.

[8] Hii, A. K., & Al-Mahaidi, R. (2006). An experimental and numerical investigation on torsional strengthening of solid and box-section RC beams using CFRP laminates. *Composite Structures*, *75*(1), 213-221.

[9] Ameli, M., Ronagh, H. R., & Dux, P. F. (2007). Behavior of FRP strengthened reinforced concrete beams under torsion. *Journal of Composites for Construction*, *11*(2), 192-200.

[10] Hii, A. K., & Al-Mahaidi, R. (2007). Torsional capacity of CFRP strengthened reinforced concrete beams. *Journal of Composites for Construction*, *11*(1), 71-80.

[11] Chalioris, C. E. (2008). Torsional strengthening of rectangular and flanged beams using carbon fibre-reinforced-polymers–Experimental study. *Construction and Building Materials*, *22*(1), 21-29.

[12] Mohammadizadeh, M. R., Fadaee, M. J., & Ronagh, H. R. (2009). Improving torsional behaviour of reinforced concrete beams strengthened with carbon fibre reinforced polymer composite. *Iranian Polymer Journal*, *18*(4), 315-327.

[13] Deifalla, A., Awad, A., & Elgarhy, M. (2013). Effectiveness of externally bonded CFRP strips for strengthening flanged beams under torsion: An experimental study. *Engineering Structures*, *56*, 2065-2075.

[14] Chai, H. K., Majeed, A. A., & Allawi, A. A. (2014). Torsional Analysis of Multicell Concrete Box Girders Strengthened with CFRP Using a Modified Softened Truss Model. *Journal of Bridge Engineering*, *20*(8), B4014001.

[15] Alabdulhady, M. Y., Sneed, L. H., & Carloni, C. (2017). Torsional behavior of RC beams strengthened with PBO-FRCM composite–An experimental study. *Engineering Structures*, *136*, 393-405.

[16] Alabdulhady, M. Y., & Sneed, L. H. (2018). A study of the effect of fiber orientation on the torsional behavior of RC beams strengthened with PBO-FRCM composite. *CONSTRUCTION AND BUILDING MATERIALS*, *166*(1), 839-854.

[17] Al-Bayati, G., Al-Mahaidi, R., & Kalfat, R. (2016). Experimental investigation into the use of NSM FRP to increase the torsional resistance of RC beams using epoxy resins and cement-based adhesives. *Construction and Building Materials*, *124*, 1153-1164.

[18] Al-Bayati, G., Al-Mahaidi, R., & Kalfat, R. (2017). Torsional strengthening of reinforced concrete beams using different configurations of NSM FRP with epoxy resins and cement-based adhesives. *Composite Structures*, *168*, 569-581.

[19] Al-Bayati, G., Al-Mahaidi, R., Hashemi, M. J., & Kalfat, R. (2018). Torsional strengthening of RC beams using NSM CFRP rope and innovative adhesives. *Composite Structures*, *187*, 190-202.

[20] ACI Committee 445. Report on torsion in structural concrete (ACI 445.1R-12). American Concrete Institute, Farmington Hills, MI, 2012, 92 pp.

[21] Pellegrino, C., & Modena, C. (2006). Fiber-reinforced polymer shear strengthening of reinforced concrete beams: Experimental study and analytical modeling. *ACI Structural Journal*, *103*(5), 720.

[22] Pellegrino, C., & Modena, C. (2008). An experimentally based analytical model for the shear capacity of FRP-strengthened reinforced concrete beams. *Mechanics of composite materials*, *44*(3), 231-244.

[23] Chen, J. F., & Teng, J. G. (2003). Shear capacity of FRP-strengthened RC beams: FRP debonding. *Construction and Building Materials*, *17*(1), 27-41.

[24] Gonzalez-Libreros, J. H., Sabau, C., Sneed, L. H., Pellegrino, C., & Sas, G. (2017). State of research on shear strengthening of RC beams with FRCM composites. *Construction and Building Materials*, *149*, 444-458.

[25] He, R., Sneed, L. H., & Belarbi, A. (2014). Torsional repair of severely damaged column using carbon fiber-reinforced polymer. *ACI Structural Journal*, *111*(3), 705.

[26] Ameli, M., & Ronagh, H. R. (2007). Analytical method for evaluating ultimate torque of FRP strengthened reinforced concrete beams. *Journal of Composites for construction*, *11*(4), 384-390.

[27] Deifalla, A., & Ghobarah, A. (2010). Full torsional behavior of RC beams wrapped with FRP: analytical model. *Journal of Composites for Construction*, *14*(3), 289-300.

[28] Chalioris, C. E. (2007). Analytical model for the torsional behavior of reinforced concrete beams retrofitted with FRP materials. *Engineering Structures*, *29*(12), 3263-3276.

[29] Zojaji, A. R., & Kabir, M. Z. (2012). Analytical approach for predicting full torsional behavior of reinforced concrete beams strengthened with FRP materials. *Scientia Iranica*, *19*(1), 51-63.

[30] Ganganagoudar, A., Mondal, T. G., & Prakash, S. S. (2016). Analytical and finite element studies on behavior of FRP strengthened RC beams under torsion. *Composite Structures*, *153*, 876-885.

[31] Chai, H. K., Majeed, A. A., & Allawi, A. A. (2014). Torsional Analysis of Multicell Concrete Box Girders Strengthened with CFRP Using a Modified Softened Truss Model. *Journal of Bridge Engineering*, *20*(8), B4014001.

[32] Shen, K., Wan, S., Mo, Y., & Jiang, Z. (2017). Theoretical analysis on full torsional behavior of RC beams strengthened with FRP materials. *Composite Structures*.

[33] Witte, F. C., & Kikstra, W. P. (2002). DIANA Finite Element Analysis, Release 8.1. *TNO Building and Construction Research, Delft, The Netherlands*.

[34] ANSYS Commands Reference, ANSYS, Inc. Southpointe, 275 Technology Drive, Canonsburg, PA 15317.

[35] ABAQUS Theory Manual 2002, ABAQUS Inc., USA.

[36] Elwan, S. K. (2016). Torsion strengthening of RC beams using CFRP (parametric study). *KSCE Journal of Civil Engineering*, 1-9.

[37] Alabdulhady, M. Y., Sneed, L. H., Abdelkarim, O. I., & ElGawady, M. A. (2017). Finite element study on the behavior of RC beams strengthened with PBO-FRCM composite under torsion. *Composite Structures*, *179*, 326-339.

[38] LS-DYNA 971 R3 [Computer software]. Livermore, CA, Livermore Software Technology.

[39] *fib* Bulletin 14 (2001). Externally bonded FRP reinforcement for RC structures. CEB-FIP, Lausanne, Switzerland, 2001, 130 pp.

[40] Zureick, A. H., Ellingwood, B. R., Nowak, A. S., Mertz, D. R., & Triantafillou, T. C. (2010). *Recommended guide specification for the design of externally bonded FRP systems for repair and strengthening of concrete bridge elements.* NCHRP Report 655. Transportation Research Board.

[41] ACI 318-14. Building code requirements for structural concrete (318-14) and commentary (318R-14). American Concrete Institute, Farmington Hills, MI, 2014, 519 pp.

II. TORSIONAL BEHAVIOR Of RC BEAMS STRENGTHENED WITH PBO-FRCM COMPOSITE – AN EXPERIMENTAL STUDY

Meyyada Y. Alabdulhady, Lesley H. Sneed, and Christian Carloni

ABSTRACT

The use of fiber reinforced cementitious matrix (FRCM) composites has been studied for flexural and shear strengthening of reinforced concrete (RC) members, but currently there are no studies on its use for torsional strengthening. This paper presents the results of an experimental study in which solid rectangular RC beams were externally strengthened with PBO-FRCM composite material in different wrapping configurations to investigate the torsional behavior in terms of strength, rotational ductility, and failure mode. Increases in the cracking torque, torsional strength, and corresponding values of twist were achieved by beams strengthened with a 4-sided wrapping configuration relative to the control (unstrengthened) beam. On the other hand, the 3-sided wrapping configuration was found to be largely ineffective in improving the torsional performance due to excessive fiber slippage. The contribution of the strengthening system to the torsional strength was reasonably predicted (+/- 20%) by the strain measured in the composite fibers. Provisions used to estimate the torsional strength of RC beams with fully-wrapped, externally-bonded fiber reinforced polymer (FRP) composites were found to be applicable to beams strengthened with PBO-FRCM composite.

HIGHLIGHTS

- RC beams were strengthened with PBO-FRCM composite and tested under torsion.
- Behavior was investigated in terms of strength, rotational ductility, failure mode.
- Strains measured in the internal and external reinforcement were evaluated.
- Analytical prediction was compared with the experimental results.
- Effectiveness of PBO-FRCM composite was compared with CFRP and GFRP composites.

KEYWORDS

Beams, fiber strain, PBO-FRCM composite, reinforced concrete, strengthening, torsion.

1. INTRODUCTION

In recent decades, repair and strengthening of reinforced concrete (RC) buildings and bridges have become increasingly common. Deficiencies in RC members may exist for several reasons, including changes in use of the structure, design and constructions errors, and degradation due to environmental conditions. RC members are commonly strengthened in flexure, shear, and/or confinement depending on the member loading conditions and type of enhancement needed. In some cases, RC members are subjected to significant torsional moments, and the torsional strength needs to be enhanced. Accordingly, methods and design provisions for strengthening RC members in torsion are needed.

Torsional behavior of RC beams strengthened with externally bonded fiber reinforced polymer (FRP) composites has been investigated since the early 2000s. Ghobarah et al. [1] investigated the behavior of RC beams with a rectangular cross-section strengthened with carbon FRP (CFRP) or glass FRP (GFRP) composite, and a simple design approach was also introduced. Panchacharam and Belarbi [2] studied the behavior of RC beams with a square cross-section strengthened with GFRP composite and proposed an analytical design equation. Salom et al. [3] tested RC beams with an L-shaped cross-section strengthened by CFRP composite to study the effectiveness of this technique on increasing the torsional strength of spandrel beams. Hii and Al-Mahaidi [4] used photogrammetry measurements to prove that externally bonded CFRP composite improves the torsional strength of RC beams by limiting crack width development and increasing aggregate interlock. Hii and Al-Mahaidi [5] investigated RC beams with solid and box sections that were strengthened in torsion with CFRP composite and compared the results with those obtained from the nonlinear finite element program DIANA. Chalioris [6] tested rectangular and T-shaped RC beams without internal transverse reinforcement and strengthened with CFRP composite in order to evaluate the contribution of the composite material to the torsional strength. Ameli et al. [7] investigated the behavior of rectangular RC beams strengthened with CFRP or GFRP composite and compared the results with those obtained from the nonlinear finite element program ANSYS. Deifalla et al. [8] tested rectangular, T-shaped, and L-shaped beams strengthened with CFRP composite to study the effectiveness of the strengthening technique on the torsional strength of beams with various cross-sections.

FRP composites have several attributes such as high strength and stiffness, light weight, resistance to corrosion, and flexibility of use that make it a suitable structural strengthening material. On the other hand, disadvantages of FRP composites include difficulty to install on wet surfaces or in low temperatures, low fire resistance, low glass transition temperature, and lack of vapor permeability, which are associated with the use of organic matrix. Recently a new type of composite called fiber reinforced cementitious matrix (FRCM) composite has been developed to overcome or reduce some of the shortcomings associated with FRP composites. In contrast to organic matrix, inorganic cementitious matrix can be applied in low temperatures and on wet surfaces, allows vapor permeability, and has better heat resistance. Different types of fibers have been used in FRCM composites systems such as carbon, glass, aramid, basalt, steel, and polyparaphenylene benzobisoxazole (PBO). The use of FRCM composites has been studied for flexural [9-11] and shear strengthening [12-15] of RC members and confinement of axially/eccentrically loaded elements [16-17], but currently there are no studies in the technical literature on its use for torsional strengthening.

The tensile force in an externally bonded composite strengthening system is transferred to the substrate through the fiber-matrix and matrix-concrete interfaces through shear. Recent studies on the fundamental bond behavior of PBO FRCM-concrete joints [18-26] indicate that the debonding failure mode is quite different from that of FRP-concrete joints. For FRP-concrete joints, failure occurs in a quasi-brittle manner within a thin mortar-rich layer of the concrete substrate, whereas with PBO FRCM-concrete joints failure occurs at the fiber-matrix interface with significant fiber slippage relative to the matrix. This difference in failure mode warrants investigation of the

fundamental torsional behavior of RC members strengthened with PBO-FRCM composites to examine the potential differences with respect to RC members strengthened with FRP composites.

The aim of this study is to investigate the torsional behavior of RC beams externally strengthened with PBO-FRCM composite in terms of torsional strength, rotational ductility, and failure mode. In this paper, the experimental results of four solid rectangular RC beams externally strengthened with PBO-FRCM composite material in different wrapping configurations are presented and compared with those of an unstrengthened control beam. The torque-twist load response and strains measured in the internal and external reinforcement are evaluated, and the applicability of design provisions for torsional strengthening using FRP composite is examined.

2. EXPERIMENTAL PROGRAM

2.1 EXPERIMENTAL DESIGN

A total of five RC beams were included in the experimental program. The beams were designed based on the ACI 318 code [27] provisions. All beams had a rectangular cross-section with the same nominal dimensions of b = 8 in. (203.2 mm) wide × h = 12 in. (304.8 mm) tall × 84 in. (2133.6 mm) long and the same internal reinforcement. Dimensions and details of the RC beams are shown in Figure 1. The beams had a test region in which the composite was applied of 60 in. (1524.0 mm) long that was reinforced with minimum torsional reinforcement in transverse direction in accordance with the ACI 318 code [27]. The volumetric reinforcement ratios of the longitudinal and transverse reinforcement were $\rho_{sl} = A_{sl}/A_c = 1.29\%$ and $\rho_{st} = \frac{A_{st}}{A_c}\frac{p_t}{s} = 0.92\%$,

respectively, where A_{sl} is the total area of longitudinal bars, A_c is the gross concrete area (A_c=bh), A_{st} is area of one leg of a stirrup, p_t is perimeter of a stirrup, and s is the center to center spacing of stirrups. The end regions of the beam (12 in. [304.8 mm] long each end) were more heavily reinforced to prevent failure in the clamp regions.

Reinforcing bars in the beam specimens were No. 3 (dia. = 9.5 mm, area = 71 mm^2) and No. 5 (dia. = 15.9 mm, area = 199 mm^2) ASTM A615 Grade 60 (Grade 420) deformed steel bars [28]. All reinforcing bars of the same size were from the same heat. Tension tests were conducted on three samples of each bar size to determine the mechanical properties. Table 1 shows the properties of the longitudinal and transverse reinforcement, which were determined based on the average of three coupon samples for each size tested according to ASTM A370 [29].

All beams were constructed at the same time with normalweight concrete without admixtures. The coarse aggregate type was crushed dolomite with 1 in. (25.4 mm) maximum aggregate size, and the fine aggregate was river sand. The compressive strength, splitting tensile strength, and modulus of elasticity of concrete were determined based on the average of three 4 in. (101.6 mm) diameter × 8 in. (203.2 mm) long cylinders tested at 28 days in accordance with ASTM C39 [30], ASTM C496 [31], and ASTM C469 [32], respectively. The concrete properties are listed in Table 1. The beams and cylinders were moist cured for four days under wet burlap then kept together in the laboratory under the same atmospheric conditions until testing.

2.2 FRCM COMPOSITE MATERIAL

The FRCM composite was comprised of PBO fibers with an inorganic matrix [33]. The PBO fibers were in the form of an unbalanced fiber net as shown in Figure 2. The net is formed with rovings spaced at 0.4 in. (10 mm) and 0.8 in. (20 mm) on center in the longitudinal and transversal directions, and the free spacing between rovings is 0.2 in. (5 mm) and 0.6 in. (15 mm), respectively. The nominal thicknesses (which is obtained by assuming the fibers are distributed evenly over the entire width of the composite) in the two fiber directions are 0.0018 in. (0.046 mm) and 0.0005 in. (0.012 mm), respectively. The total weight of PBO fibers in the mesh is 0.00013 lb/in^2 (88 g/m^2), with 0.00010 lb/in^2 (70.4 g/m^2) in the longitudinal direction and 0.000025 lb/in^2 (17.6 g/m^2) in the transversal direction.

The FRCM material properties are listed in Table 2. Tensile strength, ultimate strain, and elastic modulus of the fibers determined from tensile tests of the bare fibers were 440 ksi (3015 MPa), 0.0145, and 29,900 ksi (206 GPa), respectively [21], [23]. Mortar compressive and splitting tensile strength properties were determined from of a representative sample of matrix used to cast the FRCM composite using the average of three 2 in. (50.8 mm) diameter × 4 in. (101.6 mm) long cylinders tested at 28 days in accordance with ASTM C39 [30] and ASTM C496 [31], respectively.

2.3 FRCM COMPOSITE INSTALLATION AND WRAPPING SCHEMES

The corners of the RC beams were chamfered with a radius of 0.75 in. (19 mm) in order to reduce stress concentrations at the corners, which have been reported to lead to fiber rupture and failure of beams strengthened in torsion with FRP composites [34]. The

PBO-FRCM composite material was installed on the beams after the beams were 28 days old. The strengthening process is summarized as follows:

- The surface of the beam was sandblasted to achieve a target profile of 0.1 in. (2 mm).
- The surface of the beam was cleaned of dust and dirt.
- The surface of the beam was saturated with water before applying the first layer of matrix.
- In order to control the location and total thickness of the composite, foam strips of 0.2 in. (5 mm) thickness were mounted to the beam as shown in Figure 3.
- The first layer of cementitious matrix was applied in a layer that was approximately 0.1 in. (3 mm) thick.
- Pre-cut fibers were applied to the fresh cementitious matrix and pressed gently to ensure proper alignment and placement.
- The second 0.1 in. (2 mm) thick layer of cementitious matrix was applied to cover the fibers. The thickness of the external matrix layer was slightly less than the recommended thickness, however previous results indicate that the contribution of the external matrix layer to the load carrying capacity of the interface is much less significant than that of the internal matrix layer [35]. The total thickness of the composite was 0.2 in. (5 mm).
- For the specimen strengthened with two layers of fibers, the additional layer of fibers was pressed gently into the second layer of the fresh matrix then covered with an additional layer of cementitious matrix. The total thickness of the composite was approximately 0.4 in. (10 mm).

Four beams were strengthened, and one beam was unstrengthened for use as the control. Different wrapping schemes were used to study the torsional behavior of RC beams strengthened with the different configurations. The wrapping schemes are shown in Figure 4. One beam was strengthened with a 3-sided configuration in form of strips that were 4 in. (101.6 mm) wide with 4 in. (101.6 mm) clear spacing between strips (Figure 4b). The 3-sided configuration was investigated because in certain cases, the complete perimeter of the beam may not be accessible for strengthening, as in the case of a T-beam in monolithic construction. Three other beams were strengthened with a 4-sided configuration (i.e., fully wrapped) with one layer of strips that were 4 in. (101.6 mm) wide with 4 in. (101.6 mm) clear spacing between strips (Figure 4c), or with one or two layers continuous along the test region (Figure 4d and e). In each case, the fiber net was orientated such that the longitudinal fiber direction (Figure 2) was perpendicular to the longitudinal axis of the beam. An 8 in. (203.2 mm) overlap, corresponding to the beam width, was used for the beams that were wrapped with a 4-sided configuration. This length was slightly less than the effective bond length of the composite, defined as the minimum length needed to develop the load-carrying capacity of the interface [22], which has been shown to be approximately 10 in. (260 mm) [22].

2.4 TEST SETUP, INSTRUMENTATION, AND LOADING PROTOCOL

The test setup is shown in Figure 5. A similar test setup was previously used in the study by Panchacharam and Belarbi [2]. The torque was applied to the beam through the loading arm with an 18 in. (457 mm) eccentricity relative to the centroid of the cross-section by a hydraulic jack of 30 k (130 kN) capacity and measured by a load cell of 100

k (445 kN) capacity. The reaction arm was supported by a threaded rod that was anchored to the reaction floor. The reaction end of the beam was allowed to slide freely in the longitudinal direction to avoid axial restraint on the beam and allow the concrete cracks to open. Secondary bending effects due to self weight and to application of the load were neglected. Restraint of warping due to the clamping effects at each end was also neglected.

The average angle of twist per unit length was measured by a rotational variable differential transformer (RVDT) mounted along the east face of the beam within the test region with gage length of 45.5 in. (1155.7 mm). On the west face of the beam, the twist was determined by measuring the relative vertical displacements using two linear variable differential transformers (LVDTs) with a spacing similar to the RVDT gage length in order to verify the RVDT readings. Three additional LVDTs with inclinations of 0°, 45°, and 135° in the counterclockwise direction from the longitudinal axis of the beam in the form of rosette were used to measure the average longitudinal strain, diagonal compressive strain, and diagonal tensile strain, respectively, on the surface of the beam. Another LVDT was placed at the reaction end of the beam at the center of the cross-section to measure the deformation of the beam in the longitudinal direction. The RVDT and LVDTs are shown in Figure 6.

In order to measure the strain in the steel reinforcement, a total of 17 strain gages were mounted to the longitudinal (9) and transverse (8) bars at the middle, quarter, and third quarter of the test region. To measure the strain in the FRCM fibers, a total of 27 or 36 strain gages were used on specimens with the 3-sided or 4-sided wrapping configurations, respectively. The surface of the matrix was carefully abraded at the

location of each strain gage in order to expose the fibers as shown in Figure 7, and then the strain gages were mounted onto the fibers. The locations of the strain gages are shown in Figure 8.

The beams were tested under monotonically increasing loading resulting in torque moment T until one of the following conditions occurred: 1) after the peak torque, referred to herein as the torsional strength T_u, a significant drop in torque occurred, or 2) the maximum twist capacity of the test setup was reached. The loading was first controlled by slowly increasing the force, and then once the torsional strength was reached, the loading was controlled by slowly increasing the displacement. Electronic data collected from the instrumentation were recorded using a data acquisition system. The loading was temporarily paused at different times to mark cracks on the surface of the beam, document the damage, and take photographs.

3. EXPERIMENTAL RESULTS

3.1 GENERAL BEHAVIOR AND FAILURE MODE

The failure mode of each tested beam is shown in Figure 9. The control beam exhibited typical RC torsional behavior with spiral diagonal cracks around the cross-section in a continuous form. Two complete spiral cracks were created with a major crack angle of approximately 45° with respect to the longitudinal axis of the beam. Crushing of the concrete strut at the middle of the test region controlled the failure.

The behavior and failure mode of beam N-P-3-S-1 with a 3-sided wrapping configuration were similar to those of the control beam except the location of failure was near beam restrained end, and failure was followed by concrete cover spalling with the

composite strips still attached (Figure 9b). Excessively wide concrete cracks, oriented approximately 45° with respect to the longitudinal axis of the beam, were concentrated on the beam face without the composite near the end of the beam (Figure 9b). At the discontinuous ends of the composite, the fibers were observed to progress into the matrix indicating slippage of the fibers relative to the matrix. Whereas 3-sided unanchored wrapping configurations with FRP composite have shown to provide some improvement to the torsional performance of RC beams [3], the ineffectiveness of the 3-sided PBO-FRCM composite can be explained by the fact that PBO FRCM-concrete joints exhibit significant fiber slippage in the formation of the bond mechanism [22] that is much larger than that exhibited by FRP-composite joints (i.e., approximately 10 times). This fiber slippage is not restrained in the case of a 3-sided wrapping configuration without sufficient anchorage. Furthermore, the effective bond length of the PBO-FRCM composite used in this study was found to be approximately 10 in. (260 mm) [22], corresponding to approximately 85% of the beam height. Therefore, depending on the location of the torsional crack, the composite may not be able to develop the full stress transfer on the side faces of the beam.

Beams that were strengthened with PBO-FRCM composite with a 4-sided wrapping configuration exhibited hairline cracks on the surface of the composite that increased in number and width with increasing load and twist (see Figures 9c, d, and e). Cracks were oriented approximately 45° with respect to the longitudinal axis of the beam. Localized areas of slip between fibers and matrix were noted in the vicinity of the concrete cracks as a result of the deformation compatibility requirement between the composite and concrete. Fiber slippage was observed to increase with increasing twist,

however no measurements of fiber slippage were taken in this study. Failure was due to fiber rupture followed by crushing of the concrete struts after loss of confinement at midspan and near the reaction end for beams N-P-4-S-1 and N-P-4-C-1, respectively, while for beam N-P-4-C-2, failure occurred along the entire beam length.

The contribution of the composite to the torsional response is dependent upon the bond characteristics between the composite and the concrete. Direct-shear tests of PBO FRCM-concrete joints indicate that debonding occurs at the matrix-fiber interface with significant slippage of the fibers [22], [23]. For torsional strengthening using a 4-sided wrapping configuration, however, failure does not occur immediately after localized debonding due to the continuity of the hoop, where support to each face is provided by the adjacent faces [34]. On the other hand, since the length of the overlap provided in this study was slightly less than the effective bond length, debonding (fiber slippage relative to the embedding matrix) may have occurred at relatively large fiber strains. Such slippage around a corner and the resulting friction (interlocking) that occurs between fibers and the embedding matrix could potentially result in premature fiber rupture. For this reason, future studies should consider providing a longer overlap region on the order of the effective bond length of the composite.

After testing was completed, the FRCM composite was removed from beam N-P-4-C-2 to observe the damage in the concrete as shown in Figure 10. Numerous concrete cracks were distributed along the entire length of the beam, which suggests that the confinement helped distribute the stresses along the entire test region.

3.2 TORQUE-TWIST RESPONSE

The applied torque T versus twist per unit length ψ response for all beams is shown in Figure 11. With the exception of beam N-P-3-S-1, values of ψ in Figure 11 correspond to those measured by the RVDT. Values of ψ for beam N-P-3-S-1 were determined with the LVDTs since the RVDT detached after the peak load was reached. For all beams (with the exception of beam N-P-3-S-1), values of ψ determined with the RVDT were consistent with values computed from the LVDTs at the same load level. Drops in the response associated with pauses to mark cracks have been removed from the graph.

The overall behavior shown in Figure 11 indicates that the FRCM composite provided an increase in the torsional strength and twist at the peak load. In general, a linear behavior before cracking with high torsional stiffness was observed for each strengthened beam, then the beam suffered an increase in the twist angle without increasing of torque due to redistribution of forces from the concrete to the steel reinforcement. After this stage and before achieving the peak load, the behavior became non-linear with a reduction in torsional stiffness. The strengthened beams exhibited ductile behavior in the post-cracking stage due to yielding of the steel reinforcement and possibly slippage of the fibers in the composite.

The torque associated with cracking T_{cr} and the peak load (i.e., the torsional strength T_u), along with the corresponding angles of twist per unit length ψ_{cr}, and ψ_u, respectively, are summarized in Table 3. For the strengthened beams, Table 3 also reports the ratio of T_{cr}, T_u , ψ_{cr}, and ψ_u to the corresponding values from the control beam. The most effective wrapping scheme was that of beam N-P-4-C-2, with two layers of fully

wrapped composite, which achieved 2.09 and 2.84 times the torsional strength and corresponding angle of twist relative to the control beam, respectively. The least effective wrapping scheme was that of beam N-P-3-S-1, which had 3-sided strips, with values close to those of the control beam.

For beams with a 4-sided wrapping configuration (beams N-P-4-S-1, N-P-4-C-1, and N-P-4-C-2), Figure 11 and Table 3 show that the PBO-FRCM composite enhanced the beam stiffness by reducing ψ_{cr}, which was due to arresting the concrete cracks, and increased the cracking torque T_{cr} up to 1.40 times that of the control beam by providing an effective confinement. All three beams had a significantly higher energy absorption capability [2] (as indicated by the area under the T-ψ curve) than the control beam. Comparing the load response of beams N-P-4-S-1 and N-P-4-C-1, each of which had one layer of fibers, it can be seen that the continuous fibers were more effective in increasing the cracking torque T_{cr}, post cracking stiffness, and torsional strength T_u than the strips, which is due to the continuous confinement provided along the length. As noted by Panchacharam and Belarbi [2], strip width and spacing influences the confinement, thus affecting the post-cracking behavior.

Comparing beams N-P-4-C-1 and N-P-4-C-2, both of which had continuous fibers along the length, it can be seen that two layers of FRCM composite enhanced the post-cracking stiffness and torsional strength more effectively than one layer of composite. The increase in torsional strength was not directly proportional to the number of fiber layers (further discussion is provided in Section 5).

For the beam with a 3-sided wrapping configuration (beam N-P-3-S-1), the FRCM composite strips had a slight effect on the torsional load relative to that of the

control beam, corresponding to 11.4% and 7.4% increase in the cracking torque and torsional strength, respectively, with no increase in the twist angle at the torsional strength. Figure 11 also shows that the stiffness reduced rapidly after the peak load, which was due to the progression of concrete cracking and crushing on the face without the composite. Despite the lack of continuity of fibers around the perimeter of the member, research findings suggest that 3-sided wrapping configurations help improve the torsional strength and performance by restraining the concrete cracks [3]. This may help explain the slight increase in torsional performance of beam N-P-3-S-1 relative to that of the control beam. On the other hand, comparing beams N-P-3-S-1 and N-P-4-S-1 it can be seen that the 3-sided wrapping configuration is clearly less effective than the 4-sided configuration because of the discontinuity of the fibers around the beam perimeter. It is worth mentioning that with FRP composites, certain types of mechanical anchorage have been used to anchor the FRP to improve the contribution to the torsional resistance [2], since those types of anchorage restrain the peeling effect at the discontinuous ends of FRP composites [36]. With FRCM composites, on the other hand, it is questionable whether such anchorage would restrain the fiber slippage that characterizes debonding of PBO-FRCM composites. Future work on anchorage of FRCM composites is needed to explore this issue.

3.3 INTERNAL AND EXTERNAL REINFORCEMENT STRAINS

Strains measured in the internal and external reinforcement varied along the length of the beam due to the position of the strain gages relative to the torsional cracks in the concrete and the composite matrix. Strains measured in the fibers of beams N-P-4-

C-1 and N-P-4-C-2, with 4-sided continuous wrapping configuration, were relatively uniform along and around the beam. For beam N-P-4-S-1, with 4-sided strips, strains were relatively localized in the vicinity of torsional cracks and were not spread uniformly along the beam length.

The applied torque versus strain measured in the stirrups ε_t, longitudinal bars ε_l, and externally bonded composite fibers in the primary fiber direction (transversal direction of the beam) ε_f is shown in Figure 12 for each beam, in which the values of strain are from the strain gages that recorded the maximum corresponding values. Strain measurements are plotted until the end of the test or until the strain gage malfunctioned. Values of the yield strain of the stirrups ε_{ty} and longitudinal bars ε_{ly} determined from the tensile tests are also indicated in the graphs. Figure 12 shows that the strain in each type of reinforcement was small until concrete cracking occurred, then the strain increased rapidly after that point. The FRCM composite started to contribute to the torsional resistance once torsional cracks in the concrete formed and propagated.

The maximum strains measured in the internal reinforcement (transverse and longitudinal reinforcing steel bars) and external reinforcement (FRCM composite) at different load stages are summarized in Table 4. For the strengthened beams with a 4-sided wrapping configuration, values of strain in the stirrups at the torque moment corresponding to the torsional strength of the control beam (T=148.7 k-in. [16.8 kN-m]) were significantly lower than those in the control beam. Also, values of strain in the longitudinal reinforcement were slightly lower than those in the control beam at torque T=148.7 k-in. (16.8 kN-m). At the torsional strength of each strengthened beam, the strains in the stirrups were close to those of the control beam at its torsional strength. On

the other hand, strains measured in the longitudinal bars of the strengthened beams were much larger than those of the control beam. Therefore, it is reasonable to assume that only the primary fibers (hoop direction) contributed to the increase in torsional strength. This observation supports the design concept of using the primary fibers as the main contributor to increase beam torsional strength, as discussed further in Section 4.

4. ANALYSIS

The torsional strength of an RC member strengthened with externally bonded composite T_n can be estimated by adding the contributions of the (unstrengthened) RC member T_{RC} and the externally bonded composite strengthening system T_f as shown in Eq. (1) [37-39]. This approach assumes there is no interaction between the RC member and the externally bonded composite system and has been used to determine the contribution of FRP composite to the torsional strength of RC members [40].

$$T_n = T_{RC} + T_f \tag{1}$$

In this analysis, T_{RC} was taken as the torsional strength T_u of the control beam (148.7 k-in. [16.8 kN-m]). From Eq. (1), the contribution of the externally bonded composite to each of the strengthened beams in this study was determined by subtracting T_{RC} from the torsional strength and is reported as $T_{f,Exp}$ in Table 5.

For RC members strengthened with FRP composite, the contribution of the externally bonded composite strengthening system T_f has been estimated assuming that the externally bonded composite behaves similarly to internal stirrups, and considering the strain in the composite [37], [38], and [39]. The applicability of this model is herein explored for the case of FRCM-strengthened elements. From the *fib* provisions for FRP-

strengthened elements [38], T_f can be computed using Eq. (2) for members that are fully wrapped:

$$T_f = 2.\varepsilon_{fe}.E_f.b.h.\frac{t_f.b_f}{s_f}cot(\theta) \quad (2)$$

where ε_{fe} is the effective strain in the composite, E_f is the modulus of elasticity of the composite, t_f is the thickness of the composite, b_f is the width of the composite sheets, s_f is the center-to-center spacing of the applied composite sheets, b is the width of the cross-section, h is the height of the cross-section, and θ is the angle of diagonal crack with respect to the longitudinal axis of the member (usually assumed as 45 deg. for pure torsion). The effective strain ε_{fe} is the strain in the fiber direction along the crack when the member reaches its torsional strength, which can be used to determine the force in the composite at failure of the member. It should be noted that partial safety factors and reduction factors in the *fib* provisions [38] have been omitted from Eq. (2).

Using Eq. (2), the contribution of the FRCM composite to each of the strengthened beams with a 4-sided wrapping configuration was computed considering the maximum measured strain in the fibers corresponding to the torsional strength (Table 4) as the effective strain ε_{fe}, and values are reported as $T_{f,An}$ in Table 5. The term E_f was taken as the value corresponding to the fibers, and t_f was taken as the nominal thickness of the fibers in the primary fiber direction (discussed in Section 2.2). Values of $T_{f,An}$ are in reasonable agreement with those of $T_{f,Exp}$, within +/- 20%, which shows that this approach is applicable for the case of FRCM-strengthened elements.

It is worth noting that the design value of the effective strain in the fibers is determined in different ways in different design provisions. The *fib* provisions for FRP-

strengthened elements suggest that the design value of ε_{fe} is a function of the fiber material properties, reinforcement ratio, concrete material properties, and failure mode [38]. However, previous studies from the literature [41] have shown that for the case of PBO-FRCM composites, concrete strength may not significantly influence the load-carrying capacity of the FRCM-concrete interface. Therefore the *fib* approach to compute the effective strain may not be appropriate for FRCM composites. NCHRP provisions for the design of FRP-strengthened elements specify that the effective strain be limited to a maximum value of 0.004 to preclude the loss of aggregate interlock or delamination of the composite from the substrate [39]. Results from this study, including values of strain in the fibers at the torsional strength (Table 4), show that the limiting value of the effective strain of 0.004 [39] may also be appropriate for the design of torsional strengthening with PBO-FRCM composite for beams that are strengthened with a 4-sided wrapping configuration.

5. COMPARISON WITH OTHER COMPOSITES

In this section, the effectiveness of PBO-FRCM composite with different wrapping schemes is evaluated and compared with that of other composites. In Figure 13 the increase in torsional strength T_u for each of the beams relative to the unstrengthened beam is plotted versus the volumetric ratio of fibers ρ_f, computed using Eq. (3):

$$\rho_f = \frac{n_f.t_f.p_f}{A_c}\frac{b_f}{s_f} \tag{3}$$

where p_f is the wrapped perimeter of the beam, n_f is the number of composite layers, and the other variables were defined previously. Results in Figure 13 are supplemented with

those by Ameli et al. [7], who tested solid rectangular RC beams strengthened with CFRP or GFRP composite. The beams selected for the comparison had the same wrapping configurations as those in this study (3- or 4-sided wrapping configuration, with strips or continuous sheets), and the results are summarized in Table 6. Beams with 3- and 4-sided wrapping configurations are distinguished by different marker types in the figure. Values of ρ_f in Figure 13 are shown in units of t_f/A_c to compare beams of different cross-sections and different fiber thicknesses.

For all three series, the lowest value of ρ_f in Figure 13 corresponds to a 3-sided wrapping configuration with strips, and the remaining values correspond to a 4-sided wrapping configuration with either strips or continuous fiber sheets. In the case of the 3-sided wrapping configuration, the increase in torsional strength is relatively low for all three composite types due to the non-closed form of the strengthening material. It is likely that the increase in torsional strength for the PBO-FRCM composite was even lower than that of CFRP or GFRP composite because of fiber slippage that occurs with PBO-FRCM composites. For beams with a 4-sided wrapping configuration, Figure 13 shows that the torsional strength increased with the value of ρ_f for each composite type.

Certainly, the efficiency of the strengthening system depends on its material properties, which differ for the three composite materials included in Figure 13. The efficiency is also a function of the characteristics of the RC member that is strengthened, including concrete material properties, reinforcing bar materials properties, transverse and longitudinal reinforcement ratios and layout, etc. Therefore, comparison of the different composite material types here is intended to be viewed as qualitative and not quantitative. In general, Figure 13 shows that the PBO-FRCM composite exhibits similar

trends as GFRP and CFRP in increasing the torsional strength of a solid rectangular RC beam, where the increase in torsional strength becomes less proportional to the number of fiber layers for larger values of ρ_f.

6. CONCLUSIONS

This paper presented the results of a study aimed to understand the fundamental torsional behavior of RC members externally strengthened with PBO-FRCM composite material and the parameters that potentially influence their performance. The torque-twist load response and strains measured in the internal and external reinforcement were evaluated and discussed, and the efficiency of the PBO-FRCM composite material was compared with that of CFRP and GFRP composites from specimens reported the literature. Results of this study led to the following conclusions:

1. This study demonstrated that externally bonded PBO-FRCM composites can be used to strengthen RC beams in torsion. Failure of the strengthened beams was associated with debonding of the composite, which was characterized by significant slippage between the fibers and matrix.
2. Increases in the cracking torque, torsional strength, and corresponding values of twist were achieved by beams strengthened with a 4-sided wrapping configuration relative to the control (unstrengthened) beam. On the other hand, the 3-sided wrapping configuration was found to be largely ineffective in improving the torsional performance.

3. The 4-sided wrapping configuration improved the torsional performance by providing additional reinforcement as well as confinement, which delayed and controlled concrete cracking.
4. The contribution of the strengthening system to the torsional strength was reasonably predicted (+/- 20%) by the strains in the composite fibers. Provisions used to estimate the torsional strength of RC beams with externally-bonded FRP composites were found to be applicable for beams strengthened with FRCM composites.
5. The trend in the efficiency of PBO-FRCM composite in increasing the torsional strength of solid RC members is similar to that of GFRP and CFRP composites.
6. Further investigations are needed to study the performance of the beams with different fiber orientations and anchorage conditions.

ACKNOWLEDGEMENTS

The experimental work discussed in this paper was conducted at Missouri University of Science and Technology (Missouri S&T). Ruredil S.p.A. of San Donato Milanese, Italy, is gratefully acknowledged for providing the composite materials. The authors would like to thanks Abdeldjelil Belarbi of the University of Houston for his input regarding the test setup.

FUNDING

Funding for this work was provided by the Higher Committee for Education Development in Iraq (HCED).

Table 1. Measured concrete and steel reinforcement properties.

Material	Concrete	Steel Reinforcement	
		No. 3	No. 5
Compressive Strength, psi (MPa)	5700 (39.3)	--	--
Splitting Tensile Strength, psi (MPa)	460 (3.2)	--	--
Modulus of Elasticity ksi (GPa)	4150 (28.6)	29000 (200)	28000 (193)
Yield Strength, ksi (MPa)	--	65.8 (454)	68.0 (469)
Ultimate Strength, ksi (MPa)	--	104 (717)	107 (738)

Table 2. Measured PBO-FRCM composite material properties.

PBO Fibers	
Nominal Thickness, in. (mm)	0.002 (0.046)
Ultimate Tensile Strength, ksi (MPa)	440 (3015)
Modulus of Elasticity, ksi (GPa)	29,900 (206)
Ultimate Strain, in./in. (mm/mm)	0.0145 (0.0145)
Mortar	
Compressive Strength, psi (MPa)	3600 (24.8)
Splitting Tensile Strength, psi (MPa)	670 (4.6)

Table 3. Summary of test results.

Beam	T_{cr} k-in. (kN-m)	$\frac{T_{cr}}{T_{cr,control}}$	ψ_{cr} deg./in. (deg./m)	$\frac{\psi_{cr}}{\psi_{cr,control}}$	T_u k-in. (kN-m)	$\frac{T_u}{T_{u,control}}$	ψ_u deg./in. (deg./m)	$\frac{\psi_u}{\psi_{u,control}}$
Control	91.8 (10.4)	--	0.0042 (0.165)	--	148.7 (16.8)	--	0.085 (3.346)	--
N-P-3-S-1	102.3 (11.6)	1.11	0.0020 (0.079)	0.48	160.3 (18.1)	1.08	0.076 (2.992)	0.89
N-P-4-S-1	126.5 (14.3)	1.38	0.0034 (0.134)	0.81	193.2 (21.8)	1.30	0.245 (9.646)	2.88
N-P-4-C-1	121.6 (13.7)	1.32	0.0041 (0.161)	0.98	240.4 (27.2)	1.62	0.230 (9.055)	2.71
N-P-4-C-2	128.3 (14.5)	1.40	0.0030 (0.118)	0.71	310.6 (35.1)	2.09	0.241 (9.488)	2.84

Table 4. Maximum measured reinforcement strains.

	Strains Measured at Peak Torque of Control Beam, T=148.7 k-in (16.8 kN-m)			Strains Measured at $T=T_u$		
Beam	ε_t (%)	ε_l (%)	ε_f (%)	ε_t (%)	ε_l (%)	ε_f (%)
Control	0.252	0.165	--	0.252	0.165	--
N-P-3-S-1	0.231	0.140	0.365	0.232	0.183	0.431
N-P-4-S-1	0.050	0.108	0.004	0.295	0.287	1.026
N-P-4-C-1	0.058	0.119	0.026	0.275	0.638	0.822
N-P-4-C-2	0.016	0.104	0.005	0.305	1.137	0.653

Table 5. Contribution of the composite to the torsional strength.

Beam	T_u (k-in.) (kN-m)	$T_{f,,Exp}$ (k-in.) (kN-m)	$T_{f,An}$ (k-in.) (kN-m)	$T_{f,,Exp}/T_{f,An}$
Control	148.7 (16.8)	--	--	--
N-P-3-S-1	160.3 (18.1)	11.6 (1.3)	--	--
N-P-4-S-1	193.2 (21.8)	44.5 (5.0)	53.0 (6.0)	0.84
N-P-4-C-1	240.4 (27.2)	91.7 (10.4)	85.0 (9.6)	1.08
N-P-4-C-2	310.6 (35.1)	161.9 (18.3)	135.0 (15.3)	1.20

Table 6. Experimental results from Ameli et al. [7].

Beam	T_u (k-in.) (kN-m)	% increase in T_u relative to unstrengthened beam
CJS	154.0 (17.4)	16
CFS	192.1 (21.7)	45
CFE	247.8 (28.0)	87
CFE2	323.1 (36.5)	143
GJS	149.6 (16.9)	14
GFS	176.1 (19.9)	34
GFE	232.8 (26.3)	78
GFE2	275.3 (31.1)	110

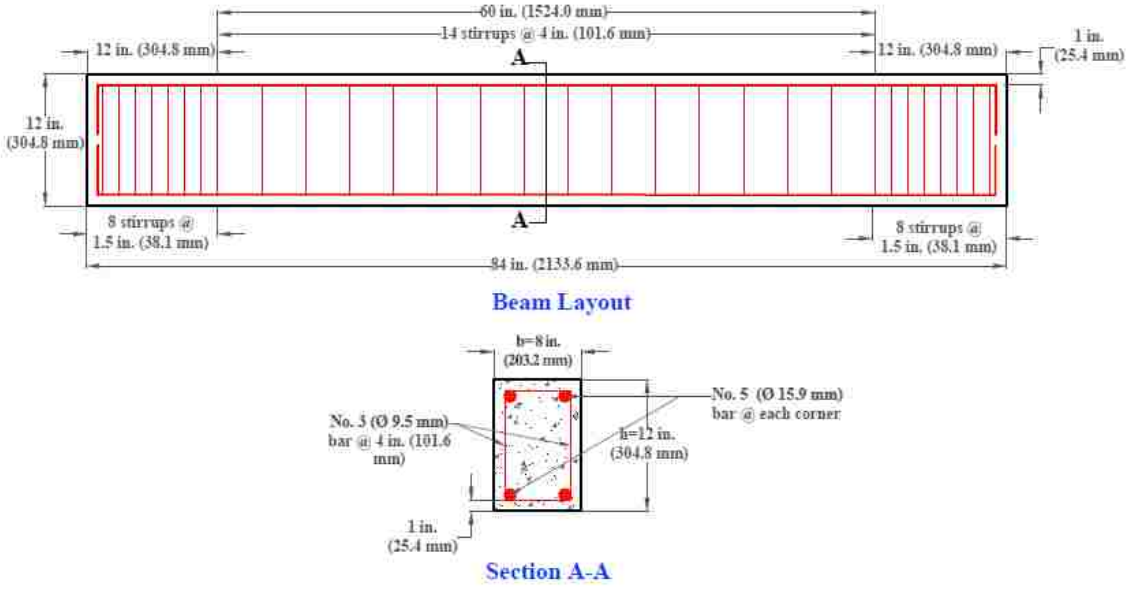

Figure 1. Beam layout and reinforcing details.

Figure 2. PBO unbalanced fiber net.

Figure 3. FRCM composite installation.

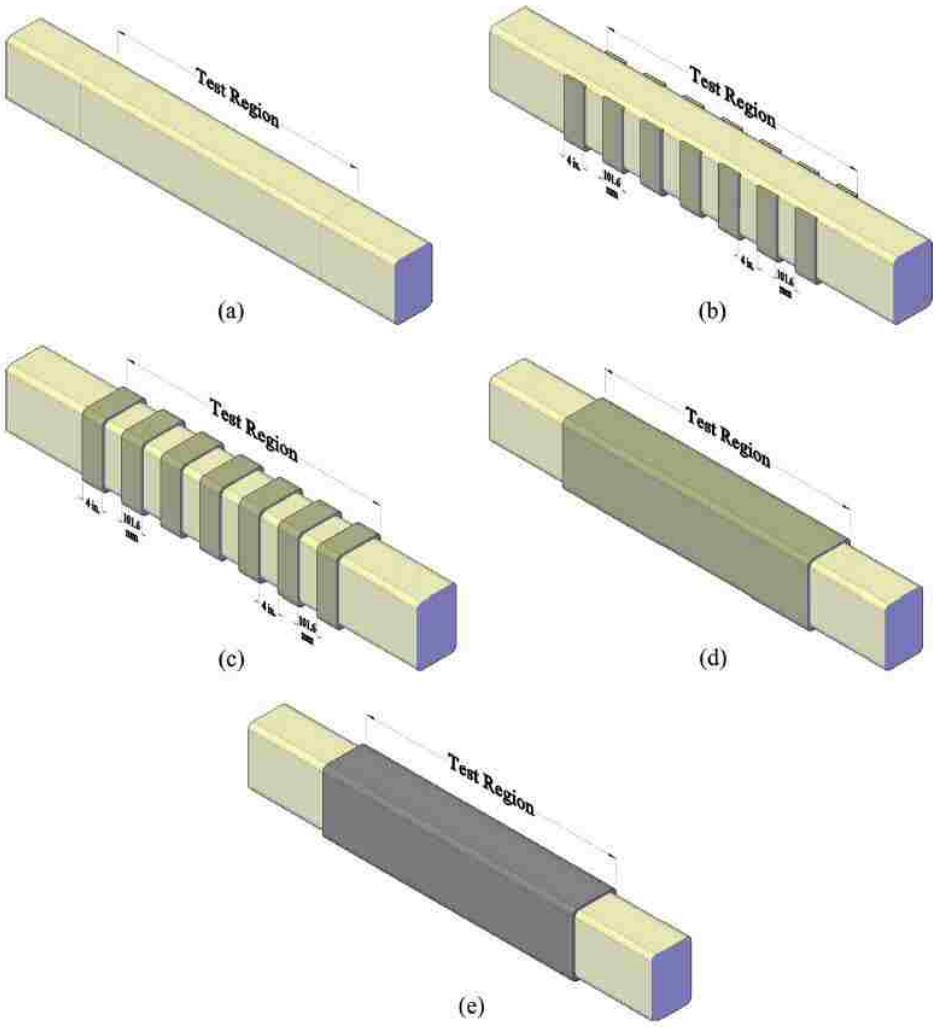

Figure 4. Schematic configuration of strengthened beams a) Control Beam, b) N-P-3-S-1, c) N-P-4-S-1, d) N-P-4-C-1, e) N-P-4-C-2.

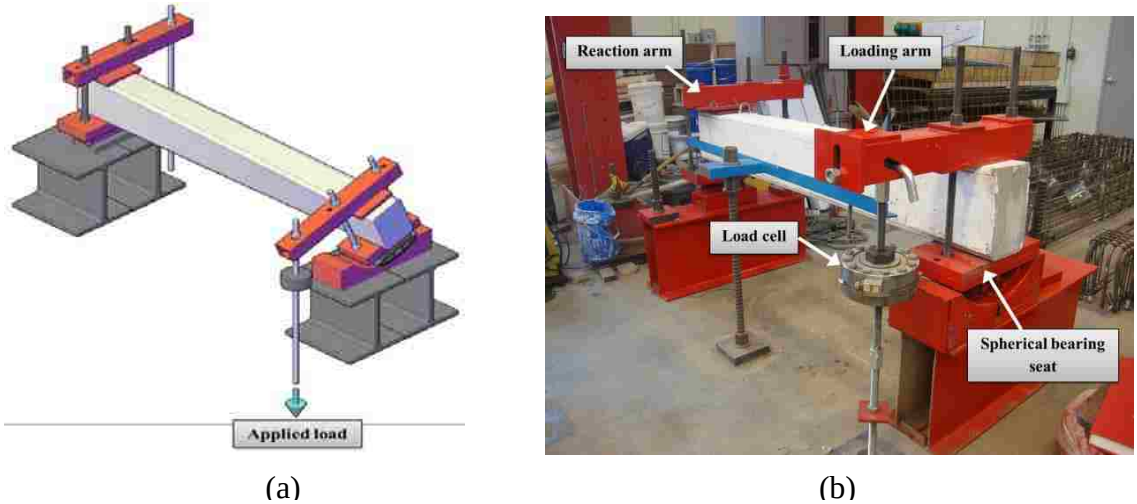

(a) (b)

Figure 5. Torsion test setup a) sketch, b) photograph.

(a) (b)

Figure 6. External instrumentation shown on a) east face, b) west face.

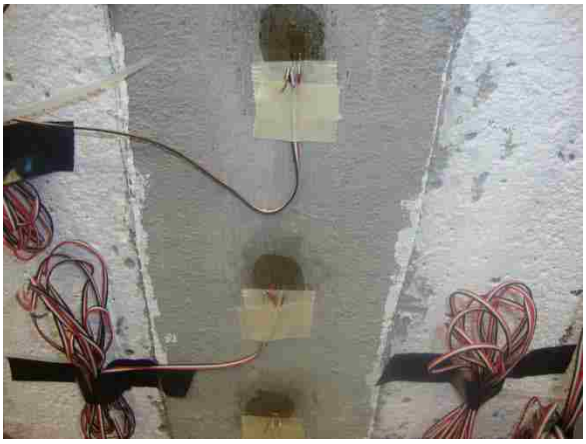

Figure 7. Strain gages on the fibers of the FRCM composite.

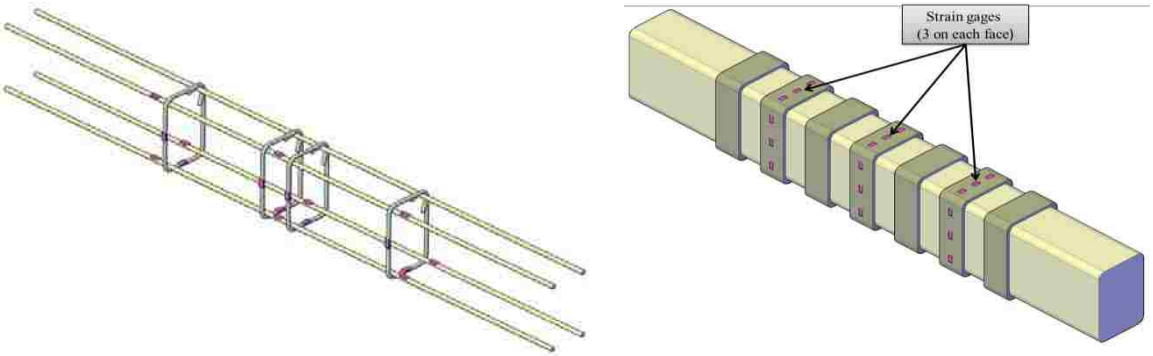

(a) (b)

Figure 8. Strain gage locations on the a) steel reinforcement (note, stirrups without strain gages not shown), b) PBO-FRCM composite.

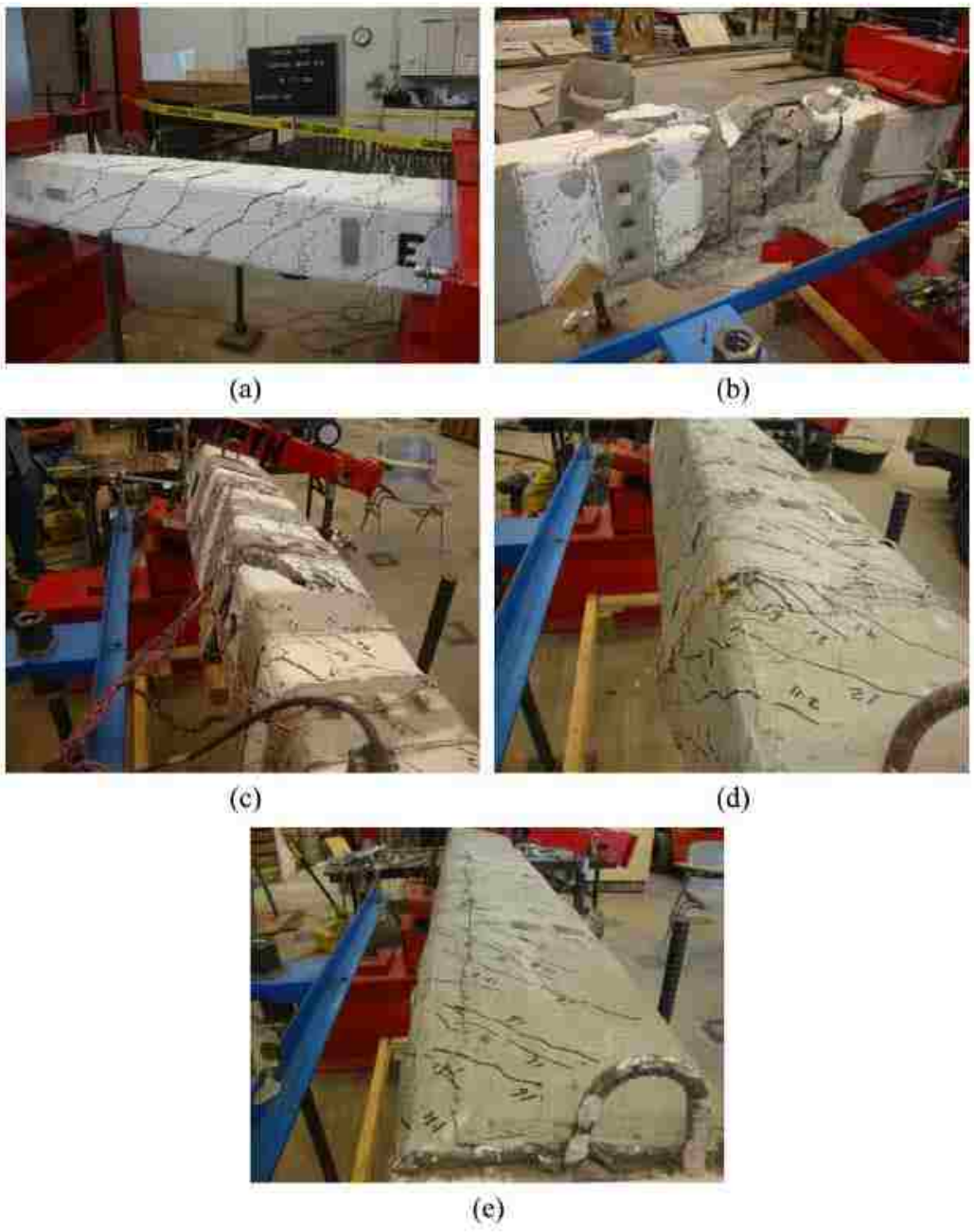

Figure 9. Failure mode of each beam a) control beam, b) N-P-3-S-1, c) N-P-4-S-1, d) N-P-4-C-1, e) N-P-4-C-2.

Figure 10. Distribution of concrete cracks beneath the FRCM composite for beam N-P-4-C-2.

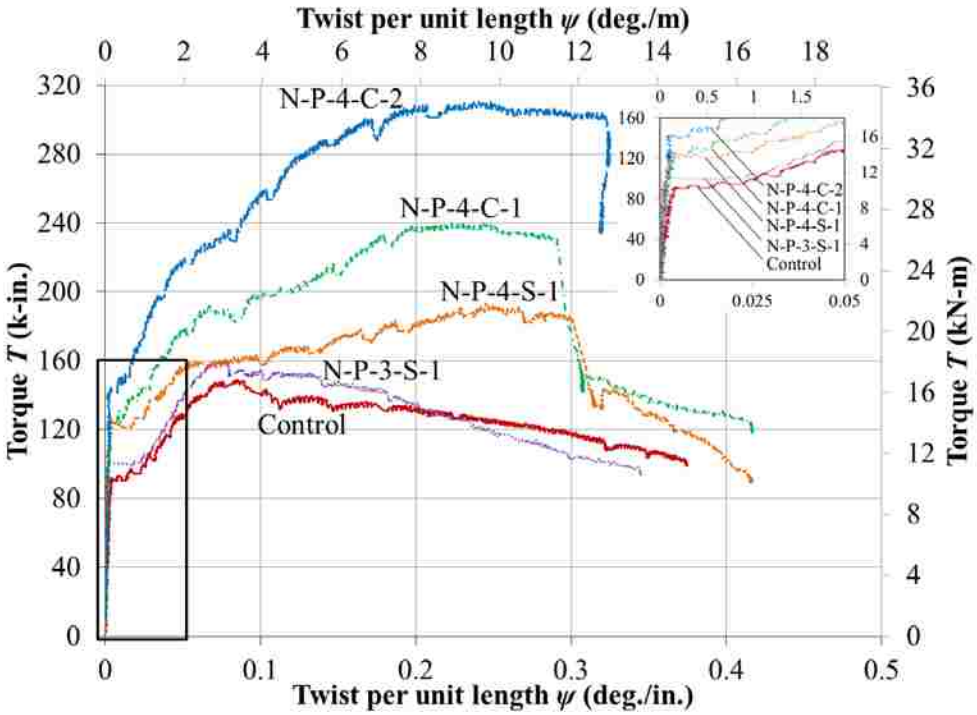

Figure 11. Experimental torque T-Twist ψ responses.

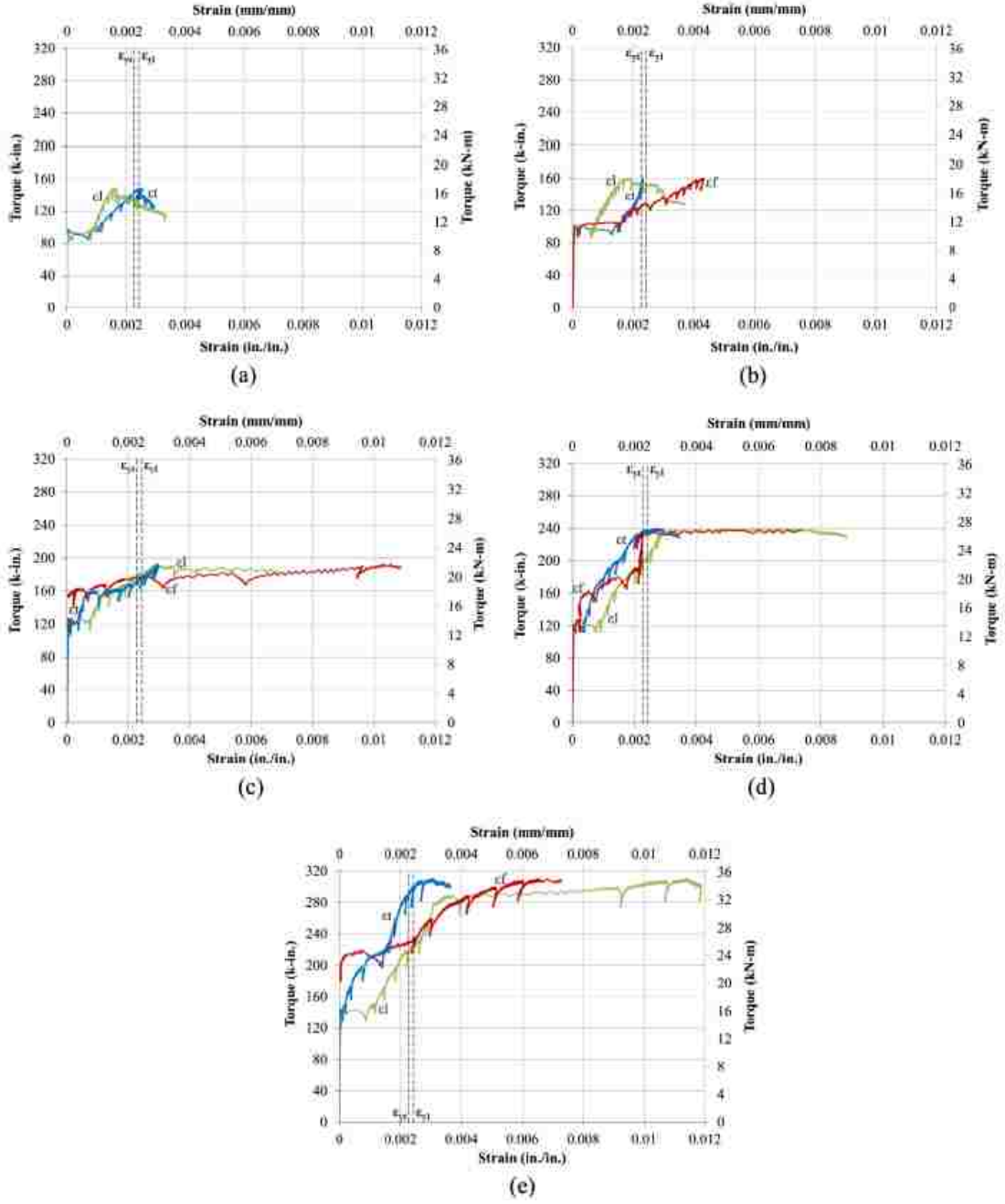

Figure 12. Torque versus reinforcement strain a) control beam, b) N-P-3-S-1, c) N-P-4-S-1, d) N-P-4-C-1, e) N-P-4-C-2.

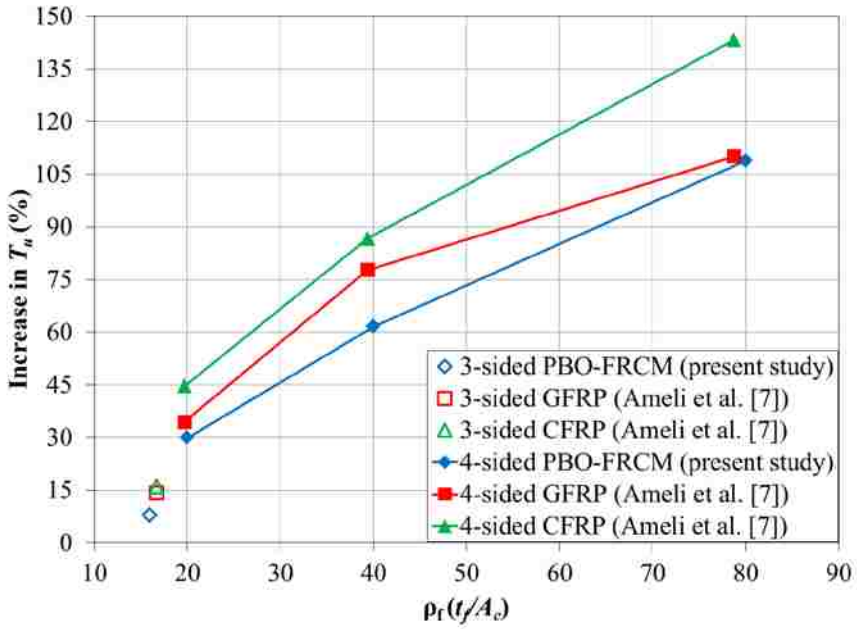

Figure 13. Influence of volumetric ratios of different wrapping systems on the increase in torsional strength relative to the unstrengthened condition.

REFERENCES

[1] Ghobarah, A., Ghorbel, M. N., & Chidiac, S. E. (2002). Upgrading torsional resistance of reinforced concrete beams using fiber-reinforced polymer. *Journal of Composites for Construction*, *6*(4), 257-263.\

[2] Panchacharam, S., & Belarbi, A. (2002). Torsional behavior of reinforced concrete beams strengthened with FRP composites. In *First FIB Congress, Osaka, Japan* (Vol. 1, pp. 01-110).

[3] Salom, P. R., Gergely, J., & Young, D. T. (2004). Torsional strengthening of spandrel beams with fiber-reinforced polymer laminates. *Journal of Composites for Construction*, *8*(2), 157-162.

[4] Hii, A. K., & Al-Mahaidi, R. (2006). Experimental investigation on torsional behavior of solid and box-section RC beams strengthened with CFRP using photogrammetry. *Journal of Composites for Construction*, *10*(4), 321-329.

[5] Hii, A. K., & Al-Mahaidi, R. (2006). An experimental and numerical investigation on torsional strengthening of solid and box-section RC beams using CFRP laminates. *Composite Structures*, *75*(1), 213-221.

[6] Chalioris, C. E. (2008). Torsional strengthening of rectangular and flanged beams using carbon fibre-reinforced-polymers–Experimental study. *Construction and Building Materials*, *22*(1), 21-29.

[7] Ameli, M., Ronagh, H. R., & Dux, P. F. (2007). Behavior of FRP strengthened reinforced concrete beams under torsion. *Journal of Composites for Construction*, *11*(2), 192-200.

[8] Deifalla, A., Awad, A., & Elgarhy, M. (2013). Effectiveness of externally bonded CFRP strips for strengthening flanged beams under torsion: An experimental study. *Engineering Structures*, *56*, 2065-2075.

[9] D'Ambrisi, A., & Focacci, F. (2011). Flexural strengthening of RC beams with cement-based composites. *Journal of Composites for Construction*, *15*(5), 707-720.

[10] Ombres, L. (2011). Flexural analysis of reinforced concrete beams strengthened with a cement based high strength composite material. *Composite Structures*, *94*(1), 143-155.

[11] Sneed, L.H., Verre, S., Carloni, C., & Ombres, L. (2016). "Flexural Behavior of RC Beams Strengthened with Steel-FRCM Composite." *Engineering Structures*, *127*, pp. 686-699.

[12] Ombres, L. (2012). Shear capacity of concrete beams strengthened with cement based composite materials. In Proceedings of the 6th International Conference on FRP Composites in Civil Engineering. (CICE 2012). Roma, Italy.

[13] Ombres, L. (2015). Structural performances of reinforced concrete beams strengthened in shear with a cement based fiber composite material. *Composite Structures*, *122*, 316-329.

[14] Trapko, T., Urbańska, D., & Kamiński, M. (2015). Shear strengthening of reinforced concrete beams with PBO-FRCM composites. *Composites Part B: Engineering*, *80*, 63-72.

[15] Loreto, G., Babaeidarabad, S., Leardini, L., & Nanni, A. (2015). RC beams shear-strengthened with fabric-reinforced-cementitious-matrix (FRCM) composite. *International Journal of Advanced Structural Engineering (IJASE)*, *7*(4), 341-352.

[16] Colajanni, P., De Domenico, F., Recupero, A., & Spinella, N. (2014). Concrete columns confined with fibre reinforced cementitious mortars: experimentation and modelling. *Construction and Building Materials*, *52*, 375-384.

[17] Carloni, C., Mazzotti, C., Savoia, M., & Subramaniam, K. V. (2014). Confinement of Masonry Columns with PBO FRCM Composites. *Key Engineering Materials*, *624*.

[18] Ombres, L. (2012). Debonding analysis of reinforced concrete beams strengthened with fibre reinforced cementitious mortar. *Engineering Fracture Mechanics*, *81*, 94-109.

[19] D'Ambrisi, A., Feo, L., & Focacci, F. (2012). Bond-slip relations for PBO-FRCM materials externally bonded to concrete. *Composites Part B: Engineering*, *43*(8), 2938-2949.

[20] D'Ambrisi, A., Feo, L., & Focacci, F. (2013). Experimental analysis on bond between PBO-FRCM strengthening materials and concrete. *Composites Part B: Engineering*, *44*(1), 524-532.

[21] D'Antino, T., Sneed, L., Carloni, C., & Pellegrino, C. (2013). Bond behavior of the FRCM-concrete interface. In *Proceedings of the 11th International Symposium on Fiber Reinforced Polymers for Reinforced Concrete Structures,(2013: Guimarães, Portugal)* (10 pp.). Institute for Sustainable an Innovation in Structural Engineering.

[22] D'Antino, T., Carloni, C., Sneed, L. H., & Pellegrino, C. (2014). Matrix–fiber bond behavior in PBO FRCM composites: A fracture mechanics approach. *Engineering Fracture Mechanics*, *117*, 94-111.

[23] Sneed, L. H., D'Antino, T., & Carloni, C. (2014). Investigation of bond behavior of PBO fiber-reinforced cementitious matrix composite-concrete interface. *ACI Materials Journal*, *111*(1-6), 1-12.

[24] Tran, C. T. M., Stitmannaithum, B., & Ueda, T. (2014). Investigation of the bond behaviour between PBO-FRCM strengthening material and concrete. *Journal of Advanced Concrete Technology*, *12*(12), 545-557.

[25] Ombres, L. (2015). Analysis of the bond between fabric reinforced cementitious mortar (FRCM) strengthening systems and concrete. *Composites Part B: Engineering*, *69*, 418-426.

[26] Sneed, L. H., D'Antino, T., Carloni, C., & Pellegrino, C. (2015). A comparison of the bond behavior of PBO-FRCM composites determined by double-lap and single-lap shear tests. *Cement and Concrete Composites*, *64*, 37-48.

[27] ACI 318-14. Building code requirements for structural concrete (318-14) and commentary (318R-14). American Concrete Institute, Farmington Hills, MI, 2014, 519 pp.

[28] ASTM A615/ A615M-16. Standard specification for deformed and plain carbon-steel bars for concrete reinforcement. ASTM International, West Conshohocken, PA, 2015, 8 pp.

[29] ASTM A370-16. Standard test methods and definitions for mechanical testing of steel products. ASTM International, West Conshohocken, PA, 2016, 49 pp.

[30] ASTM C39/C39M-16b. Standard test method for compressive strength of cylindrical concrete specimens. ASTM International, West Conshohocken, PA, 2016, 7 pp.

[31] ASTM C496/ C496M-11. Standard test method for splitting tensile strength of cylindrical concrete specimens. ASTM International, West Conshohocken, PA, 2011, 5 pp.

[32] ASTM C469/C469M-14. Standard test method for static modulus of elasticity and Poisson's ratio of concrete in compression. ASTM International, West Conshohocken, PA, 2014, 5 pp.

[33] Ruredil. X Mesh Gold Data Sheet. Ruredil S.p.A. 2012, Milan, Italy. <http://english.ruredil.it/SchedeProdottoENG/RuredilXMeshGOLD_ing_1.pdf>.

[34] Hii, A. K., & Al-Mahaidi, R. (2007). Torsional capacity of CFRP strengthened reinforced concrete beams. *Journal of Composites for Construction*, *11*(1), 71-80.

[35] Carloni, C., D'Antino, T., Sneed, L.H., and Pellegrino, C. (2015). "Role of the Matrix Layers in the Stress-Transfer Mechanism of FRCM Composites Bonded to a Concrete Substrate." *Journal of Engineering Mechanics. 141*(6).

[36] Grelle, S. V., & Sneed, L. H. (2013). Review of anchorage systems for externally bonded FRP laminates. *International Journal of Concrete Structures and Materials*, *7*(1), 17-33.

[37] Matthys, S., and Triantafillou, T. (2001). "Shear and Torsion Strengthening with Externally Bonded FRP Reinforcement." *Proceedings of the International Workshop on Composites in Construction: A Reality*, E. Cosensa, G. Manfredi, and A. Nanni, eds., Capri, Italy, pp. 203-210.

[38] *fib* Bulletin 14 (2001). Externally bonded FRP reinforcement for RC structures. CEB-FIP, Lausanne, Switzerland, 2001, 130 pp.

[39] Zureick, A. H., Ellingwood, B. R., Nowak, A. S., Mertz, D. R., & Triantafillou, T. C. (2010). *Recommended guide specification for the design of externally bonded FRP systems for repair and strengthening of concrete bridge elements.* NCHRP Report 655. Transportation Research Board.

[40] He, R., Sneed, L. H., & Belarbi, A. (2014). Torsional repair of severely damaged column using carbon fiber-reinforced polymer. *ACI Structural Journal*, *111*(3), 705-716.

[41] D'Antino T., Sneed L.H., Carloni C., & Pellegrino C. (2015). "Influence of the Substrate Characteristics the Bond Behaviour of FRCM-Concrete Joints", *Construction and Building Materials*, *101*(1), 838-850.

III. A STUDY OF THE EFFECT OF FIBER ORIENTATION ON THE TORSIONAL BEHAVIOR OF RC BEAMS STRENGTHENED WITH PBO-FRCM COMPOSITE

Meyyada Y. Alabdulhady and Lesley H. Sneed

ABSTRACT

Repair and rehabilitation of reinforced concrete (RC) structures with different types of external reinforcement has been investigated widely. Fiber reinforced cementitious matrix (FRCM) is a new type of composite system that contains continuous fibers embedded in inorganic matrix. This system has been proven to be effective for strengthening RC members under flexure, shear, and axial loadings. However, studies on the use of FRCM composite for torsional strengthening are very limited. This study investigated experimentally the torsional behavior of solid rectangular RC beams strengthened with externally bonded PBO-FRCM composite in different wrapping configurations. The study focused on the effect of fiber orientation as well as other parameters that influence the torsional strength, torsional moment-twist per unit length response, and mode of failure including fiber continuity and number of composite layers. The strains in the internal and external reinforcement and the longitudinal elongation of the strengthened beams were examined, and a comparison with other types of fiber reinforced composite was also discussed. The 90° fiber orientation (perpendicular to the beam longitudinal axis) was more effective in increasing the torsional strength than the 45° fiber orientation since premature debonding of the fibers occurred at the ends of the 45° strips, which contrasted the potential benefits from optimizing the fiber orientation and led to the underutilization of the composite. The 90° fiber orientation was also more effective than the 0° fiber orientation.

HIGHLIGHTS

- RC beams strengthened with PBO-FRCM composite were tested under torsional moment.
- The effect of composite fiber orientation on the torsional response was studied.
- Internal and external reinforcement strains were presented.
- Longitudinal elongation of the strengthened beams was examined.

KEYWORDS

Fiber orientation; fiber strain; PBO-FRCM composite; RC beams; strengthening; torsion.

1. INTRODUCTION

Fiber reinforced cementitious matrix (FRCM) composite material has been used recently in repair and strengthening of reinforced concrete (RC) members in buildings and bridges [1-3]. This type of composite, which is comprised of continuous fibers embedded in an inorganic matrix, has favorable features over fiber reinforced composites with organic resin, such as fiber reinforced polymer (FRP) composites, due to its higher temperature resistance and reversibility, ability to be installed onto wet surfaces or in low temperatures, and good vapor permeability due to compatibility with concrete and masonry substrates. Therefore, FRCM composites appear to be highly promising, especially for application to historical constructions [4]. Different types of fibers have been used in FRCM composite systems including carbon, glass, basalt, steel, and polyparaphenylene benzobisoxazole (PBO). The use of FRCM composites has been studied for flexural [5-8] and shear strengthening [9-15] of RC members and confinement

of axially and eccentrically loaded elements [16-18]. On the other hand, very few studies are available in the technical literature on its use for torsional strengthening [19].

Torsional behavior of RC beams strengthened with externally bonded FRP composites has been investigated since the early 2000s [20-24]. Some authors have studied the effect of the FRP fiber orientation on the torsional strength. Panchacharam and Belarbi [25] studied the behavior of RC beams with a square cross-section strengthened with glass FRP (GFRP) composite in different fiber orientations (0° and 90° relative to the longitudinal axis of the beam) and wrapping configurations. The results showed that fibers with 0° orientation increase the torsional moment associated with concrete cracking, although they were ineffective for increasing the torsional strength. Ghobarah et al. [26] investigated the behavior of RC beams with a rectangular cross-section strengthened with GFRP or carbon FRP (CFRP) composite with different fiber orientations (45° and 90° relative to the longitudinal axis of the beam) and wrapping schemes (continuous along the length or discrete strips with different widths and spacings). Findings showed that spiral wrap with a 45° fiber orientation is more efficient in terms of increasing the torsional strength than fibers a 90° orientation. Deifalla et al. [27] tested rectangular, T-shaped, and L-shaped beams strengthened with CFRP composite with fibers oriented in the 45° and 90° directions to study the effectiveness of the strengthening technique on increasing the torsional strength of beams with various cross-sections. The results showed that the torsional strength and rotational capacity of L-shaped RC beams with anchored, inclined U-jackets were increased by 12% relative to those with anchored, vertical U-jackets. Furthermore, anchored 45° U-jacket strips were found to be more effective than unanchored 45° U-jacket strips, while anchored 45° U-

jacket strips were comparable to 45° fully wrapped strips. This study investigates the torsional behavior of RC beams strengthened with PBO-FRCM composite. The experimental results of 10 solid rectangular RC beams externally strengthened with PBO-FRCM composite material in different wrapping configurations are presented and compared with those of an unstrengthened control beam. The aim of the present study is to investigate the effect of fiber orientation and wrapping configuration on the torsional strength, behavior, and failure mode of FRCM strengthened RC beams.

2. EXPERIMENTAL PROGRAM

2.1 MATERIAL PROPERTIES

The RC beams in this study were constructed with normalweight concrete. The coarse aggregate was a crushed dolomitic limestone with 1 in. (25.4 mm) maximum aggregate. The fine aggregate was natural river sand. The beams were constructed in two batches, named Batch 1 and Batch 2, with the same concrete mixture proportions summarized in Table 1. The compressive strength, splitting tensile strength, and modulus of elasticity of each batch of concrete were determined from the average of three 4 in. (101.6 mm) diameter × 8 in. (203.2 mm) long cylinders cast at the same time and cured in the same manner as the concrete beams and tested at 28 days in accordance with ASTM C39 [28], ASTM C496 [29], and ASTM C469 [30], respectively. The measured concrete properties are summarized in Table 2. The concrete beams and cylinders were covered with wet burlap for four days then kept together in the laboratory under the same atmospheric conditions until testing.

Reinforcing bars were ASTM A615 Grade 60 (Grade 420) deformed steel bars of sizes No. 3 (dia. = 9.5 mm, area = 71 mm^2) and No. 5 (dia. = 15.9 mm, area = 199 mm^2) [31]. Reinforcing bars of the same size were from the same heat of material. Three coupon samples of each bar size were tested according to ASTM A370 [32] to obtain the material properties, and the results are provided in Table 2.

The FRCM composite used in this study was comprised of a bidirectional PBO fiber net embedded in an inorganic matrix [33]. The PBO fiber net is shown in Figure 1. The fiber net rovings were spaced 0.4 in. (10 mm) and 0.8 in. (20 mm) center-to-center in the longitudinal and transversal directions of the net. The clear spacing between rovings was 0.2 in. (5 mm) and 0.6 in. (15 mm), respectively. The nominal thicknesses (obtained by assuming the fibers are distributed evenly over the entire width of the composite) in the two fiber directions were 0.0018 in. (0.046 mm) and 0.0005 in. (0.012 mm), respectively. The weight of PBO fibers in the mesh was 0.00010 lb/in^2 (70.4 g/m^2) and 0.000025 lb/in^2 (17.6 g/m^2) in the longitudinal and transversal directions, respectively, with a total weight of 0.00013 lb/in^2 (88 g/m^2). Tensile strength, ultimate strain, and elastic modulus of the PBO fibers determined from tensile tests of the bare fibers were 440 ksi (3015 MPa), 0.0145, and 29,900 ksi (206 GPa), respectively [34], [35].

The FRCM composite matrix was an inorganic cementitious mortar. The FRCM composite was applied to the RC beams in two batches, referred to as Batch 1 and Batch 2, corresponding to the two batches of concrete used to cast the beams. Mortar compressive and splitting tensile strength properties were determined for each batch from of a representative sample of matrix used to cast the FRCM composite as the average of three 2 in. (50.8 mm) diameter × 4 in. (101.6 mm) long cylinders tested at 28 days in

accordance with ASTM C39 [28] and ASTM C496 [29], respectively. The FRCM material properties are summarized in Table 3.

2.2 BEAMS UNDER INVESTIGATION

A total of 11 RC beams were included in the experimental program, 10 of which were strengthened, and one was unstrengthened for use as the control. Five of the 11 beams, including the control beam, were included in the first phase of an experimental campaign previously published by the authors [19]. The six additional strengthened beams presented in this paper were included in the second phase of the experimental campaign, which involved additional test variables including composite fiber orientation.

All RC beams had a solid rectangular cross-section and the same nominal geometrical and mechanical properties. The nominal dimensions were b=8 in. (203.2 mm) wide × h=12 in. (304.8 mm) tall × 84 in. (2133.6 mm) long. The RC beams were designed based on the ACI 318 code [36] provisions and had the same internal reinforcement. The beams had a test region in which the composite was applied of 60 in. (1524.0 mm) long that was reinforced with minimum torsional reinforcement in the beam transverse direction in accordance with the ACI 318 code [36]. The internal transverse reinforcement was in the form of closed stirrups oriented perpendicular to the longitudinal axis of the beam. The volumetric reinforcement ratio of the longitudinal reinforcement was $\rho_{sl} = A_{sl}/A_c = 1.29\%$, and of the transverse reinforcement was $\rho_{st} = \frac{A_{st}}{A_c}\frac{p_t}{s} = 0.92\%$, where A_{sl} is the total area of longitudinal bars, A_c is the gross concrete area (A_c=bh), A_{st} is area of one leg of a stirrup, p_t is perimeter of a stirrup, and s

is the spacing of stirrups (center-to-center). The beam end regions (12 in. [304.8 mm] long each end) were more heavily reinforced internally with stirrups and externally with CFRP composite material (strengthened beams only) with unidirectional fibers oriented perpendicular to the longitudinal axis of the beam to prevent failure in the end (clamp) regions. Figure 2 shows the dimensions and reinforcement details of the RC beams.

The strengthened beams were wrapped with PBO-FRCM composite applied in different configurations. The wrapping schemes are shown in Figure 3. The strengthened beams were designated as N-P-X-(α or *w*)Y-Z, where N identifies the concrete type (normalweight), P identifies the fiber type in the composite (PBO), X indicates the number of wrapped sides (3 or 4), Y indicates whether the composite was applied in discrete strips or continuous along the length of the test region (S or C, respectively), and Z indicates the number of composite layers (1 or 2). The term α, where indicated, designates the primary fiber direction of the fiber layer (α=0°, 45°, or 90°) relative to the longitudinal axis of the beam, starting with the innermost layer for the case of multiple fiber layers. Unless noted otherwise, α=90°. The term *w*, where indicated, designates a relatively wide strip was used (*w*=8 in. [203.2 mm]). Unless noted otherwise, *w*=4 in. (101.6 mm). The clear spacing between strips was *s*=4 in. (101.6 mm). The 3-sided configuration was investigated because in certain cases the complete perimeter of the beam may not be accessible for strengthening, as in the case of a T-beam or spandrel beam in monolithic concrete construction.

Before the composite was applied, the corners of the RC beams were rounded with a radius of 0.75 in. (19 mm) to reduce stress concentrations at the corners [37]. The PBO-FRCM composite material was installed on the beams after they were 28 days old.

The concrete surface was sandblasted to a target profile of 0.1 in. (2 mm), then dust and loose particles were removed. The concrete surface was then wetted before applying the first layer of matrix. Foam strips of 0.2 in. (5 mm) thickness were mounted to the surface of the beam to control the location and total thickness of the composite (Figure 4). For beams strengthened with one layer of composite, the first (internal) layer of matrix of approximately 0.1 in. (3 mm) thick was applied, then pre-cut fibers were applied onto the fresh matrix and pressed gently to ensure proper alignment and placement. The second (external) layer of matrix of approximately 0.1 in. (2 mm) thick was applied to cover the fibers. The thickness of the external matrix layer was slightly less than the recommended thickness, however previous results have shown that the contribution of the external matrix layer to the load carrying capacity of the interface is much less significant than that of the internal matrix layer [38]. For beams strengthened with one layer of fibers, the total thickness of the composite was 0.2 in. (5 mm). For beams strengthened with two layers of fibers, the second layer of fibers was applied to the fresh matrix, then it was covered with an additional layer of matrix. The thickness of composite with two layers was approximately 0.4 in. (10 mm). Finally, the surface of the matrix was removed at the location of each strain gage in order to expose the fibers and apply the gage to the bare fibers. Figure 4 shows the composite application process.

For beams wrapped with a 4-sided configuration and a 90° fiber orientation, an 8 in. (203.2 mm) overlap, corresponding to the beam width, was provided on the top surface of the beam. The overlap length was slightly less than the effective bond length of the composite, defined as the minimum length needed to fully develop the FRCM-substrate joint load-carrying capacity [39], which was determined to be approximately 10

in. (260 mm) for the PBO-FRCM composite in this study [39]. It is important to highlight that for strengthened beams with 45° or 0° fiber orientation, even those with a 4-sided wrapping configuration, the fibers sheets did not overlap at the ends of the fiber sheet (see Figures 3f and 3h, for example). Fiber sheets terminated at the end of the test region and did not extend into the clamp regions in order to avoid restraint from the clamping. The termination of sheets at the member end may also be required in certain practical cases, such as in the case of a beam-column joint in monolithic concrete construction.

2.3 TEST SETUP, INSTRUMENTATION, AND LOADING PROCEDURE

Figure 5 shows the test setup used in this study. Torsional moment was applied to the beam through the loading arm, which had an 18 in. (457 mm) eccentricity relative to the centroid of the cross-section, using a 30 k (130 kN) capacity hydraulic jack and measured by a 100 k (445 kN) capacity load cell. The opposite end of the beam was restrained with a reaction arm anchored to the strong floor with a threaded rod. The beam was allowed to slide freely in the longitudinal direction at the reaction end to avoid axial restraint and allow concrete cracks to open. Effects of secondary bending due to self weight and to application of the load were neglected. Additionally, the restraint of warping at the clamped ends was also neglected.

A rotational variable differential transformer (RVDT) mounted along the east face of the beam within the test region with gage length of 45.5 in. (1155.7 mm) was used to measure the average angle of twist per unit length (directions are indicated in Figure 5). Measurements from the RVDT were confirmed with values determined from measurements of vertical displacement acquired from two linear variable differential

transformers (LVDTs) mounted on the west face of the beam. Another LVDT was placed at the center of the cross-section at the reaction end of the beam to measure longitudinal deformation of the beam. The RVDT and LVDTs are shown in Figure 6.

A total of 17 uniaxial electrical resistance strain gages were mounted to the longitudinal (9) and transverse (8) reinforcing bars at the middle and quarter points of the beam test region (Figure 7a). A total of 27 or 36 strain gages were used to measure FRCM fiber strains for specimens with a 3-sided or 4-sided wrapping configuration, respectively (Figure 7b).

The beams were subjected to monotonically increasing loading resulting in constant torsional moment T along the length. Loading continued until either a significant reduction in torsional moment occurred, or the twist capacity of the test setup was reached. At the beginning of the test, the loading was controlled by slowly increasing the force. After the peak torsional moment (i.e., the torsional strength) was reached, the loading was controlled by slowly increasing the displacement. The loading was paused to mark cracks and photgraph the condition of the beam at various stages during testing.

3. EXPERIMENTAL RESULTS

3.1 SUMMARY OF CRACKING AND PEAK TORSIONAL MOMENT AND CORRESPONDING TWIST

This section summarizes and compares the salient results from the experiments conducted in this study. Values of the cracking and peak torsional moment (T_{cr} and T_u, respectively), along with the corresponding angles of twist per unit length (ψ_{cr} and ψ_u, respectively), are listed in Table 4. Values of the torsional moment T for all tested beams

were normalized for purpose of comparison since the beams had different measured concrete compressive strengths. Since torsional moment is proportional to the value $\sqrt{f_c'}$ [36], the normalized values of torsional moment, denoted as $\widetilde{T}$, were obtained by multiplying the torsional moment T by the factor $\sqrt{\bar{f}_c'/f_c'}$, where $\bar{f}_c'$ is the average concrete compressive strength of the two concrete batches ($\bar{f}_c'$ =5350 psi [36.9 MPa]). Nomalized values of the cracking and peak torsional moment ($\widetilde{T_{cr}}$ and $\widetilde{T_u}$, respectively) are listed in Table 4. For the strengthened beams, Table 4 also summarizes the increase in normalized cracking and peak torsional moment and twist per unit length relative to the corresponding normalized value of the control beam.

Table 4 shows that the normalized cracking torsional moment for all strengthened beams was larger than that of the control beam. The largest increase was for beam N-P-4-C-2 due to the confinement effect of the two layers of fibers with 90° orientation. With the exception of beam N-P-3-S-1, with a 3-sided wrapping configuration, the normalized peak torsional moment of all strengthened beams was larger than that of the control beam. The largest increase in normalized peak torsional moment was achieved by beam N-P-4-C-2 with two layers of fibers with 90° fiber orientation.

3.2 TORSIONAL BEHAVIOR AND MODE OF FAILURE

3.2.1 Control Beam. The torsional behavior and mode of failure of the control beam is shown in Figure 8. The ascending region of the normalized torsional moment-twist per unit length curve in Figure 8a can be described by three stages: an initial linear

behavior with high torsional stiffness until cracking of concrete, then an increase in twist angle without increasing torsional moment due to redistribution of forces from the concrete to the internal steel reinforcement, followed by a non-linear behavior with a reduction in torsional stiffness until the normalized peak torsional moment is achieved. The post-peak response can be described as gradual reduction in torsional moment with increasing twist per unit length.

The cracking pattern of the control beam was characterized by the formation spiral diagonal cracks around the perimeter of the beam (see Figure 8b). The inclination of the major cracks was approximately 45° with respect to the beam longitudinal axis. Failure of the control beam was due to crushing of the concrete struts at the mid-length of the test region.

3.2.2 Strengthened Beams with 3-Sided Wrapping Configurations. Figure 9 shows the $\tilde{T}$-ψ response of the strengthened beams with 3-sided wrapping, i.e., beams N-P-3-S-1, N-P-3-45S-1, and N-P-3-C-1, along with the control beam for comparison. Only slight differences in normalized cracking and peak torsional moment relative to the control beam were achieved, regardless of fiber orientation.

The mode of failure of the strengthened beams with 3-sided wrapping configurations was the same as that of the control beam, except the location of failure was near the beam restrained end, and failure was followed by concrete cover spalling with the composite strips still attached (Figure 10). Excessively wide concrete cracks, oriented between 42° and 47° with respect to the longitudinal axis of the beam, were concentrated on the unwrapped beam face near the end of the beam. This damage led to premature failure of beam N-P-3-45S-1 with a slightly lower normalized peak torsional

moment (3%) compared to the control beam. During loading, the slippage of the fibers relative to the matrix was observed at the ends of the fiber sheets. The orientation of the fibers did not play a significant role in the behavior of the strengthened beams with 3-sided wrapping configurations due to the fact that PBO-FRCM-concrete joints exhibit significant fiber slippage in the formation of the bond mechanism [39]. This fiber slippage is not restrained in the case of a 3-sided wrapping configuration without sufficient anchorage.

3.2.3 Strengthened Beams with 4-Sided Wrapping Configurations and One Layer of Fibers. The $\tilde{T}$-ψ response of the beams strengthened with 1-layer, 4-sided wrapping configurations (beams N-P-4-S-1, N-P-4-45S-1, N-P-4-8S-1, N-P-4-0C-1, and N-P-4-C-1), along with the control beam, is shown in Figure 11. Comparing the response of beam N-P-4-0C-1, with fibers oriented parallel to the longitudinal axis of the beam, with that of the control beam indicates that the 0° orientation was ineffective for increasing the normalized peak torsional moment, although it did increase the normalized cracking torsional moment (1.22 times that of the control beam). On the other hand, beam N-P-4-C-1, with fibers oriented in the 90° direction, had larger normalized cracking and peak torsional moments than that of the control beam (1.33 and 1.62 times, respectively).

The mode of failure and the failure location of beams with 4-sided wrapping configurations varied based on the wrapping scheme and fiber orientation as shown in Figure 12. The major cracks were oriented between 40° and 48° with respect to the longitudinal axis of the beam. For N-P-4-S-1, N-P-4-8S-1 and N-P-4-C-1, with 90° fiber orientation, fiber rupture followed by concrete strut crushing due to loss of confinement governed the failure, which occurred at mid-length, the loading end, and the restrained

end, respectively (Figures 12a, c, and e). The external layer of the matrix exhibited fine cracks during the test, which indicates slippage of the fibers relative to the cementitious matrix. For beams N-P-4-45S-1 and N-P-4-0C-1, with 45° and 0° fiber orientation respectively, failure initiated by debonding of the fibers at the loading end followed by crushing of the concrete struts (Figure 12b, and d).

It is interesting to note that results of beams strengthened with FRP composite showed that the 45° fiber orientation is more effective than the 90° orientation since the inclined fibers are generally perpendicular to the diagonal concrete cracks [26]. In this study, however, strips oriented at 90° were more effective at increasing the cracking and peak torsional moment than those oriented at 45° due to premature debonding failure mode of the beam with inclined strips. Other studies have found that fibers oriented at 0° were able to contribute to the torsional strength of RC members [40]. As discussed in Section 2.2, even though beams N-P-4-45S-1 and N-P-4-0C-1 had a continuous wrapping configuration along the length of the test region, the fiber sheets were effectively unanchored at the ends of the test region, which resulted in premature failure of these beams. It is possible that the lower mechanical properties of the mortar matrix for these specimens (Batch 2, see Table 3) had an influence on the load at which debonding occurred. Further studies are needed to determine a suitable anchorage system to prevent the debonding failure of fibers with 45° and 0° orientations. The influence of fiber orientation is discussed further in Section 4.

3.2.4 Strengthened Beams with 4-Sided Wrapping Configurations and Two Layers of Fibers. Figure 13 shows the $\tilde{T}$-ψ response of beams strengthened with 2-layer, 4-sided wrapping configurations (beams N-P-4-0/90C-2 and N-P-4-C-2), along with the

response of the control beam. The normalized cracking and peak torsional moments of beam N-P-4-0/90C-2 were 1.48 and 1.80 times those of the control beam. The normalized cracking and peak torsional moments of beam N-P-4-C-2 were 1.58 and 2.09 times those of the control beam. The increase in $\widetilde{T_{cr}}$ and $\widetilde{T_u}$ for beam N-P-4-C-2 was larger than for beam N-P-4-0/90C-2 due to the confinement effect provided by the two layers of wrapping. The increase in $\widetilde{T_{cr}}$ and $\widetilde{T_u}$ for beam N-P-4-C-2 was also larger than that for beam N-P-4-C-1 (1.33 and 1.62 times that of the control beam, respectively, see Section 3.2.3) due to the increased number of fiber layers (two versus one, respectively).

Debonding of the inner composite layer (0°) from the concrete substrate at the restrained end followed by concrete strut crushing governed the failure of beam N-P-4-0/90C-2 (Figure 14a). Fiber rupture followed by concrete strut crushing due to loss of confinement governed the failure of beam N-P-4-C-2 (Figure 14b). The major cracks were oriented between 42°and 45° with respect to the longitudinal axis for beams N-P-4-0/90C-2 and N-P-4-C-2, respectively.

3.3 STRAINS IN THE INTERNAL AND EXTERNAL REINFORCEMENT

The applied torsional moment versus strain measured in the internal transverse reinforcement (stirrups) ε_t and externally bonded composite ε_f is shown in Figures 15 and 16, respectively. The values of strain in the figures are from the strain gages that recorded the maximum corresponding values at the peak torsional moment. Strain measurements are plotted until the end of the test or until the strain gage malfunctioned. Values of the cracking and ultimate torsional moment are indicated in each graph. Also, values of the yield strain of the stirrups ε_{ty} determined from the tensile coupons (Section 2.1) are

shown in Figure 15. Figures 15 and 16 show that the strain in each type of reinforcement was small until concrete cracking occurred, then the strain increased rapidly after that point. The FRCM composite started to contribute to the torsional resistance once torsional cracks in the concrete formed and propagated (see Figure 16).

The maximum strains measured in the internal reinforcement (transverse and longitudinal reinforcing steel bars) and external reinforcement (FRCM composite) at the peak torsional moment and at the normalized peak torsional moment of the control beam are summarized in Table 5. The maximum strain in the stirrups varied based on the external reinforcement fiber orientation and the mode of failure. For strengthened beams with 4-sided 90° fiber orientation, the strains in the stirrups and longitudinal bars at the peak torsional moment were larger than those of the control beam. On the other hand, values of strain for the strengthened beams with 4-sided 45° or 0° fiber orientation, which failed due to debonding of the composite (i.e., beams N-P-4-45S-1 and N-P-4-0C-1), were lower than those of the control beam. In fact, beams N-P-3-45S-1, N-P-4-45S-1, and N-P-4-0C-1 were the only strengthened beams in which yielding of the stirrups did not occur (see Table 5) because premature failure occurred due to either damage of the concrete struts (beam N-P-3-45S-1) or debonding of the composite (beams N-P-4-45S-1 and N-P-4-0C-1).

The maximum strain in the FRCM composite fibers varied based on the fiber orientation and the mode of failure. The effect of confinement can be seen clearly at the early loading stages corresponding to the normalized peak torsional moment of the control beam (Table 5). Beams with 3-sided wrapping configurations had higher strain values due to slippage of the fibers at the crack locations, while very small strain values

were recorded for beams with 4-sided wrapping configurations. Furthermore, higher values of strain were achieved in strengthened beams with 4-sided 90° orientation at the peak torsional moment due to the full utility of the fibers until rupture. Values of strain measured for beam N-P-4-0C-1, with 0° orientation, were lower than that of beam N-P-4-C-1, with 90° orientation, since the contribution of the composite in the longitudinal direction to the torsional strength was small as discussed in Section 3.2.3.

3.4 LONGITUDINAL ELONGATION RESPONSE

The longitudinal elongation of all beams is shown in Figure 17. As expected, all beams elongated longitudinally after reaching the cracking torsional moment due to the formation and widening of concrete cracks. The elongation values measured at the peak torsional moment and at the normalized peak torsional moment of the control beam are summarized in Table 6.

The largest values of elongation at the peak torsional moment occurred in beams N-P-4-S-1 and N-P-4-C-2 (0.21 in. [5.4 mm] for both beams). In real structures, and especially monolithic concrete construction, this elongation may be restrained by the supporting members. However, the effects of this elongation (or its restraint) may require additional consideration. Results in Table 6 show that at the peak torsional moment of the control beam, the strengthened beams with a 3-sided wrapping configuration exhibited the same elongation as that of the control beam except for beam N-P-3-45S-1, which failed at torsional moment slightly lower than the control beam. In other words, the presence of the 3-sided jacket did not influence the beam elongation. For beams with a 4-sided wrapping configuration, the beam elongation at the torsional moment

corresponding to the peak torsional moment of the control beam reduced by 18-92% relative to that of the control beam. This reduction is due to the concrete crack arresting capability of the fibers, which prevented the beams from elongating at the early loading stages.

4. EFFECT OF FIBER ORIENTATION

As discussed in Section 1, most experimental work on torsional strengthening of RC beams with externally bonded composites reported in the literature is with beams that are wrapped with a fiber orientation of 90°. Few studies have investigated the effects of different composite fiber orientations. In this section, the effect of composite fiber orientation on the torsional strength is examined. Results of beams strengthened with FRCM composites from the current study are compared with those from experimental studies by Panchacharam and Belarbi [25] and Ghobarah et al. [26], who studied the torsional response of RC beams strengthened with GFRP and CFRP composites. Beams selected from those studies and from the current study for the comparison are from series in which the parameter varied was fiber orientation. The selected beams, strengthening configurations, and experimental results are summarized in Table 7.

Figure 18 shows the increase in torsional strength relative to the corresponding unstrengthened beam for strengthened beams with different fiber orientations, where the different series are indicated with different markers. It should be noted that the values of torsional strength increase are not comparable among the different series due to different geometrical and material properties of the beams and strengthening systems, as well as different strengthening configurations. Comparing the results of beams strengthened with

0° and 90° fiber orientations, Figure 18 shows that the trend for PBO-FRCM composite-strengthened beams is the same as for GFRP-strengthened beams, i.e., the 90° fiber orientation is more effective in increasing the torsional strength than the 0° orientation. On the other hand, comparing the results of beams strengthened with 45° and 90° fiber orientations, Figure 18 shows that the 45° fiber orientation is more effective than the 90° orientation for CFRP-strengthened beams, while PBO-FRCM composite-strengthened beams exhibit the opposite trend. As discussed in Section 3.2.3, the 45° fiber orientation should be more effective than the 90° orientation since the inclined fibers are generally perpendicular to the diagonal cracks [26]. However, the contribution of the PBO-FRCM composite to the torsional strength was much lower for the beam with 45° strips (N-P-4-45S-1) than the beam with 90° strips (N-P-4-S-1) due to the debonding of the composite from the concrete substrate at the end of the strip, which occurred since the fiber sheets were effectively unanchored at the ends of the test region. As discussed in Section 2.2, a length of approximately 10 in. (260 mm) is needed to fully develop the load-carrying capacity of the PBO-FRCM concrete interface (Section 2.2), however considering a 45° crack orientation and the geometry of the beam, the available length beyond the crack may be considerably less (see Figure 12b, for example). Therefore, this condition contrasted the potential benefits from optimizing the fiber orientation and led to the underutilization of the composite. This observation emphasizes the need for suitable anchorage systems for beams strengthened with PBO-FRCM composite without adequate overlap at the ends of the fiber sheets (in the fiber direction).

5. CONCLUSIONS

This paper discussed the influence of the fiber orientation, fiber continuity, and number of composite layers on the torsional strength, torsional moment-twist per unit length response, and mode of failure of PBO-FRCM strengthened concrete beams subjected to pure torsion. Strains measured in the internal and external reinforcement and the beam elongation with respect to the beam longitudinal axis were evaluated. Furthermore, the efficiency the PBO-FRCM composite material was compared with that of CFRP and GFRP composites from studies in the literature. The main conclusions from this study are summarized below:

1. The normalized cracking torsional moment of all strengthened beams was larger than that of the unstrengthened beam, with a maximum increase of 58%. The maximum increase in the normalized peak torsional moment relative to control beam was 109%. These results indicate that PBO-FRCM composite can be a suitable material for torsional strengthening of RC beams.
2. The normalized cracking torsional moment of the beam with one layer of fibers with 4-sided 0° fiber orientation (parallel to the longitudinal axis of the beam) was increased relative to that of the control beam, while no significant increase in the normalized peak torsional moment was observed. However, the normalized cracking and peak torsional moments were improved significantly for beams with 4-sided, 90° fiber orientation.

3. No significant increase in normalized cracking or peak torsional moment was achieved for beams with 3-sided wrapping configuration, regardless of fiber orientation or wrapping configuration.
4. Concrete crushing governed the failure of the unstrengthened control beam and the strengthened beams with 3-sided wrapping configurations. Fiber rupture followed by concrete crushing and preceded by stirrup yielding governed the failure for beams strengthened with 1-layer, 4-sided, 90° fiber orientation and the beam strengthened with 2-layers, 4-sided, 90° fiber orientation.
5. Debonding of the fibers from the concrete substrate governed the failure of the strengthened beams with 4-sided, 45° strips, the strengthened beam with 4-sided, 0° continuous wrapping, and the strengthened beam with two layers (0°/90°) fiber orientation.
6. The FRCM composite reduced the longitudinal elongation of the strengthened beams up to 92% compared to the control beam at the peak load of the control beam.
7. Similar to GFRP-strengthened beams, the 90° fiber orientation was more effective in increasing the torsional strength than the 0° orientation for PBO-FRCM strengthened beams. On the other hand, the 45° fiber orientation was more effective than the 90° orientation for CFRP-strengthened beams, while PBO-FRCM composite-strengthened beams exhibited the opposite trend. Debonding of the PBO-FRCM composite fibers at the ends of the strips contrasted the potential benefits from optimizing the fiber orientation and led to the underutilization of the composite.

8. Further investigations are needed to select a suitable anchorage system for beams strengthened with PBO-FRCM composite without overlap at the ends of the fiber sheets.

ACKNOWLEDGEMENTS

The experimental work discussed in this paper was conducted at Missouri University of Science and Technology (Missouri S&T). Ruredil S.p.A. of San Donato Milanese, Italy, is gratefully acknowledged for providing the composite materials. The authors would also like to acknowledge Mr. Zuhair Al Jaberi for his assistance with the experimental work.

FUNDING

Funding for this work was provided by the Higher Committee for Education Development in Iraq (HCED).

Table 1. Concrete mixture proportions.

Material	Quantity
Water, lb/yd^3 (kg/m^3)	270 (160)
Cement Type I/II, lb/yd^3 (kg/m^3)	517 (307)
Coarse Aggregate, lb/yd^3 (kg/m^3)	1700 (1009)
Fine Aggregate, lb/yd^3 (kg/m^3)	1450 (860)

Table 2. Measured concrete and steel reinforcement material properties.

Material	Concrete		Steel reinforcing bars	
	Batch 1	Batch 2	No. 3	No. 5
Compressive strength, psi (MPa)	5700 (39.3)	5000 (34.5)	--	--
Splitting tensile strength, psi (MPa)	460 (3.2)	400 (2.8)	--	--
Modulus of elasticity ksi (GPa)	4150 (28.6)	4150 (28.6)	29000 (200)	28000 (193)
Yield strength, ksi (MPa)	--	--	65.8 (454)	68.0 (469)
Ultimate strength, ksi (MPa)	--	--	104 (717)	107 (738)

Table 3. Measured PBO-FRCM composite material properties.

PBO fibers		
Ultimate tensile strength, ksi (MPa)	440 (3015)	
Modulus of elasticity, ksi (GPa)	29,900 (206)	
Ultimate strain, in./in. (mm/mm)	0.0145 (0.0145)	
Mortar		
	Batch 1	Batch 2
Compressive strength, psi (MPa)	3600 (24.8)	2200 (15.2)
Splitting tensile strength, psi (MPa)	670 (4.6)	520 (3.6)

Table 4. Summary of test results.

Beam	Concrete batch and composite matrix batch	T_{cr} k-in. (kN-m)	$\widetilde{T_{cr}}$ k-in. (kN-m)	$\frac{\widetilde{T_{cr}}}{\widetilde{T_{cr,control}}}$	ψ_{cr} deg./in. (deg./m)	$\frac{\psi_{cr}}{\psi_{cr,control}}$	T_u k-in. (kN-m)	$\widetilde{T_u}$ k-in. (kN-m)	$\frac{\widetilde{T_u}}{\widetilde{T_{u,control}}}$	ψ_u deg./in. (deg./m)	$\frac{\psi_u}{\psi_{u,control}}$
Control	1	91.8 (10.4)	88.9 (10.0)	--	0.0042 (0.165)	--	148.7 (16.8)	144.0 (16.4)	--	0.085 (3.346)	--
N-P-3-S-1	1	102.3 (11.6)	99.1 (11.2)	1.11	0.0020 (0.079)	0.48	160.3 (18.1)	155.3 (17.5)	1.08	0.076 (2.992)	0.89
N-P-3-45S-1	2	90.6 (10.2)	93.7 (10.6)	1.05	0.0049 (0.193)	1.17	134.5 (15.2)	139.1 (15.7)	0.97	0.065 (2.559)	0.76
N-P-3-C-1	2	97.3 (11.0)	100.7 (11.4)	1.14	0.0027 (0.106)	0.64	140.3 (15.9)	145.1 (16.4)	1.01	0.068 (2.677)	0.8
N-P-4-S-1	1	126.5 (14.3)	122.5 (13.8)	1.38	0.0034 (0.134)	0.81	193.2 (21.8)	187.1 (21.1)	1.30	0.245 (9.646)	2.88
N-P-4-45S-1	2	109.6 (12.4)	113.3 (12.8)	1.27	0.0029 (0.114)	0.69	163.7 (18.5)	169.4 (19.1)	1.18	0.074 (2.913)	0.87
N-P-4-8S-1	2	90.0 (10.2)	93.1 (10.5)	1.05	0.0027 (0.106)	0.64	179.1 (20.2)	185.2 (20.9)	1.29	0.227 (8.937)	2.67
N-P-4-0C-1	2	105.3 (11.9)	108.9 (12.3)	1.22	0.0037 (0.146)	0.88	149.9 (16.9)	155.1 (17.5)	1.08	0.053 (2.087)	0.62
N-P-4-C-1	1	121.6 (13.7)	117.8 (13.3)	1.33	0.0041 (0.161)	0.98	240.4 (27.2)	232.9 (26.3)	1.62	0.230 (9.055)	2.71
N-P-4-(0/90)C-2	2	125.5 (14.2)	129.8 (14.7)	1.48	0.0042 (0.165)	1.00	249.3 (28.2)	257.9 (29.1)	1.80	0.223 (8.780)	2.62
N-P-4-C-2	1	144.4 (16.3)	139.9 (15.8)	1.58	0.0040 (0.157)	0.95	310.6 (35.1)	300.9 (34.0)	2.09	0.241 (9.488)	2.84

Note: T_{cr}= cracking torsional moment; $\widetilde{T_{cr}}$= normalized cracking torsional moment; $\widetilde{T_{cr,control}}$= normalized cracking torsional moment of control beam; ψ_{cr}= cracking twist per unit length; $\psi_{cr,control}$= cracking twist per unit length of control beam; T_u= peak torsional moment; $\widetilde{T_u}$= normalized peak torsional moment; $\widetilde{T_{u,control}}$= normalized peak torsional moment of control beam; ψ_u= peak twist per unit length; $\psi_{u,control}$= peak twist per unit length of control beam.

Table 5. Maximum measured reinforcement strains.

	Strains measured at normalized peak torsional moment of control beam, $T_{u,control}^{\sim}$			Strains measured at peak torsional moment T_u		
Beam	ε_t (%)	ε_l (%)	ε_f (%)	ε_t (%)	ε_l (%)	ε_f (%)
Control	0.252	0.165	--	0.252	0.165	--
N-P-3-S-1	0.231	0.140	0.365	0.232	0.183	0.431
N-P-3-45S-1	--	--	--	0.208	0.183	0.367
N-P-3-C-1	0.224	0.444	0.359	0.224	0.537	0.359
N-P-4-S-1	0.050	0.108	0.004	0.295	0.287	1.026
N-P-4-45S-1	0.095	0.111	0.435	0.164	0.177	0.562
N-P-4-8S-1	0.069	0.166	0.000	0.386	0.347	0.506
N-P-4-0C-1	0.162	0.141	0.030	0.192	0.164	0.210
N-P-4-C-1	0.058	0.119	0.026	0.275	0.638	0.822
N-P-4-(0/90)C-2	0.108	0.085	0.012	0.345	0.631	0.848
N-P-4-C-2	0.016	0.104	0.005	0.305	1.137	0.653

Note: $T_{u,control}^{\sim}$= normalized peak torsional moment of control beam; T_u= peak torsional moment; ε_t= strain measured in the internal transverse reinforcement (stirrups); ε_l= strain measured in the internal longitudinal reinforcement; ε_f= strain measured in the externally bonded composite.

Table 6. Beam longitudinal elongation.

Beam	Longitudinal elongation at normalized peak torsional moment of control beam, $T=T_{u,\widetilde{control}}$	% Reduction relative to unstrengthened beam	Longitudinal elongation at $T=T_u$ in. (mm)	% Increase relative to unstrengthened beam (at peak torsional moment)
Control	0.077 (1.96)	--	0.077 (1.96)	--
N-P-3-S-1	0.076 (1.93)	--	0.101 (2.57)	25
N-P-3-45S-1	(Note 1)	--	0.072 (1.83)	--
N-P-3-C-1	0.079 (2.01)	--	0.085 (2.16)	13
N-P-4-S-1	0.063 (1.63)	18	0.213 (5.41)	163
N-P-4-45S-1	0.058 (1.47)	25	0.095 (2.41)	25
N-P-4-8S-1	0.056 (1.42)	27	0.184 (4.67)	125
N-P-4-0C-1	0.058 (1.47)	25	0.070 (1.78)	--
N-P-4-C-1	0.029 (0.74)	62	0.176 (4.47)	125
N-P-4-(0/90)C-2	0.027 (0.69)	65	0.190 (4.83)	138
N-P-4-C-2	0.006 (0.15)	92	0.213 (5.41)	163

Note: 1. Peak torsional moment is lower than that of the control beam.

$T_{u,\widetilde{control}}$= normalized peak torsional moment of control beam; T_u= peak torsional moment.

Table 7. Summary of experimental results of strengthened beams with different fiber orientations from current study, Panchacharam and Belarbi [25], and Ghobarah et al. [26].

Author	Beam	Composite type and wrapping configuration	T_u k-in. (kN-m)	% increase in T_u relative to unstrengthened beam	% change in T_u relative to 90° configuration
Current study	N-P-4-S-1	PBO-FRCM 90° strips	187.1 (21.1)*	30	--
	N-P-4-45S-1	PBO-FRCM 45° strips	169.4 (19.1)*	18	-12
	N-P-4-C-1	PBO-FRCM 90° continuous	232.9 (26.3)*	62	--
	N-P-4-0C-1	PBO-FRCM 0° continuous	155.1 (17.5)*	8	-54
Panchacharam and Belarbi [25]	A90W4	GFRP 90° continuous	398.3 (45)	149	--
	A0L4	GFRP 0° continuous	256.7 (29)	62	-87
Ghobarah et al. [26]	C2	CFRP 90° strips	123.6 (14.0)	27	--
	C6	CFRP 45° strips	148.9 (16.8)	55	28

Note: *Normalized by the factor $\sqrt{\bar{f}_c'/f_c'}$

T_u= peak torsional moment.

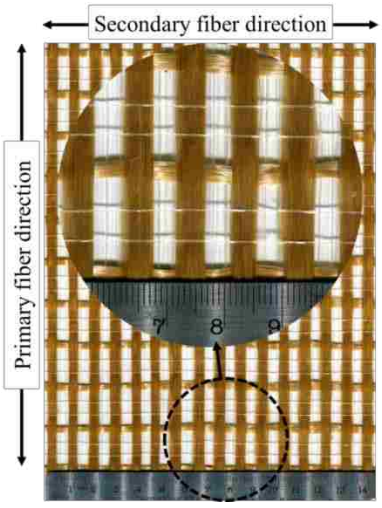

Figure 1. PBO unbalanced fiber net.

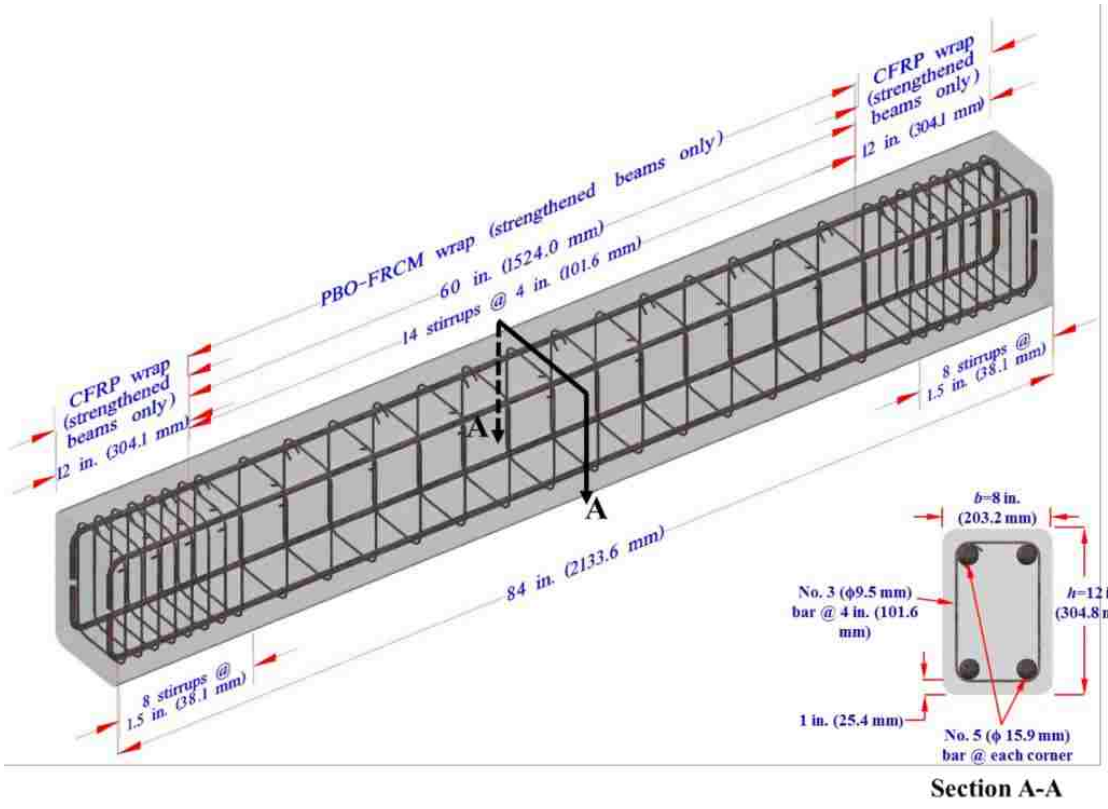

Figure 2. Beam reinforcement layout and dimensions.

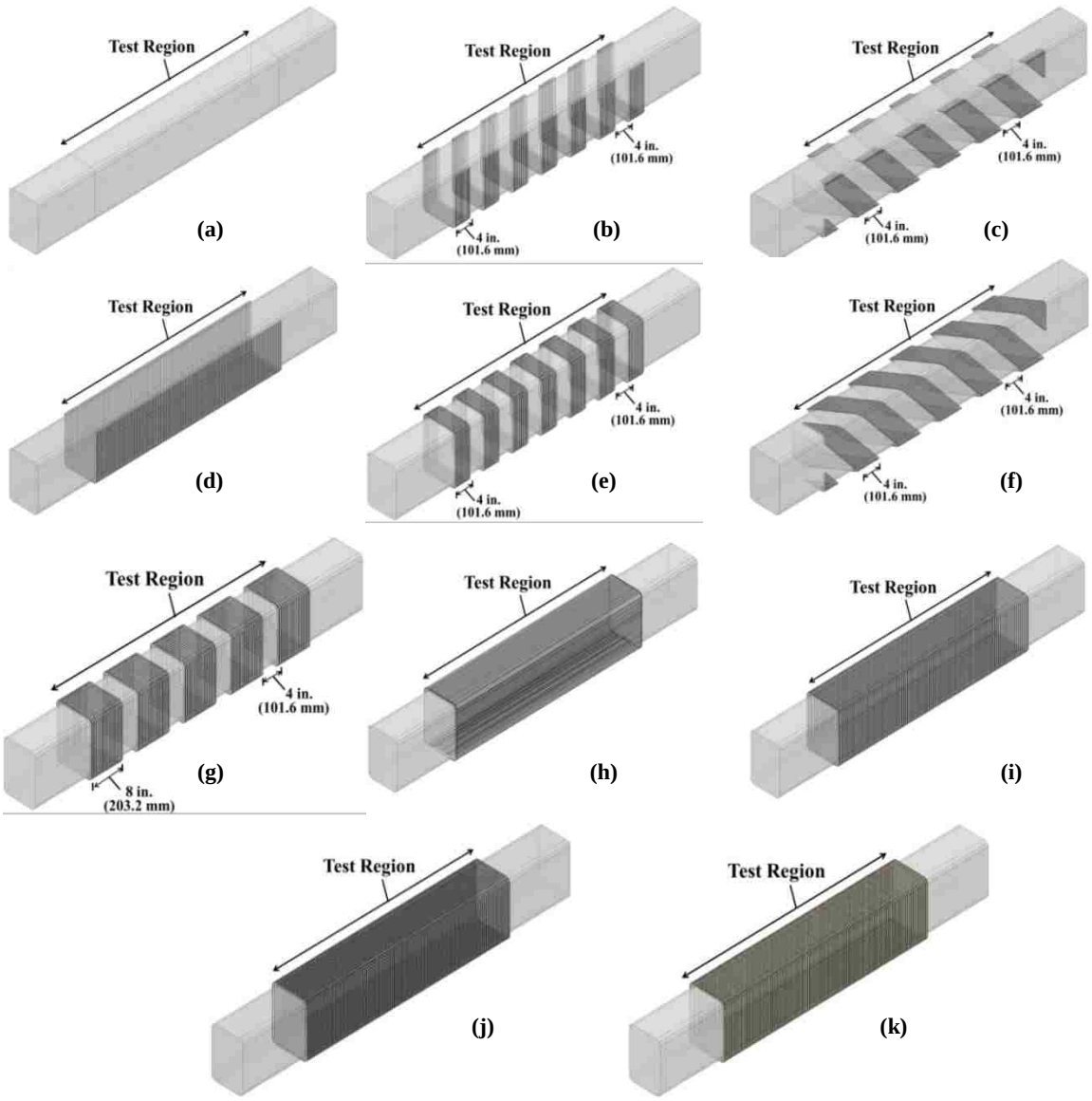

Figure 3. Schematic configuration of the RC beams: a) control beam, b) one layer, 3-sided, 90°, strips (N-P-3-S-1), c) one layer, 3-sided, 45°, strips (N-P-3-45S-1), d) one layer, 3-sided, 90°, continuous (N-P-3-C-1), e) one layer, 4-sided, 90°, strips (N-P-4-S-1), f) one layer, 4-sided, 45°, strips (N-P-4-45S-1), g) one layer, 4-sided, 90°, strips (N-P-4-8S-1), h) one layer, 4-sided, 0°, continuous (N-P-4-0C-1), i) one layer, 4-sided, 90°, continuous (N-P-4-C-1), j) two layers, 4-sided, 0°/90°, continuous (N-P-4-0/90C-2), k) two layers, 4-sided, 90°, continuous (N-P-4-C-2).

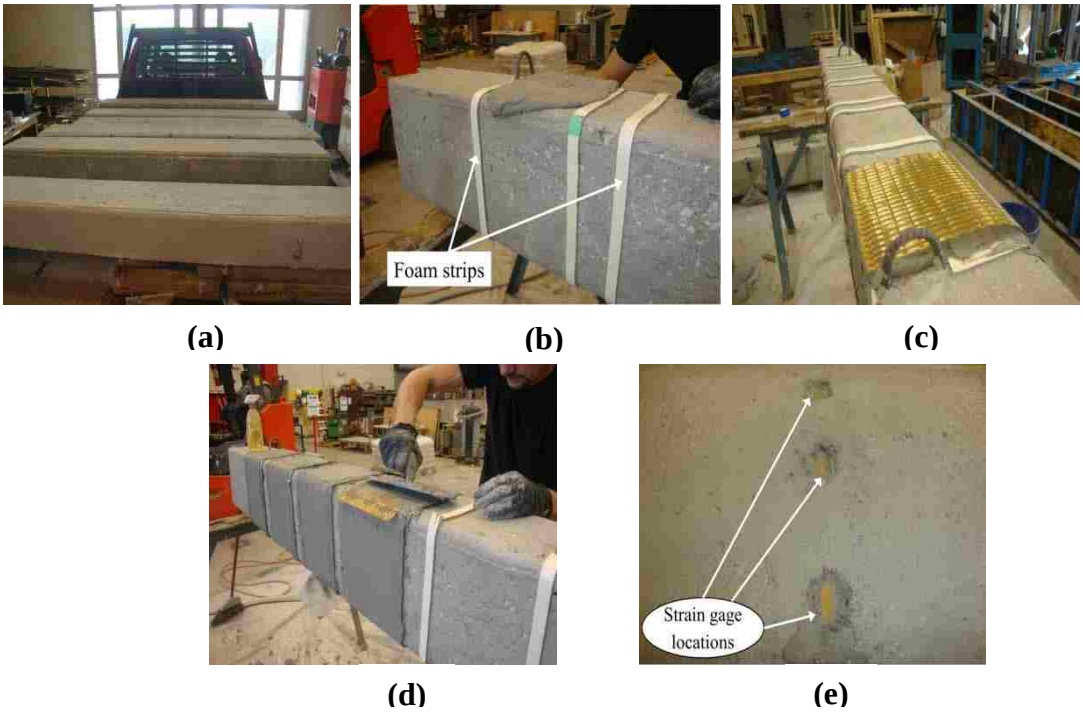

Figure 4. FRCM-composite installation process: a) sand blasted concrete surface, b) adding the first layer of matrix, c) applying the fibers, d) adding the second layer of matrix, e) strain gage locations.

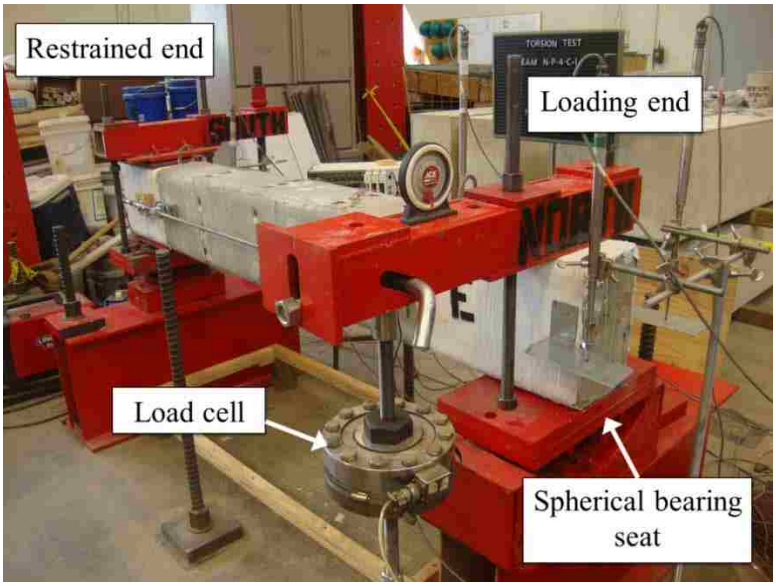

Figure 5. Torsion test setup.

(a) **(b)**

Figure 6. External instrumentation on a) east side, b) west side of the beam.

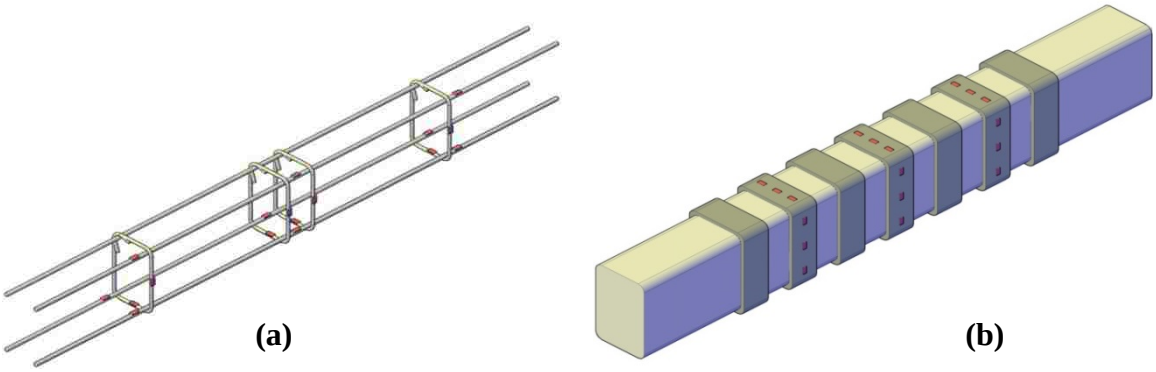

(a) **(b)**

Figure 7. Strain gage locations: a) on the steel reinforcing bars, b) on the PBO-FRCM composite.

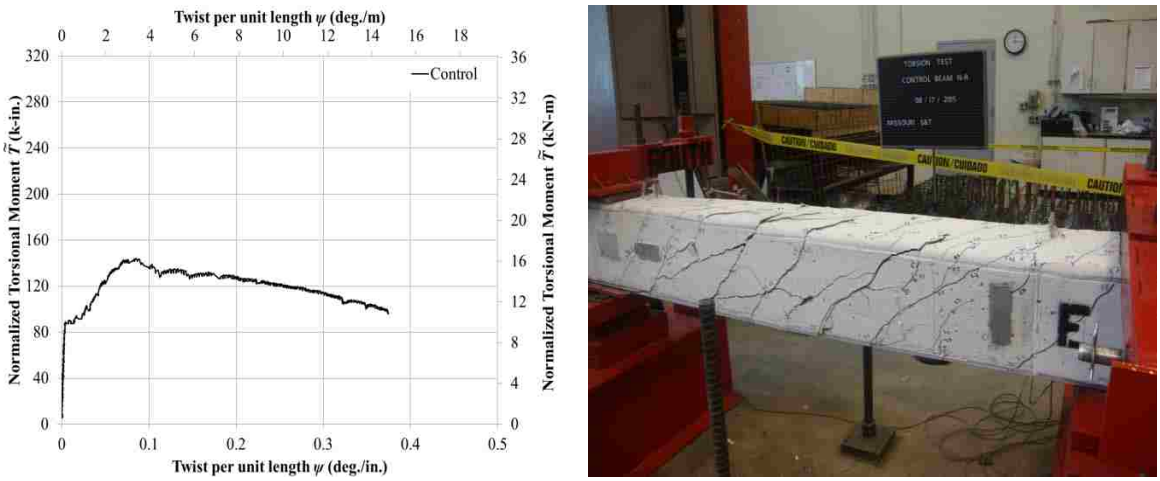

Figure 8. Experimental results for control beam: a) normalized torsional moment $\tilde{T}$-twist per unit length ψ response, b) mode of failure.

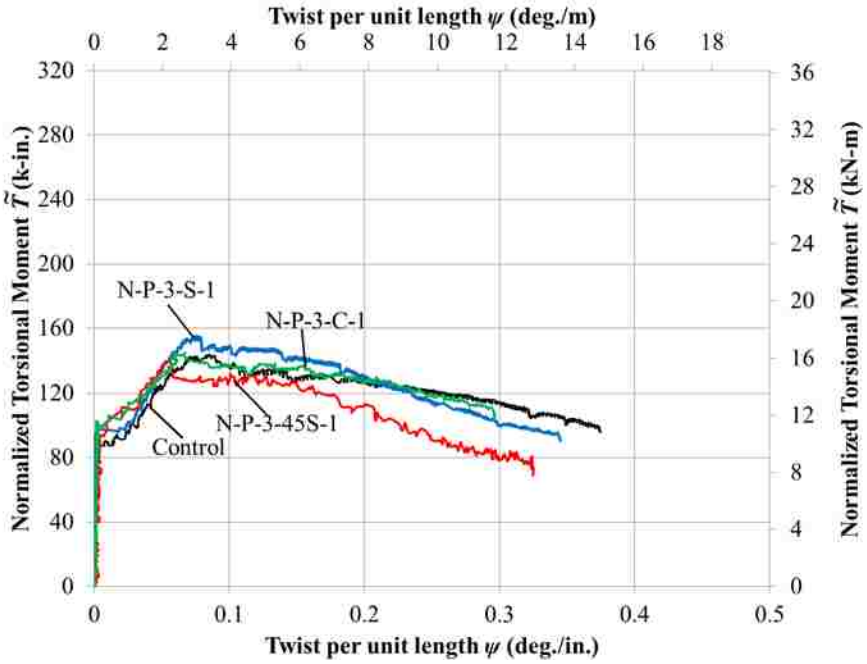

Figure 9. Normalized torsional moment $\tilde{T}$-twist per unit length ψ responses for strengthened beams with 3-sided wrapping configurations.

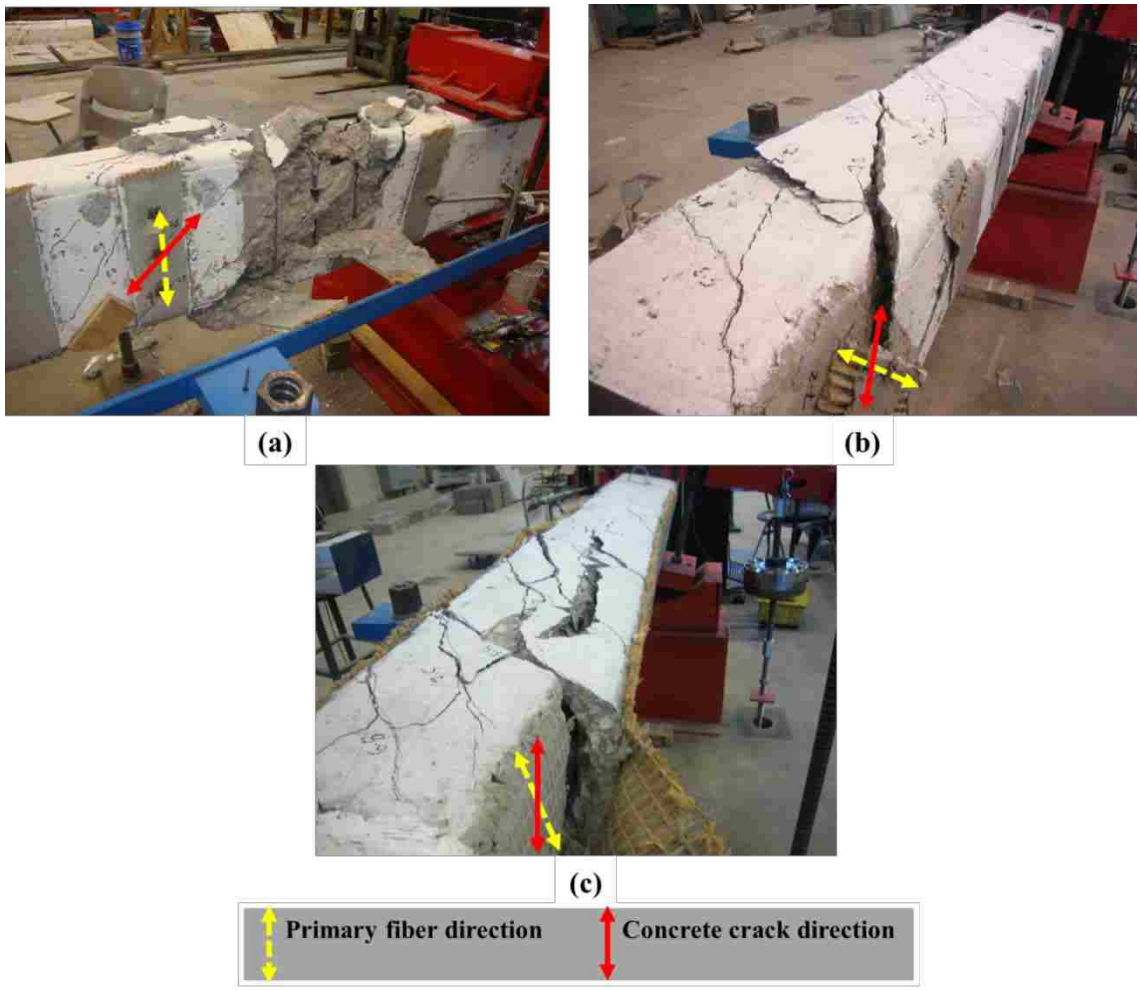

Figure 10. Mode of failure for strengthened beams with 3-sided wrapping configurations: a) N-P-3-S-1, b) N-P-3-45S-1, c) N-P-3-C-1.

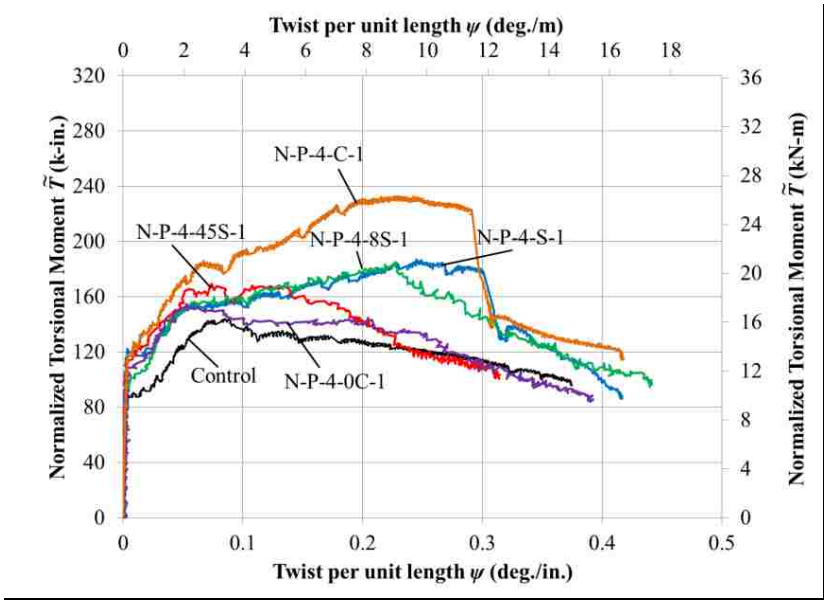

Figure 11. Normalized torsional moment $\tilde{T}$-twist per unit length ψ responses for strengthened beams with 1-layer, 4-sided wrapping configurations.

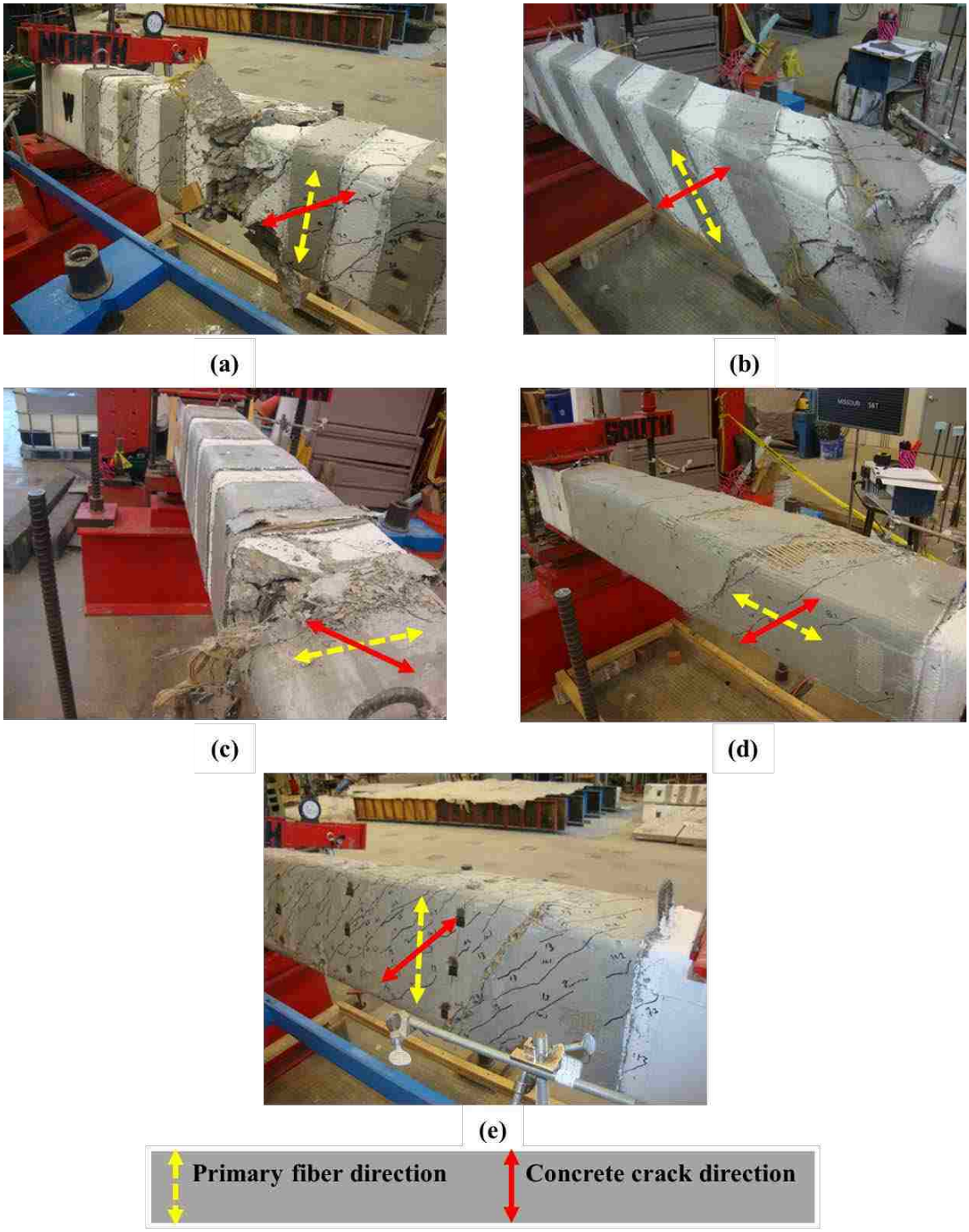

Figure 12. Mode of failure for strengthened beams with 1-layer, 4-sided wrapping configurations: a) N-P-4-S-1, b) N-P-4-45S-1, c) N-P-4-8S-1, d) N-P-4-0C-1, e) N-P-4-C-1.

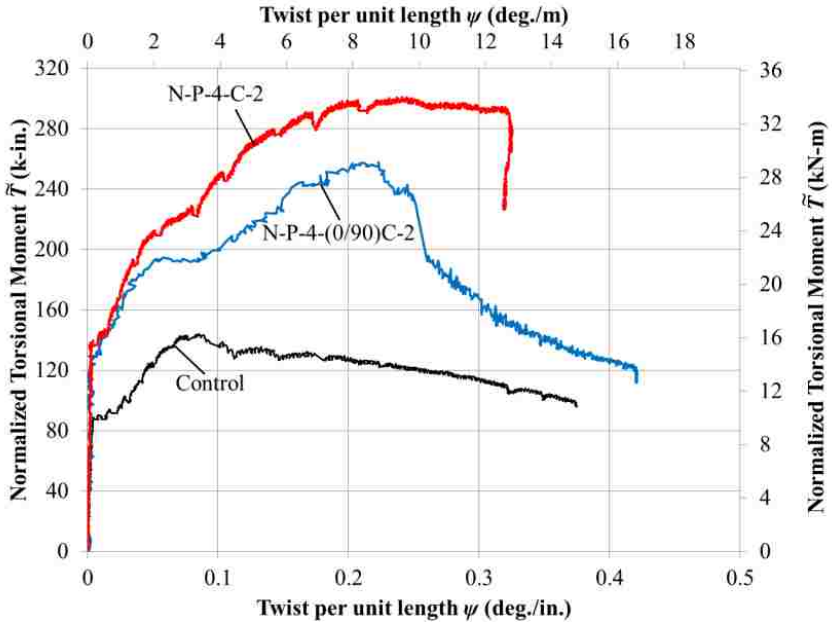

Figure 13. Normalized torsional moment $\tilde{T}$-twist ψ per unit length responses for strengthened beams with 2-layer, 4-sided wrapping configurations.

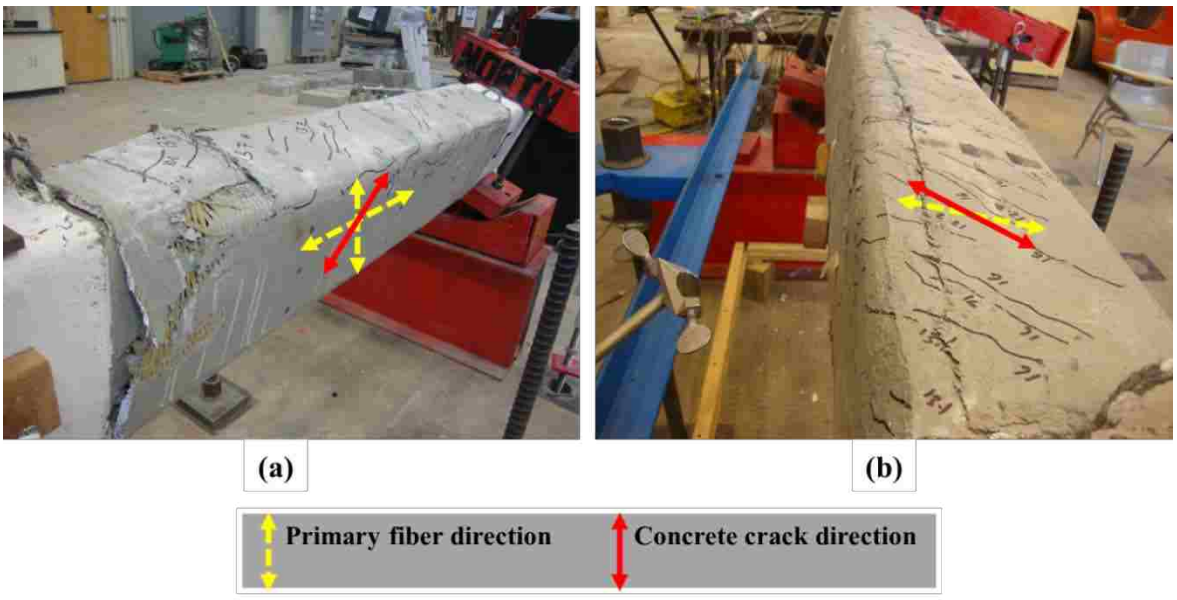

Figure 14. Mode of failure for strengthened beams with 2-layer, 4-sided wrapping configurations: a) N-P-4-0/90C-2, b) N-P-4-C-2.

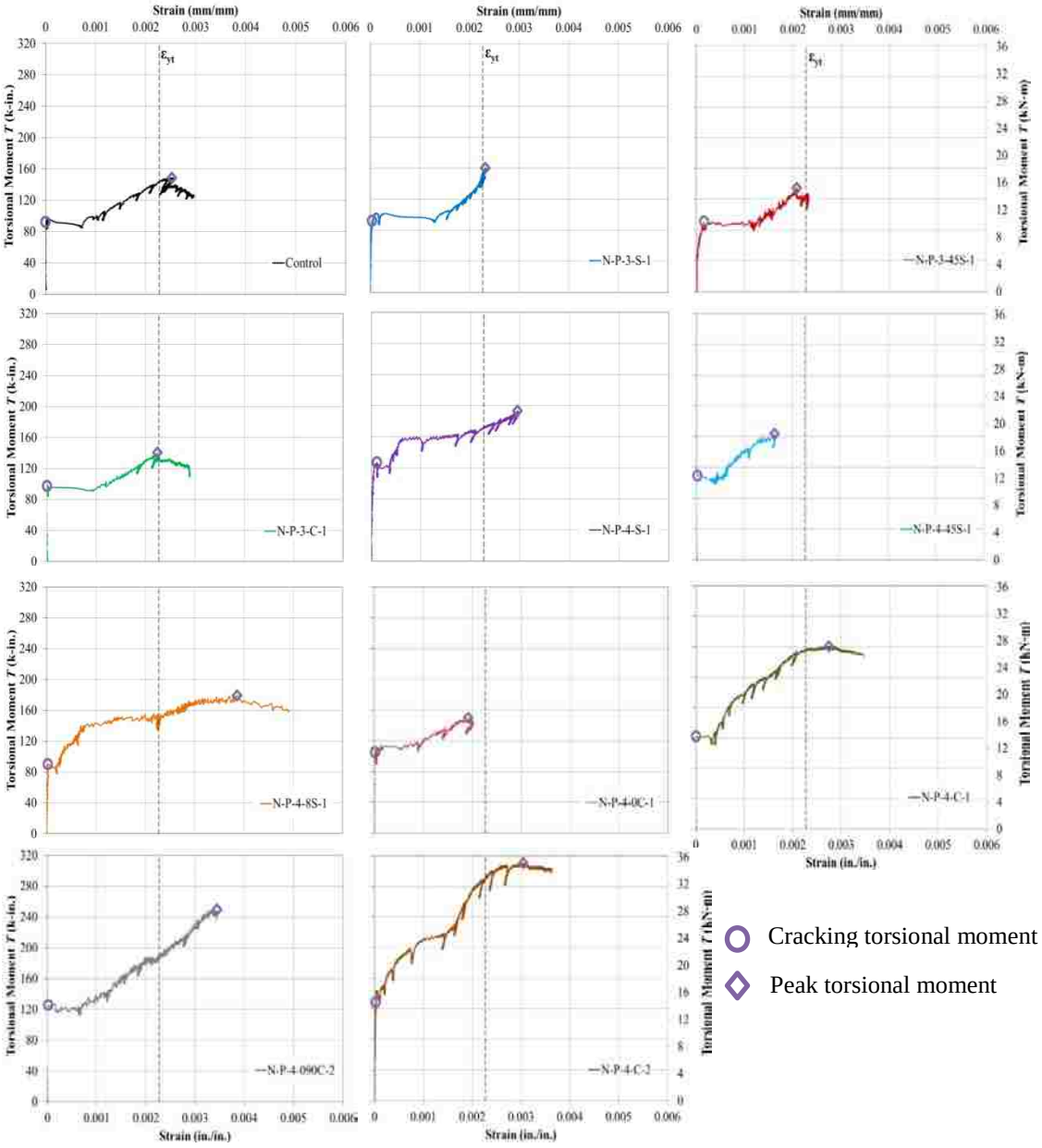

Figure 15. Torsional moment *T* versus stirrup strain.

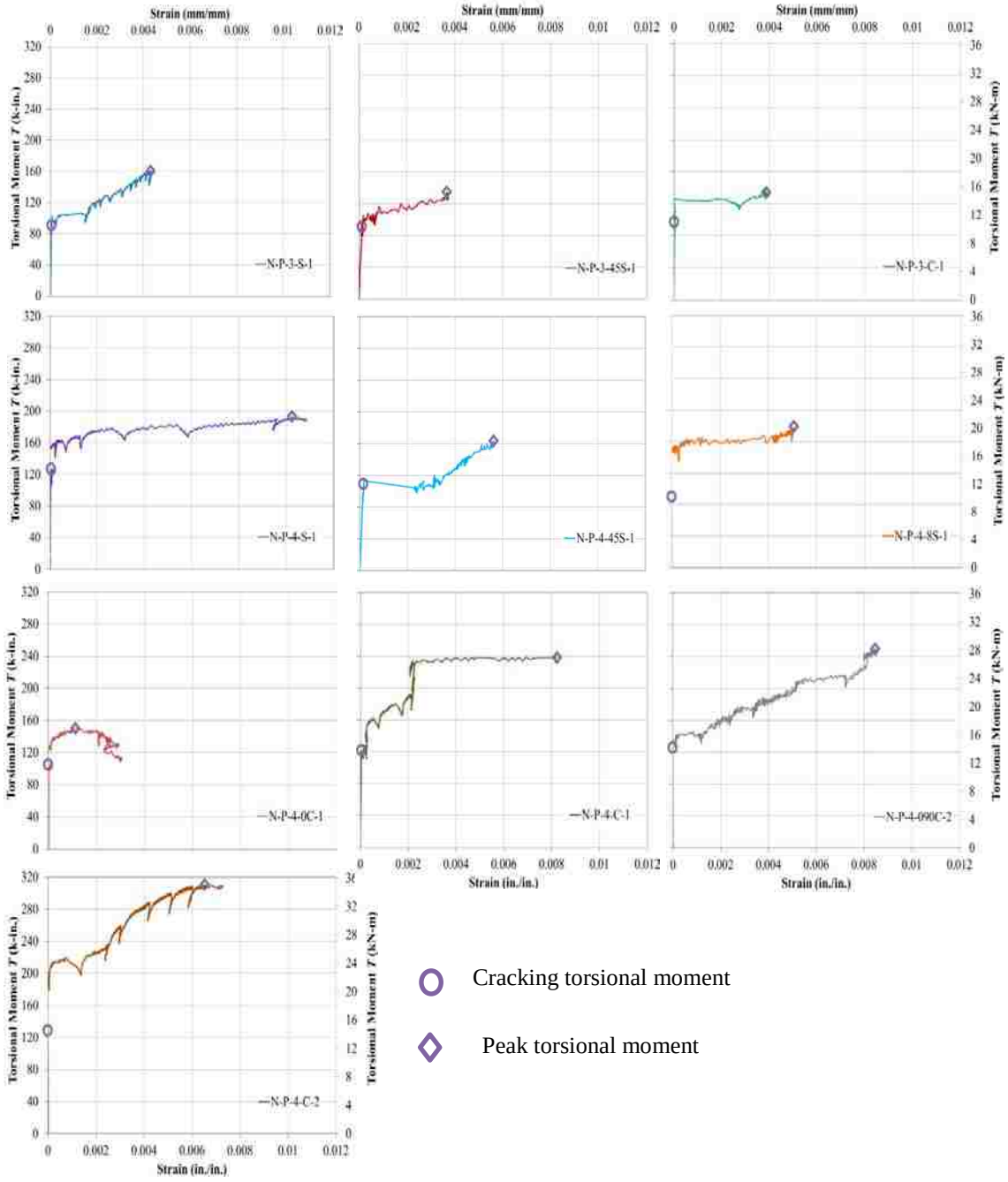

Figure 16. Torsional moment *T* versus FRCM composite fiber strain.

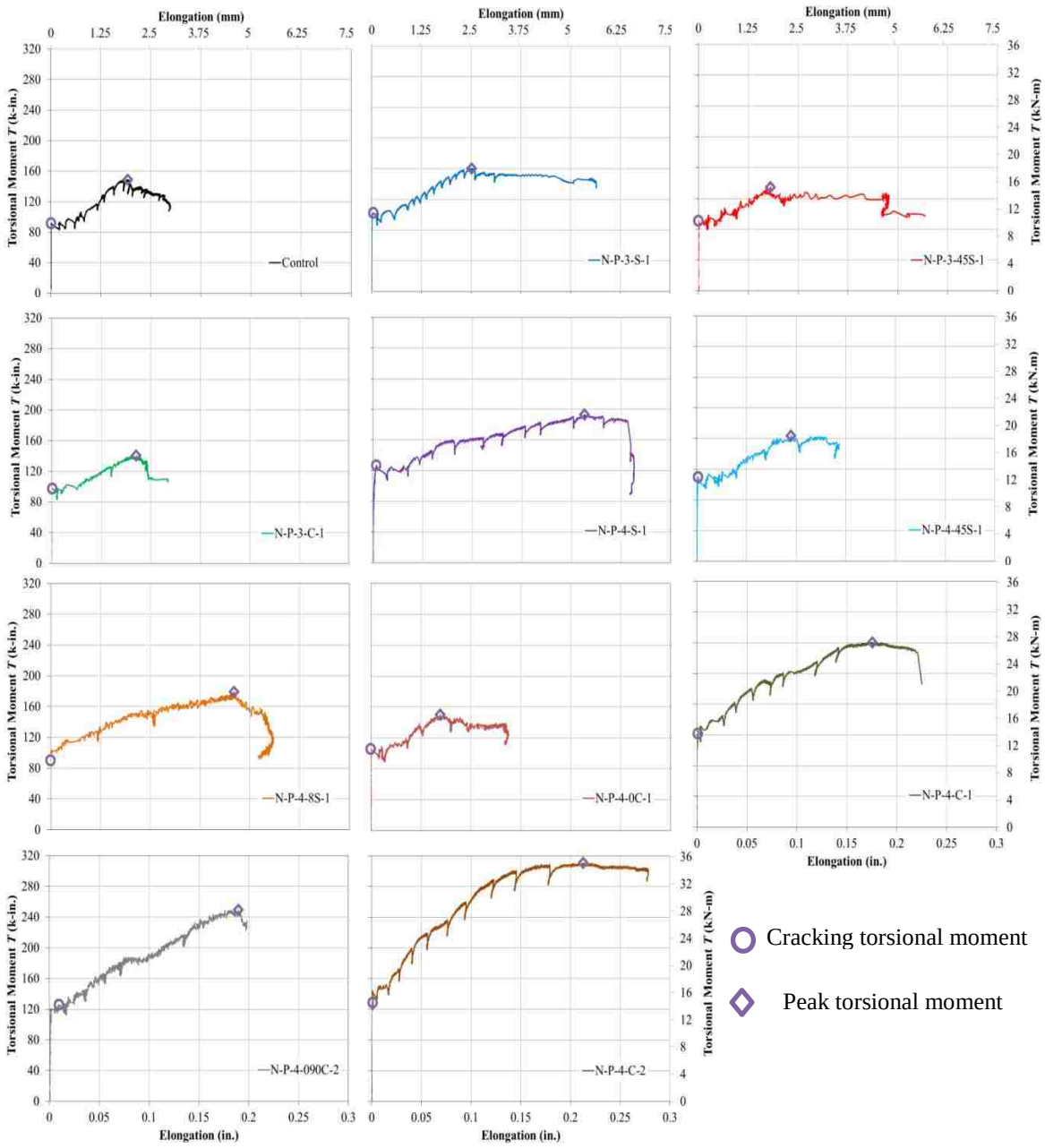

Figure 17. Torsional moment *T* versus longitudinal elongation.

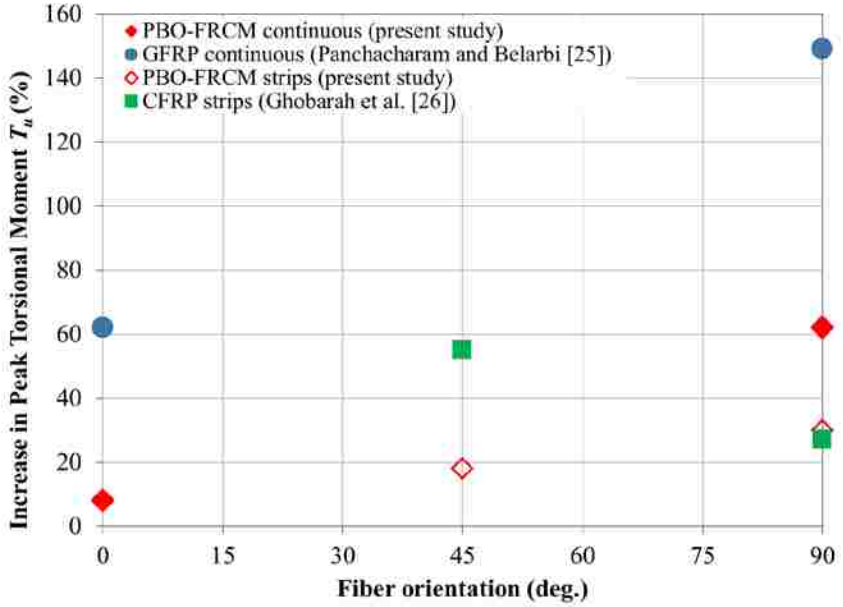

Figure 18. Influence of composite fiber orientation (with respect to the longitudinal axis of the beam) on the increase in torsional strength relative to the unstrengthened condition.

REFERENCES

[1] Bentur, A., & Mindess, S. (2006). *Fibre reinforced cementitious composites*. CRC Press.

[2] Täljsten, B., & Blanksvärd, T. (2008). Strengthening of concrete structures with cement based bonded composites. *Nordic Concrete Research*, *2*(38), 133-153.

[3] Nanni, A. (2012). A new tool for concrete and masonry repair: strengthening with fiber-reinforced cementitious matrix composites. *Concrete international*, *34*(4), 43-49.

[4] Alecci, V., Focacci, F., Rovero, L., Stipo, G., & De Stefano, M. (2016). Extrados strengthening of brick masonry arches with PBO–FRCM composites: Experimental and analytical investigations. *Composite Structures*, *149*, 184-196.

[5] D'Ambrisi, A., & Focacci, F. (2011). Flexural strengthening of RC beams with cement-based composites. Journal of Composites for Construction, 15(5), 707-720.

[6] Ombres, L. (2011). Flexural analysis of reinforced concrete beams strengthened with a cement based high strength composite material. Composite Structures, 94(1), 143-155.

[7] Babaeidarabad, S., Loreto, G., & Nanni, A. (2014). Flexural strengthening of RC beams with an externally bonded fabric-reinforced cementitious matrix. *Journal of Composites for Construction*, 18(5), 04014009.

[8] Sneed, L.H., Verre, S., Carloni, C., & Ombres, L., 2016. "Flexural Behavior of RC Beams Strengthened with Steel-FRCM Composite." *Engineering Structures*, 127, pp. 686-699.

[9] Ombres, L. (2012). Shear capacity of concrete beams strengthened with cement based composite materials. In Proceedings of the 6th International Conference on FRP Composites in Civil Engineering. (CICE 2012). Roma, Italy.

[10] Ombres, L. (2015). Structural performances of reinforced concrete beams strengthened in shear with a cement based fiber composite material. Composite Structures, 122, 316-329.

[11] Trapko, T., Urbańska, D., & Kamiński, M. (2015). Shear strengthening of reinforced concrete beams with PBO-FRCM composites. Composites Part B: Engineering, 80, 63-72.

[12] Loreto, G., Babaeidarabad, S., Leardini, L., & Nanni, A. (2015). RC beams shear-strengthened with fabric-reinforced-cementitious-matrix (FRCM) composite. International Journal of Advanced Structural Engineering (IJASE), 7(4), 341-352.

[13] Aljazaeri, Z. R., & Myers, J. J. (2017). Strengthening of Reinforced-Concrete Beams in Shear with a Fabric-Reinforced Cementitious Matrix. *Journal of Composites for Construction*, *21*(5), 04017041.

[14] Gonzalez-Libreros, J. H., Sabau, C., Sneed, L. H., Pellegrino, C., & Sas, G. (2017). State of research on shear strengthening of RC beams with FRCM composites. *Construction and Building Materials*, *149*, 444-458.

[15] Gonzalez-Libreros, J. H., Sneed, L. H., D'Antino, T., & Pellegrino, C. (2017). Behavior of RC beams strengthened in shear with FRP and FRCM composites. *Engineering Structures*, *150*, 830-842.

[16] Colajanni, P., De Domenico, F., Recupero, A., & Spinella, N. (2014). Concrete columns confined with fibre reinforced cementitious mortars: experimentation and modelling. Construction and Building Materials, 52, 375-384.

[17] Carloni, C., Mazzotti, C., Savoia, M., & Subramaniam, K. V. (2014). Confinement of Masonry Columns with PBO FRCM Composites. *Key Engineering Materials*, *624*.

[18] Sneed, L. H., Carloni, C., Baietti, G., & Fraioli, G. (2017). Confinement of Clay Masonry Columns with SRG. In *Key Engineering Materials* (Vol. 747, pp. 350-357). Trans Tech Publications.

[19] Alabdulhady, M. Y., Sneed, L. H., & Carloni, C. (2017). Torsional behavior of RC beams strengthened with PBO-FRCM composite–An experimental study. *Engineering Structures*, *136*, 393-405.

[20] Salom, P. R., Gergely, J., & Young, D. T. (2004). Torsional strengthening of spandrel beams with fiber-reinforced polymer laminates. *Journal of Composites for Construction*, *8*(2), 157-162.

[21] Hii, A. K., & Al-Mahaidi, R. (2006). Experimental investigation on torsional behavior of solid and box-section RC beams strengthened with CFRP using photogrammetry. *Journal of Composites for Construction*, *10*(4), 321-329.

[22] Hii, A. K., & Al-Mahaidi, R. (2006). An experimental and numerical investigation on torsional strengthening of solid and box-section RC beams using CFRP laminates. *Composite Structures*, *75*(1), 213-221.

[23] Ameli, M., Ronagh, H. R., & Dux, P. F. (2007). Behavior of FRP strengthened reinforced concrete beams under torsion. *Journal of Composites for Construction*, *11*(2), 192-200.

[24] Chalioris, C. E. (2008). Torsional strengthening of rectangular and flanged beams using carbon fibre-reinforced-polymers–Experimental study. *Construction and Building Materials*, *22*(1), 21-29.

[25] Panchacharam, S., & Belarbi, A. (2002). Torsional behavior of reinforced concrete beams strengthened with FRP composites. In *First FIB Congress, Osaka, Japan* (Vol. 1, pp. 01-110).

[26] Ghobarah, A., Ghorbel, M. N., & Chidiac, S. E. (2002). Upgrading torsional resistance of reinforced concrete beams using fiber-reinforced polymer. *Journal of Composites for Construction*, *6*(4), 257-263.

[27] Deifalla, A., Awad, A., & Elgarhy, M. (2013). Effectiveness of externally bonded CFRP strips for strengthening flanged beams under torsion: An experimental study. *Engineering Structures*, *56*, 2065-2075.

[28] Standard, A. S. T. M. (2014). C39. Standard test method for compressive strength of cylindrical concrete specimens. *ASTM International*, 7.

[29] Standard, A. S. T. M. (2011). C496/ C496M. Standard test method for splitting tensile strength of cylindrical concrete specimens.

[30] Standard, A. S. T. M. (2011). C469/ C469M. Standard test method for static modulus of elasticity and Poisson's ratio of concrete in compression.

[31] Standard, A. S. T. M. (2015). A615/ A615M, Standard specification for deformed and plain carbon-steel bars for concrete reinforcement.

[32] Standard, A. S. T. M. (2013). A370, Standard test methods and definitions for mechanical testing of steel products.

[33] Ruredil. X Mesh Gold Data Sheet. Ruredil S.p.A. 2012, Milan, Italy. <http://english.ruredil.it/SchedeProdottoENG/RuredilXMeshGOLD_ing_1.pdf>.

[34] D'Antino, T., Sneed, L., Carloni, C., & Pellegrino, C. (2013). Bond behavior of the FRCM-concrete interface. In *Proceedings of the 11th International Symposium on Fiber Reinforced Polymers for Reinforced Concrete Structures,(2013: Guimarães, Portugal)* (10 pp.). Institute for Sustainable an Innovation in Structural Engineering.

[35] Sneed, L. H., D'Antino, T., & Carloni, C. (2014). Investigation of bond behavior of PBO fiber-reinforced cementitious matrix composite-concrete interface. *ACI Materials Journal*, *111*(1-6), 1-12.

[36] ACI Committee, American Concrete Institute, & International Organization for Standardization. (2014). Building code requirements for structural concrete (ACI 318-14) and commentary. American Concrete Institute.

[37] ACI Committee 549, ACI 549.4R-13– Guide to Design and construction of externally bonded fabric-reinforced cementitious matrix (FRCM) systems for repair and strengthening concrete and masonry structures, (2013).

[38] Carloni, C., D'Antino, T., Sneed, L.H., and Pellegrino, C. (2015). "Role of the Matrix Layers in the Stress-Transfer Mechanism of FRCM Composites Bonded to a Concrete Substrate." *Journal of Engineering Mechanics. 141*(6), 04014165.

[39] D'Antino, T., Carloni, C., Sneed, L. H., & Pellegrino, C. (2014). Matrix–fiber bond behavior in PBO FRCM composites: A fracture mechanics approach. *Engineering Fracture Mechanics*, *117*, 94-111.

[40] He, R., Sneed, L.H., and Belarbi, A. (2014). "Torsional Repair of Severely Damaged Column Using Carbon Fiber-Reinforced Polymer." ACI Structural Journal, American Concrete Institute, Farmington Hills, MI, V. 111, No. 3, pp. 705-716.

IV. FINITE ELEMENT STUDY ON THE BEHAVIOR OF RC BEAMS STRENGTHENED WITH PBO-FRCM COMPOSITE UNDER TORSION

Meyyada Y. Alabdulhady, Lesley H. Sneed, Omar I. Abdelkarim, Mohamed A. ElGawady

ABSTRACT

This paper describes the results of numerical simulation performed to investigate the torsional behavior of reinforced concrete (RC) beams strengthened with externally bonded fiber reinforced cementitious matrix (FRCM) composite. A nonlinear finite element analysis was performed using LS-DYNA. FE predictions were in reasonable agreement with experimental results of FRCM-strengthened beams under torsional loading in terms of failure mode, torsional strength, and corresponding twist per unit length. A parametric study was also carried out to study the influence of concrete compressive strength and FRCM composite strip width and spacing. Results showed that the torsional strength increases with increasing concrete compressive strength when failure is governed by crushing of the concrete strut. When failure is governed by fiber rupture, the torsional strength was not sensitive to concrete compressive strength. The parametric study also showed that the torsional strength increases with increasing fiber reinforcement ratio, although the increase in torsional strength is not directly proportional to the increase in fiber reinforcement ratio.

HIGHLIGHTS

- Torsional behavior of RC beams strengthened with PBO-FRCM composite was evaluated numerically.

- Torsional behavior in terms of strength and failure mode was validated with experimental results.
- Strains measured in the stirrups and fibers were evaluated and compared with experimental results.
- The influence of different parameters on the torsional strength and behavior were studied.

KEYWORDS

Finite element analysis; PBO-FRCM composite; parametric study; RC beams; strengthening; torsion.

1. INTRODUCTION

In the past several decades, investigators have explored experimentally and numerically the behavior of reinforced concrete (RC) beams strengthened with externally bonded fiber reinforced polymer (FRP) composite under different loading conditions. While significant efforts have been made to study the response of FRP-strengthened RC members subjected to flexure, shear, and axial loading, fewer studies have focused on the response of members subjected to torsional loading. Ghobarah et al. [1] studied the torsional behavior of rectangular RC beams strengthened with carbon FRP (CFRP) or glass FRP (GFRP) composite. Panchacharam and Belarbi [2] tested GFRP-strengthened RC beams with a square cross-section and proposed equations to calculate the cracking torque and torsional strength of the strengthened beams. Salom et al. [3] studied the effectiveness of CFRP composite on increasing the torsional strength of RC spandrel

beams with an L-shaped cross-section. Hii and Al-Mahaidi [4] used photogrammetry measurements to study the concrete cracking behavior and aggregate interlocking action of CFRP-strengthened RC beams under torsional loading. Hii and Al-Mahaidi [5] tested CFRP-strengthened RC beams with solid and box sections under torsional loading and compared the results with those obtained from the nonlinear finite element program DIANA [6]. Chalioris [7] tested CFRP-strengthened rectangular and flanged RC beams with no internal transverse reinforcement to evaluate the contribution of the composite to the torsional strength. Ameli et al. [8] tested CFRP and GFRP-strengthened RC beams with a rectangular cross-section and compared the results with those obtained from the nonlinear finite element program ANSYS [9]. Deifalla et al. [10] experimentally investigated the effectiveness of CFRP composite on increasing the torsional strength of RC beams with various cross-sectional shapes. Ganganagoudar et al. [11] introduced a modified softened membrane model for torsion, taking into account the influence of externally bonded FRP on the compressive behavior of cracked concrete, and compared the results with those obtained from experiments and a nonlinear finite element study using ABAQUS [12]. Elwan [13] conducted a parametric study on the effects of volumetric ratio of composite, number of composite layers, composite strength, and U-jacket configuration on the torsional behavior of rectangular and T-shaped RC beams using the nonlinear finite element program ANSYS [9]. Other researchers have examined the response of FRP-jacketed RC columns with square, oval, or hollow circular cross-sections subjected to torsional loading [14-18].

While FRP composites have been proven to be effective in different strengthening applications of RC structures, certain characteristics including their difficulty to install

onto wet surfaces or in low temperatures, low fire resistance, low glass transition temperature, and lack of vapor permeability, which are associated with the use of organic matrix, have prompted the development of new innovative composite strengthening materials. One promising material is fiber reinforced cementitious matrix (FRCM) composites. FRCM composites avoid the toxicity of the epoxy resin and overcome some of the aforementioned limitations of using FRP strengthening material. FRCM composite material is comprised of continuous fibers in an inorganic mortar matrix that is more compatible with concrete and masonry substrates, can be applied onto wet surfaces, and has better heat resistance than FRP composites. Because the matrix is a mortar, the resulting thickness of FRCM composites is generally larger than that of FRP composites (on the order of 5 times). Different types of fibers including carbon, glass, aramid, basalt, steel, and polyparaphenylene benzobisoxazole (PBO) have been used in FRCM composites. FRCM composites have been studied for flexural strengthening [e.g., 19-23], shear strengthening [e.g., 24-28], and confinement applications [e.g., 29-30] for RC members, but studies in the technical literature on their use for torsional strengthening are extremely limited [31].

In order to gain a better understanding of the torsional behavior of FRCM-strengthened RC beams, the main objective of this paper is to evaluate numerically the response of PBO-FRCM composite-strengthened RC beams with different strengthening schemes. The simulation is performed with the software program package LS-DYNA 971 R3 [32]. Torsional strength, torque-twist per unit length response, and strains in the internal and external reinforcement are evaluated and compared with experimental results to validate the model and determine its accuracy. The model is further used for a

parametric study in order to shed light on the influence of concrete compressive strength and composite strip width and spacing on the torsional response of FRCM-strengthened RC beams.

2. EXPERIMENTAL PROGRAM

Experimental results of six RC beams subjected to torsional loading were used for model validation. Five of the beams were strengthened, and one beam was unstrengthened and was used as the control specimen. Four of the six beams were included in the first phase of an experimental campaign previously published by the authors [31]. The beams selected from [31] for the purpose of the numerical simulation in this paper included the control beam and strengthened beams that were fully wrapped around the cross-section. Two additional strengthened beams included in this paper were included in the second phase of the experimental campaign, which involved different test variables. The experimental program for both phases is summarized briefly in this section. Additional information is provided in [31].

2.1 EXPERIMENTAL DESIGN

The beams were designed based on the ACI 318 code provisions [33]. All beams had a rectangular cross-section with the same nominal dimensions of b=8 in. (203.2 mm) wide × h=12 in. (304.8 mm) deep × 84 in. (2133.6 mm) long and the same internal reinforcement. Dimensions and reinforcement details of the RC beams are shown in Figure 1. The beams had a test region in which the FRCM composite was applied of length 60 in. (1524.0 mm) that was reinforced with minimum internal steel torsional

reinforcement in the transverse direction in accordance with the ACI 318 code. The corresponding reinforcement ratios of the internal longitudinal and transverse reinforcement were $\rho_{sl} = \frac{A_{sl}}{A_c} = 1.29\%$ and $\rho_{st} = \frac{A_{st}}{A_c}\frac{p_t}{s_t} = 0.92\%$, respectively, where A_{sl} is the total area of longitudinal bars, A_c is the gross concrete area (A_c=bh), A_{st} is area of one leg of a stirrup, p_t is perimeter of a stirrup, and s_t is the center-to-center spacing of stirrups. The end regions of the beam (12 in. [304.8 mm] long each end) were more heavily reinforced internally with stirrups and externally with CFRP composite material (strengthened beams only, see Figure 1) with unidirectional fibers oriented perpendicular to the longitudinal axis of the beam to prevent failure in the clamp regions.

Reinforcing bars in the beam specimens were No. 3 (dia. = 0.375 in. [9.5 mm], area = 0.11 in^2 [71 mm^2]) and No. 5 (dia. = 0.625 in. [15.9 mm], area = 0.31 in^2 [199 mm^2]) ASTM A615 Grade 60 (Grade 420) deformed steel bars [34]. All reinforcing bars of the same size were produced from the same heat. Tension tests were conducted on three samples of each bar size to determine the mechanical properties. Table 1 shows the properties of the longitudinal and transverse reinforcement, which were determined based on the average of three coupon samples for each bar size and tested according to ASTM A370 [35].

The concrete beams were constructed with normalweight concrete cast in two batches: Batch 1 for the phase 1 beams and Batch 2 for the phase 2 beams. The coarse aggregate type was crushed dolomite with 1 in. (25.4 mm) maximum aggregate size, and the fine aggregate was river sand. The compressive strength f'_c, splitting tensile strength f_{ct}, and modulus of elasticity E_c of concrete were determined for each batch based on the average of three 4 in. (101.6 mm) diameter × 8 in. (203.2 mm) long cylinders tested at 28

days in accordance with ASTM C39 [36], ASTM C496 [37], and ASTM C469 [38], respectively. The concrete properties are summarized in Table 1. The beams and cylinders were moist cured for four days under wet burlap then kept together in the laboratory under the same atmospheric conditions until testing.

2.2 FRCM COMPOSITE

The FRCM composite was comprised of PBO fibers with an inorganic matrix. The PBO fibers were in the form of a bidirectional (orthogonal) unbalanced fiber net as shown in Figure 2. The net was formed with rovings spaced at 0.4 in. (10 mm) and 0.8 in. (20 mm) on center in the primary and secondary directions, and the free spacing between rovings was 0.2 in. (5 mm) and 0.6 in. (15 mm), respectively. The nominal thickness of the fibers (which is obtained by assuming the fibers are distributed evenly over the entire width of the composite) in the two fiber directions was 0.0018 in. (0.046 mm) and 0.0005 in. (0.012 mm), respectively. The weight of PBO fibers in the mesh was 0.00010 lb/in^2 (70.4 g/m^2) in the primary direction and 0.000025 lb/in^2 (17.6 g/m^2) in the secondary direction, with a total weight of 0.00013 lb/in^2 (88 g/m^2). The total thickness of the composite was 0.2 in. (5 mm) per composite layer.

The FRCM composite material properties are listed in Table 2. Tensile strength, ultimate strain, and elastic modulus of the fibers determined from tensile tests of the bare fibers were 440 ksi (3015 MPa), 0.0145, and 29,900 ksi (206 GPa), respectively [39]. Compressive strength f'_{cm} and splitting tensile strength of the mortar were determined from a representative sample of matrix used to cast the FRCM composite using the average of three 2 in. (50.8 mm) diameter × 4 in. (101.6 mm) long cylinders tested at 28

days in accordance with ASTM C39 [36] and ASTM C496 [37], respectively. Mortar Batch 1 corresponds to the phase 1 beams, whereas Mortar Batch 2 corresponds to the phase 2 beams.

Different wrapping schemes were used to study the torsional behavior of RC beams strengthened with PBO-FRCM composite. Figure 3a shows the control beam, and Figures 3b-f show the different wrapping schemes of the strengthened beams. All strengthened beams considered in this paper were fully wrapped around the perimeter. Two beams were strengthened with one layer of discontinuous strips, one with w=4 in. (101.6 mm) wide strips with s=4 in. (101.6 mm) clear spacing between strips (beam N-P-4-S-1, Figure 3b), and the other with w=8 in. (203.2 mm) wide strips with s=4 in. (101.6 mm) clear spacing between strips (beam N-P-4-8S-1, Figure 3c) with the fiber net orientated such that the primary fiber direction was perpendicular to the longitudinal axis of the beam. Three other beams were strengthened continuously along the test region. Beam N-P-4-C-1 was strengthened with one layer (Figure 3d), and beam N-P-4-C-2 was strengthened with two layers (Figure 3f), with the fiber net orientated such that the primary fiber direction was perpendicular to the longitudinal axis of the beam. Beam N-P-4-(0/90)C-2 (Figure 3e) was strengthened with two layers of fibers, the first (inner) layer of fibers oriented with the primary fiber direction parallel to the longitudinal axis of the beam (shown in Figure 2), and the second layer of fibers oriented with primary fiber direction perpendicular to the longitudinal axis.

2.3 TEST SETUP AND INSTRUMENTATION

The test setup is shown in Figure 4. The torque was applied to the beam through the loading arm with an 18 in. (457 mm) eccentricity relative to the centroid of the cross-section by a hydraulic jack of 30 k (130 kN) capacity and measured by a load cell of 100 k (445 kN) capacity. The reaction arm was supported by a threaded rod that was anchored to the reaction floor. Rollers were provided at the reaction end of the beam to allow it to slide freely in the longitudinal direction and allow the concrete cracks to open. Secondary bending effects due to the beam self weight and to application of the load were neglected. Restraint of warping due to the clamping effects at each end was also neglected.

The average angle of twist per unit length was measured by a rotational variable differential transformer (RVDT) mounted to the east face of the beam within the test region with gage length of 45.5 in. (1155.7 mm). On the west face of the beam, the twist was determined by measuring the relative vertical displacements using two linear variable differential transformers (LVDTs) with spacing similar to the RVDT gage length. The RVDT and LVDs are shown in Figure 5a.

A total of 17 strain gages were mounted to the longitudinal (9) and transverse (8) bars at the middle, quarter, and third quarter of the test region to measure strain in the internal reinforcement. A total of 36 strain gages were used to measure the strain in the FRCM fibers. The surface of the matrix was carefully abraded at the location of each strain gage in order to expose the fibers, and then the strain gages were mounted onto the fibers. The locations of the strain gages are shown in Figure 5b, c.

3. FINITE ELEMENT MODEL

To study more thoroughly the torsional behavior of RC beams strengthened with PBO-FRCM composite material, a nonlinear finite element analysis was carried out to analyze the experimentally tested beams described in Section 2. The analysis was performed using the finite element package LS-DYNA. The validation was developed in order to verify the accuracy of the finite element procedure. The accuracy of the finite element model was determined by ensuring that the peak torque (i.e., the torsional strength) was reasonably close to the experimental results and that the predicted torsional moment-twist per unit length response followed closely the experimental response.

3.1 MODEL GEOMETRY

The modeled beam in LS-DYNA is shown in Figure 6. Model parameters, including mesh size and contact element type, were investigated through a sensitivity analysis in order to obtain the most accurate results as compared with the experimental values and to minimize the computational effort. Elements with 2 in. (50 mm) size in three directions x, y, and z (beam length, width, and depth, respectively, see Figure 6) were chosen. Concrete, steel plates, and the FRCM composite internal matrix layer were modeled using 8-nodes solid elements with constant stress element formulation. Steel reinforcing bars in the beam longitudinal and transverse directions were modeled using 2 nodes beam-elements. PBO and carbon fibers were modeled as shell elements with 4 nodes Belytschko-Tsay element formulation [40]. The solid elements for the model are based on a linear shape function using one point integration and hourglass control, which has the lowest time cost [41]. Hourglass type 5 was used with a default hourglass

coefficient of 0.1 to maintain modal stability. The Lagrange_In_Solid constraint command was used to tie steel/concrete interfaces with perfect bond, while merge command nodes (i.e., perfect bond) were used to connect the other elements. The modeled beam components are shown in Figure 7.

3.2 MATERIAL MODELS

Plasticity based material model type MAT_CONCRETE_DAMAGE_REL3 [42] was used to model both the concrete of the beam and the matrix of the FRCM composite. This material is a three-invariant model as shown in Figure 8a in which $\Delta\sigma$ is the stress difference which limits the second invariant of the deviatoric stress tensor, p is the pressure (i.e., normal stress, positive in compression), and ξ is the ratio of the tensile to compressive meridian [43]. The model uses three shear failure surfaces (the initial yield surface, the maximum yield surface, and the residual yield surface) and includes damage effects. This material model can account for important features of concrete such as tensile fracture energy, effect of confinement, and shear dilation [43]. A summary of the model and its development can be found in [44]. A key feature of this model is that model parameters can be generated solely from the unconfined compressive strength of concrete [43]. Accordingly, the constitutive material parameters were automatically generated using the measured values of the unconfined concrete and matrix compressive strength, f'_c and $f'_{cm,}$ presented in Tables 1 and 2, respectively. The fractional dilatancy ω, which takes into consideration the association rules [45], was set equal to 0.65 for all beams.

Steel reinforcing bars were modeled using material model type MAT_PLASTIC_KINEMATIC [42]. This material is suited to model isotropic and kinematic hardening plasticity. The parameters needed are the modulus of elasticity *E*, poisson's ratio PR, yield stress SIGY, and tangent modulus ETAN. The modulus of elasticity and yield strength are listed in Table 1. PR was set equal to 0.3, and ETAN was taken as 10% of the *E* value. The material behavior is shown in Figure 8b in which l_0 and *l* are the undeformed and deformed lengths of a uniaxial tension specimen respectively.

To model the PBO FRCM composite fibers, only the fibers in the primary fiber direction were considered. Material MAT_ORTHOTROPIC_ELASTIC type 2 [42] was used for both PBO and carbon fibers. This material is valid for modeling the elastic-orthotropic behavior of solids, shells, and thick shells. The main parameters needed in this model are *E*, PR, and shear modulus *G* in three orthogonal directions, and fiber direction is defined by a vector. The properties of fibers are listed in Table 3, and the material behavior is shown in Figure 8c. Due to numerical instability with the small shell thickness, a slightly larger fiber thickness t_f^* was used. To avoid altering the structural behavior of the beams, the stiffnesses of the fibers were kept the same by introducing reduced modulus E^* and G^*, where E^* and G^* in Table 3 can be calculated using Equation 1:

$$(E \ or \ G)^* = \frac{(E \ or \ G) \times t_f}{t_f^*} \quad (1)$$

Material MAT_ELASTIC type 1 [42] was used to model the steel plates at the restrained end of the beam and the loading arm in order to prevent a stress concentration problem. The parameters needed in this model are *E* and PR. In order to ensure that the

steel plates and arm would remain elastic, a large value of *E* was used. PR was set equal to 0.3.

3.3 LOADING STRATEGY AND BOUNDARY CONDITIONS

The load was applied at the same location as in the experiments (Section 2.3) using explicit time integration algorithms. This type of solution method is faster and requires lower storage space than the implicit method. The explicit analysis is an iterative process that solves the incremental procedure by updating the stiffness matrix at the end of each increment of load based on changes in geometry and material. Accordingly, convergence problems do not occur at the peak load for nonlinear material models.

Steel plates with 1 in. (25 mm) thickness were added at the support locations in order to avoid stress concentration problems. The nodes at the restrained end of the beam were prevented from translation and rotation in all directions, except the beam displacement in the axial direction was allowed for elongation to simulate the boundary conditions used in the experimental work. At the other end (loading end), the beam was free to rotate around the x-axis as in Figure 6, with no other actions.

4. RESULTS

4.1 TORQUE-TWIST PER UNIT LENGTH RESPONSE

The experimental and FE load responses of each beam are shown in Figure 9. Values of the torque and angle of twist per unit length in the simulation were determined in the same way as in the experimental program. The post-peak region of the experimental and FE responses are plotted until the torque reduced by 20% with respect

to the peak value. Figure 9 shows that the initial torsional stiffness of all beams was well predicted by the FE model, and then the beam suffered an increase in the twist angle without increasing of torque due to redistribution of forces from the concrete to the steel reinforcement. After this stage, the behavior became non-linear up to the peak torque T_u (i.e., the torsional strength). Although the FE load responses deviate from the experimental load responses after cracking of concrete, they are in reasonable agreement in terms of determining the peak torque. Similar limitations have also been reported with FE models of FRP-strengthened beams under torsional loading [5,8,11],

Values of T_u and the corresponding angle of twist per unit length ψ_u for each beam are summarized in Table 4. Results in Table 4 show that the model was able to predict the peak torque with an error in the range of 1-18%. Regarding values of ψ_u, most beams had an acceptable error ranging from 8-20% with the exception of beam N-P-4-C-2, for which the error was 32%. It is possible that differential slippage of the two fiber layers delayed the fiber rupture in the experiment, and this slippage was not considered in the FE model. Figure 9 shows that the model was also able to predict the ultimate torque and corresponding angle of twist per unit length, considered herein as the terminal values of the load responses as discussed previously, reasonably well.

4.2 MODE OF FAILURE

The mode of failure predicted by the FE model was examined for each beam and compared with the experimental results to ensure the model accuracy. Figure 10 compares the damage to each beam at failure observed in the experiments and the FE results. For the FE results, the failure is depicted by the distribution of the effective

plastic strain (damage) in the concrete and the 1st principle strain (tensile strain) in the fibers at the peak torque. The color of the fringe for the effective plastic strain is an indicator of the level of damage which is scaled between 0 and 2 based on the three failure surfaces. The values from 0 to 1 indicate the material transitions from the yield failure surface to the maximum failure surface, and values from 1 to 2 indicate the material transitions from the maximum failure surface to the residual failure surface [42].

In the experimental program, the control beam exhibited typical RC torsional behavior with the formation of continuous spiral diagonal cracks around the cross section, followed by yielding of the stirrup near the restrained end and crushing of the concrete strut. The same mode of failure was observed with the modeled control beam (Figure 10a), which failed due to yielding of the transverse reinforcement near the loading arm followed by concrete crushing.

Regarding the strengthened beams, in the experiments, the beams that were strengthened with PBO-FRCM composite failed due to fiber rupture at the beam corners followed by concrete crushing except for beam N-P-4-(0/90)C-2, which failed due to premature debonding of the inner layer of composite (at the restrained end zone). The location of the failure with respect to the beam length was near the loading zone for beam N-P-4-8S-1, in the middle of the test region for beam N-P-4-S-1, and along the entire test region for beam N-P-4-C-2. The mode of failure predicted by the FE model for all strengthened beams was fiber rupture at the beam corners preceded by concrete and matrix cracking and followed by concrete crushing (Figures 10b, c, d and f), which was consistent with the experimental results except for beam N-P-4-(0/90)C-2 (Figure 10e). The location of the failure for all modeled beams was at the loading zone (the area with

the higher stresses due to the applied load). Furthermore, Figures 10b-f show that the effective plastic strain in the concrete for the strengthened beams was distributed along the entire test region, while in the case of the control beam, the effective plastic strain in the concrete was nonuniform along the test region (Figure 10a). These results indicate that the strengthening system provides a better utilization of the concrete strength due to confinement. This observation was also reported in the experimental program [31].

4.3 STRAINS IN INTERNAL REINFORCEMENT AND COMPOSITE FIBERS

The maximum values of strain at the peak torque in the transverse reinforcing bars ε_t and FRCM composite fibers ε_f determined by the experiments and FE results are summarized in Table 5. Reasonable agreement was achieved between the experimental and FE results.

The experimental and FE torque versus strain responses at the midlength of beams N-P-4-S-1, N-P-4-C-1, and N-P-4-C-2 are shown in Figure 11. (For the sake of brevity, three strengthened beams were selected for illustration herein and are representative of all strengthened beams in this study.) Values of strain plotted from the experiments correspond to the strain gage at the midlength of the beam that measured the maximum strain at the peak torque in order to compare FE and experimental values at the same location. The FE model was able to predict the same behavior as in the experimental results, that is, a linear response up to the cracking torque followed by a nonlinear trend up to the peak torque.

Internal reinforcement strains at the peak torque predicted by the FE model at different locations of each beam were investigated to gain a better understanding of the

yielding zone. Generally, the model showed that the stirrups yielded within the vicinity of the loading end, while the longitudinal reinforcement yielded near the restrained end. These locations are consistent with the experimental results except for beam N-P-4-(0/90)C-2. In the experimentally tested beam, the yielded stirrups were located at the midlength and at the restrained end due to debonding of the internal layer of composite at the restrained end, which prevented the stresses from distributing to the loading end.

5. PARAMETRIC STUDY

The verified FE model was used to study the influence of different parameters on the torsional strength and behavior of RC beams strengthened with PBO-FRCM composite to archive more data and to provide more information about the most effective parameters to be considered in design. Parameters investigated in the parametric study were the compressive strength of concrete f'_c, and the FRCM composite strip width w and clear spacing s. In each case, the FE model corresponding to one of the experimentally tested beams was selected for the baseline comparison, and then the parameter of interest was varied to study its influence on the response. The FE model for beam N-P-R-4-C-1 was selected for studying the parameter f'_c, and the FE model for the control beam was selected for studying the parameters w and s. The results are discussed in the sections that follow.

5.1 CONCRETE COMPRESSIVE STRENGTH

The concrete compressive strength f'_c was varied from 3000 psi to 8000 psi (20.7 MPa 55.2 MPa) for beam N-P-4-C-1 to study its influence on the torsional strength and

behavior of PBO-FRCM strengthened beams. The value of f'_c in the baseline model was 5700 psi (39.3 MPa) (Batch 1, Table 1). As shown in Figure 12a, the torsional behavior was similar for all models, with lower initial stiffness for strengthened beams with lower concrete compressive strength. Beams with f'_c less than that of the baseline model had lower values of peak torque relative to the baseline model (Table 6). Strengthened beams with lower concrete compressive strength failed due to crushing of the concrete strut. At failure, the strains in the fibers were very low and more distributed along the entire beam length (Figure 12b) compared with those in the baseline beam (N-P-4-C-1) (Figure 12c), which had a higher concentration of strain at the beam corner (fiber rupture). On the other hand, no increase in peak torque was achieved for values of f'_c higher than the value of the baseline model (in other words, f'_c =5700 psi is the saturation point for this particular case). Fiber rupture governed the mode of failure for strengthened beams with higher concrete compressive strength.

5.2 FRCM COMPOSITE STRIP WIDTH AND SPACING

Different composite wrapping schemes were modeled to investigate the influence of strip width *w* and clear spacing *s*. Values of *w* and *s* ranged from 0 in. to 8 in. (0 mm to 203.2 mm), where the maximum value of *s* considered corresponded to the beam width in this study. Strips with only a single layer of composite were considered in this parametric study, since experimental results showed that the increase in torsional strength is not directly proportional to the number of composite layers [31]. Further work is needed to study the torsional behavior of beams strengthened with multiple layers of FRCM composite.

The results are compared with the control (unstrengthened) beam in Figure 13a and Table 6. The FE results of beam N-P-4-C-1, which was strengthened continuously along the length, and beam N-P-4-S-1, with w=4 in. (101.6 mm) and s=4 in. (101.6 mm), are also included for comparison. Both beams N-P-4-C-1 and N-P-4-S-1 were constructed with the same batch of concrete as the control beam (Batch 1, Table 1). The control beam failed due to crushing of the concrete strut, whereas all strengthened beams failed due to fiber rupture.

The volumetric ratio of the fibers ρ_f, computed using Eq. (2) for each different wrapping scheme considered, is included in Table 6:

$$\rho_f = \frac{n_f.t_f.p_f.w}{A_c.s_f} \tag{2}$$

where p_f is the wrapped perimeter of the beam, n_f is the number of layers of the composite, w is the width of the composite sheets, s_f is the center-to-center spacing of the applied composite sheets (s_f=w+s), and A_c was defined previously. Values of percent increase in T_u relative to the control beam versus ρ_f are plotted in Figure 13b. Results in Figure 13b and Table 6 show that T_u increases with increasing ρ_f, however the increase in T_u is not directly proportional to the increase in ρ_f. Beams with the same value of ρ_f but different values of w and s exhibited similar increases in T_u relative to the control beam.

6. CONCLUSIONS

This paper discussed the numerical simulation of PBO-FRCM composite-strengthened RC beams with different reinforcement schemes under torsional loading using the software program package LS-DYNA 971 R3. Torsional strength, torque-twist

per unit length response, and strains in the internal and external reinforcement were evaluated and compared with experimental results to validate the model and determine the accuracy. A parametric study was conducted to investigate the effects of concrete compressive strength and FRCM composite strip width and spacing. The important points concluded from this study are listed below:

1. The general torsional behavior of the experimentally tested beams was predicted accurately by the finite element model in terms of initial stiffness and peak torque.
2. The peak torque and twist per unit length were predicted by the model with maximum error of 18% and 32%, respectively. Values of strains in the internal reinforcement and the composite fibers determined by the experiments and FE results at the peak torque were compared at the beam midlength. Reasonable agreement was achieved between the experimental and FE results.
3. Results of the parametric study showed that values of concrete compressive strength higher than that of the baseline beam (f'_c=5,700 psi) (39.3 MPa) did not increase the torsional strength. On the other hand, a reduction in torsional strength was observed for values of concrete compressive strength lower than that of the baseline beam. The difference is due to different failure modes, namely fiber rupture for beams with higher values of f'_c and crushing of the concrete strut for lower values of f'_c.
4. The parametric study also showed that the torsional strength increases with increasing fiber reinforcement ratio, although the increase in torsional strength is not directly proportional to the increase in fiber reinforcement ratio. Beams with the same fiber reinforcement ratio but different strip width and spacing exhibited similar increases in torsional strength relative to the control beam.

ACKNOWLEDGEMENTS

The experimental work discussed in this paper was conducted at Missouri University of Science and Technology (Missouri S&T). Ruredil S.p.A. of San Donato Milanese, Italy, is gratefully acknowledged for providing the composite materials. The authors would also like to acknowledge Ahmed Gheni for his assistance with this work.

FUNDING

Funding for this work was provided by the Higher Committee for Education Development in Iraq (HCED).

Table 1. Measured concrete and steel reinforcement properties.

Material	Concrete		Steel Reinforcement	
	Batch 1	Batch 2	No. 3	No. 5
Compressive Strength, psi (MPa)	5700 (39.3)	5000 (34.5)	--	--
Splitting Tensile Strength, psi (MPa)	460 (3.2)	400 (2.8)	--	--
Modulus of Elasticity ksi (GPa)	4150 (28.6)	4150 (28.6)	29000 (200)	28000 (193)
Yield Strength, ksi (MPa)	--		65.8 (454)	68.0 (469)
Ultimate Strength, ksi (MPa)	--		104 (717)	107 (738)

Table 2. Measured PBO-FRCM composite material properties.

PBO Fibers		
Nominal Thickness in Primary Fiber Direction, in. (mm)	0.0018 (0.046)	
Ultimate Tensile Strength, ksi (MPa)	440 (3015)	
Modulus of Elasticity, ksi (GPa)	29,900 (206)	
Ultimate Strain, in./in. (mm/mm)	0.0145 (0.0145)	
Mortar		
	Batch 1	Batch 2
Compressive Strength, psi (MPa)	3600 (24.8)	2200 (15.2)
Splitting Tensile Strength, psi (MPa)	670 (4.6)	520 (3.6)

Table 3. PBO and carbon fiber properties in LS-DYNA.

Fiber type	E*a ksi (GPa)	E*b ksi (GPa)	E*c ksi (GPa)	PRba	PRca	PRcb	G*ab ksi (GPa)	G*bc ksi (GPa)	G*ca ksi (GPa)
Carbon	5750 (39.6)	575 (4.0)	575 (4.0)	0.01	0.01	0.25	514 (3.5)	230 (1.6)	230 (1.6)
PBO	1350 (9.3)	135 (0.9)	135 (0.9)	0.01	0.01	0.25	120 (0.8)	54 (0.4)	54 (0.4)

Table 4. Experimental and FE peak torque T_u and corresponding twist per unit length ψ_u.

Experimental Campaign Phase	Beam ID	Concrete Batch	Matrix Batch	T_u k-in. (kN-m)			ψ_u deg/in. (deg/m)		
				Exp.	FE	FE/Exp.	Exp.	FE	FE/Exp.
1 [31]	Control	A	A	148.7 (16.8)	151.1 (17.1)	1.02	0.085 (3.346)	0.078 (3.071)	0.92
1 [31]	N-P-4-S-1	A	A	193.2 (21.8)	213.7 (24.1)	1.11	0.245 (9.646)	0.202 (7.953)	0.83
2	N-P-4-8S-1	B	B	179.1 (20.2)	211.6 (23.9)	1.18	0.227 (8.937)	0.207 (8.150)	0.90
1 [31]	N-P-4-C-1	A	A	240.4 (27.2)	239.0 (27.0)	0.99	0.230 (9.055)	0.203 (7.992)	0.88
2	N-P-4-(0/90)C-2	B	B	249.3 (28.2)	261.9 (29.6)	1.05	0.223 (8.780)	0.178 (7.008)	0.80
1 [31]	N-P-4-C-2	A	A	310.6 (35.1)	293.0 (33.1)	0.94	0.241 (9.488)	0.163 (6.417)	0.68

Table 5. Maximum strains in the internal transverse reinforcing bars and composite. fibers at peak torque T_u.

Phase	Beam	Internal Transverse Reinforcement Strain			Composite Fiber Strain		
		ε_t (%) (Exp.)	ε_t (%) (FE)	FE/Exp.	ε_f (%) (Exp.)	ε_f (%) (FE)	FE/Exp.
1 [31]	Control	0.252	0.231	0.92	-	-	-
1 [31]	N-P-4-S-1	0.295	0.240	0.81	1.026	1.147	1.12
2	N-P-4-8S-1	0.386	0.240	0.62	0.505	1.127	2.23
1 [31]	N-P-4-C-1	0.275	0.236	0.86	0.822	1.257	1.53
2	N-P-4-(0/90)C-2	0.345	0.228	0.66	0.848	1.010	1.19
1 [31]	N-P-4-C-2	0.305	0.213	0.70	0.653	0.970	1.49

Table 6. Effect of parameters on peak torque T_u.

Parameters and Values		% Change in T_u (Relative to Baseline)
Concrete Compressive Strength, f'_c psi (MPa)	3000 (20.7)	-16
	4000 (27.6)	-9
	5000 (34.5)	-3
	5700 (39.3)*	-
	7000 (48.3)	0
	8000 (55.2)	2
Strip Width *w* and Spacing *s*, in. (mm), Composite Fiber Reinforcement Ratio ρ_f %	Control*	-
	w=2 (50.8) *s*=4 (101.6) ρ_f =0.025	32
	w=2 (50.8) *s*=2 (50.8) ρ_f=0.038	36
	N-P-4-S-1 *w*=4 (101.6) *s*=4 (101.6) ρ_f =0.038	41
	w=8 (203.2) *s*=8 (203.2) ρ_f =0.038	44
	w=4 (101.6) *s*=2 (50.8) ρ_f =0.050	48
	w=8 (203.2) *s*=4 (101.6) ρ_f =0.050	48
	N-P-4-C-1 *w*=60 (1524.0) *s*=0 (0) ρ_f =0.075	58

*Indicates baseline for comparison

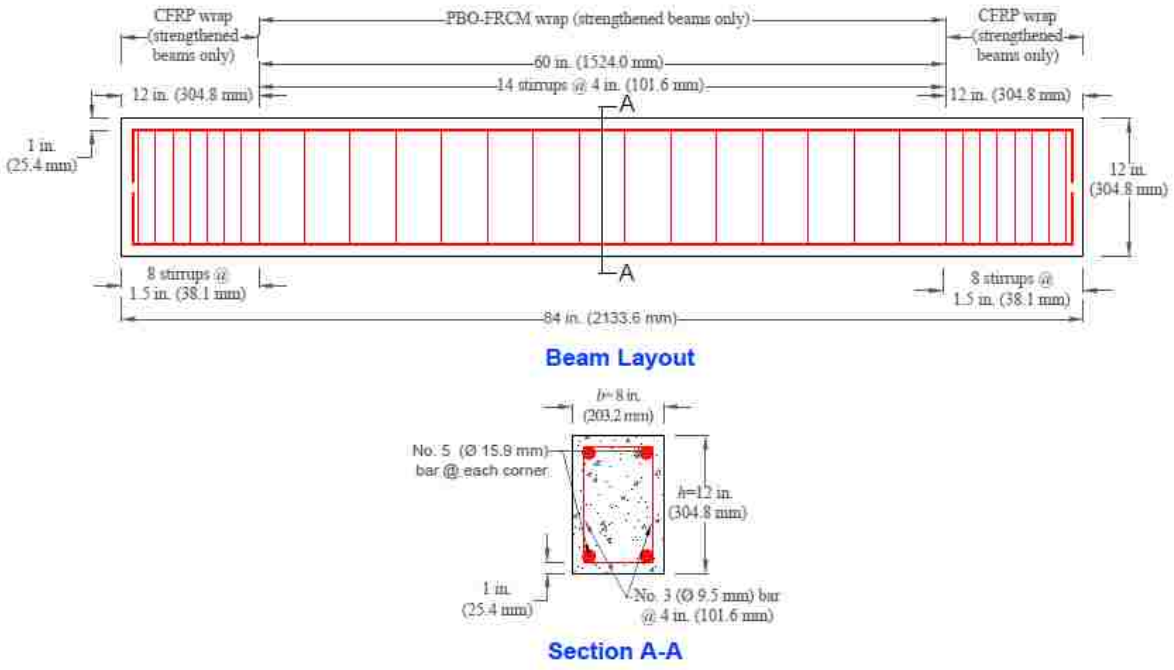

Figure 1. Beam layout and reinforcing details.

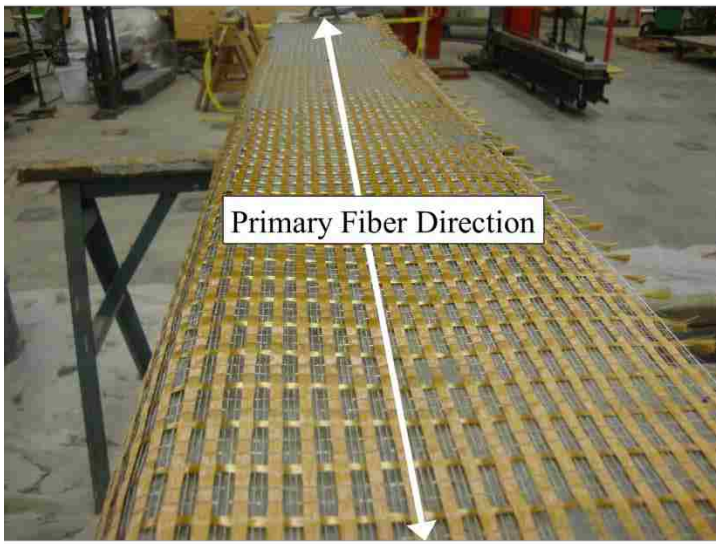

Figure 2. PBO unbalanced fiber net.

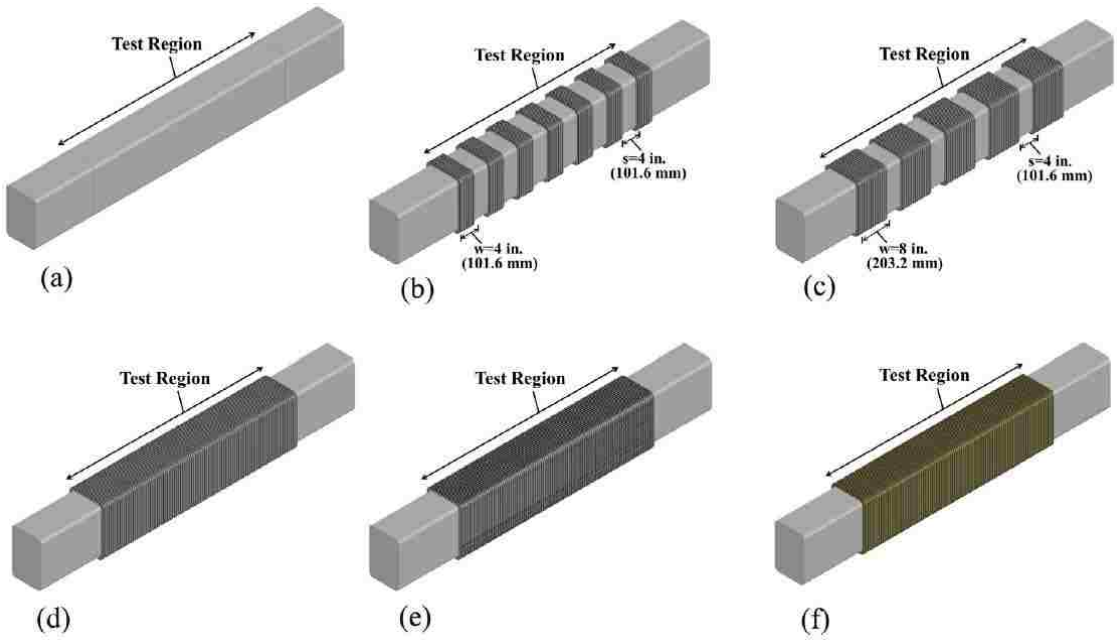

Figure 3. Schematic configuration of unstrengthened and strengthened beams: a) control beam, b) one layer, 90° strips (N-P-4-S-1), c) one layer, 90° strips (N-P-4-8S-1), d) one layer, 90° continuous (N-P-4-C-1), e) two layers, (0/90)° continuous (N-P-4-(0/90)C-2), f) two layers, 90° continuous (N-P-4-C-2).

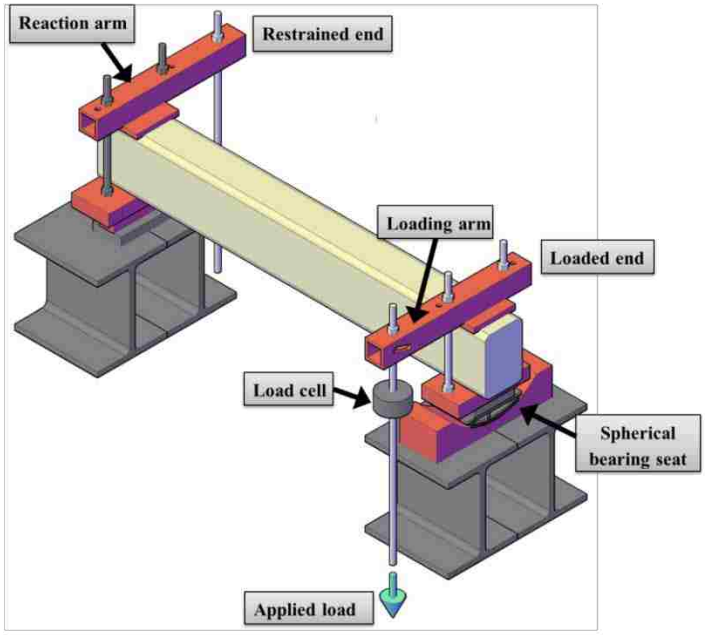

Figure 4. Torsion test setup.

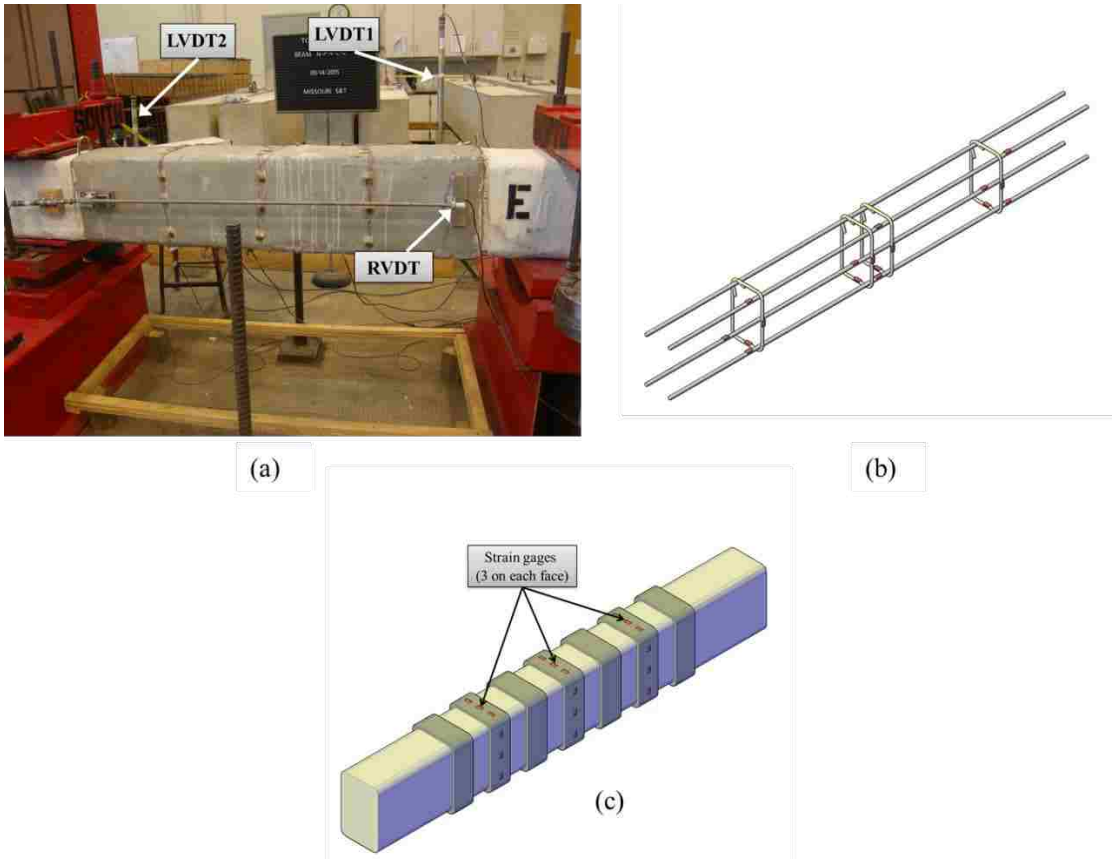

Figure 5. Instrumentation: a) RVDT and LVDTs, b) strain gages on the steel reinforcement, c) strain gages on the PBO-FRCM composite.

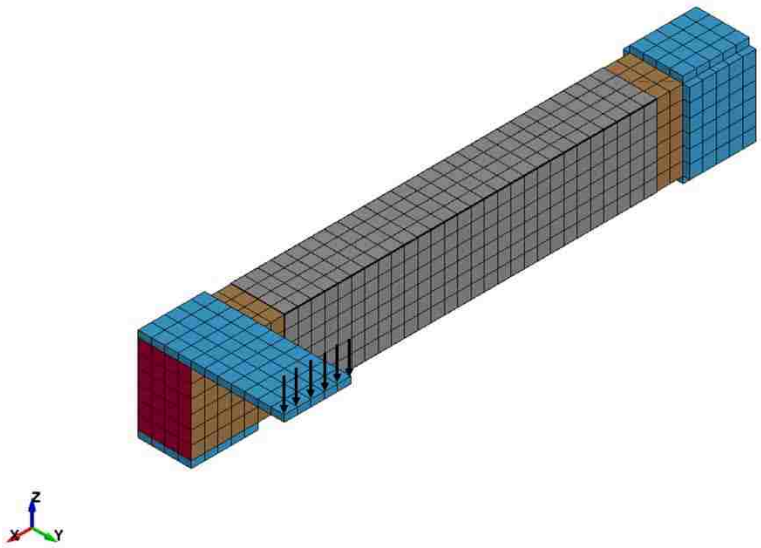

Figure 6. Modeled beam in LS-DYNA.

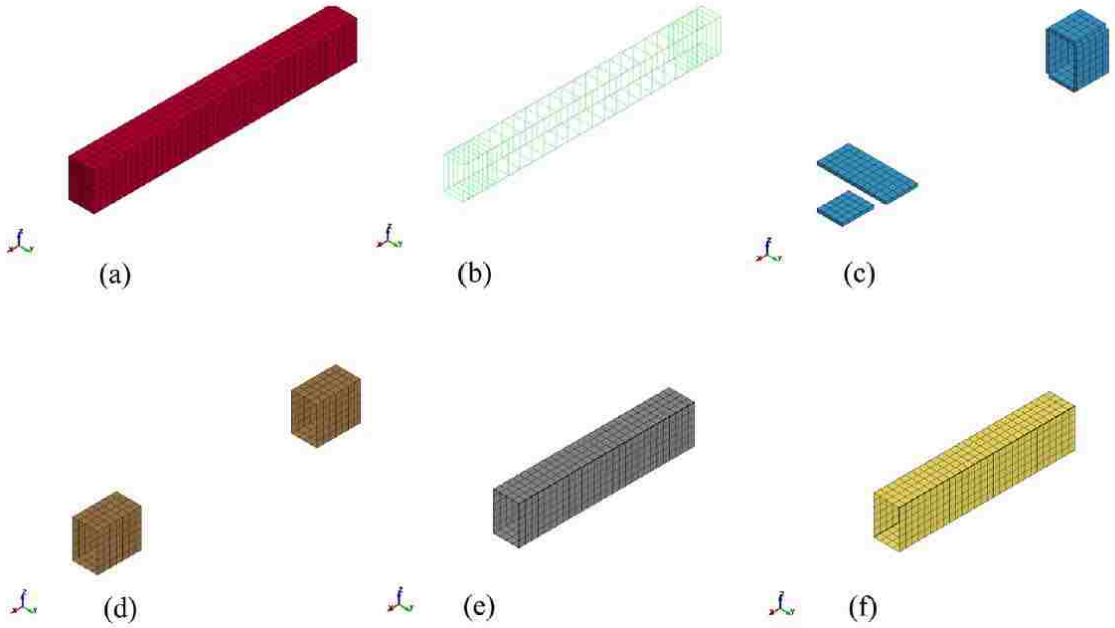

Figure 7. Modeled components: a) concrete beam, b) internal steel reinforcement, c) steel plates and loading arm, d) carbon fiber, e) cementitious matrix, f) PBO fiber.

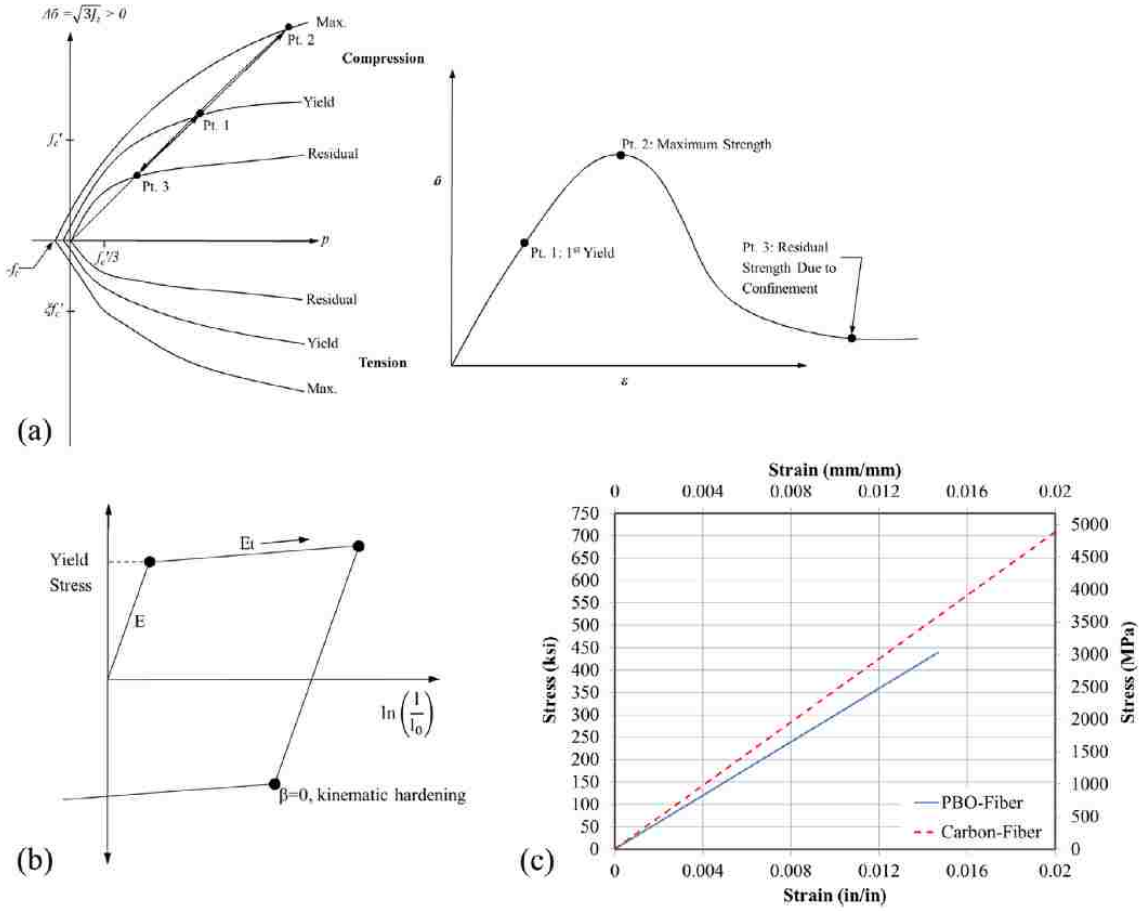

Figure 8. a) Three failure surfaces of concrete and matrix (adapted from [43]), b) elastic-plastic behavior with kinematic hardening for steel reinforcing bars (adapted from [42]), c) stress-strain relationship for PBO and carbon fibers.

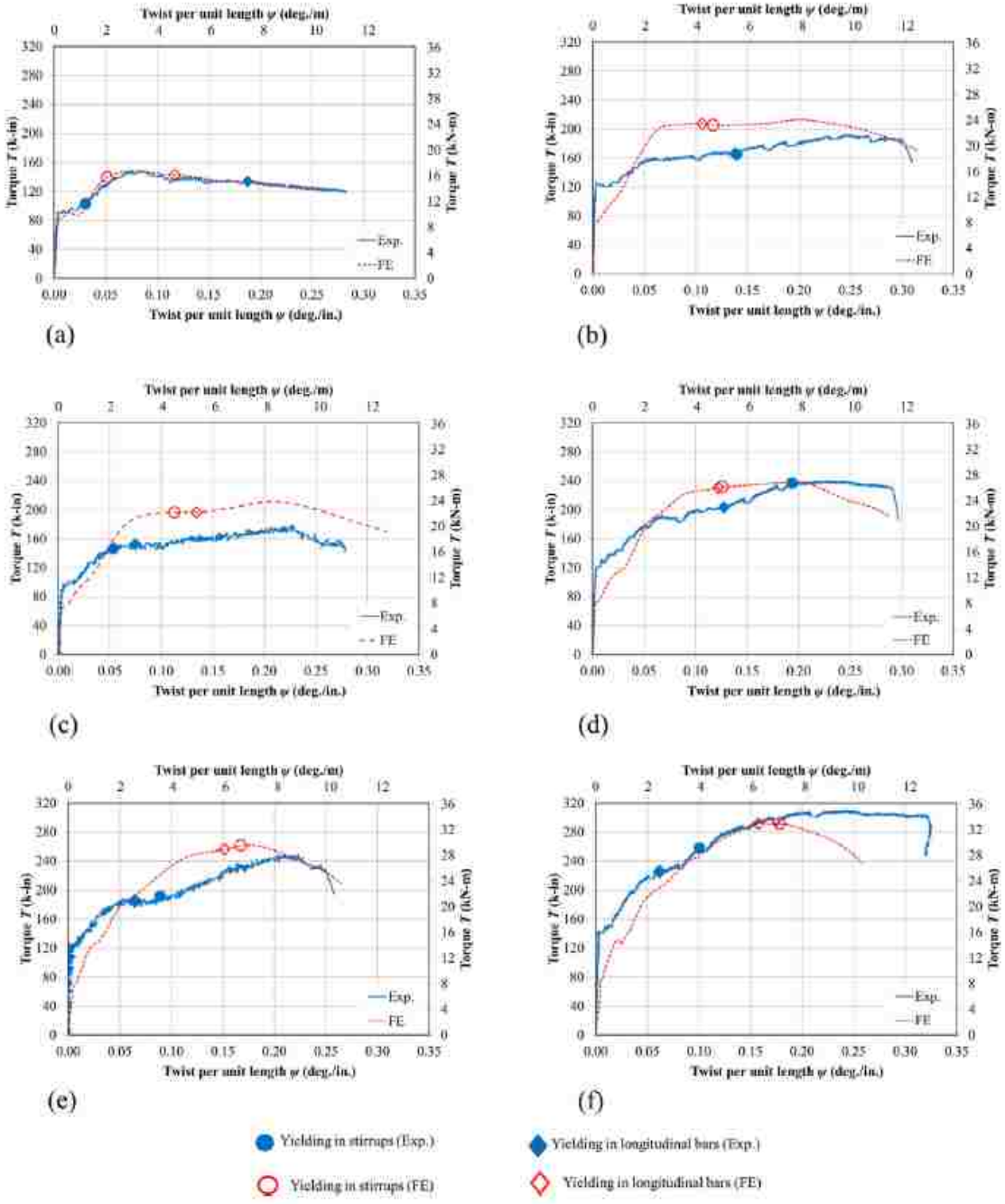

Figure 9. Experimental versus FE torque-twist per unit length response: a) control beam, b) N-P-4-S-1, c) N-P-4-8S-1, d) N-P-4-C-1, e) N-P-4-(0/90)C-2, f) N-P-4-C-2.

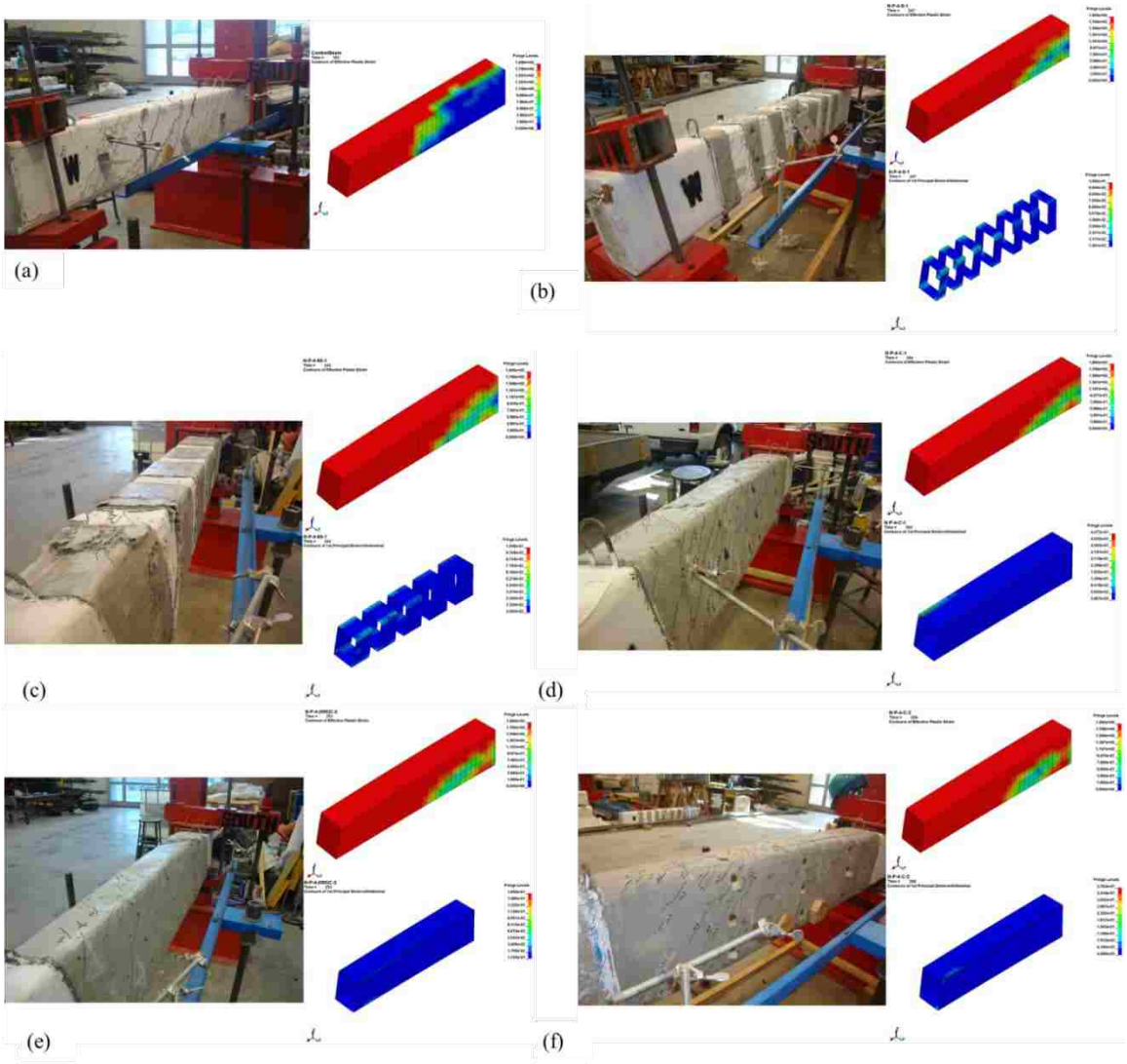

Figure 10. Comparison of failure mode (experimental and FE) for validated beams: a) control beam, b) N-P-4-S-1, c) N-P-4-8S-1, d) N-P-4-C-1, e) N-P-4-(0/90)C-2, f) N-P-4-C-2.

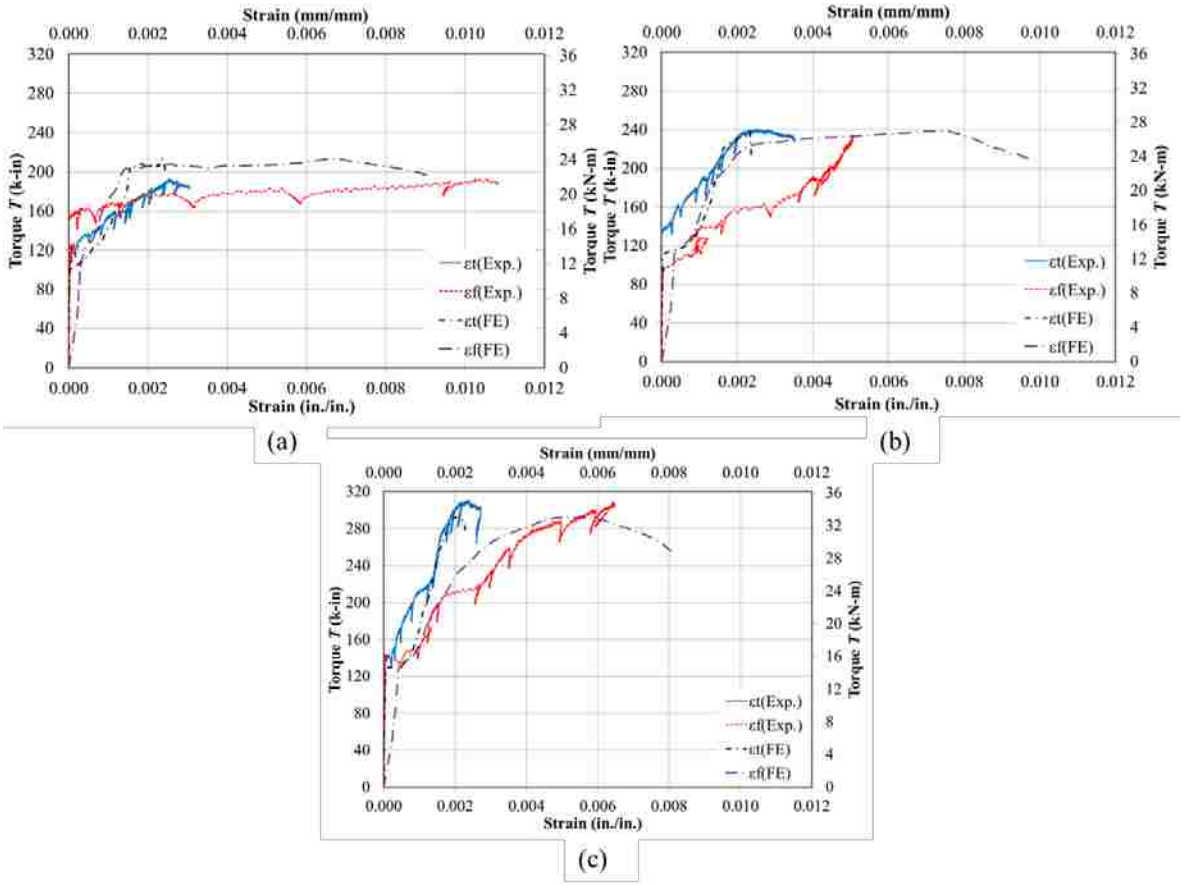

Figure 11. Torque versus strain at midlength a) N-P-4-S-1, b) N-P-4-C-1, and c) N-P-4-C-2.

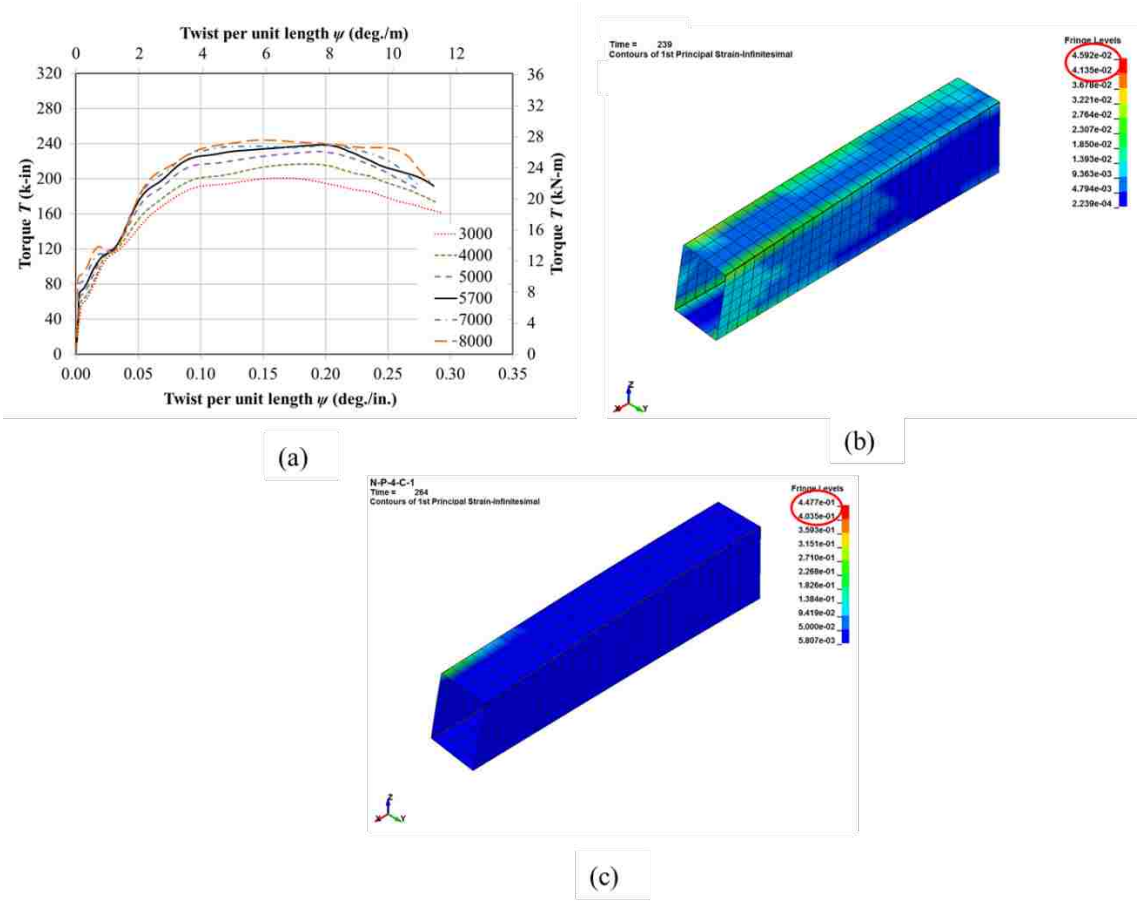

Figure 12. a) Influence of concrete compressive strength f'_c on torsional behavior, b) strain distribution in the fibers at the peak torque T_u for beam with f'_c =3000 psi (20.7 MPa), c) strain distribution in the fibers at the peak torque T_u for baseline beam (N-P-4-C-1) with f'_c =5700 psi (39.3 MPa).

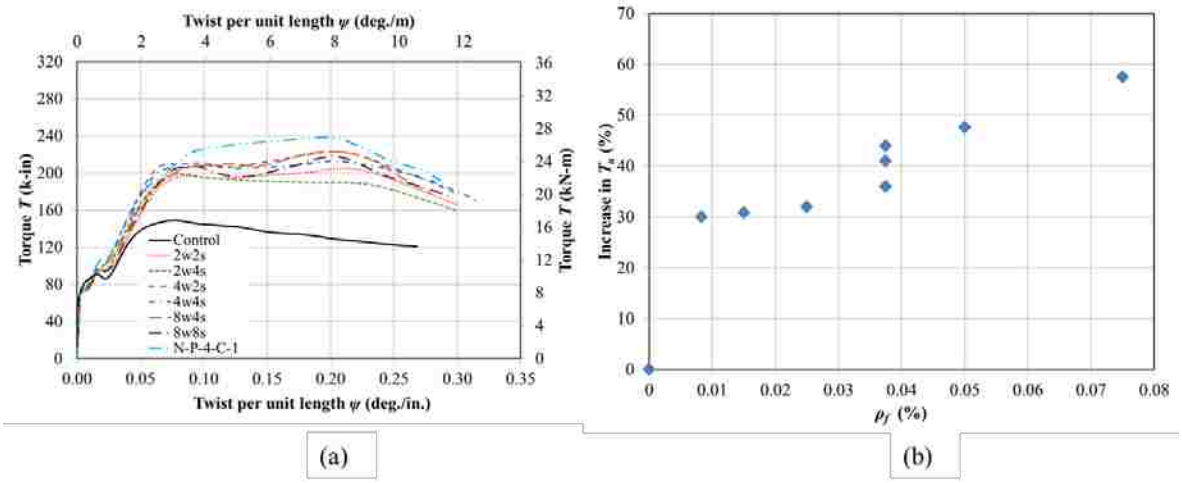

Figure 13. a) Influence of composite strip width w and spacing s on the torsional response, b) effect of volumetric fiber ratio ρ_f on the increase in peak torque T_u relative to the control beam.

REFERENCES

[1] Ghobarah, A., Ghorbel, M. N., & Chidiac, S. E. (2002). Upgrading torsional resistance of reinforced concrete beams using fiber-reinforced polymer. *Journal of Composites for Construction*, *6*(4), 257-263.

[2] Panchacharam, S., & Belarbi, A. (2002). Torsional behavior of reinforced concrete beams strengthened with FRP composites. In *First FIB Congress, Osaka, Japan* (Vol. 1, pp. 01-110).

[3] Salom, P. R., Gergely, J., & Young, D. T. (2004). Torsional strengthening of spandrel beams with fiber-reinforced polymer laminates. *Journal of Composites for Construction*, *8*(2), 157-162.

[4] Hii, A. K., & Al-Mahaidi, R. (2006). Experimental investigation on torsional behavior of solid and box-section RC beams strengthened with CFRP using photogrammetry. *Journal of Composites for Construction*, *10*(4), 321-329.

[5] Hii, A. K., & Al-Mahaidi, R. (2006). An experimental and numerical investigation on torsional strengthening of solid and box-section RC beams using CFRP laminates. *Composite Structures*, *75*(1), 213-221.

[6] Witte, F. C., & Kikstra, W. P. (2002). DIANA Finite Element Analysis, Release 8.1. *TNO Building and Construction Research, Delft, The Netherlands*.

[7] Chalioris, C. E. (2008). Torsional strengthening of rectangular and flanged beams using carbon fibre-reinforced-polymers–Experimental study. *Construction and Building Materials*, *22*(1), 21-29.

[8] Ameli, M., Ronagh, H. R., & Dux, P. F. (2007). Behavior of FRP strengthened reinforced concrete beams under torsion. *Journal of Composites for Construction*, *11*(2), 192-200.

[9] ANSYS Commands Reference, ANSYS, Inc. Southpointe, 275 Technology Drive, Canonsburg, PA 15317.

[10] Deifalla, A., Awad, A., & Elgarhy, M. (2013). Effectiveness of externally bonded CFRP strips for strengthening flanged beams under torsion: An experimental study. *Engineering Structures*, *56*, 2065-2075.

[11] Ganganagoudar, A., Mondal, T. G., & Prakash, S. S. (2016). Analytical and finite element studies on behavior of FRP strengthened RC beams under torsion. *Composite Structures*, *153*, 876-885.

[12] ABAQUS Theory Manual 2002, ABAQUS Inc., USA.

[13] Elwan, S. K. (2016). Torsion strengthening of RC beams using CFRP (parametric study). *KSCE Journal of Civil Engineering*, 1-9.

[14] He, R., Sneed, L. H., & Belarbi, A. (2013). Rapid repair of severely damaged RC columns with different damage conditions: An experimental study. *International Journal of Concrete Structures and Materials*, *7*(1), 35-50.

[15] He, R., Sneed, L. H., & Belarbi, A. (2014). Torsional repair of severely damaged column using carbon fiber-reinforced polymer. *ACI Structural Journal*, *111*(3), 705.

[16] Yang, Y., Sneed, L. H., Morgan, A., Saiidi, M. S., & Belarbi, A. (2015). Repair of RC bridge columns with interlocking spirals and fractured longitudinal bars–An experimental study. *Construction and Building Materials*, *78*, 405-420.

[17] Yang, Y., Sneed, L., Saiidi, M. S., Belarbi, A., Ehsani, M., & He, R. (2015). Emergency repair of an RC bridge column with fractured bars using externally bonded prefabricated thin CFRP laminates and CFRP strips. *Composite Structures*, *133*, 727-738.

[18] Abdelkarim, O. I., ElGawady, M. A., Gheni, A., Anumolu, S., & Abdulazeez, M. (2016). Seismic Performance of Innovative Hollow-Core FRP–Concrete–Steel Bridge Columns. *Journal of Bridge Engineering*, *22*(2), 04016120.

[19] D'Ambrisi, A., & Focacci, F. (2011). Flexural strengthening of RC beams with cement-based composites. *Journal of Composites for Construction*, *15*(5), 707-720.

[20] Ombres, L. (2011). Flexural analysis of reinforced concrete beams strengthened with a cement based high strength composite material. *Composite Structures*, *94*(1), 143-155.

[21] Paliga, C. M., Real, M. D. V., & Campos Filho, A. (2013). Numerical analysis of reinforced concrete beams strengthened with high strength cement-based composite material. *Revista IBRACON de Estruturas e Materiais*, *6*(2), 211-226.

[22] Babaeidarabad, S., Loreto, G., & Nanni, A. (2014). Flexural strengthening of RC beams with an externally bonded fabric-reinforced cementitious matrix. *Journal of Composites for Construction*, 18(5), 04014009.

[23] Sneed, L. H., Verre, S., Carloni, C., & Ombres, L. (2016). Flexural behavior of RC beams strengthened with steel-FRCM composite. *Engineering Structures*, *127*, 686-699.

[24] Ombres, L. (2012). Shear capacity of concrete beams strengthened with cement based composite materials. In Proceedings of the 6th International Conference on FRP Composites in Civil Engineering. (CICE 2012). Roma, Italy.

[25] Ombres, L. (2015). Structural performances of reinforced concrete beams strengthened in shear with a cement based fiber composite material. *Composite Structures*, *122*, 316-329.

[26] Trapko, T., Urbańska, D., & Kamiński, M. (2015). Shear strengthening of reinforced concrete beams with PBO-FRCM composites. *Composites Part B: Engineering*, *80*, 63-72.

[27] Loreto, G., Babaeidarabad, S., Leardini, L., & Nanni, A. (2015). RC beams shear-strengthened with fabric-reinforced-cementitious-matrix (FRCM) composite. *International Journal of Advanced Structural Engineering (IJASE)*, *7*(4), 341-352.

[28] Gonzalez-Libreros, J.H., Sabau, C., Sneed, L.H., Pellegrino, C., & Sas, G. (2017). State of research on shear strengthening of RC Beams using FRCM composites." *Construction and Building Materials*, *149*, 444-458.

[29] Colajanni, P., De Domenico, F., Recupero, A., & Spinella, N. (2014). Concrete columns confined with fiber reinforced cementitious mortars: experimentation and modelling. *Construction and Building Materials*, *52*, 375-384.

[30] Carloni, C., Mazzotti, C., Savoia, M., & Subramaniam, K. V. (2014). Confinement of Masonry Columns with PBO FRCM Composites. *Key Engineering Materials*, *624*.

[31] Alabdulhady, M. Y., Sneed, L. H., & Carloni, C. (2017). Torsional behavior of RC beams strengthened with PBO-FRCM composite–An experimental study. *Engineering Structures*, *136*, 393-405.

[32] LS-DYNA 971 R3 [Computer software]. Livermore, CA, Livermore Software Technology.

[33] ACI 318-14. Building code requirements for structural concrete (318-14) and commentary (318R-14). American Concrete Institute, Farmington Hills, MI, 2014, 519 pp.

[34] ASTM A615/ A615M-16. Standard specification for deformed and plain carbon-steel bars for concrete reinforcement. ASTM International, West Conshohocken, PA, 2015, 8 pp.

[35] ASTM A370-16. Standard test methods and definitions for mechanical testing of steel products. ASTM International, West Conshohocken, PA, 2016, 49 pp.

[36] ASTM C39/C39M-16b. Standard test method for compressive strength of cylindrical concrete specimens. ASTM International, West Conshohocken, PA, 2016, 7 pp.

[37] ASTM C496/ C496M-11. Standard test method for splitting tensile strength of cylindrical concrete specimens. ASTM International, West Conshohocken, PA, 2011, 5 pp.

[38] ASTM C469/C469M-14. Standard test method for static modulus of elasticity and Poisson's ratio of concrete in compression. ASTM International, West Conshohocken, PA, 2014, 5 pp.

[39] Sneed, L. H., D'Antino, T., & Carloni, C. (2014). Investigation of bond behavior of PBO fiber-reinforced cementitious matrix composite-concrete interface. *ACI Materials Journal*, *111*(1-6), 1-12.

[40] Belytschko, T., Lin, J. I., & Chen-Shyh, T. (1984). Explicit algorithms for the nonlinear dynamics of shells. *Computer methods in applied mechanics and engineering*, *42*(2), 225-251.

[41] Abdelkarim, O. I., & ElGawady, M. A. (2014). Analytical and finite-element modeling of FRP-concrete-steel double-skin tubular columns. *Journal of Bridge Engineering*, *20*(8), B4014005.

[42] Livermore Software Technology Corporation (LSTC) (2007). LS-DYNA Keyword User's Manual Volume II (Material Models), Version 971, Livermore, California.

[43] Malvar, L. J., & Simons, D. (1996). Concrete material modeling in explicit computations. In *Proceedings, Workshop on Recent Advances in Computational Structural Dynamics and High Performance Computing, USAE Waterways Experiment Station, Vicksburg, MS* (pp. 165-194).

[44] Lin, X., Zhang, Y.X., & Hazell, P.J. (2014). Modelling the response of reinforced concrete panels under blast loading. *Materials & Design, 56*, 620-628.

[45] Youssf, O., ElGawady, M. A., Mills, J. E., & Ma, X. (2014). Finite element modelling and dilation of FRP-confined concrete columns. *Engineering Structures, 79*, 70-85.

V. ANALYTICAL STUDY ON THE TORSIONAL BEHAVIOR OF REINFORCED CONCRETE BEAMS STRENGTHENED WITH FRCM COMPOSITE

Meyyada Y. Alabdulhady, Khalid Aljabery, and Lesley H. Sneed

ABSTRACT

In this study, an analytical approach was used to predict the full torsional response of RC beams strengthened with externally bonded fiber reinforced cementitious matrix (FRCM) composite. The analytical model was based on the softened membrane model for torsion (SMMT) modified for fiber reinforced polymer (FRP)-strengthened beams. As a first attempt, fully wrapped beams with fiber rupture governing the mode of failure were considered in this study. The model was validated by comparing the analytical response to the experimental response of five solid, rectangular RC beams. The model was able to predict values of the cracking and ultimate torsional moment and corresponding angles of twist per unit length with reasonable accuracy. Also, good agreement was achieved between the experimental and analytical results of the strain in the stirrups and composite fibers. The results confirm the feasibility of the SMMT model to predict the torsional response of FRCM-strengthened beams. However, additional modifications are required to extend the model to U-wrapped configurations and composite debonding failure modes.

KEYWORDS

Fiber strain; PBO-FRCM composite; RC beams; softened membrane model; strengthening; torsion.

1. INTRODUCTION

Externally bonded fiber reinforced composites have been widely used for strengthening and repairing reinforced concrete (RC) elements in buildings and bridges. Fiber reinforced polymer (FRP) composite material is the most common system used for this purpose. However, in some situations it is difficult to use FRP composite material as an external strengthening system due to its inability to install onto wet surfaces or in low temperatures. Furthermore, the epoxy resin, which is used as the binder between the fibers and the substrate, has poor properties such as low fire resistance and lack of vapor permeability. Therefore, a new type of composite system, referred to as fiber reinforced cementitious matrix (FRCM) composite, has been investigated recently as an alternative strengthening technique to overcome the shortcomings of the well-known FRP composite system. The inorganic cementitious matrix in the FRCM composite system affords better compatibility with concrete and masonry substrates and has better heat resistance than the epoxy resin in the FRP composite system. Different types of fibers have been used in FRCM composite systems such as polyparaphenylene benzobisoxazole (PBO), carbon, glass, aramid, basalt, and steel. The use of PBO-FRCM composite, which is the composite used in the present study, has been studied for flexural strengthening [e.g., D'Ambrisi and Focacci 2011, Ombres 2011, Babaeidarabad et al. 2014, Sneed et al. 2016], shear strengthening [e.g., Ombres 2012, Ombres 2015, Trapko et al. 2015, Loreto et al. 2015, Aljazaeri and Myers 2017, Gonzalez-Libreros et al. 2017, Gonzalez-Libreros et al. 2017], and confinement of axially/eccentrically loaded RC elements [e.g., Colajanni et al. 2014, Carloni et al. 2014, Sneed et al. 2017], but currently there are very few studies in the technical literature on its use for torsional strengthening [Alabdulhady et al.

2017, Alabdulhady and Sneed 2018]. Since the early of 2000s, researchers have investigated experimentally the torsional behavior of RC beams strengthened with externally bonded FRP composites [Ghobarah et al. 2002, Panchacharam and Belarbi 2002, Salom et al. 2004, Hii and Al-Mahaidi 2006, Hii and Al-Mahaidi 2006, Ameli et al. 2007, Chalioris 2008, Deifalla et al. 2013]. Furthermore, analytical studies have been conducted to predict the torsional behavior of RC beams strengthened with FRP composite material by implementing different approaches. Ameli and Ronagh [2007] developed a method based on the compression field theory (CFT) to determine the torsional strength of FRP-strengthened RC beams. Deifalla and Ghobarah [2010] developed an analytical model based on the modified compression field theory (MCFT), the hollow tube analogy, and compatibility at the corner of the cross section to predict the full torsional behavior of RC beams strengthened with FRP composite. Their model considered the tensile stress in concrete and took into account different composite wrapping schemes, including U-wrapped and side-bonded configurations, fiber orientations, and failure modes.

Chalioris [2007] introduced an approach to predict the full torsional behavior of RC beams strengthened with FRP composite material by combining two different theoretical models: the smeared crack model for plain concrete in torsion to predict the elastic (pre-cracking) response, and a modified softened truss model for torsion (STMT) that takes into account the contribution of the FRP composite to predict the post-cracking response. The model also considered different composite wrapping schemes, fiber orientations, and failure modes but did not include the tensile stress in concrete. Chai et al. [2014] proposed an analytical method to predict the torsional capacity and behavior of

RC multicell box girders strengthened with CFRP sheets based on the extension and modification of the softened truss model for torsion (STMT) algorithm. Extending the work by Chalioris [2007] and Chai et al. [2014], Shen et al. [2017] proposed an analytical model based on a modification of the STMT to predict the full torsional response of RC beams externally wrapped with FRP composite considering the influence of the tensile stress in concrete and the effect of FRP confinement.

Ganganagoudar et al. [2016] introduced a modified softened membrane model for torsion (SMMT) taking into account the influence of externally bonded FRP on the compressive behavior of cracked concrete and the tensile stress in concrete. The model considered the fiber rupture failure mode of FRP; debonding of the composite was outside the scope of the study. Analytical results were compared with those determined from experiments and a nonlinear finite element analysis, which were in reasonable agreement with the analytical results. Zojaji and Kabir [2012] developed a procedure to predict the full torsional response of RC beams strengthened with externally bonded FRP composite based on the SMMT model and considering the tensile stress in concrete. Different failure modes were considered, including composite fiber rupture and debonding, and the analytical results were in good agreement with experimental results.

The aim of the present study is to predict the full torsional response of RC beams strengthened with externally bonded PBO-FRCM composite. The analytical model is based on the SMMT due to its ability to predict the entire torque-twist response (pre-cracking, post-cracking, and post-peak stages) of FRP-strengthened RC beams with reasonable accuracy. As a first attempt, fully wrapped beams with fiber rupture governing the mode of failure are considered in this study. The results from an experimental

program conducted by the authors [Alabdulhady et al. 2017, Alabdulhady and Sneed 2018] are used to validate the analytical model. Furthermore, the strains measured in the internal and external reinforcement and the behavior of concrete and steel reinforcement are evaluated.

2. ANALYTICAL MODEL

2.1 OVERVIEW

The softened membrane model for torsion (SMMT) was first introduced by Jeng and Hsu [2009] for RC beams subjected to pure torsion. Zojaji and Kabir [2012] modified the Jeng and Hsu [2009] model to include the effect of externally bonded FRP composite on the torsional behavior of strengthened RC beams. The model was validated with solid and hollow rectangular beams with different FRP materials and strengthening configurations. The modified SMMT model by Zojaji and Kabir [2012] was adopted in the current study in an attempt to model the response of solid, rectangular RC beams strengthened with externally bonded FRCM composite described in Section 3.

In the SMMT model of an externally strengthened RC beam, torsional moment after concrete cracking is resisted by truss action of compressive stresses in the diagonal concrete struts and tensile stresses in the internal and external reinforcement. Equations of equilibrium and compatibility are solved with the constitutive relationships of an element taken from a member under pure torsional moment (see Figure 1). The strengthening system is considered in the model by the addition of terms to the equilibrium equations in the longitudinal and transverse directions, as applicable. The effect of confinement provided by the strengthening system is considered in the

constitutive relationship of concrete in compression. Variables in this section are defined in the Nomenclature section.

2.2 EQUILIBRIUM EQUATIONS

The torsional moment *T* applied to a rectangular RC prism that is strengthened with externally bonded fiber reinforced composite (Figure 1) is resisted by the internal uniform shear stresses (τ) formed by the circulatory shear flow q developed in the center of the shear flow zone that has an effective thickness t_d [Hsu 1990]. A membrane element subjected to in-plane stresses and the corresponding internal stress components of the concrete, internal reinforcement, and external reinforcement are shown in Figure 1. The state of the in-plane stresses of element A (Figure 1) can be represented by Mohr's circle [Hsu 1993] as shown in Figure 2, where the *l-t* coordinate is defined as the direction of the longitudinal and transverse reinforcing steel bars, and the 2-1 coordinate is defined as the direction of the principle applied stresses. The in-plane equilibrium equations for element A are then given by Equation 1:

$$б_l = б_2^c cos^2\alpha_2 + б_1^c sin^2\alpha_2 + 2\tau_{21}^c sin\alpha_2 cos\alpha_2 + \rho_{sl} f_{sl} + \rho_{fl} f_{fl} \quad (1a)$$

$$б_t = б_2^c sin^2\alpha_2 + б_1^c cos^2\alpha_2 - 2\tau_{21}^c sin\alpha_2 cos\alpha_2 + \rho_{st} f_{st} + \rho_{ft} f_{ft} \quad (1b)$$

$$\tau_{lt} = (-б_2^c + б_1^c) - 2\tau_{21}^c sin\alpha_2 cos\alpha_2 + \rho_{st} f_{st} + \rho_{ft} f_{ft} \quad (1c)$$

For an RC beam subjected to pure torsion, element A is subjected to pure shear $\tau_{lt} = q/t_d$, with the normal stresses $б_l = б_t = 0$ and $\alpha_2 = 45°$. The torsional moment *T* can be calculated from Equation 2, which is adopted from Bredt's equation for an equivalent thin walled cross section [Bredt 1896]:

$$T = 2A_0 q = 2A_0 t_d \tau_{lt} \quad (2)$$

2.3 COMPATIBILITY EQUATIONS

The in-plane compatibility of the shear in element A (Figure 1) must be ensured. Equation 3 [Hsu and Zhu 2002] presents the compatibility equations, which are represented by Mohr's circle in Figure 3:

$$\varepsilon_l = \varepsilon_2 cos^2\alpha_2 + \varepsilon_1 sin^2\alpha_2 + \gamma_{21} sin\alpha_2 cos\alpha_2 \quad (3a)$$

$$\varepsilon_t = \varepsilon_2 sin^2\alpha_2 + \varepsilon_1 cos^2\alpha_2 - \gamma_{21} sin\alpha_2 cos\alpha_2 \quad (3b)$$

$$\gamma_{lt} = 2(-\varepsilon_2 + \varepsilon_1) sin\alpha_2 cos\alpha_2 + \gamma_{21}(cos\alpha_2 - sin\alpha_2) \quad (3c)$$

Since the constitutive relationships of the materials are calculated from the uniaxial strain, the uniaxial strain is related to the biaxial strain using the relationships given by Zhu and Hsu below [Zhu and Hsu 2002].

Concrete uniaxial strain:

$$\bar{\varepsilon_1} = \frac{1}{1-\nu_{12}\nu_{21}}\varepsilon_1 + \frac{\nu_{12}}{1-\nu_{12}\nu_{21}}\varepsilon_2 \quad (4a)$$

$$\bar{\varepsilon_2} = \frac{\nu_{12}}{1-\nu_{12}\nu_{21}}\varepsilon_1 + \frac{1}{1-\nu_{12}\nu_{21}}\varepsilon_2 \quad (4b)$$

$$\bar{\gamma_{21}} = \gamma_{21} \quad (4c)$$

Steel reinforcing bar uniaxial strain:

$$\bar{\varepsilon_l} = \bar{\varepsilon_2} cos^2\alpha_2 + \bar{\varepsilon_1} sin^2\alpha_2 + \gamma_{21} sin\alpha_2 cos\alpha_2 \quad (5a)$$

$$\bar{\varepsilon_t} = \bar{\varepsilon_2} sin^2\alpha_2 + \bar{\varepsilon_1} cos^2\alpha_2 - \gamma_{21} sin\alpha_2 cos\alpha_2 \quad (5b)$$

The other two compatibility equations that relate the shear strain to the angle of twist per unit length ψ and curvature ϕ are given by Equations 6 and 7, respectively [Hsu 1993]:

$$\psi = \frac{p_0}{2A_0}\gamma_{lt} \quad (6)$$

$$\phi = \psi sin2\alpha_2 = \frac{p_0}{2A_0}\gamma_{lt} sin2\alpha_2 \quad (7)$$

The curvature ϕ results in a strain gradient in the concrete struts as shown in Figure 4. The triangular strain distribution in the 1- and 2- directions is assumed to be linear based on the rotating angle theories, and the depth of the compression zone of the concrete struts is assumed to be the effective thickness of the shear flow zone t_d. Therefore, t_d can be calculated by Equation 8 [Jeng and Hsu 2009]:

$$t_d = \frac{\bar{\varepsilon}_{2s}}{\phi} \tag{8}$$

Substitution and manipulation of Equations 7 and 8 with the equations for computing p_0 and A_0 in the Nomenclature section yields to Equation 9 for calculating the effective thickness of shear flow zone t_d [Jeng and Hsu 2009]:

$$t_d = \frac{1}{2(Q+4)}\left[p_c\left(1+\frac{Q}{2}\right) - \sqrt{\left(1+\frac{Q}{2}\right)^2 p_c^2 - 4Q(Q+4)A_c)}\right] \tag{9}$$

where:

$$Q = \frac{2\bar{\varepsilon}_{2s}}{\gamma_{lt} sin2\alpha_2} = \frac{4\bar{\varepsilon}_s}{\gamma_{lt} sin2\alpha_2} \tag{10}$$

2.4 CONSTITUTIVE RELATIONSHIPS OF MATERIALS

The constitutive relationships of the concrete, steel reinforcing bars, and composite fibers are discussed in detail in this section and are illustrated in Figure 5. Parameters in the equations that follow are given in units of (mm, MPa) except for E_f, which is given in (GPa) according to FIB [fib 2001].

2.4.1 Concrete in Compression. The stress-strain response of the SMMT model was developed by Belarbi and Hsu [1995] for a softened compressive concrete and then modified by Chalioris [2007] to include the effect of confinement provided by external

reinforcement using the method proposed by Vintzileou and Panagiotidou [2008]. The stress-strain relationship of concrete in compression is given by Equation 11, and the behavior is illustrated in Figure 5a:

$$\sigma_2^c = k_{1c}\zeta f_c' \tag{11}$$

$$k_{1c} = \frac{\bar{\varepsilon}_{2s}}{k^2\zeta\varepsilon_0} - \frac{(\bar{\varepsilon}_{2s})^2}{3(k^2\zeta\varepsilon_0)^2} \qquad \text{for } \frac{\bar{\varepsilon}_{2s}}{k^2\zeta\varepsilon_0} \leq 1$$

$$k_{1c} = 1 - \frac{k^2\zeta\varepsilon_0}{3\bar{\varepsilon}_{2s}} \qquad \text{for } \frac{\bar{\varepsilon}_{2s}}{k^2\zeta\varepsilon_0} > 1 \tag{12}$$

$$\zeta = \frac{0.9}{\sqrt{(1+400\bar{\varepsilon}_1)}} \tag{13}$$

where:

$$k = 1 + 1.3\alpha_n\omega_n \tag{14}$$

$$\alpha_n = 1 - \frac{b^2+h^2}{3A_c} \tag{15}$$

$$\omega_n = \frac{Volume\ of\ composite\ material}{Volume\ of\ the\ confined\ concrete\ core}\frac{f_{fu}}{f_c'} \tag{16}$$

2.4.2 Concrete in Tension. The model by Belarbi and Hsu [1995] for the tensile behavior of concrete in shear was modified by Jeng and Hsu [2009] for concrete in torsion to account for an increase in the pre-cracking stiffness and strain at peak tensile stress. The concrete behavior in tension is shown in Figure 5b, and the tensile stress is calculated as follows:

$$\sigma_1^c = k_{1t}f_{cr} \tag{17}$$

$$k_{1t} = \frac{\bar{\varepsilon}_{1s}}{2\varepsilon_{cr}} \qquad \text{for } \frac{\bar{\varepsilon}_{1s}}{\varepsilon_{cr}} \leq 1$$

$$k_{1t} = \frac{\varepsilon_{cr}}{2\bar{\varepsilon}_{1s}} + \frac{(\varepsilon_{cr})^{0.4}}{0.6\bar{\varepsilon}_{1s}}[(\bar{\varepsilon}_{1s})^{0.6} - (\varepsilon_{cr})^{0.6}] \qquad \text{for } \frac{\bar{\varepsilon}_{1s}}{\varepsilon_{cr}} > 1 \tag{18}$$

where:

$$f_{cr} = E_c \varepsilon_{cr} \tag{19}$$

$$E_c = 5620\sqrt{f_c'} \tag{20}$$

and ε_{cr} is taken as 0.000116.

The concrete shear stress is related to the shear strain by Equation 21:

$$\tau_{21}^c = \frac{\sigma_1^c - \sigma_2^c}{2(\varepsilon_1 - \varepsilon_2)} \gamma_{21} \tag{21}$$

2.4.3 Steel Reinforcing Bars. The stress-strain response for the longitudinal and transverse steel reinforcement is shown in Figure 5c, and the relationship is given below [Jeng and Hsu 2009]:

$$f_s = E_s \bar{\varepsilon_s} \qquad \text{for } \bar{\varepsilon_s} \le \bar{\varepsilon_n}$$

$$f_s = f_{sy}\left[(0.91 - 2B) + (0.02 + 0.25B)\frac{\bar{\varepsilon_s}}{\varepsilon_{sy}}\right] \qquad \text{for } \bar{\varepsilon_s} > \bar{\varepsilon_n} \tag{22}$$

where:

$$B = \left(f_{cr}/f_{sy}\right)^{1.5}/\rho \tag{23}$$

$$\bar{\varepsilon_n} = \varepsilon_{sy}(0.93 - 2B) \tag{24}$$

2.4.4 Composite Fibers. The tensile behavior of the composite material is assumed to be linear elastic up to failure as shown in Figure 5d. Accordingly, only the fibers are considered, and the influence of the matrix is neglected. The constitutive law is based on Hook's law:

$$f_f = E_f \varepsilon_f \qquad \text{for } \varepsilon_f \le \varepsilon_{fe} \tag{25}$$

where ε_{fe} is the effective tensile strain, which is determined based on the mode of failure and wrapping configuration of the RC beam strengthened with external reinforcement. In

the modified SMMT model for FRP-strengthened beams by Zojaji and Kabir [2012], failure modes that were considered included composite debonding, peeling off, and fiber rupture for the case of fully-wrapped beams, and composite debonding for the case of U-wrapped beams. For PBO FRCM-strengthened beams with fibers fully wrapped around the cross-section and oriented perpendicular to the longitudinal axis of the beam, previous studies reported that fiber rupture governed the failure mode [Alabdulhady et al. 2017, Alabdulhady and Sneed 2018]. Therefore in the present study, the fiber rupture failure mode is considered, and the equation proposed by Deifalla and Ghobarah [2010] and utilized in the SMMT model modified by Zojaji and Kabir [2012] is employed herein:

$$\varepsilon_{fe} = 0.1(E_f \rho_f)^{-0.86} \varepsilon_{fu} \tag{26}$$

For failure modes associated with composite debonding, on the other hand, it has been noted that determining the effective fiber strain is extremely challenging [fib 2001], especially since experimental data on strengthened RC beams subjected to torsion is limited in the technical literature. Different models have been proposed to compute the effective fiber strain for debonding of FRP composites, however, it must be noted that such models are generally not applicable to FRCM composites since the bond behavior is different. With FRP composites, debonding typically occurs within a thin layer of the concrete substrate, and therefore models for the effective fiber strain for FRP composites are usually a function of the concrete strength [fib 2001]. For PBO-FRCM composite, on the other hand, debonding has been associated with slippage of the fibers relative to the embedding matrix [Sneed et al. 2014], and the concrete strength does not significantly influence the bond behavior [D'Antino et al. 2015]. Recent work has examined the

effective fiber strain for FRCM-strengthened RC beams subjected to shear that failed due to composite debonding [Gonzalez-Libreros et al. 2017], however more work is needed for FRCM-strengthened RC beams subjected to torsion with this failure mode.

2.5 SOLUTION ALGORITHM

The solution algorithm was implemented using the program MATLAB [2016a]. The solution steps are illustrated in the flow chart shown in Figure 6. The basic equilibrium equations in Equation 1 were summed and subtracted to obtain Equations 27 and 28, which were extended from Hsu and Zhu [2002] and used as a convergence criterion for the solution procedure. A trial and error procedure was implemented to calculate each point of the torsional moment – twist per unit length (*T- ψ)* curve.

$$\rho_{sl}f_{sl} + \rho_{fl}f_{fl} + \rho_{st}f_{st} + \rho_{ft}f_{ft} = (б_l + б_t) - (б_2^c + б_1^c) \quad (27)$$

$$\rho_{sl}f_{sl} + \rho_{fl}f_{fl} - \rho_{st}f_{st} - \rho_{ft}f_{ft} = (б_l - б_t) - (б_2^c - б_1^c)\, cos\, 2\alpha_2 - 2\tau_{21}^c sin2\alpha_2 \quad (28)$$

It should be noted that Equations 27 and 28 are written in general form to include terms for composite fibers oriented in both the transverse and longitudinal directions. In this study, only the contribution of the composite fibers in the transverse (wrap) direction ($\rho_{ft}f_{ft}$) were considered since fibers in the longitudinal direction debonded prematurely [Alabdulhady and Sneed 2018], and the debonding failure mode is not considered (Section 2.4).

The maximum values of the main variables in this study (ε_2, ε_1, and γ_{12}) were taken as (0.0035, 0.05, and 0.01), respectively. These values were set to arbitrarily large values in order to enable the complete solution.

3. VALIDATION OF THE MODEL

The model was validated by comparing the analytical response with the experimental response of five RC beams tested by the authors. The experiments are summarized briefly in Section 3.1. The predicted torsional moment T versus twist per unit length ψ behavior of the unstrengthened (control) beam was generated based on the SMMT model for unstrengthened RC beams presented by Jeng and Hsu [2009]. Then, modifications based on the Zojaji and Kabir model [2012] discussed in Section 2 were implemented to predict the T-ψ response of the four PBO FRCM-strengthened beams. The analytical results are summarized and compared with the experimental results in Sections 3.2-3.4.

3.1 EXPERIMENTS

In order to examine the applicability of the SMMT model proposed by Zojaji and Kabir [2012] to the FRCM composite material investigated in this study, five beams were selected from the experimental program conducted by the authors discussed in detail in [Alabdulhady et al. 2017, Alabdulhady and Sneed 2018]. Four of the five beams were strengthened, and one beam was unstrengthened for use as the control (see Figure 7a). The RC beams had a rectangular cross section and internal reinforcement illustrated in Figure 8. The FRCM composite in this study was comprised of PBO fibers with an inorganic matrix. The PBO fibers were in the form of a bidirectional unbalanced fiber net as shown in Figure 9. The properties of the materials in this study (concrete, steel reinforcing bars, and composite fibers) are summarized in Table 1. The nominal thickness of the composite fibers t_f was obtained by assuming the fibers in the primary

fiber direction (defined in Figure 9) were distributed evenly across the width of the composite.

The strengthened beams that were considered in the analytical study were those that failed due to composite fiber rupture and were fully wrapped around the perimeter with the primary fiber direction (defined in Figure 9) oriented perpendicular to the longitudinal axis of the beam. Two beams (beams N-P-4-S-1 and N-P-4-8S-1) were strengthened with one layer of discontinuous strips, with strip width and strip spacing indicated in Figures 7b and 7c. Two other beams (beams N-P-4-C-1 and N-P-4-C-2) were strengthened continuously along the test region. Beam N-P-4-C-1 was strengthened with one layer of composite (Figure 7d), and beam N-P-4-C-2 was strengthened with two layers of composite (Figure 7e). The beams are listed in Table 2, which also indicates the concrete batch (see Table 1) used to construct each beam.

The beams were tested under monotonic loading conditions. The response was measured by a variety of instruments including a load cell at the beam loading end, linear variable differential transformers (LVDTs) mounted at different positions and inclinations along the beam length, a rotational variable differential transformer (RVDT) mounted along the side face, and strain gages mounted to the reinforcing bars and composite fibers at different positions along the length. The experimental response is compared with the analytical response in the sections that follow. Additional information on the experimental program is discussed in detail in [Alabdulhady et al. 2017, Alabdulhady and Sneed 2018].

3.2 TORSIONAL MOMENT – TWIST PER UNIT LENGTH (T-ψ) RESPONSE

The experimental and analytical T-ψ response for all beams is plotted in Figure 10. Results in Figure 10 show that the analytical model predicted the different stages of the experimental response, characterized by a linear behavior before cracking with high initial torsional stiffness (pre-cracking stage), followed by an increase in the twist angle without increasing torsional moment due to the redistribution of forces from the concrete to the steel reinforcement. Then, the behavior became non-linear up to the peak torsional moment T_u (i.e., the torsional strength). The drop in the T-ψ response after the peak torsional moment (post-peak stage) was also predicted by the analytical model.

Values of the experimental and analytical cracking moment and peak torsional moment, T_{cr} and T_u, respectively, and the corresponding angle of twist per unit length, ψ_{cr} and ψ_u, respectively, for each beam are summarized in Table 2. Results in Table 2 show that the model was able to predict the values of T_{cr} and ψ_{cr} with an error in the range of 6-23% and 3-36%, respectively. The values of T_u and ψ_u were predicted with an error in the range of 0-22% and 1-24%, respectively.

3.3 STRAIN IN STEEL REINFORCING BARS AND PBO FIBERS

The maximum values of strain at the peak torsional moment T_u in the transverse reinforcing bars (stirrups) ε_t and the FRCM composite fibers ε_f determined by the experimental and analytical model results are summarized in Table 3. Reasonable agreement was achieved between the experimental and analytical results.

Results in Table 3 show that at the peak torsional moment, the analytical strain in the PBO fibers for beams strengthened with one and two layers of continuous wrapping

(beams N-P-4-C-1 and N-P-4-C-2) was lower than that in beams with discontinuous strips. Furthermore, the analytical strain in fibers for beam N-P-4-C-2, which had two layers of composite, was lower than in beam N-P-4-C-1, which had one layer of composite. The same variation in fiber strain with respect to the number of composite layers was also reported by Zojaji and Kabir [2012] for FRP-strengthened beams. The trend is also in agreement with experimental results, which showed that the contribution of the composite to the torsional strength reduces with an increasing number of composite layers [Alabdulhady et al. 2017]. For both beams N-P-4-C-1 and N-P-4-C-2, the strain in the fibers is significantly lower than the ultimate strain of the fibers (1.45%, Table 1), which is also in agreement with results by Zojaji and Kabir [2012] for FRP-strengthened beams. The effective fiber strain given by Equation 26 is a function of concrete section dimensions and the effective shear flow thickness (t_d). In fact, the effective strain of the fiber is only a practical criterion for analytical models [Zojaji and Kabir 2012].

3.4 ANALYTICAL BEHAVIOR OF CONCRETE AND STEEL REINFORCEMENT IN FRCM-STRENGTHENED BEAMS

The aim of this section is to illustrate the effect of the composite system on the material behavior of the FRCM-strengthened beams. Figure 11 plots the analytical stress-strain behavior of the concrete and steel reinforcing bars for the control beam and beam N-P-4-C-1 as a representative comparison between the unstrengthened and strengthened beams. Locations of reinforcing steel yielding and peak torsional moment are indicated in the graphs. The applied shear stress τ_{lt} versus shear strain γ_{lt} (Figure 11a) and the concrete

behavior (Figures 11b,c) was different in both cases. The strengthened beam had higher values of stresses with larger corresponding strains due to the effect of confinement and the contribution of the composite to the overall behavior as shown in Figures 11a-c. Furthermore, for the control (unstrengthened) beam, the location of the peak torsional moment on the curves is close to the peak stress and with approximately at the same strain value (Figures 11a-c). On the other hand, the peak torsional moment of the strengthened beam (N-P-4-C-1) occurs at a stress that is lower than the peak stress and with a larger strain value. This indicates that the FRCM-strengthened beam was able to carry additional load even though the concrete had reached its ultimate capacity due to the effect of confinement provided by the composite system.

4. CONCLUSIONS

A softened membrane model for torsion (SMMT) for FRP-wrapped beams introduced by Zojaji and Kabir [2012] was implemented in this study to predict the full torsional response of RC beams externally bonded with PBO-FRCM composite. Experimental results from five beams tested by the authors [Alabdulhady et al. 2017, Alabdulhady and Sneed 2018] were considered in this paper to validate the applicability and the accuracy of the model. The response of the control (unstrengthened) beam was compared with the response predicted by the Jeng and Hsu [2009] model, then modifications based on the Zojaji and Kabir model [2012] were implemented to predict the full torsional moment – twist per unit length response for the strengthened beams. The most significant conclusions from this study are summarized below:

1. The torsional behavior of the experimentally tested beams was reasonably predicted by the analytical model in terms of initial stiffness, cracking torsional moment, and peak torsional moment and the corresponding angles of twist per unit length. These results confirm the feasibility of the SMMT model to predict the torsional response of FRCM-strengthened beams.
2. Values of the cracking and peak torsional moment and corresponding twist per unit length were predicted analytically with maximum error of (23%, 22%), and (36% and 24%), respectively.
3. Beams with fully wrapped (continuous and strips) configurations were considered in this study. The mode of failure for all strengthened beam was governed by composite fiber rupture. Further modifications are required to extend the model to the composite debonding failure mode.
4. Reasonable agreement was achieved between the experimental and analytical model values of strain in the stirrups and the composite fibers at the peak torsional moment.
5. The effect of confinement and the contribution of the composite on the concrete strength could be seen clearly by the higher concrete stress with larger corresponding strain for the strengthened beams compared with the unstrengthened beam at peak torsional moment.

APPENDIX: EXAMPLE

A representative example of beam N-P-4-C-1 is provided in this appendix to illustrate the calculation details. Table A shows the results of three points from the torsional moment – twist per unit length response curve (first yield, second yield, and

peak torsional moment). The results in this section were compared with the SMM analytical model study on shear presented by Hsu and Zhu [2002] due to lack of examples and information on torsion with the SMMT model. Signs and the predicted values were in agreement with the calculated values of Hsu and Zhu example [Hsu and Zhu 2002].

ACKNOWLEDGEMENTS

The authors would like to thanks the Higher Committee for Education Development in Iraq (HCED) for the financial support.

NOMENCLATURE

A_0	area enclosed by the centerline of shear flow; $A_0 = A_c - 0.5p_c t_d + t_d^2$
A_c	cross sectional area bounded by the outer perimeter of the concrete
A_{fl}	fiber area in the longitudinal direction; $A_{fl} = n_{fl} t_{fl} p_{fl}$
A_{ft}	fiber area in the transverse direction; $A_{ft} = n_{ft} t_{ft} w_f$
A_{sl}	total cross sectional area of the longitudinal steel bars
A_{st}	cross sectional area of one transverse steel bar
b	width of the beam section
E_c	elastic modulus of the concrete
E_f	elastic modulus of the fibers
E_s	elastic modulus of steel reinforcing bars
$f'c$	concrete cylinder compressive strain

f_{cr}	cracking stress of the concrete
f_{fl} , f_{ft}	fiber stresses in the longitudinal and transverse direction, respectively
f_f	tensile strength in the direction of the fiber
f_{fe}	effective tensile strength of the fibers
f_{fu}	ultimate tensile strength of the fibers
f_s	smeared (average) stress of the steel reinforcing bars
f_{sl} , f_{st}	smeared (average) steel stresses in the longitudinal and transverse direction, respectively
f_{su}	maximum stress of the steel reinforcing bars
f_{sy}	yield stress of the steel reinforcing bars
h	height of the beam section
k	composite confinement parameter
k_{1c}	ratio of the average compressive stress to the peak compressive stress in the concrete struts, taking into account the tensile stress of concrete
k_{1t}	ratio of the average tensile stress to the peak tensile stress in the concrete struts
L_e	effective bond length
n_{fl}	number of composite layer in the longitudinal direction
n_{ft}	number of composite layer in the transverse direction
p_0	perimeter of centerline of shear flow zone; $p_0 = p_c - 4t_d$
p_c	perimeter of outer concrete cross section
p_{st}	perimeter of the area enclosed by the stirrup
p_{fl}	perimeter of the strengthened beam cross section enclosed by the composite in the longitudinal direction

p_{ft}	perimeter of the strengthened beam cross section enclosed by the composite in the transverse direction
q	shear flow
s	center-to-center spacing of the transverse reinforcing bars (stirrups)
s_f	center-to-center spacing between the centerline of the composite strips
T	torsional moment
t_d	effective thickness of shear flow zone
t_{fl}	fiber thickness in the longitudinal direction of the beam
t_{ft}	fiber thickness in the transverse direction of the beam
w	out-of-plane displacement in the direction normal to the membrane element as shown in Figure 4
w_f	width of the composite strip
α	rotating angle, angle of applied principle compressive stress (2-axis) with respect to longitudinal steel bars (l-axis)
α_2	fixed angle, angle of applied principle compressive stress (2-axis) with respect to the longitudinal steel reinforcing bars (*l*-axis)
α_f	constant parameter taking into account the difference in stress distribution between continuous composite sheets and strips
α_n	in-section coefficient of effectiveness of the confinement
β	deviation angle taken as $0.5tan^{-1}(\gamma_{21}/(\varepsilon_2 - \varepsilon_1))$
ε_0	concrete strain at the peak compressive stress $f'c$ taken as -0.00235
ε_2 , ε_1	smeared (average) biaxial strain of concrete in the 2-direction and the 1-direction, respectively
$\overline{\varepsilon_2}$, $\overline{\varepsilon_1}$	smeared (average) uniaxial strain of concrete in the 2-direction and the 1-direction, respectively

$\bar{\varepsilon_{2s}}$, $\bar{\varepsilon_{1s}}$	maximum uniaxial strain at the surface in the 2-direction and the 1-direction, respectively; $\bar{\varepsilon_{2s}} = 2\bar{\varepsilon_2}$ and $\bar{\varepsilon_{1s}} = 2\bar{\varepsilon_1}$
ε_{cr}	cracking strain of concrete
ε_{cu}	maximum strain of concrete
ε_f	fiber tensile strain
ε_{fe}	effective fiber tensile strain
ε_{fu}	ultimate fiber tensile strain
ε_l , ε_t	smeared (average) biaxial strain of steel bars in the *l*-direction and the *t*-direction, respectively
$\bar{\varepsilon_l}$, $\bar{\varepsilon_t}$	smeared (average) uniaxial strain of steel bars in the *l*-direction and the *t*-direction, respectively
ε_s	smeared (average) strain of steel reinforcing bars
$\bar{\varepsilon_n}$	smeared (average) uniaxial yield strain of the steel reinforcing bars
$\bar{\varepsilon_s}$	smeared (average) uniaxial strain of the steel reinforcing bars
ε_{sf}	smeared (average) strain of steel reinforcing bars that yield first
ε_{su}	maximum strain of steel reinforcing bar
ε_{sy}	yield strain of steel reinforcing bar
γ_{21}	smeared (average) biaxial shear strain of concrete in the 2-1direction
$\bar{\gamma}_{21}$	smeared (average) uniaxial shear strain of concrete in the 2-1direction
γ_{lt}	smeared (average) shear strain of steel reinforcing bars in the *l*-*t* direction
$б_2^c$, $б_1^c$	smeared (average) normal stresses of concrete in the 2-direction and the 1-direction, respectively
$б_l$, $б_t$	applied normal stresses of steel reinforcing bars in the *l*-direction and the *t*-direction, respectively.
τ_{21}^c	smeared (average) shear stress of concrete in 2-1 coordinate

τ_{lt} applied shear stress in the *l*-*t* coordinate of the steel bars

ρ steel reinforcement ratio

ρ_{fl}, ρ_{ft} longitudinal and transverse fiber ratios, respectively; $\rho_{fl} = A_{fl}/p_0\, t_d$ and $\rho_{ft} = A_{ft}p_{ft}/p_0\, t_d s_f$

ρ_{sl}, ρ_{st} longitudinal and transverse steel ratios, respectively; $\rho_{sl} = A_{sl}/p_0\, t_d$ and $\rho_{st} = A_{st}p_{st}/p_0\, t_d s$

ν_{12}, ν_{21} Hsu/Zhu ratios used in the SMM: $\nu_{12} = 0.2 + 850\varepsilon_{sf}$ for $\varepsilon_{sf} \leq \varepsilon_y$ or $\nu_{12} = 1.9$ for $\varepsilon_{sf} > \varepsilon_y$; $\nu_{21} = 0$

ψ angle of twist per unit length

ϕ curvature of the concrete struts along the 2-direction

φ curvature of the concrete struts along the 1-direction

ω_n volumetric mechanical ratio of external confinement

ζ softened coefficient of concrete in compression

Table 1. Measured concrete, steel reinforcement and PBO fiber properties.

Concrete		
	Batch 1	Batch 2
Compressive strength, MPa	39.3	34.5
Splitting tensile strength, MPa	3.2	2.8
Modulus of elasticity, GPa	28.6	28.6
Steel reinforcing bars		
	No. 3	No. 5
Modulus of elasticity, GPa	200	193
Yield strength, MPa	454	469
Ultimate strength, MPa	717	738
PBO Fiber		
Nominal thickness in primary fiber direction, mm	0.046	
Ultimate tensile strength, MPa	3015	
Modulus of elasticity, GPa	206	
Ultimate tensile strain, mm/mm	0.0145	

Table 2. Summary of experimental and analytical torsional moment and corresponding twist per unit length.

Beam ID	Concrete Batch	T_{cr} kN-m			Ψ_{cr} deg./m			T_u kN-m			ψ_u deg./m		
		Exp.	Ana.	Ana. /Exp.	Exp.	Ana.	Ana. /Exp.	Exp.	Ana.	Ana. /Exp.	Exp.	Ana.	Ana. /Exp.
Control [Alabdulhady et al. 2017, Alabdulhady and Sneed 2018]	1	10.4	11.0	1.06	0.165	0.209	1.25	16.8	16.9	1.00	3.346	3.583	1.08
N-P-4-S-1 [Alabdulhady et al. 2017, Alabdulhady and Sneed 2018]	1	14.3	11.9	0.84	0.134	0.138	1.03	21.8	25.9	1.19	9.646	9.567	0.99
N-P-4-8S-1 [Alabdulhady and Sneed 2018]	2	11.1	12.1	1.09	0.244	0.157	0.64	20.2	24.8	1.22	8.937	7.559	0.85
N-P-4-C-1 [Alabdulhady et al. 2017, Alabdulhady and Sneed 2018]	1	13.7	11.8	0.86	0.161	0.173	1.07	27.2	27.3	1.01	9.055	8.622	0.95
N-P-4-C-2 [Alabdulhady et al. 2017, Alabdulhady and Sneed 2018]	1	16.3	12.5	0.77	0.157	0.185	1.18	35.1	36.3	1.03	9.488	7.165	0.76

Table 3. Strain in the transverse reinforcing bars and composite fibers at the peak torsional moment.

Beam	Transverse reinforcing bar strain			Composite fiber strain		
	ε_t (%) (Exp.)	ε_t (%) (Ana.)	Ana. /Exp.	ε_f (%) (Exp.)	ε_f (%) (Ana.)	Ana. /Exp.
Control	0.252	0.239	0.95	--	--	--
N-P-4-S-1	0.295	0.424	1.44	1.026	0.707	0.69
N-P-4-8S-1	0.386	0.396	1.03	0.506	0.935	1.85
N-P-4-C-1	0.275	0.358	1.30	0.822	0.395	0.48
N-P-4-C-2	0.305	0.165	0.54	0.653	0.248	0.38

Table 4. Representative example of beam (N-P-4-C-1).

Variable	Equation #	Unit	Calculated Values		
			First Yield	Second Yield	Peak Torque
ε_2	Selected		-0.00069	-0.00119	-0.00266
ε_1	Assumed		0.00454	0.00710	0.01292
γ_{12}	Assumed		-0.00072	-0.00103	-0.00196
ε_l	Eq. 3a		0.00157	0.00244	0.00415
ε_t	Eq. 3b		0.00228	0.00347	0.00611
ν_{12}	Nomenclature		1.9	1.9	1.9
$\overline{\varepsilon_2}$	Eq. 4b		-0.00069	-0.00119	-0.00266
$\overline{\varepsilon_1}$	Eq. 4a		0.00323	0.00484	0.00787
$\overline{\varepsilon_l}$	Eq. 5a		0.00091	0.00131	0.00163
$\overline{\varepsilon_t}$	Eq. 5b		0.00163	0.00234	0.00358
ζ	Eq. 13		0.595	0.525	0.442
$б_2^c$	Eq. 11	MPa	-15.16	-16.93	-16.19
$б_1^c$	Eq. 17	MPa	1.28	1.10	0.92
$б_l$	Eq. 1a	MPa	-2.56	-1.59	-0.58
$б_t$	Eq. 1b	MPa	2.37	2.23	1.57
τ_{21}^c	Eq. 21	MPa	-1.13	-1.12	-1.07
f_l	Eq. 22	MPa	175.67	252.97	313.85
f_t	Eq. 22	MPa	325.16	388.70	392.11
ρ_{sl}	Nomenclature		0.0313	0.0294	0.0259
ρ_{st}	Nomenclature		0.0213	0.0200	0.0176
ρ_{ft}	Nomenclature		0.00183	0.00172	0.00151
ε_{ef}	Eq. 26		0.00335	0.00354	0.00395
f_f	Eq. 25	MPa	690.78	729.48	813.61
τ_{lt}	Eq. 1a	MPa	8.22	9.01	8.56
γ_{lt}	Eq. 3c		0.00523	0.00829	0.01558
t_d	Eqs. 9 &10	mm	28.28	30.41	35.30
T	Eq. 2	kN-m	22.48	25.99	27.32
ψ	Eq. 6	deg./m	2.80	4.49	8.62

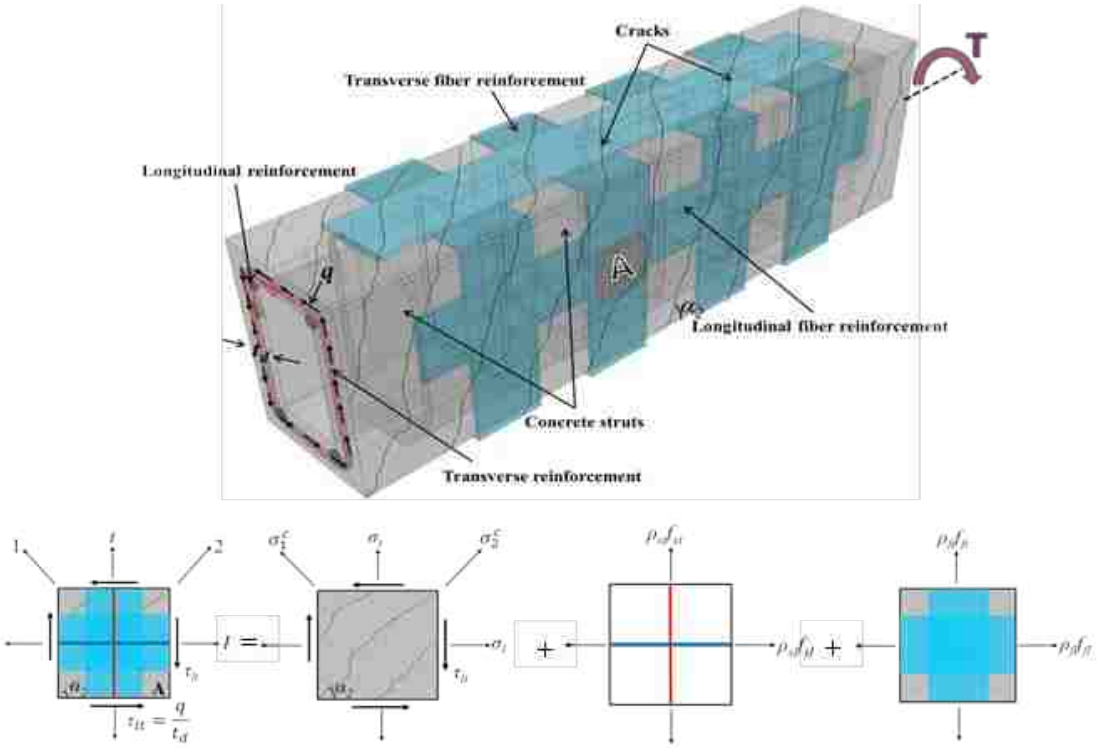

Figure 1. Torsional deformation of fiber reinforced composite-strengthened RC beam and in-plane stresses of an element taken from shear flow zone (adapted from [Chalioris 2007]).

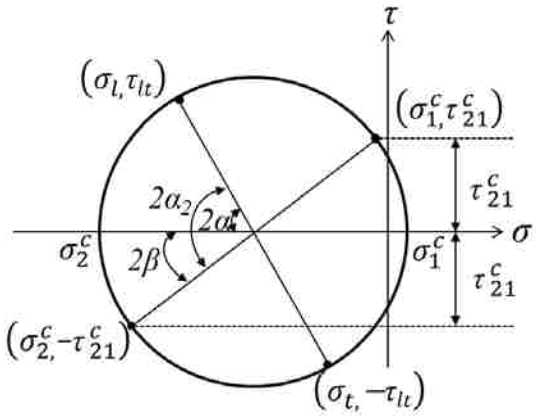

Figure 2. Mohr circle for stresses.

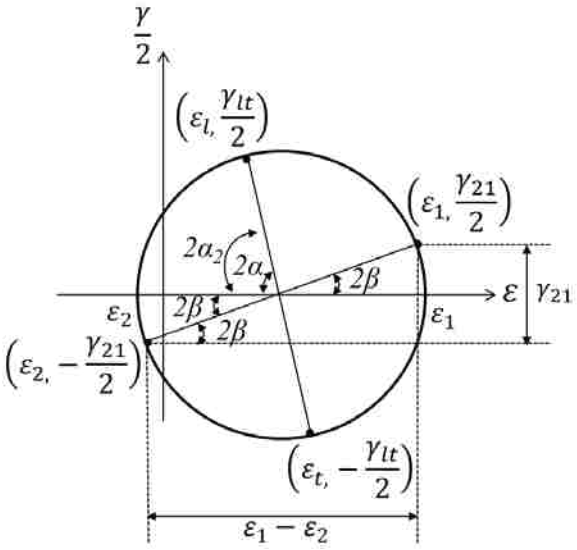

Figure 3. Mohr circle for strains.

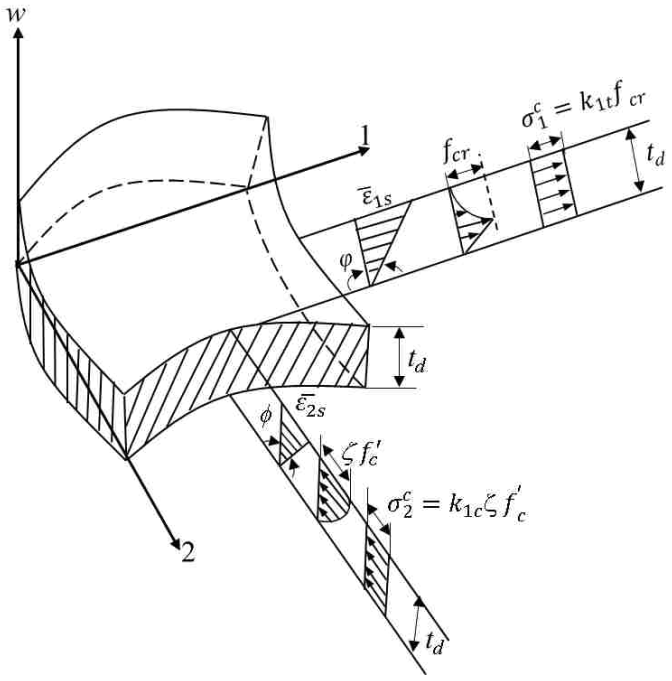

Figure 4. In-plane biaxial stress state with out-of-plane bending (adapted from [Jeng and Hsu 2009]).

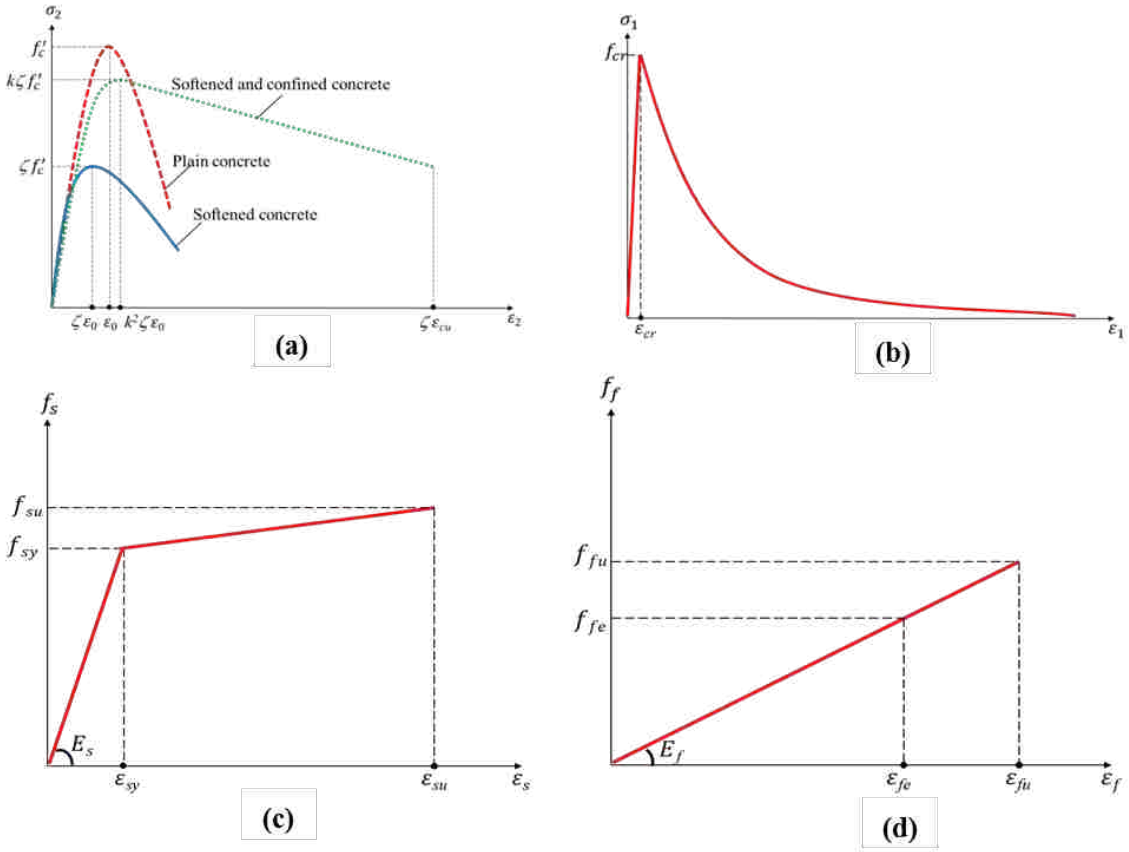

Figure 5. Constitutive stress–strain relationships for the materials: (a) concrete in compression, (b) concrete in tension, (c) steel reinforcing bar in tension; (d) composite fiber in tension.

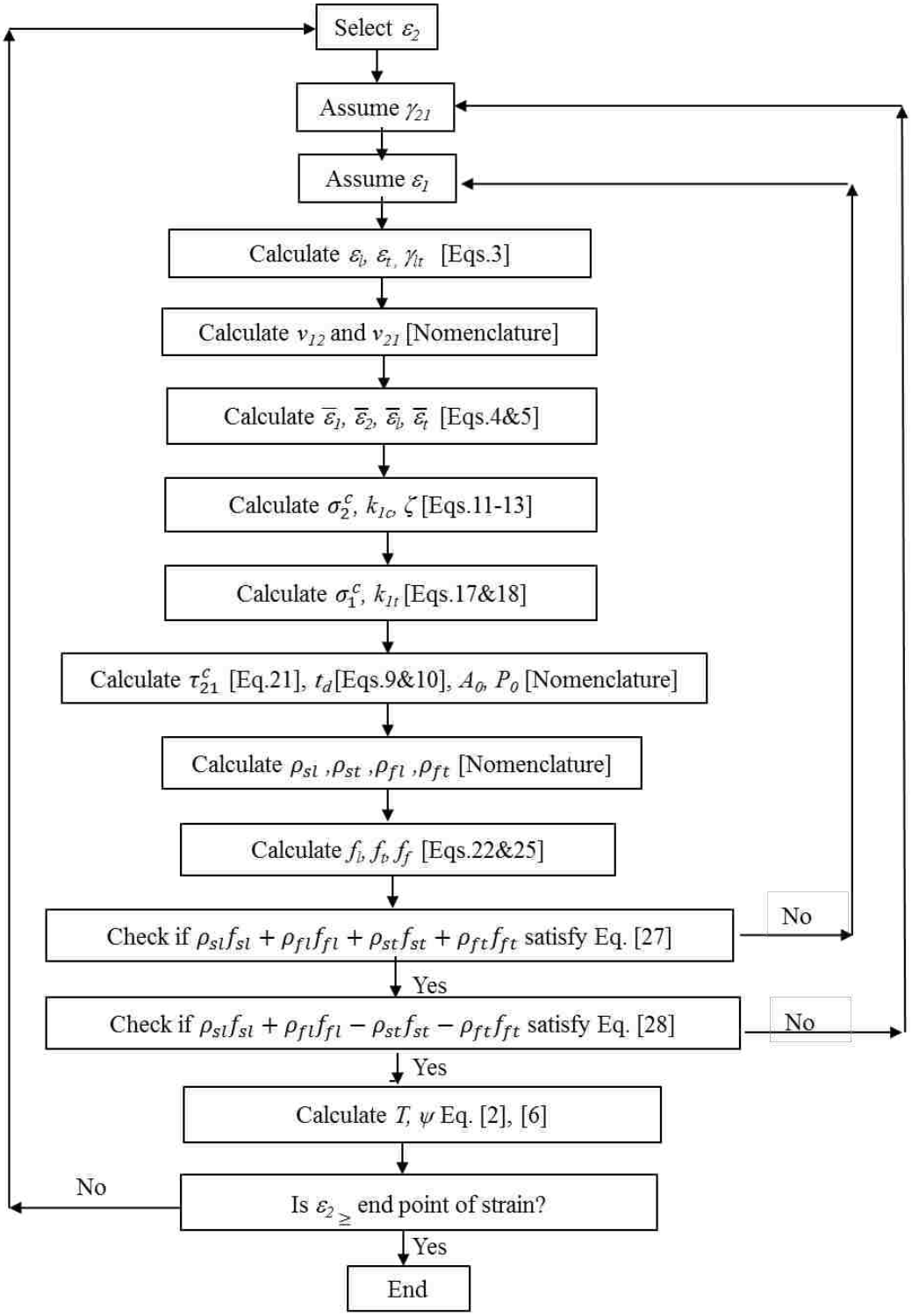

Figure 6. Solution algorithm.

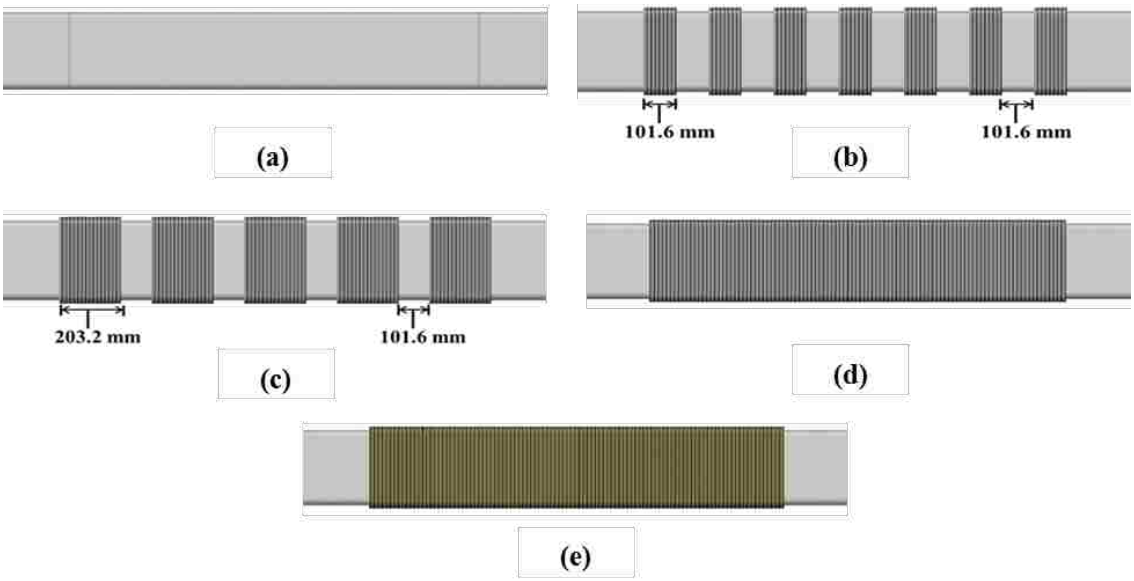

Figure 7. Schematic configuration of beams considered in this study: a) control beam, b) one layer, 90° strips (N-P-4-S-1), c) one layer, 90° strips (N-P-4-8S-1), d) one layer, 90° continuous (N-P-4-C-1), e) two layers, 90° continuous (N-P-4-C-2).

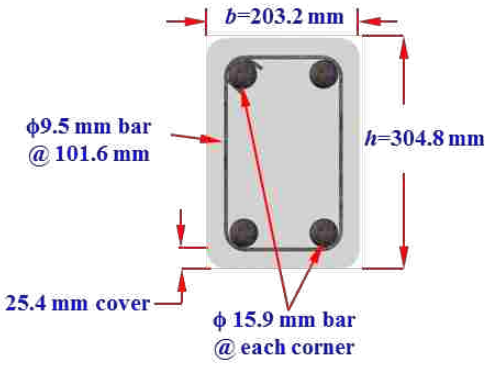

Figure 8. Internal reinforcement details.

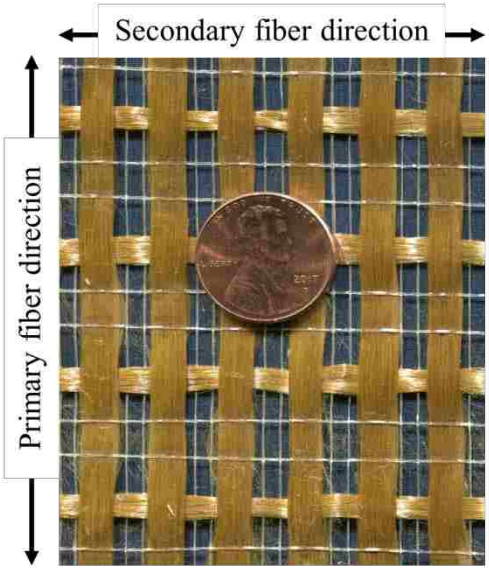

Figure 9. PBO fiber directions.

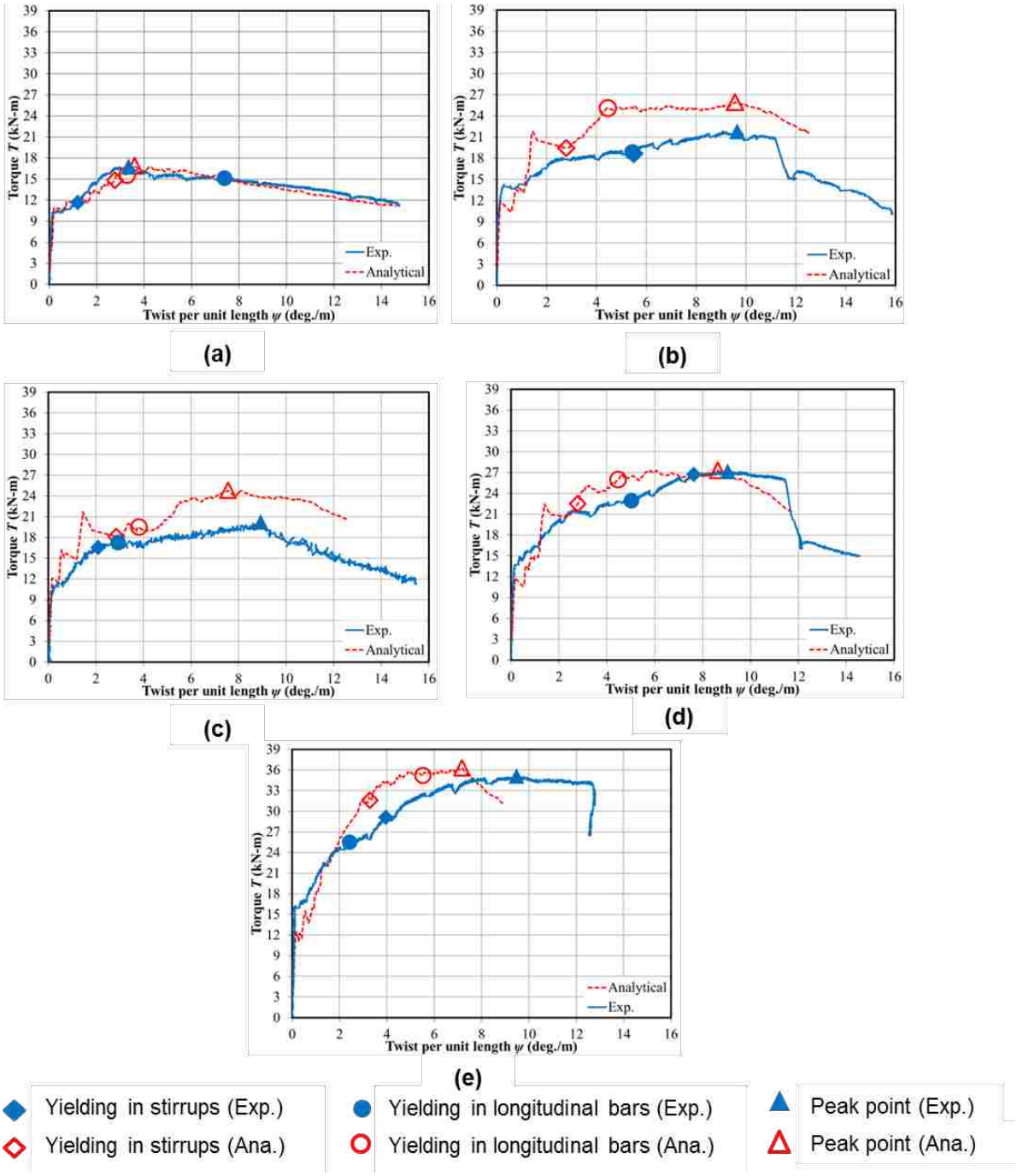

Figure 10. Experimental and analytical torsional moment-twist per unit length (T-ψ) response: a) control beam, b) N-P-4-S-1, c) N-P-4-8S-1, d) N-P-4-C-1, e) N-P-4-C-2.

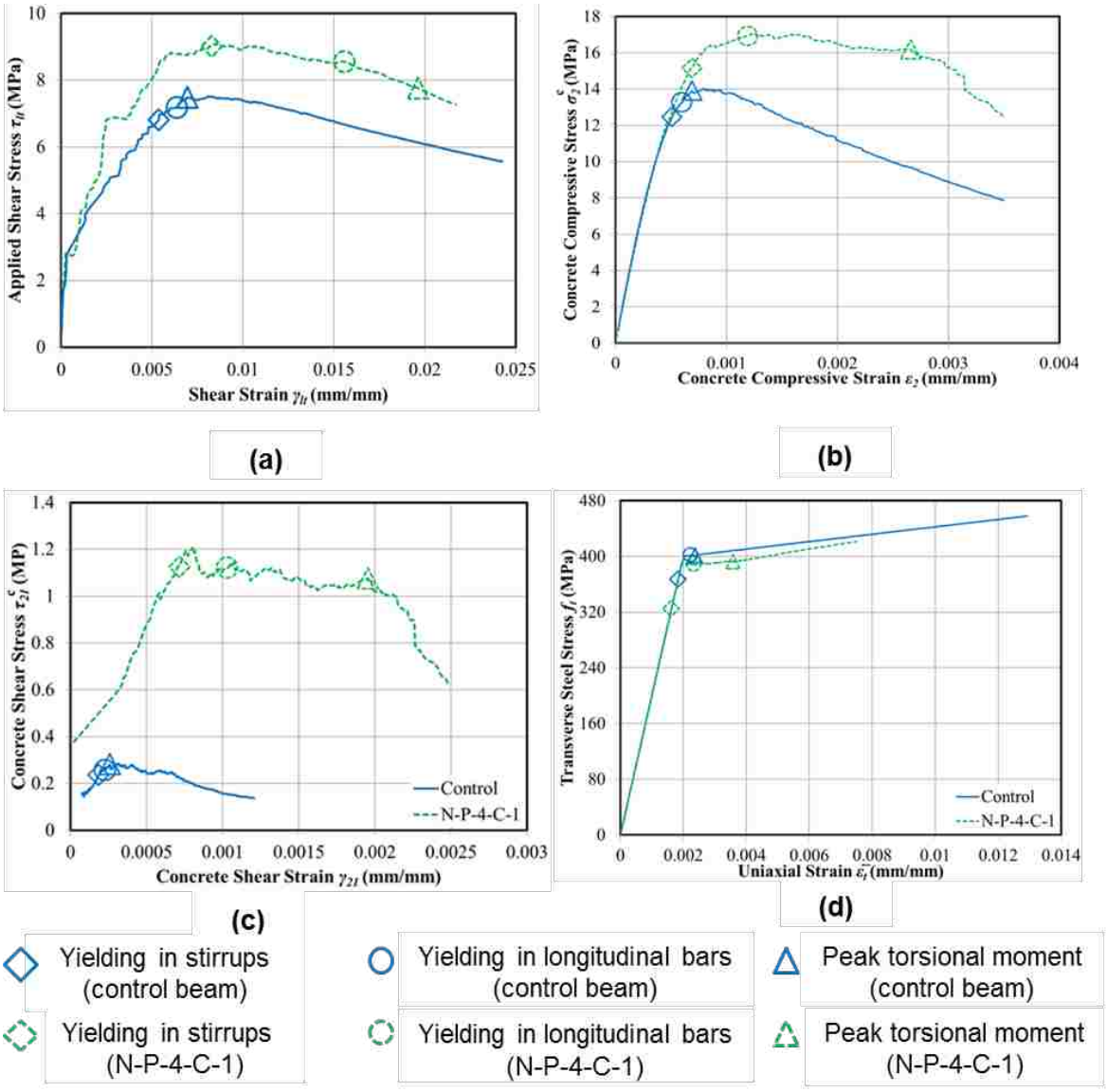

Figure 11. Comparison of analytical material behavior for the control beam and beam N-P-4-C-1: a) applied shear stress τ_{lt} vs. shear strain γ_{lt}, b) concrete compressive stress $\acute{o}_2^c$ vs. compressive strain ε_2, c) concrete shear stress τ_{21}^c vs. shear strain γ_{21}, d) transverse steel stress f_t vs. uniaxial steel strain $\bar{\varepsilon_t}$.

REFERENCES

Alabdulhady, M. Y., & Sneed, L. H. (2018). A study of the effect of fiber orientation on the torsional behavior of RC beams strengthened with PBO-FRCM composite. *Construction and Building Materials*, *166*, 839-854.

Alabdulhady, M. Y., Sneed, L. H., & Carloni, C. (2017). Torsional behavior of RC beams strengthened with PBO-FRCM composite–An experimental study. *Engineering Structures*, *136*, 393-405.

Aljazaeri, Z. R., & Myers, J. J. (2017). Strengthening of Reinforced-Concrete Beams in Shear with a Fabric-Reinforced Cementitious Matrix. *Journal of Composites for Construction*, *21*(5), 04017041.

Ameli, M., & Ronagh, H. R. (2007). Analytical method for evaluating ultimate torque of FRP strengthened reinforced concrete beams. *Journal of Composites for construction*, *11*(4), 384-390.

Ameli, M., Ronagh, H. R., & Dux, P. F. (2007). Behavior of FRP strengthened reinforced concrete beams under torsion. *Journal of Composites for Construction*, *11*(2), 192-200.

Babaeidarabad, S., Loreto, G., & Nanni, A. (2014). Flexural strengthening of RC beams with an externally bonded fabric-reinforced cementitious matrix. *Journal of Composites for Construction*, 18(5), 04014009.

Belarbi, A., & Hsu, T. T. (1995). Constitutive laws of softened concrete in biaxial tension compression. *Structural Journal*, *92*(5), 562-573.

Bredt, R. (1896). Kritische Bemerkungen zur drehungselastizitat. *Zeitschrift des Vereines Deutscher Ingenieure*, *40*(28), 785-790.

Carloni, C., Mazzotti, C., Savoia, M., & Subramaniam, K. V. (2014). Confinement of Masonry Columns with PBO FRCM Composites. *Key Engineering Materials*, *624*.

Chai, H. K., Majeed, A. A., & Allawi, A. A. (2014). Torsional Analysis of Multicell Concrete Box Girders Strengthened with CFRP Using a Modified Softened Truss Model. *Journal of Bridge Engineering*, *20*(8), B4014001.

Chalioris, C. E. (2007). Analytical model for the torsional behavior of reinforced concrete beams retrofitted with FRP materials. *Engineering Structures*, *29*(12), 3263-3276.

Chalioris, C. E. (2008). Torsional strengthening of rectangular and flanged beams using carbon fibre-reinforced-polymers–Experimental study. *Construction and Building Materials*, *22*(1), 21-29.

Colajanni, P., De Domenico, F., Recupero, A., & Spinella, N. (2014). Concrete columns confined with fibre reinforced cementitious mortars: experimentation and modelling. Construction and Building Materials, 52, 375-384.

D'Ambrisi, A., & Focacci, F. (2011). Flexural strengthening of RC beams with cement-based composites. Journal of Composites for Construction, 15(5), 707-720.

D'Antino, T., Sneed, L. H., Carloni, C., & Pellegrino, C. (2015). Influence of the substrate characteristics on the bond behavior of PBO FRCM-concrete joints. *Construction and Building Materials*, *101*, 838-850.

Deifalla, A., & Ghobarah, A. (2010). Full torsional behavior of RC beams wrapped with FRP: analytical model. *Journal of Composites for Construction*, *14*(3), 289-300.

Deifalla, A., Awad, A., & Elgarhy, M. (2013). Effectiveness of externally bonded CFRP strips for strengthening flanged beams under torsion: An experimental study. *Engineering Structures*, *56*, 2065-2075.

fib Bulletin 14 (2001). Externally bonded FRP reinforcement for RC structures. CEB-FIP, Lausanne, Switzerland, 2001, 130 pp.

Ganganagoudar, A., Mondal, T. G., & Prakash, S. S. (2016). Analytical and finite element studies on behavior of FRP strengthened RC beams under torsion. *Composite Structures*, *153*, 876-885.

Ghobarah, A., Ghorbel, M. N., & Chidiac, S. E. (2002). Upgrading torsional resistance of reinforced concrete beams using fiber-reinforced polymer. *Journal of Composites for Construction*, *6*(4), 257-263.

Gonzalez-Libreros, J. H., Sabau, C., Sneed, L. H., Pellegrino, C., & Sas, G. (2017). State of research on shear strengthening of RC beams with FRCM composites. *Construction and Building Materials*, *149*, 444-458.

Gonzalez-Libreros, J. H., Sabau, C., Sneed, L. H., Pellegrino, C., & Sas, G. (2017). State of research on shear strengthening of RC beams with FRCM composites. *Construction and Building Materials*, *149*, 444-458.

Gonzalez-Libreros, J. H., Sneed, L. H., D'Antino, T., & Pellegrino, C. (2017). Behavior of RC beams strengthened in shear with FRP and FRCM composites. *Engineering Structures*, *150*, 830-842.

Hii, A. K., & Al-Mahaidi, R. (2006). An experimental and numerical investigation on torsional strengthening of solid and box-section RC beams using CFRP laminates. *Composite Structures, 75*(1), 213-221.

Hii, A. K., & Al-Mahaidi, R. (2006). Experimental investigation on torsional behavior of solid and box-section RC beams strengthened with CFRP using photogrammetry. *Journal of Composites for Construction*, *10*(4), 321-329.

Hsu, T. T. (1990). Shear flow zone in torsion of reinforced concrete. *Journal of Structural Engineering*, *116*(11), 3206-3226.

Hsu, T. T. (1993). Unified theory of reinforced concrete. *Boca Raton (FI): CRC*.

Hsu, T. T., & Zhu, R. R. (2002). Softened membrane model for reinforced concrete elements in shear. *Structural Journal*, *99*(4), 460-469.

Jeng, C. H., & Hsu, T. T. (2009). A softened membrane model for torsion in reinforced concrete members. *Engineering Structures*, *31*(9), 1944-1954.

Loreto, G., Babaeidarabad, S., Leardini, L., & Nanni, A. (2015). RC beams shear-strengthened with fabric-reinforced-cementitious-matrix (FRCM) composite. International Journal of Advanced Structural Engineering (IJASE), 7(4), 341-352.

MATLAB and Statistics Toolbox Release 2016a. The MathWorks, Inc., Natick, Massachusetts, United States.

Ombres, L. (2011). Flexural analysis of reinforced concrete beams strengthened with a cement based high strength composite material. Composite Structures, 94(1), 143-155.

Ombres, L. (2012). Shear capacity of concrete beams strengthened with cement based composite materials. In Proceedings of the 6th International Conference on FRP Composites in Civil Engineering. (CICE 2012). Roma, Italy.

Ombres, L. (2015). Structural performances of reinforced concrete beams strengthened in shear with a cement based fiber composite material. Composite Structures, 122, 316-329.

Panchacharam, S., & Belarbi, A. (2002). Torsional behavior of reinforced concrete beams strengthened with FRP composites. In *First FIB Congress, Osaka, Japan* (Vol. 1, pp. 01-110).

Salom, P. R., Gergely, J., & Young, D. T. (2004). Torsional strengthening of spandrel beams with fiber-reinforced polymer laminates. *Journal of Composites for Construction*, *8*(2), 157-162.

Shen, K., Wan, S., Mo, Y., & Jiang, Z. (2017). Theoretical analysis on full torsional behavior of RC beams strengthened with FRP materials. *Composite Structures*.

Sneed, L. H., Carloni, C., Baietti, G., & Fraioli, G. (2017). Confinement of Clay Masonry Columns with SRG. In *Key Engineering Materials* (Vol. 747, pp. 350-357). Trans Tech Publications.

Sneed, L. H., D'Antino, T., & Carloni, C. (2014). Investigation of bond behavior of PBO fiber-reinforced cementitious matrix composite-concrete interface. *ACI Materials Journal*, *111*(1-6), 1-12.

Sneed, L.H., Verre, S., Carloni, C., & Ombres, L., 2016. "Flexural Behavior of RC Beams Strengthened with Steel-FRCM Composite." *Engineering Structures*, 127, pp. 686-699.

Trapko, T., Urbańska, D., & Kamiński, M. (2015). Shear strengthening of reinforced concrete beams with PBO-FRCM composites. Composites Part B: Engineering, 80, 63-72.

Vintzileou, E., & Panagiotidou, E. (2008). An empirical model for predicting the mechanical properties of FRP-confined concrete. *Construction and Building Materials*, *22*(5), 841-854.

Zhu, R. R., & Hsu, T. T. (2002). Poisson effect in reinforced concrete membrane elements. *Structural Journal*, *99*(5), 631-640.

Zojaji, A. R., & Kabir, M. Z. (2012). Analytical approach for predicting full torsional behavior of reinforced concrete beams strengthened with FRP materials. *Scientia Iranica*, *19*(1), 51-63.

SECTION

2. SUMMARY, CONCLUSIONS, AND RECOMMENDATIONS

2.1 SUMMARY OF RESEARCH WORK

The aim of this research was to study the torsional behavior of RC beams strengthened externally with PBO-FRCM composite. Experimental, numerical, and analytical studies were included in this study.

The experimental program included 11 beams, one without strengthening as a control beam and 10 strengthened with PBO-FRCM composite material in different wrapping configurations. The effect of different parameters such as number of wrapped sides, the continuity of composite layer (along the beam length), number of composite layers and fiber orientation on the torque-twist response, rotational capacity, and mode of failure was introduced and discussed. Strains measured in the internal and external reinforcement and the longitudinal elongation of the beam with respect to its axis were examined. The contribution of the strengthening system to the torsional strength was evaluated by the strain measured in the composite fibers. Provisions used to estimate the torsional strength of RC beams with fully-wrapped, externally-bonded fiber reinforced polymer (FRP) composites were explored to examine their applicability on the beams strengthened with PBO-FRCM composite.

In order to gain a better understanding of the torsional behavior of FRCM-strengthened RC beams, six beams with different strengthening schemes were evaluated numerically by implementing a nonlinear software program package LS-DYNA 971 R3. Torsional strength, torsional moment-twist per unit length response, and strains in the

internal and external reinforcement were evaluated and compared with experimental results to validate the model and determine its accuracy. The model was further used for a parametric study in order to shed light on the influence of concrete compressive strength and composite strip width and spacing on the response of FRCM-strengthened RC beams. Furthermore, an analytical study based on the softened membrane model for torsion (SMMT) was conducted to study the full torsional response of PBO-FRCM-strengthened beams.

2.2 CONCLUSIONS

This section summarizes the conclusions from the experimental, numerical, and analytical studies on torsional strengthening of RC beams strengthened with PBO-FRCM composite. With regard to the experimental work, the following conclusions are presented:

- This study demonstrated that externally bonded PBO-FRCM composites can be used to strengthen RC beams in torsion. Failure of the strengthened beams was associated with debonding of the composite, which was characterized by significant slippage between the fibers and matrix.
- Increases in the cracking torque, torsional strength, and corresponding values of twist were achieved by beams strengthened with a 4-sided wrapping configuration relative to the control (unstrengthened) beam. On the other hand, the 3-sided wrapping configuration was found to be largely ineffective in improving the torsional performance.

- The 4-sided wrapping configuration improved the torsional performance by providing additional reinforcement as well as confinement, which delayed and controlled concrete cracking.
- The normalized cracking torsional moment of all strengthened beams was larger than that of the unstrengthened beam, with a maximum increase of 58%. The maximum increase in the normalized peak torsional moment relative to control beam was 109%. These results indicate that PBO-FRCM composite can be a suitable material for torsional strengthening of RC beams.
- The normalized cracking torsional moment of the beam with one layer of fibers with 4-sided 0° fiber orientation (parallel to the longitudinal axis of the beam) was increased relative to that of the control beam, while no significant increase in the normalized peak torsional moment was observed. However, the normalized cracking and peak torsional moments were improved significantly for beams with 4-sided, 90° fiber orientation.
- Concrete crushing governed the failure of the unstrengthened control beam and the strengthened beams with 3-sided wrapping configurations. Fiber rupture followed by concrete crushing and preceded by stirrup yielding governed the failure for beams strengthened with 1-layer, 4-sided, 90° fiber orientation and the beam strengthened with 2-layers, 4-sided, 90° fiber orientation.

- Debonding of the fibers from the concrete substrate governed the failure of the strengthened beams with 4-sided, 45° strips, the strengthened beam with 4-sided, 0° continuous wrapping, and the strengthened beam with two layers (0°/90°) fiber orientation.
- The FRCM composite reduced the longitudinal elongation of the strengthened beams up to 92% compared to the control beam at the peak load of the control beam.
- The contribution of the strengthening system to the torsional strength was reasonably predicted (+/- 20%) by the strains in the composite fibers. Provisions used to estimate the torsional strength of RC beams with externally-bonded FRP composites were found to be applicable for beams strengthened with FRCM composites.
- The trend in the efficiency of PBO-FRCM composite in increasing the torsional strength of solid RC members is similar to that of GFRP and CFRP composites.
- Similar to GFRP-strengthened beams, the 90° fiber orientation was more effective in increasing the torsional strength than the 0° orientation for PBO-FRCM strengthened beams. On the other hand, the 45° fiber orientation was more effective than the 90° orientation for CFRP-strengthened beams, while PBO-FRCM composite-strengthened beams exhibited the opposite trend. Debonding of the PBO-FRCM composite fibers at the ends of the strips contrasted the potential benefits from optimizing the fiber orientation and led to the underutilization of the composite.

- Further investigations are needed to select a suitable anchorage system for beams strengthened with PBO-FRCM composite without overlap at the ends of the fiber sheets.

Based on the numerical study, the following conclusions are presented:

- The general torsional behavior of the experimentally tested beams was predicted accurately by the finite element model in terms of initial stiffness and peak torque.
- The peak torque and twist per unit length were predicted by the model with maximum error of 18% and 32%, respectively. Values of strains in the internal reinforcement and the composite fibers determined by the experiments and FE results at the peak torque were compared at the beam midlength. Reasonable agreement was achieved between the experimental and FE results.
- Results of the parametric study showed that values of concrete compressive strength higher than that of the baseline beam (f'_c=5,700 psi) (39.3 MPa) did not increase the torsional strength. On the other hand, a reduction in torsional strength was observed for values of concrete compressive strength lower than that of the baseline beam. The difference is due to different failure modes, namely fiber rupture for beams with higher values of f'_c and crushing of the concrete strut for lower values of f'_c.
- The parametric study also showed that the torsional strength increases with increasing fiber reinforcement ratio, although the increase in torsional strength is not directly proportional to the increase in fiber reinforcement ratio. Beams

with the same fiber reinforcement ratio but different strip width and spacing exhibited similar increases in torsional strength relative to the control beam.

Based on the analytical study, the following conclusions are presented:

- The torsional behavior of the experimentally tested beams was reasonably predicted by the analytical model in terms of initial stiffness, cracking torsional moment, and peak torsional moment and the corresponding angles of twist per unit length. These results confirm the feasibility of the SMMT model to predict the torsional response of FRCM-strengthened beams.
- Values of the cracking and peak torsional moment and corresponding twist per unit length were predicted analytically with maximum error of (23%, 22%), (36% and 24%), respectively.
- Beams with fully wrapped (continuous and strips) configurations were considered in this study. The mode of failure for all strengthened beam was governed by composite fiber rupture. Further modifications are required to extend the model to the composite debonding failure mode.
- Reasonable agreement was achieved between the experimental and analytical model values of strain in the stirrups and the composite fibers at the peak torsional moment.
- The effect of confinement and the contribution of the composite on the concrete strength could be seen clearly by the higher concrete stress with larger corresponding strain for the strengthened beams compared with the unstrengthened beam at peak torsional moment.

2.3 RECOMMENDATIONS

Based on the objective and scope of work of this study, the following aspects are recommended for future research:

1. Further investigations are needed to study the torsional behavior of RC beams strengthened with PBO-FRCM with a suitable anchorage system.
2. The torsional behavior of RC beams strengthened with PBO-FRCM under cyclic loading should be investigated.
3. Beams in this study had solid, rectangular cross sections. The torsional behavior of hollow and T- or L-shaped RC beams strengthened with PBO-FRCM composite needs further study.
4. The behavior of RC beams strengthened with PBO-FRCM composite under combined loading (shear, flexure, axial, and torsion) should be investigated.
5. Further experimental and numerical studies are needed for torsional behavior of plain concrete beams (i.e., without internal transverse reinforcement) externally strengthened with PBO-FRCM composite.
6. The analytical model presented in this thesis work considered fiber rupture failure mode. Further research is needed to extend the model to the composite debonding failure mode.

REFERENCES

ABAQUS Theory Manual 2002, ABAQUS Inc., USA.

Abdelkarim, O. I., & ElGawady, M. A. (2014). Analytical and finite-element modeling of FRP-concrete-steel double-skin tubular columns. *Journal of Bridge Engineering*, *20*(8), B4014005.

Abdelkarim, O. I., ElGawady, M. A., Gheni, A., Anumolu, S., & Abdulazeez, M. (2016). Seismic Performance of Innovative Hollow-Core FRP–Concrete–Steel Bridge Columns. *Journal of Bridge Engineering*, *22*(2), 04016120.

ACI 318-14. Building code requirements for structural concrete (318-14) and commentary (318R-14). American Concrete Institute, Farmington Hills, MI, 2014, 519 pp.

ACI Committee 445. Report on torsion in structural concrete (ACI 445.1R-12). American Concrete Institute, Farmington Hills, MI, 2012, 92 pp.

ACI Committee 549, ACI 549.4R-13– Guide to Design and construction of externally bonded fabric-reinforced cementitious matrix (FRCM) systems for repair and strengthening concrete and masonry structures, (2013).

Alabdulhady, M. Y., & Sneed, L. H. (2018). A study of the effect of fiber orientation on the torsional behavior of RC beams strengthened with PBO-FRCM composite. *Construction and Building Materials*, *166*, 839-854.

Alabdulhady, M. Y., Sneed, L. H., & Carloni, C. (2017). Torsional behavior of RC beams strengthened with PBO-FRCM composite–An experimental study. *Engineering Structures*, *136*, 393-405.

Alabdulhady, M. Y., Sneed, L. H., Abdelkarim, O. I., & ElGawady, M. A. (2017). Finite element study on the behavior of RC beams strengthened with PBO-FRCM composite under torsion. *Composite Structures*, *179*, 326-339.

Al-Bayati, G., Al-Mahaidi, R., & Kalfat, R. (2016). Experimental investigation into the use of NSM FRP to increase the torsional resistance of RC beams using epoxy resins and cement-based adhesives. *Construction and Building Materials*, *124*, 1153-1164.

Al-Bayati, G., Al-Mahaidi, R., & Kalfat, R. (2017). Torsional strengthening of reinforced concrete beams using different configurations of NSM FRP with epoxy resins and cement-based adhesives. *Composite Structures*, *168*, 569-581.

Al-Bayati, G., Al-Mahaidi, R., Hashemi, M. J., & Kalfat, R. (2018). Torsional strengthening of RC beams using NSM CFRP rope and innovative adhesives. *Composite Structures, 187*, 190-202.

Alecci, V., Focacci, F., Rovero, L., Stipo, G., & De Stefano, M. (2016). Extrados strengthening of brick masonry arches with PBO–FRCM composites: Experimental and analytical investigations. *Composite Structures, 149*, 184-196.

Aljazaeri, Z. R., & Myers, J. J. (2017). Strengthening of Reinforced-Concrete Beams in Shear with a Fabric-Reinforced Cementitious Matrix. *Journal of Composites for Construction*, *21*(5), 04017041.

Ameli, M., & Ronagh, H. R. (2007). Analytical method for evaluating ultimate torque of FRP strengthened reinforced concrete beams. *Journal of Composites for construction*, *11*(4), 384-390.

Ameli, M., Ronagh, H. R., & Dux, P. F. (2007). Behavior of FRP strengthened reinforced concrete beams under torsion. *Journal of Composites for Construction*, *11*(2), 192-200.

ANSYS Commands Reference, ANSYS, Inc. Southpointe, 275 Technology Drive, Canonsburg, PA 15317.

ASTM A370-16. Standard test methods and definitions for mechanical testing of steel products. ASTM International, West Conshohocken, PA, 2016, 49 pp.

ASTM A615/ A615M-16. Standard specification for deformed and plain carbon-steel bars for concrete reinforcement. ASTM International, West Conshohocken, PA, 2015, 8 pp.

ASTM C39/C39M-16b. Standard test method for compressive strength of cylindrical concrete specimens. ASTM International, West Conshohocken, PA, 2016, 7 pp.

ASTM C469/C469M-14. Standard test method for static modulus of elasticity and Poisson's ratio of concrete in compression. ASTM International, West Conshohocken, PA, 2014, 5 pp.

ASTM C496/ C496M-11. Standard test method for splitting tensile strength of cylindrical concrete specimens. ASTM International, West Conshohocken, PA, 2011, 5 pp.

Babaeidarabad, S., Loreto, G., & Nanni, A. (2014). Flexural strengthening of RC beams with an externally bonded fabric-reinforced cementitious matrix. *Journal of Composites for Construction*, 18(5), 04014009.

Belarbi, A., & Hsu, T. T. (1995). Constitutive laws of softened concrete in biaxial tension compression. *Structural Journal*, *92*(5), 562-573.

Belytschko, T., Lin, J. I., & Chen-Shyh, T. (1984). Explicit algorithms for the nonlinear dynamics of shells. *Computer methods in applied mechanics and engineering*, *42*(2), 225-251.

Bentur, A., & Mindess, S. (2006). *Fibre reinforced cementitious composites*. CRC Press.

Bredt, R. (1896). Kritische Bemerkungen zur drehungselastizitat. *Zeitschrift des Vereines Deutscher Ingenieure*, *40*(28), 785-790.

Carloni, C., D'Antino, T., Sneed, L.H., and Pellegrino, C. (2015). "Role of the Matrix Layers in the Stress-Transfer Mechanism of FRCM Composites Bonded to a Concrete Substrate." *Journal of Engineering Mechanics. 141*(6), 04014165.

Carloni, C., Mazzotti, C., Savoia, M., & Subramaniam, K. V. (2014). Confinement of Masonry Columns with PBO FRCM Composites. *Key Engineering Materials*, *624*.

Chai, H. K., Majeed, A. A., & Allawi, A. A. (2014). Torsional Analysis of Multicell Concrete Box Girders Strengthened with CFRP Using a Modified Softened Truss Model. *Journal of Bridge Engineering*, *20*(8), B4014001.

Chalioris, C. E. (2007). Analytical model for the torsional behavior of reinforced concrete beams retrofitted with FRP materials. *Engineering Structures*, *29*(12), 3263-3276.

Chalioris, C. E. (2008). Torsional strengthening of rectangular and flanged beams using carbon fibre-reinforced-polymers–Experimental study. *Construction and Building Materials*, *22*(1), 21-29.

Chen, J. F., & Teng, J. G. (2003). Shear capacity of FRP-strengthened RC beams: FRP debonding. Construction and Building Materials, 17(1), 27-41.

Colajanni, P., De Domenico, F., Recupero, A., & Spinella, N. (2014). Concrete columns confined with fiber reinforced cementitious mortars: experimentation and modelling. *Construction and Building Materials*, *52*, 375-384.

D'Ambrisi, A., & Focacci, F. (2011). Flexural strengthening of RC beams with cement-based composites. *Journal of Composites for Construction*, *15*(5), 707-720.

D'Ambrisi, A., Feo, L., & Focacci, F. (2012). Bond-slip relations for PBO-FRCM materials externally bonded to concrete. *Composites Part B: Engineering*, *43*(8), 2938-2949.

D’Ambrisi, A., Feo, L., & Focacci, F. (2013). Experimental analysis on bond between PBO-FRCM strengthening materials and concrete. *Composites Part B: Engineering*, *44*(1), 524-532.

D’Antino, T., Carloni, C., Sneed, L. H., & Pellegrino, C. (2014). Matrix–fiber bond behavior in PBO FRCM composites: A fracture mechanics approach. *Engineering Fracture Mechanics*, *117*, 94-111.

D’Antino, T., Sneed, L. H., Carloni, C., & Pellegrino, C. (2015). Influence of the substrate characteristics on the bond behavior of PBO FRCM-concrete joints. *Construction and Building Materials*, *101*, 838-850.

D'Antino, T., Sneed, L., Carloni, C., & Pellegrino, C. (2013). Bond behavior of the FRCM-concrete interface. In *Proceedings of the 11th International Symposium on Fiber Reinforced Polymers for Reinforced Concrete Structures,(2013: Guimarães, Portugal)* (10 pp.). Institute for Sustainable an Innovation in Structural Engineering.

Deifalla, A., & Ghobarah, A. (2010). Full torsional behavior of RC beams wrapped with FRP: analytical model. *Journal of Composites for Construction*, *14*(3), 289-300.

Deifalla, A., Awad, A., & Elgarhy, M. (2013). Effectiveness of externally bonded CFRP strips for strengthening flanged beams under torsion: An experimental study. *Engineering Structures*, *56*, 2065-2075.

Elwan, S. K. (2016). Torsion strengthening of RC beams using CFRP (parametric study). *KSCE Journal of Civil Engineering*, 1-9.

fib Bulletin 14 (2001). Externally bonded FRP reinforcement for RC structures. CEB-FIP, Lausanne, Switzerland, 2001, 130 pp.

Ganganagoudar, A., Mondal, T. G., & Prakash, S. S. (2016). Analytical and finite element studies on behavior of FRP strengthened RC beams under torsion. *Composite Structures*, *153*, 876-885.

Ghobarah, A., Ghorbel, M. N., & Chidiac, S. E. (2002). Upgrading torsional resistance of reinforced concrete beams using fiber-reinforced polymer. *Journal of Composites for Construction*, *6*(4), 257-263.

Gonzalez-Libreros, J. H., Sabau, C., Sneed, L. H., Pellegrino, C., & Sas, G. (2017). State of research on shear strengthening of RC beams with FRCM composites. *Construction and Building Materials*, *149*, 444-458.

Gonzalez-Libreros, J. H., Sneed, L. H., D'Antino, T., & Pellegrino, C. (2017). Behavior of RC beams strengthened in shear with FRP and FRCM composites. *Engineering Structures*, *150*, 830-842.

Grelle, S. V., & Sneed, L. H. (2013). Review of anchorage systems for externally bonded FRP laminates. *International Journal of Concrete Structures and Materials*, *7*(1), 17-33.

He, R., Sneed, L. H., & Belarbi, A. (2013). Rapid repair of severely damaged RC columns with different damage conditions: An experimental study. *International Journal of Concrete Structures and Materials*, *7*(1), 35-50.

He, R., Sneed, L. H., & Belarbi, A. (2014). Torsional repair of severely damaged column using carbon fiber-reinforced polymer. *ACI Structural Journal*, *111*(3), 705.

Hii, A. K., & Al-Mahaidi, R. (2006). An experimental and numerical investigation on torsional strengthening of solid and box-section RC beams using CFRP laminates. *Composite Structures*, *75*(1), 213-221.

Hii, A. K., & Al-Mahaidi, R. (2006). Experimental investigation on torsional behavior of solid and box-section RC beams strengthened with CFRP using photogrammetry. *Journal of Composites for Construction*, *10*(4), 321-329.

Hii, A. K., & Al-Mahaidi, R. (2007). Torsional capacity of CFRP strengthened reinforced concrete beams. *Journal of Composites for Construction*, *11*(1), 71-80.

Holman, J. W., & Cook, J. P. (1984). Steel plates for torsion repair of concrete beams. *Journal of Structural Engineering*, *110*(1), 10-18.

Hsu, T. T. (1990). Shear flow zone in torsion of reinforced concrete. *Journal of Structural Engineering*, *116*(11), 3206-3226.

Hsu, T. T. (1993). Unified theory of reinforced concrete. *Boca Raton (FI): CRC*.

Hsu, T. T., & Zhu, R. R. (2002). Softened membrane model for reinforced concrete elements in shear. *Structural Journal*, *99*(4), 460-469.

Jeng, C. H., & Hsu, T. T. (2009). A softened membrane model for torsion in reinforced concrete members. *Engineering Structures*, *31*(9), 1944-1954.

Lin, X., Zhang, Y.X., & Hazell, P.J. (2014). Modelling the response of reinforced concrete panels under blast loading. *Materials & Design*, *56*, 620-628.

Livermore Software Technology Corporation (LSTC) (2007). LS-DYNA Keyword User's Manual Volume II (Material Models), Version 971, Livermore, California.

Loreto, G., Babaeidarabad, S., Leardini, L., & Nanni, A. (2015). RC beams shear-strengthened with fabric-reinforced-cementitious-matrix (FRCM) composite. *International Journal of Advanced Structural Engineering (IJASE), 7*(4), 341-352.

LS-DYNA 971 R3 [Computer software]. Livermore, CA, Livermore Software Technology.

Malvar, L. J., & Simons, D. (1996). Concrete material modeling in explicit computations. In *Proceedings, Workshop on Recent Advances in Computational Structural Dynamics and High Performance Computing, USAE Waterways Experiment Station, Vicksburg, MS* (pp. 165-194).

MATLAB and Statistics Toolbox Release 2016a. The MathWorks, Inc., Natick, Massachusetts, United States.

Matthys, S., and Triantafillou, T. (2001). "Shear and Torsion Strengthening with Externally Bonded FRP Reinforcement." *Proceedings of the International Workshop on Composites in Construction: A Reality*, E. Cosensa, G. Manfredi, and A. Nanni, eds., Capri, Italy, pp. 203-210.

McCormac, J. C., & Brown, R. H. (2015). *Design of reinforced concrete*. John Wiley & Sons.

Mohammadizadeh, M. R., Fadaee, M. J., & Ronagh, H. R. (2009). Improving torsional behaviour of reinforced concrete beams strengthened with carbon fibre reinforced polymer composite. *Iranian Polymer Journal*, *18*(4), 315-327.

Nanni, A. (2012). A new tool for concrete and masonry repair: strengthening with fiber-reinforced cementitious matrix composites. *Concrete international*, *34*(4), 43-49.

Ombres, L. (2011). Flexural analysis of reinforced concrete beams strengthened with a cement based high strength composite material. *Composite Structures*, *94*(1), 143-155.

Ombres, L. (2012). Debonding analysis of reinforced concrete beams strengthened with fibre reinforced cementitious mortar. *Engineering Fracture Mechanics*, *81*, 94-109.

Ombres, L. (2012). Shear capacity of concrete beams strengthened with cement based composite materials. In Proceedings of the 6th International Conference on FRP Composites in Civil Engineering. (CICE 2012). Roma, Italy.

Ombres, L. (2015). Analysis of the bond between fabric reinforced cementitious mortar (FRCM) strengthening systems and concrete. *Composites Part B: Engineering*, *69*, 418-426.

Ombres, L. (2015). Structural performances of reinforced concrete beams strengthened in shear with a cement based fiber composite material. *Composite Structures*, *122*, 316-329.

Paliga, C. M., Real, M. D. V., & Campos Filho, A. (2013). Numerical analysis of reinforced concrete beams strengthened with high strength cement-based composite material. *Revista IBRACON de Estruturas e Materiais*, *6*(2), 211-226.

Panchacharam, S., & Belarbi, A. (2002). Torsional behavior of reinforced concrete beams strengthened with FRP composites. In *First FIB Congress, Osaka, Japan* (Vol. 1, pp. 01-110).

Pellegrino, C., & Modena, C. (2006). Fiber-reinforced polymer shear strengthening of reinforced concrete beams: Experimental study and analytical modeling. ACI Structural Journal, 103(5), 720.

Pellegrino, C., & Modena, C. (2008). An experimentally based analytical model for the shear capacity of FRP-strengthened reinforced concrete beams. Mechanics of composite materials, 44(3), 231-244.

Ruredil. X Mesh Gold Data Sheet. Ruredil S.p.A. 2012, Milan, Italy. <http://english.ruredil.it/SchedeProdottoENG/RuredilXMeshGOLD_ing_1.pdf>.

Salom, P. R., Gergely, J., & Young, D. T. (2004). Torsional strengthening of spandrel beams with fiber-reinforced polymer laminates. *Journal of Composites for Construction*, *8*(2), 157-162.

Shen, K., Wan, S., Mo, Y., & Jiang, Z. (2017). Theoretical analysis on full torsional behavior of RC beams strengthened with FRP materials. *Composite Structures*.

Sneed, L. H., Carloni, C., Baietti, G., & Fraioli, G. (2017). Confinement of Clay Masonry Columns with SRG. In *Key Engineering Materials* (Vol. 747, pp. 350-357). Trans Tech Publications.

Sneed, L. H., D'Antino, T., & Carloni, C. (2014). Investigation of bond behavior of PBO fiber-reinforced cementitious matrix composite-concrete interface. *ACI Materials Journal*, *111*(1-6), 1-12.

Sneed, L. H., D'Antino, T., Carloni, C., & Pellegrino, C. (2015). A comparison of the bond behavior of PBO-FRCM composites determined by double-lap and single-lap shear tests. *Cement and Concrete Composites*, *64*, 37-48.

Sneed, L. H., Verre, S., Carloni, C., & Ombres, L. (2016). Flexural behavior of RC beams strengthened with steel-FRCM composite. *Engineering Structures*, *127*, 686-699.

Täljsten, B., & Blanksvärd, T. (2008). Strengthening of concrete structures with cement based bonded composites. *Nordic Concrete Research*, *2*(38), 133-153.

Tran, C. T. M., Stitmannaithum, B., & Ueda, T. (2014). Investigation of the bond behaviour between PBO-FRCM strengthening material and concrete. *Journal of Advanced Concrete Technology*, *12*(12), 545-557.

Trapko, T., Urbańska, D., & Kamiński, M. (2015). Shear strengthening of reinforced concrete beams with PBO-FRCM composites. *Composites Part B: Engineering*, *80*, 63-72.

Vintzileou, E., & Panagiotidou, E. (2008). An empirical model for predicting the mechanical properties of FRP-confined concrete. *Construction and Building Materials*, *22*(5), 841-854.

Witte, F. C., & Kikstra, W. P. (2002). DIANA Finite Element Analysis, Release 8.1. *TNO Building and Construction Research, Delft, The Netherlands*.

Yang, Y., Sneed, L. H., Morgan, A., Saiidi, M. S., & Belarbi, A. (2015). Repair of RC bridge columns with interlocking spirals and fractured longitudinal bars–An experimental study. *Construction and Building Materials*, *78*, 405-420.

Yang, Y., Sneed, L., Saiidi, M. S., Belarbi, A., Ehsani, M., & He, R. (2015). Emergency repair of an RC bridge column with fractured bars using externally bonded prefabricated thin CFRP laminates and CFRP strips. *Composite Structures*, *133*, 727-738.

Youssf, O., ElGawady, M. A., Mills, J. E., & Ma, X. (2014). Finite element modelling and dilation of FRP-confined concrete columns. *Engineering Structures*, *79*, 70-85.

Zhang, J. W., Lu, Z. T., & Zhu, H. (2001). Experimental study on the behaviour of RC torsional members externally bonded with CFRP. In *FRP Composites in Civil Engineering. Proceedings of the International Conference on FRP composites in Civil Engineering* (No. Volume 1).

Zhu, R. R., & Hsu, T. T. (2002). Poisson effect in reinforced concrete membrane elements. *Structural Journal*, *99*(5), 631-640.

Zojaji, A. R., & Kabir, M. Z. (2012). Analytical approach for predicting full torsional behavior of reinforced concrete beams strengthened with FRP materials. *Scientia Iranica*, *19*(1), 51-63.

Zureick, A. H., Ellingwood, B. R., Nowak, A. S., Mertz, D. R., & Triantafillou, T. C. (2010). *Recommended guide specification for the design of externally bonded FRP systems for repair and strengthening of concrete bridge elements.* NCHRP Report 655. Transportation Research Board.

VITA

Meyyada Yahya Mohammed Alabdulhady was born in Basrah, Iraq in 1984. She received her bachelor and master's degree in Civil Engineering both with distinction from University of Basrah - Iraq in 2006 and 2009 respectively. She started her graduate studies with research focused on the torsional strength of RC spandrel beams in October 2006. She published her masters' research titled "Prediction of Ultimate Torsional Strength of Spandrel Beams using Artificial Neural Networks" in Basrah Journal for Engineering Science, 2011.

She worked as an assistant lecturer at the University of Basrah, College of engineering, civil department. During her career, she taught several classes and coauthored a book titled "Structural Analysis" with Prof. Nabeel A. Jasim published in 2010.

In 2011, she won a scholarship to complete her PhD in Missouri University of Science and Technology and started her Ph.D. program in Civil Engineering. Her research focus on the torsional behavior of RC beams strengthened with PBO-FRCM composite system. She published several papers in Elsavier {Engineering Structures, Composite Structures, and Construction & Building Materials} journals. She received her PhD in Civil Engineering from Missouri University of Science and Technology in May 2018.